2009

Utilization of mononuclear trivalent lanthanide complexes for the assembly of heteronuclear (d-f) metal complexes

Ritu Raturi
University of Windsor

Utilization of Mononuclear Trivalent Lanthanide Complexes for the Assembly of Heteronuclear (*d-f*) Metal Complexes

by

Ritu Raturi

A Dissertation
Submitted to the Faculty of Graduate Studies through
Chemistry and Biochemistry
in Partial Fulfillment of the Requirements for
the Degree of Doctor of Philosophy at the
University of Windsor

Windsor, Ontario, Canada
2009

Your file Votre référence
ISBN: 978-0-494-57656-4
Our file Notre référence
ISBN: 978-0-494-57656-4

Declaration of Previous Publication

This thesis includes 6 Chapters, out of which Chapter-3 "A Phosphine Mediated Through-Space Exchange Coupling Pathway for Unpaired Electrons in a Heterobimetallic *d-f* Metal Complexes" has been previously published in one of the reputed journals. I was the principal investigator in the above mentioned publication and I had a significant role in the manuscript preparation. I acknowledge my supervisor as a co-author in this work as he has also made a significant contribution to the writing of manuscript and the acquisition of computational data. Other listed authors on manuscript contributed through raw data acquisition.

I certify that I have obtained a written permission from the copyright owner to include the above published material in my thesis. I certify that the above material describes work completed during my registration as graduate student at the University of Windsor. I declare that this thesis, and the research related to this, are the product of my own work and that any ideas form the work of other people, published or otherwise, are fully acknowledged in accordance with the standard referencing practices of the discipline. I also declare that this is a true copy of my thesis, and that this thesis has not been submitted for a higher degree to any other University or Institution.

ABSTRACT

Lanthanides are known for their distinctive magnetic properties and have been utilized for the design of multinuclear single-molecule magnets. Mononuclear trivalent lanthanide complexes were prepared from the reaction of tripodal amido ligands $[P(CH_2NHAr^R)_3]$ and $Ln[N(SiMe_3)_2]$ (Ar^R = C_6H_5, 3,5-Me_2 and 3,5-$(CF_3)_2$ and Ln = Y, Tb, Dy, Ho, Er, Tm and Yb) in the presence of THF. These mononuclear lanthanide complexes were then further utilized for the syntheses of *d-f* heteronuclear compounds, using various transition metal complexes such as Pt(cyclooctadiene)Me_2, Ni(acetylacetonate)$_2$ and Co-porphyrin.

Mononuclear trivalent lanthanide complexes, prepared using 2-methyl anthranilate, contained a rigid chelate ring with six proton environments. The $^{31}P\{^1H\}$ NMR spectra demonstrated a through-space interaction between the minor lobe of phosphine lone pair and the yttrium metal. Binding of a paramagnetic cobalt metal complex to the unbound phosphine lone pair provided heterodinuclear *d-f* metal complexes. The EPR spectra and the magnetic study of heterodinuclear complexes indicated the through-space antiferromagnetic coupling between unpaired electrons of gadolinium and cobalt centers.

Magnetic anisotropy of lanthanide complexes with more than C_2 symmetry can be easily measured by their NMR shifts due to the presence of dipolar contribution. According to Bleaney, temperature dependence of the magnetic anisotropy of lanthanide complexes should be proportional to T^{-2} and the crystal field parameter (a_{20}).

$$\chi_{\parallel} - \chi_{\perp} = \frac{K_0}{T^2} a_{20} \qquad \text{(eq. 1)}$$

McGarvey later expanded the temperature dependence of the anisotropy by including a term that is proportional to T^{-3} and other crystal field parameters (equation 2).

$$\chi_{\parallel} - \chi_{\perp} = C_2 T^{-2} + C_3 T^{-3} \qquad \text{(eq. 2)}$$

From our calculations, we demonstrated the dependence of higher terms ($>T^{-2}$) for the calculation of magnetic anisotropy near room temperature. These higher terms showed the contribution of 20-90 % of the T^{-2} term.

Estimation of crystal field parameters (related with magnetic properties) generally requires low temperature optical spectroscopy or a SQUID magnetometer. Our trivalent mononuclear lanthanide complexes have C_3 symmetry, which required 6 crystal field parameters, B_{20}, B_{40}, B_{60}, B_{43}, B_{63} and B_{66}. Here, we utilized variable temperature NMR spectra to calculate the set of crystal field parameters. A best set of crystal-field parameters were then obtained by comparing experimental and theoretical magnetic anisotropies. In the future, these parameters can be further utilized for the electronic structure of lanthanide complexes.

Dedicated to Arun and Avani (Meri Lado)

Acknowledgments

After a long period, the journey has ended in the form of this thesis. I was not alone in this journey, there were many people, who accompanied me and made this journey easier for me. I would like to gratefully acknowledge all those people without whom it was almost impossible to make this thesis successful.

I wish to express my thanks to my supervisor, Dr. Samuel Johnson, for giving me an opportunity to pursue this research work. Next I would like to acknowledge my committee members Dr. Stephen Loeb, Dr. James Green, Dr. Maria Cioppa and my external examiner Dr. Laurel Schafer for being a part of my committee, and for all the valuable advice, and suggestions. My heartiest thanks to Dr. Charles Macdonald for his immense support and ideas he gave me during my PhD.

I am indebted to my many student colleagues for providing a stimulating and fun environment. Many thanks to former and current members of Johnson and Macdonald groups: Jill, Meghan, Ben, Raj, Erin. Special thanks to Jill for editing my thesis as well as for babysitting my daughter whenever she was in the department with me. I would also like to thank Harman, Sapna and Rafiq for their help. Many thanks to Marlene Bezaire and Una Lee for their entire help during my studies.

Special thanks to Mrs. Macdonald (Inga Slišković) for her help and support, especially when it was needed the most; and yes Inga for babysitting Avi too!

I wish to thank my Maa, Papa and my big brother Alok for loving me, supporting me and for trusting me in all my endeavours. I would also like to thank my in-laws for providing a loving environment for me.

Lastly, and the most importantly, my wonderful husband, Dr. Arun Raturi who held my hand through every step, words can not express his invaluable support or my gratitude. He always pushes me to do my best for his continuous support and without him I could not have accomplished this goal. So hey, I love you more than any one else does and you know I mean it.

No acknowledgement can express my feeling for my daughter, Avani. The only thing, which I can say here, is that Mamma adores you and dedicates this thesis to the most important persons in my life (you and your Dad).

TABLE OF CONTENTS

LIST OF FIGURES

LIST OF TABLES

LIST OF ABBREVIATIONS

Å	Angstrom
Anal.	Analysis
Ar^R	C_6H_5, 3,5-$Me_2C_6H_3$, 3,5-$(CF_3)_2C_6H_3$
Ar^{Me}	3,5-$Me_2C_6H_3$
Ar^{CF3}	3,5-$(CF_3)_2C_6H_3$
$A_{P\parallel}$	Parallel superhyperfine coupling constant to phosphorus
$A_{P\perp}$	Perpendicular superhyperfine coupling constant to phosphorus
aq	Aqueous
br	Broad
^{n}Bu	*n*-Butyl group
^{t}Bu	Tertiary butyl group
^{13}C	Carbon-13
Calcd.	Calculated
cm	Centimetre
CFP	Crystal field parameter
COSY	Correlation spectroscopy
Cp	Cyclopentadienyl
°C	Degree Celsius
d	Doublet
dd	Doublet of doublets
dt	Doublet of triplets
deg	Degree
DMF	Dimethyl formamide
ER	Endoplasmic Reticulum
EPR	Electron paramagnetic resonance
^{19}F	Fluorine-19
g	Grams
g_J	Landé factor
GOOF	Goodness of fit

Hapen	*N,N'*-ethylenebis(*o*-hydroxyacetophenoneiminato)
h	Hour
$\{^1H\}$	Proton decoupled
^1H	Proton
H	Hertz
Hhmp	2-(hydroxymethyl)-pyridine
Hmmi	2-hydroxymethyl-1-methyl-imidazole
IR	Infrared
J	Coupling constant
K	Kelvin
KTp	Potassium salt of tris(pyrazolyl) borate
Ln	Lanthanide
mg	Milligram
min	Minute
mL	Milliliter
mmol	Millimole
mol	Mole
m	Multiplet
m	*Meta*
M	Molarity
MPMS	Magnetic Property Measurement System
μ_{eff}	Effective magnetic moment
NMR	Nuclear magnetic resonance
o	*Ortho*
ORTEP	Oakridge thermal ellipsoid plotting program
$^{31}P\{^1H\}$	Phosphorus-31
Ph	Phenyl group
ppm	Parts per million
R_w	Weighted residual
RT	Room temperature
Salen	*N,N'*-ethylenebis(salicylaldiminato)*o*-hydroxyacetophenoneiminato)

s	Singlet
S	Total spin angular momentum
SMM	Single molecule magnet
SQUID	Superconducting quantum interference device
t	Triplet
T	Temperature
T^{-n}	Temperature to the exponent −n
VT	Variable-temperature
TCNE	Tetracyanoethane
TNOP	bis{3-(*N*-*tert*-butyloxyamino)-5-*tert*-butylphenyl}aminoxyl
THF	Tetrahydrofuran
TPP	5,10,15,20–tetrakis(4–methoxyphenyl)porphyrin)
$\chi_{\parallel}/\chi_{\perp}$	Anisotropy
χ_m	Molar magnetic susceptibility
δ	Chemical shift (ppm)

CHAPTER-1

Molecular Magnetism and Tripodal Amido Ligands

1. Overview of Dissertation

This Ph.D. dissertation covers a synthetic approach to tripodal amido ligand-stabilized mononuclear trivalent lanthanide complexes, which act as building blocks for heterodinuclear complexes. The aim of this research is to utilize the magnetic properties of lanthanides for the assembly of magnetic molecules. This thesis is divided into six chapters. The first Chapter provides an introduction to the thesis and is divided into two sections: the first section provides a review of lanthanide complexes, their

References begin on page 30

syntheses and applications in molecular magnetism, while the second section reviews tripodal amido ligands and other ligands such as ligands containing phosphorus and nitrogen donor atoms, tris(pyrazolyl)borate, and their metal complexes. Some of the tripodal amido ligands reported in this thesis have also been utilized to generate multinuclear complexes with potential application as molecular magnets.[1, 2]

Chapter 2 describes the syntheses of mononuclear trivalent lanthanide compounds and their heterodinuclear *d–f* metal complexes using an appropriate transition metal complex to observe magnetic interactions. Chapter 3 describes the design of a new tripodal amido ligand with amido nitrogens, ester functionality oxygens, and a phosphine donor and its utilization in mono and heterodinuclear complexes (published 2007). For the last few decades, due to the presence of unique magnetic properties, such as large magnetic anisotropies and large zero field splitting, lanthanide complexes have been used for the syntheses of various magnetic molecules and heteronuclear complexes. The large magnetic anisotropy of lanthanide complexes depends on the crystal field splitting and temperature. The magnetic anisotropy is also responsible for large NMR shifts of paramagnetic lanthanide complexes; therefore, the paramagnetic NMR shifts are also temperature dependent. Thus Chapter 4 of the thesis focuses on the temperature dependent terms of magnetic anisotropy (T^{-2}, T^{-3}..... T^{-n}) and their relevance on pseudocontact shifts. Crystal field parameters, which are essential to define magnetic properties of lanthanide complexes, are mostly determined by low temperature optical spectroscopy. In Chapter 5, a new approach is proposed by which the crystal field parameters of trivalent lanthanide complexes can be determined by using variable-temperature NMR spectroscopy. Chapter 6 summarizes this thesis with a

References begin on page 30

few preliminary results obtained from synthesizing heteronuclear *d-d* metal complexes and the potential future approaches towards other heteronuclear complexes.

The long term goals of this research work are: 1) preparation of multinuclear complexes and clusters with specific magnetic properties, and 2) to develop new molecular magnets such as single molecule magnets (SMMs). The ultimate goal of this study is to incorporate these SMMs and molecular molecules in information storage devices.

1.1 Molecular Magnetism

Fundamentally, metal complexes exhibit two types of magnetic behaviours: diamagnetism (paired electrons) and paramagnetism (unpaired electrons). Unlike diamagnetism, in paramagnetism, the spin of one or more electrons does not get cancelled by electrons with opposite spin, which causes magnetic dipole. In an external magnetic field, the magnetic dipoles present in the compound align with the field, which causes magnetization that creates an induced field within the substance called the magnetic induction (*B*). It can be expressed as:

$$B = H + 4\pi M \qquad (1.1)$$

H = external magnetic field
M = magnetization

However, commonly the magnetization is expressed in terms of magnetic susceptibility (χ) and can be written as:

$$\chi = M/H \qquad (1.2)$$

References begin on page 30

While diamagnetism is characterized by small negative χ values, paramagnetism yields large positive χ values. Magnetic calculations depend on the population of different energy levels (Boltzmann distribution), which defines the magnetic susceptibility at any particular temperature. For example, for any unpaired electron ($S = ½$), there are two levels of interest and in the absence of a magnetic field, the $S = ½$ state possesses two energetically degenerate quantum levels referred to as a Kramer's' doublet. This degeneracy, after applying an external magnetic field, splits into two quantum levels, $m_s = +½$ and $m_s = -½$. As shown in Figure 1.1, this splitting of Kramers' doublet is called Zeeman splitting.

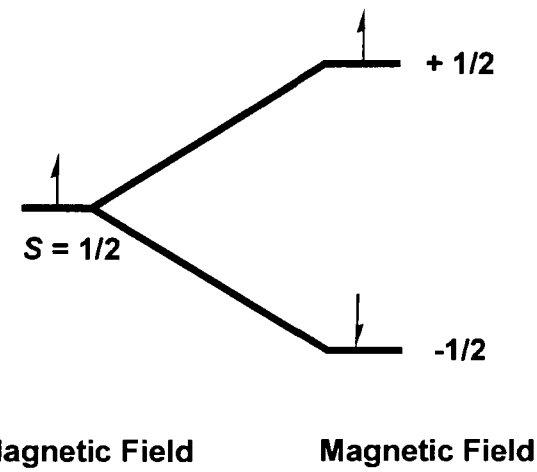

Figure 1.1. Zeeman splitting effect of an unpaired electron ($S = ½$)

In transition metal complexes, the presence of supporting ligands is responsible for the distribution of electrons in *d*-orbitals, while lanthanide complexes are not strongly influenced by ligand field splitting. Traditional equations that describe the magnetic moment of transition metal complexes generally fail to account for the large unquenched orbital angular momentum of lanthanides. For example, in transition metal

References begin on page 30

complexes, the magnetic moment is the result of only spin angular momentum and can be calculated as given in equation 1.3.

$$\mu_{eff} = g\sqrt{S(S+1)} \qquad (1.3)$$

μ_{eff} = magnetic moment

g = g-factor

S = total spin angular momentum

Calculation of the magnetic moment of the paramagnetic lanthanide complexes requires additional parameters such as orbital angular momentum and spin-orbital coupling. With the exception of Gd^{3+} and Eu^{3+}, which have orbitally non-degenerate ground states,[3] the unquenched orbital angular momentum (L) and spin angular momentum (S) interact further to produce several new micro states. These micro states arise from the spin-orbit coupling and are defined as the total angular momentum (J). The values of $J = L+S, L+S-1, L+S-2, L+S-3.....L-S$.

For most of the trivalent lanthanide ions, the excited J levels are thermally accessible due to the large spin-orbit coupling; thus, their magnetic behaviour is generally determined by the ground spin-orbit coupled state. At room temperature, the magnetic moment of lanthanides can be defined as shown in equation (1.4):

$$\mu_{eff} = g_J\sqrt{J(J+1)} \qquad (1.4)$$

$$g_J = \frac{3}{2} + \frac{S(S+1)-L(L+1)}{2J(J+1)} \qquad (1.5)$$

References begin on page 30

g_J = Landé factor

S = total spin angular momentum

L = total orbital angular momentum

J = total angular momentum

As shown in Table 1.1, paramagnetic lanthanide metal ions exhibit large magnetic moment and this property of lanthanides has been exploited to synthesize several magnetic materials.[4, 5]

Table 1.1. Magnetic Properties of Ln^{3+} at Room Temperature.

Ln^{3+}	f^n	Ground State	μ_{eff}[a]	$\chi_m T(cm^3 mol^{-1} K)$[b]
La	f^0	$^1S_0$	0	0
Ce	f^1	$^2F_{5/2}$	2.54	0.80
Pr	f^2	$^3H_4$	3.58	1.60
Nd	f^3	$^4I_{9/2}$	3.68	1.64
Pm	f^4	$^5I_4$	2.83	0.90
Sm	f^5	$^6H_{5/2}$	0.85	0.09
Eu	f^6	$^7F_0$	0	0
Gd	f^7	$^8S_{7/2}$	7.94	7.88
Tb	f^8	$^7F_6$	9.72	11.82
Dy	f^9	$^6H_{15/2}$	10.63	14.72
Ho	f^{10}	$^5I_8$	10.60	14.07
Er	f^{11}	$^4I_{15/2}$	9.59	11.48
Tm	f^{12}	$^3H_6$	7.57	7.15
Yb	f^{13}	$^2F_{7/2}$	4.53	2.57
Lu	f^{14}	$^1S_0$	0	0

[a,b] μ_{eff} is the magnetic moment and $\chi_m T$ is the product of magnetic susceptibility and temperature for *f*-block metal ions (Ln^{3+})

f^n = no. of *f*-electrons

References begin on page 30

For lanthanide complexes, splitting of ground state multiplets depends on the surrounding ligands and can be described by crystal field theory. To fully understand the magnetic behaviour of lanthanide complexes, understanding of crystal field parameters are require, which are require for the splitting of ground state multiplets. Total six crystal field parameters, B_{20}, B_{40}, B_{43}, B_{60}, B_{63} and B_{66} are require for lanthanide complexes with C_3 symmetry. These crystal filed parameters are responsible for the splitting of ground state multiplets. In lanthanide complexes while spin-orbit coupling is responsible for splitting on the order of 50-2000 cm^{-1}, crystal field splitting is on order of 30-200 cm^{-1}.[5] Crystal field splitting introduces magnetic anisotropy into the magnetic susceptibility, defined as the difference between minimum and maximum susceptibility. For the axially symmetric lanthanide complexes, the relationship between magnetic susceptibility and anisotropy can be written as given in equations.1.6-1.8.[6, 7]

$$\chi_{zz} - \bar{\chi} = \tfrac{2}{3}(\chi_{\parallel} - \chi_{\perp}) \qquad (1.6)$$

$$\bar{\chi} = (\chi_{zz} + \chi_{xx} + \chi_{yy})/3 \qquad (1.7)$$

$$\chi_{zz} = \chi_{\parallel} \text{ and } \chi_{xx} = \chi_{yy} = \chi_{\perp} \qquad (1.8)$$

Magnetic anisotropy is a temperature dependent term and gives higher values at low temperatures due to the presence of the thermally populated ground state. Increasing the temperature increases the number of thermally populated excited states, and thus, decreases the magnetic anisotropy. In simple way, the magnetic anisotropy of lanthanide complex can be determined from crystal field parameters and has temperature dependence. Magnetic anisotropy also induces paramagnetic NMR shifts in lanthanide

References begin on page 30

complexes, that allows them to serve as a lanthanide shift reagent, for the structural determination of complicated bio and organic molecules.[8, 9] Paramagnetic shifts of lanthanides are the combination of contact and pseudocontact shifts.[10] While contact shifts arise from the delocalization of metal spin density to the substrate nuclei, pseudocontact shifts arise from the dipolar contribution and provide structural information of the lanthanide complexes. Paramagnetic pseudocontact shifts can be utilized to measure the magnetic anisotropy as shown in equation 1.9.[10]

$$\Delta\delta = \frac{(3\cos^2\theta - 1)}{2R^3}(\chi_{zz} - \overline{\chi}) \qquad (1.9)$$

$\Delta\delta$ = chemical shifts

R = distance between lanthanide metal and substrate nuclei

θ = angle between lanthanide metal and substrate nuclei

A large magnetic anisotropy is a desirable property in magnetic molecules for observing through-space magnetic interaction. Commonly, in magnetic molecules, exchange coupling between metal center ions is calculated by spin Hamiltonian ($\hat{H}$), as given in equation (1.10).[6, 11]

$$\hat{H} = (-J)(\hat{S}_1 \cdot \hat{S}_2) \qquad (1.10)$$

$-J$ = antiferromagnetic coupling constant

$+J$ = ferromagnetic coupling coupling constant

$\hat{S}_1$ and $\hat{S}_2$ = spin operators associated with both metal centers

As shown in Figure 1.2., the net magnetic moment (S) of a magnetic molecule is the result of the net effect of the atomic moments of each paramagnetic ion. Depending upon the direction of the magnetic moment of both metals, their interaction can be of

References begin on page 30

three types. **A**) Ferromagnetic, which is the strongest interaction and occurs even in the absence of the magnetic field. Ferromagnetic interaction is due to the parallel arrangement of atomic moments, which align in the same direction. **B**) Antiferromagnetic interaction, which is due to the antiparallel arrangement of atomic moments, resulting in a net zero magnetization value, and **C**) ferrimagnetic interaction, which is a special case of antiferromagnetic interaction, where the net magnetization value cannot be zero. In this type of magnetic interaction, the adjacent magnetic spins with different magnitude align themselves antiparallel to each other, resulting a non zero magnetic moment.

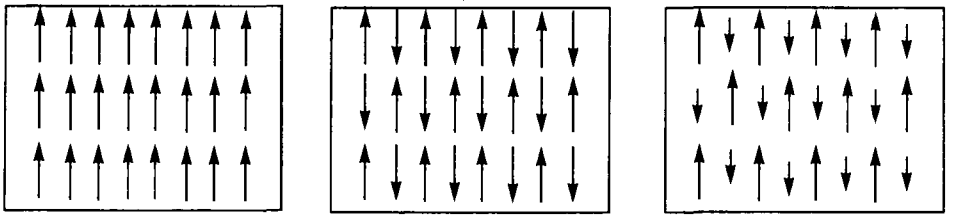

Figure 1.2. Different types of magnetic interactions showing the net magnetic moment.

Lanthanide metal ions exhibit weak interactions between *f-f* metal centers due to the presence of unquenched orbital angular momentum and the internal nature of *f* electrons. Complexes containing both paramagnetic lanthanides (*f*) and transition metal ions (*d*) produce measurable effects due to stronger magnetic interaction and hence have been used for various magnetic molecules. Most of the *d-f* metal complexes reported in the literature are the Gd^{3+} and Cu^{2+} coupled system because of the non-degenerate ground state of Gd^{3+}, which simplifies the magnetic analysis.[12, 13] Bencini *et al.* first reported a magnetic study of two trinuclear Gd-Cu complexes containing two copper

References begin on page 30

metal ions within the trinuclear units. Both the *d-f* metal complexes showed a ferromagnetic interaction between the two Cu^{2+} ions and one Gd^{3+} ion within the trinuclear units.[14] With the exception of a few examples, most of the Gd^{3+} and Cu^{2+} containing *d-f* metal complexes showed ferromagnetic interactions between Gd-Cu.[15, 16]

The first magnetic molecule, diethydithiocarbamate iron chloride, was synthesized and characterized by Wickman *et al.* in 1967.[17] One of the recently developed giant magnetic molecules also contains transition metal ions (Mo-Fe system) with a total of 30 trivalent iron metal ions (S = 5/2), $Mo_{72}Fe_{30}O_{252}(Mo_2O_7(H_2O))_2(Mo_2O_8H_2)(H_2O))(CH_3COO)_{12}(H_2O)_{91}]\cdot 150H_2O$ $Mo_{72}Fe_{30}$).[18]

The contribution of magnetism or magnetic materials in different area involve: a) synthetic chemistry- designing of molecular systems that contain magnetic properties i.e. molecular magnets[19-23] and single-molecule magnets[24-26] and b) molecular electronics, where these molecular systems can be used in electronic devices. Synthetic approaches towards molecular magnets have grown rapidly in the last few years due to the increasing demand for magnetic molecules in various fields. Not only in information storage industries or academic research, magnetic molecules have also found their place in biomedicine, such as use of magneto fluorescent nanoparticles and magnetic materials for sensing, imaging, and magnetic separation[27-29] Bruck in 2005 focused on the improvements and developments on magnetic refrigerator, which are analogues of commercially available refrigerators but with environmental friendly features such as water coolants, a gas free compressor, and low electricity consumption.[30]

Molecular magnetism, which involves magnetic molecules formed due to the magnetic interaction between metallic centers, is a significant large area in material

References begin on page 30

chemistry. These magnetic molecules act as building block and can be further used to build molecules for designing electronics and magnetic materials, such as molecular wires, medical devices, microphones, data storage devices, motors, and generators.[31] Traditional magnetic materials are the combination of two- or three-dimensional arrays of inorganic molecules that are composed of paramagnetic transition or lanthanides metal ions. Production of these materials requires high-temperature metallurgical processes. In contrast to these traditional magnetic materials, molecular magnets are comprised of paramagnetic metal ions or organic radicals and require low temperature synthetic processes.[31, 32]

Most of the early reported magnetic molecules are the combination of either transition metals or transition and lanthanide based metal systems, rather than lanthanide metal ions exclusively, since the *f-f* interaction is comparatively smaller than the interaction between *f* and *s, p* or *d* electrons. Though the heteronuclear complexes containing *d* and *f* block metal ions first appeared in early 1970's, detailed studies on the magnetic chemistry of heteronuclear complexes containing *d* and *f* block metals remain less understood than *d-d* metal ions.[33-41] Due to the increasing demand for new molecular-based materials, there has been a significant amount of research dedicated to the syntheses of new *d-f* heteronuclear complexes providing a better understanding of exchange-coupling/magnetic interactions. However, designing appropriate chelating ligands that can provide a close proximity between both metals is still a great challenge.

References begin on page 30

1.1.1 Exchange Interaction

In the case of traditional magnets, a net magnetic moment involves the alignment of unpaired electron spins via a mechanical effect. The magnetic moment of molecular magnets or magnetic coupling between unpaired electrons of paramagnetic metal ions is the result of one of the following two main mechanisms:

1.1.1.1 Superexchange- A process in which paramagnetic metal ions are bridged via bridging ligands and the exchange interaction occurs by charge transfer between metal ions and ligands.[7, 42-44] Superexchange interactions can be expressed by the spin-Hamiltonian as shown in equation (1.10). Goodenough and coworkers proposed a mechanism for superexchange coupling from which the exchange coupling constant can be predicted.[45] In 1993, Kahn and coworkers suggested that in the case of lanthanide complexes, the sign of the interaction (J) depends on the number of unpaired f-electrons and is antiferromagnetic if J is negative ($-J$).[36] Due to the shielding effect of $4f$-electrons by $5s$ and $5p$ orbitals, f-orbitals are weakly delocalized towards the surrounding ligands. Therefore, interaction between ligand and metal ions is due to the electron exchange process.

1.1.1.2 Direct exchange- This type of interaction mainly occurs due to overlapping of the orbitals of paramagnetic metal ions.[46, 47]

In recent years, increasing demands for nanoscale magnetic materials have developed into a new scientific field involving the design of intricate architectures, including macromolecular polynuclear complexes, 1-D wires, and 2-D or 3-D networks.[48] In order to act as a magnetic material, the specific molecular cluster or polynuclear complex must enable the transmission of exchange coupling via the same

References begin on page 30

bonding interactions that assemble these complexes and networks. The superexchange coupling is often performed by single atom bridged metal centres, but larger π-conjugated bridging ligands are also capable of propagating exchange. In addition to these properties, magnetic anisotropy also plays an important role in enhancing the magnetic interaction between metal ions in polynuclear magnetic complexes. Cyanido-metallate complexes have recently revolutionized the design of magnetic network-structures[43, 49] and single molecule magnets.[50, 51] In these cyanido-bridged complexes, the cyanido group provides an exchange pathway for the interaction between the metal centers. Other bridging ligands that have been utilized successfully to design polynuclear complexes and magnetic network are tetracyanoethene (TCNE),[23, 42, 52, 53] bis{3-(*N-tert*-butoxyamino)-5-*tert*-butylphenyl}aminoxyl (TNOP),[54, 55] Hhmp (2-(hydroxymethyl)-pyridine),[56] Hmmi (2-hydroxymethyl-1-methylimidazole),[57] and azacyano-carbanions.[58] Hhmp is a well known bridging ligand in the synthesis of Mn single-molecule magnets (SMMs) (Figure 1.3).[32]

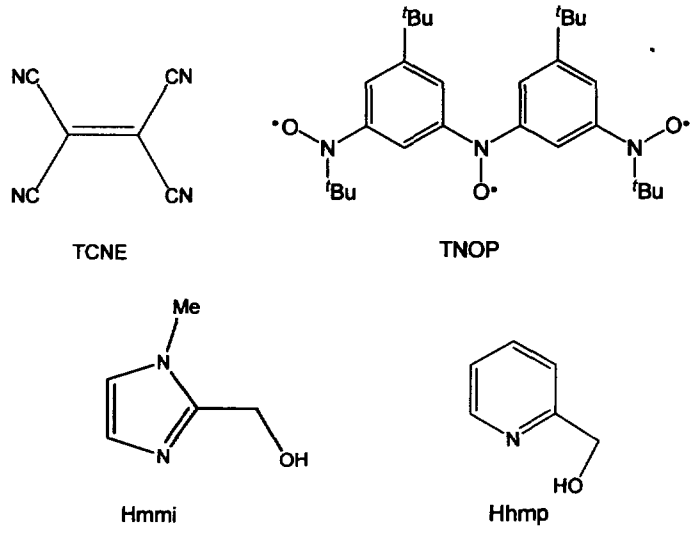

Figure 1.3. Bridging ligands for magnetic complexes.

References begin on page 30

The lanthanide complexes discussed in the present thesis are supported by tripodal amido ligands, which provide two different active sites to accommodate two different metal ions while also serving as a bridging ligand between the metal ions.

1.1.2 Single Molecule Magnets (SMMs)

Single molecule magnets[24, 59, 60] are the class of molecule-based magnet in which each and every molecule behaves as a magnet, yet do not magnetically interact with each other. SMMs require a combination of large axial magnetic anisotropy, or negative zero field splitting ($-D$) and large spin ground states, ($S = +S$ (↑) or $-S$ (↓)) which results in the formation of a significant barrier (U) with the maximum value of $U = S^2|D|$ or $U = (S^2-{}^1/_4)|D|$ depending upon the integer or non–integer spins respectively as shown in Figure 1.4.[61]

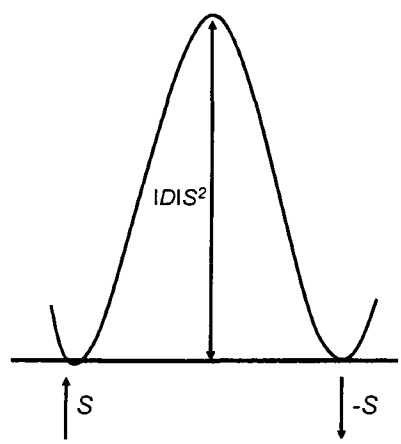

Figure 1.4. Potential energy diagram with negative zero field splitting ($-D$) and energy barrier $U = S^2|D|$

The first SMM reported by Caneschi *et al.* is the Mn-acetate cluster $Mn_{12}O_{12}(MeCO_2)_{16}(H_2O)_4$, which contained four inner Mn-ions surrounded by outer

References begin on page 30

eight Mn-ions, bridged by oxygens (Figure 1.5).[62] The net spin (S = 10) of the cluster was the result of the spin of each four inner Mn^{3+} ($S = {}^3/_2$) and eight outer (S = 2) Mn^{4+} ions giving large zero field splitting and slow relaxation magnetization at low temperature. Both inner (Mn^{3+}) and outer (Mn^{4+}) metal ions showed antiferromagnetic coupling between each other.

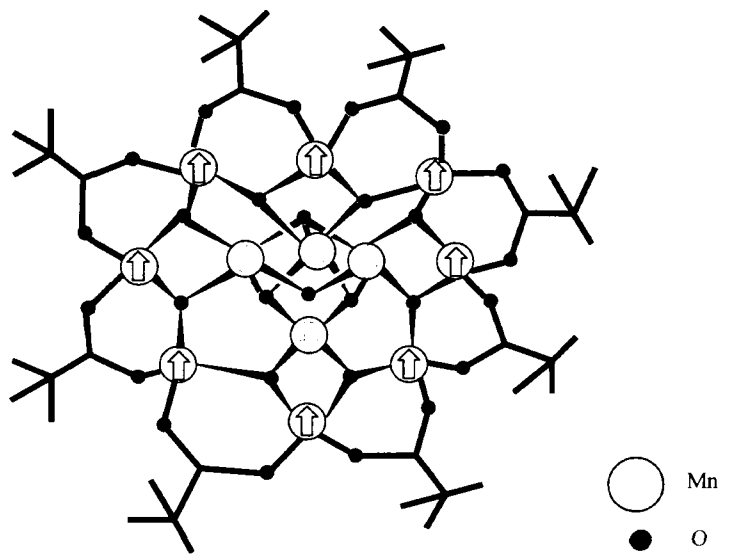

Figure 1.5. Structure of $Mn_{12}O_{12}(MeCO_2)_{16}(H_2O)_4$ showing magnetic coupling between Mn ions. Ferromagnetically coupled inner Mn^{3+} ($S = {}^3/_2$) with total spin S = 6 and outer eight Mn^{4+} (S = 2) with total spin S = 16. Net spin results due to the antiferromagnetic exchange, $S = 16-6 = 10$.

It has been reported by Waldmann recently, that the most important factor to obtain a good quality SMM is a larger zero-field splitting,[63, 64] while the previously reported SMMs were based on large spin ground states.[24, 65] The large spin ground state

References begin on page 30

values of any SMM are the result of either ferromagnetic or antiferromagnetic exchange coupling between metal ions by which SMMs behave like super paramagnets. In the case of SMMs, the magnetic moment of each paramagnetic molecule aligns parallel to the applied external magnetic field and remains magnetized at low temperature, even after the removal of the magnetic field. At low temperatures, in the absence of a magnetic field, SMMs develop an energy barrier, which requires reversing the direction of the magnetization. As shown below in Figure 1.6, in the absence of a magnetic field, all micro spin states are at the same energy levels and become unequal only after the application of an external magnetic field (field direction is parallel to z-axis). At low temperature, one of the spin states becomes populated and magnetization reaches its saturation point. Removal of the external magnetic field reverts the system to its original equilibrium position via a process called relaxation, thereby creating an energy barrier, which is a necessary requirement for SMM.

References begin on page 30

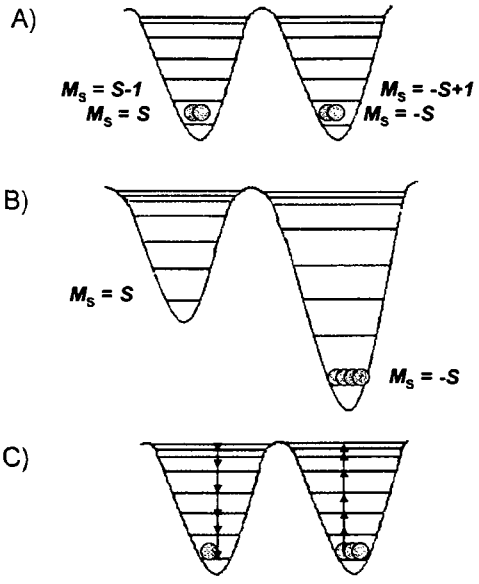

Figure 1.6. Energy levels for a spin state S with easy axis magnetic anisotropy. Left well shows $+M_S$ levels and the right well $-M_S$ levels. A) Equally populated wells in the absence of magnetic field, B) Highly populated right well in the presence of magnetic field, and C) removal of field creates multiple steps to return to equilibrium.

Another known SMM is $[\{Fe_8O_2(OH)_{12}(tacn)_6\}Br_7 \cdot H_2O]Br \cdot 8H_2O$, (Where, tacn is 1,4,7–triazacyclononane) with a ground state of $S = 10$ in which the iron metal ions are bridged by oxygen and hydroxyl groups.[60] Although most of the reported SMMs contain primarily Mn^{3+} ions, it is known that the spin of transition metal ions affect the rate of magnetization.[66] SMMs, containing other metal ions include, tetranuclear Co_4L_4, where L = *N,N'*-di[1-(2-hydroxypheny)ethlidene]hydrazone,[67] $[Ni(hmp)(CH_2OH)Cl]_4$, where hmp = monoanion of 2-hydroxymethylpyridine with four Ni^{2+} and four hmp^- at alternating corners[63], mononuclear bis(pthalocyanato)Tb^-, bis(phthalocyanin)Dy^- [64, 68]

References begin on page 30

and heterometallic complexes such as tetranuclear $[Cu^{II}LTb^{III}(hfac)_2]_2$ and $[Cu^{II}LDy^{III}(hfac)_2]_2$ (Where, hfac = hexafluoroacetylacetone and H_3L = 1-2(-hydroxybenzamide)-2-(2-hydroxy-3-methoxybenzylideneamino)ethane)[69] and $[Mn_{11}Dy_4O_8(OH)_6(OMe)_2(O_2CPh)_{16}(NO_3)_5(H_2O)_3]_{15}\cdot MeCN(1.15MeCN)$ with five or nine coordinate Mn^{3+} and Dy^{3+} ions respectively.[35, 70] Properties of the SMMs composed of *d-f* metal complexes depend on both metal ions and can be tuned by using appropriate combination of metals. For example, the above given Mn-Dy-complex is the first known *d-f* SMM and has an energy barrier of 9 K,[70] which is lower than other heterometallic complexes containing Tb-Cu systems (21 K and 14 K).[39] Trivalent Tb and Dy metal ions play a significant role in increasing anisotropy and can also lead to fast tunneling at H = 0. Recently Ishikawa reported a SMM made of trivalent Terbium and Dysprosium ions sandwiched with two phthalocyaninato molecules to form a double-decker structure.[71]

1.1.3 Building Block Approach Toward Magnetism

The properties of molecular magnetic materials can be controlled by using an ideal geometrical arrangement of building blocks. Depending upon the assembly of the polynuclear complexes, molecular magnets can be 0-D (SMM), 1-D [Single Chain Magnet (SCM)], 2-D or 3-D networks.[48] Single chain magnets are the extended form of single molecule magnets, including molecular wires.[72-74] A strong easy axis anisotropy and a stronger intra-chain interaction rather than inter-chain interaction, differentiate a SCM from SMM.[32] The first cyano-bridged 1-D molecular chain compounds contained Gd^{III} and Cr^{III} metal ions and displayed antiferromagnetic coupling between both the metals.[75] A large energy barrier of 154 K has been reported for the SCM

References begin on page 30

$[Co(hfac)_2(NiTPhOMe)]$, which is almost double than that has been reported for Mn_{12}acetate (SMM).[76]

The first heterometallic SCM complex $[Mn_2(saltmen)_2Ni(pao)_2L_2]A_2$ (where saltmen^{2-} = *N,N'*-(1,1,2,2–tetramethylene)bis(salicylideneiminate), pao$^-$ = pyridine-2-aldoximate, L = nitrogen donor and A = univalent anion) reported in 2002 contains antiferromagnetically coupled Ni(II) and Mn(III) bridged by a single aldoxime ligand. The SCM contained two ferromagnetically coupled Mn(III) ions, bridged by double phenolate-oxo ligands and showed slow magnetic relaxation below 3.5 K.[77] Several single-chain compounds contain a combination of transition metal ions with lanthanide ions due to the high magnetic anisotropy of lanthanides. Among all the lanthanide series, Tb^{III} and Dy^{III} are the typically used lanthanides that have been involved in the formation of magnetic molecules. The first 1-D polymer system $[\{Ln(O_2NO)(H_2O)_3\}\{Ni(bpca)_2\}](NO_3)_2\cdot 3H_2O]$ (Ln^{III} = Gd, Dy or Tb) contains $Ni(bpca)_2$ (where bpca = bis(2-pyridylcarbonyl)amine) coordinated with Gd^{III}, Tb^{III} and Dy^{III} metal ions and showed weak interactions.[78] Heteronuclear (*d-f*) metal phosphonates containing Ln^{III}-Cu^{II} (Ln^{III} = La, Pr, Nd, Gd, Sm, Tb, Dy or Ho) are the first example of heterometallic phosphonates, where Ln^{III} = Gd, Pr or Nd were ferromagnetically coupled with the Cu^{II} metal ion.[79]

Ligand choice plays an important role in observing a magnetic interaction between metal ions in heterometallic complexes. Cyanometallates and metal oxalates are common building blocks used in the syntheses of multidimensional systems, where cyano ligands act as the bridging ligand and facilitate interactions between metal ions.[80] The most commonly used cyano-metal anionic building blocks for magnetic materials

References begin on page 30

are $[M(CN)_6]^{n-}$ (M = Cr(III), Fe(II), Fe(III), Mn(II) or Co(III)).[72-74, 80-83] Cotton *et al.* reported dinuclear ruthenium carboxylate complexes,[84] which can also be used as building blocks for magnetic material using appropriate bridging ligands.

1. 2 Tripodal Amido Ligands

In organometallic chemistry, modification of the reactivity of metal-carbon bonds introduced amido ligands that are very well suited for early as well as for late transition metals with higher oxidation states.[85] Due to the stable nature of bonding between amides and metal ions, amido ligands have been utilized in the formation of various polynuclear complexes and clusters.[86, 87] In lanthanide chemistry cyclopentadienyl ligands (Cp) play an important role and it has been shown that LnCp complexes possess unique catalytic reactivity in a variety of reactions including hydrogenation, polymerization, hydroamination, and hydrosilation.[88-91] Efforts have also been made to develop another suitable ligand system as an alternative in which nitrogen-based inorganic amido ligands (eg benzamidinates,[92] aminotroponiminates,[93, 94] and P–N ligands[92]) were used to stabilize lanthanide metal complexes. Similar to Cp-metal complexes ligands, reactivity and stability of amido ligand supported complexes can be altered by changing the electronic and steric properties of the ligands. Lanthanocene amides have also been reported for catalyzing a variety of catalytic reactions.[95] Lanthanide metal complexes containing inorganic tripodal amido ligands have also been involved in nuclear medicinal chemistry.[96, 97] Multidentate ligands are suitable for the formation of lanthanide complexes with high coordination numbers.[98-100]

References begin on page 30

Amido ligands are one of the multidentate ligands, which are important in observing interaction between two metal ions of heterometallic complexes. The connectivity between two metals requires an appropriate ligand design especially for heteronuclear complexes, where ligands containing hard and soft donor moieties are desirable for two different types of metal ions. Modification in the reactivity as well as in the selectivity of these ligands can result in the suitable combination of two metals associated together in heterometallic complexes. One of the desirable properties of amido ligands is their ability to stabilize metal-metal bonds in polynuclear complexes and thus, these can be used for studying the interaction between metal ions. Currently, heteronuclear complexes containing *d*- and *f*- block metals are of great interest because of their unique properties and various applications such as in the modelling of metalloenzymes and catalytic reactions.[101-103] The combination of paramagnetic *d* and *f*-block metals is also very well suited for the development of magnetic materials and molecular based magnets.[23, 49, 57]

Modification in either the electronic or the steric property of the amido ligand $[NR_2]^-$ by changing both substituents (R) can greatly affect the chemistry of the attached metal center.[104-108] It also affects the stability of polynuclear complexes since amido ligands act as building blocks for these complexes.[109-113] Most tripodal amido ligands reported to date act as chelating ligands in which the nitrogen atoms, with its substituents, create a coordination sphere, which kinetically stabilize the polynuclear complexes. Depending upon the number of substituents attached to the nitrogen atom and its availability for binding a metal center, amido ligands are divided into mono, bi, tri and polydentate ligands. Amido donors are very well known π and σ donors, and act

References begin on page 30

as hard Lewis bases for hard metals such as lanthanides.[104, 114] Tripodal amido ligands are also associated with supramolecular coordination chemistry but their use in lanthanide supramolecular chemistry[115] is still less studied in comparison to transition metals.[116, 117]

Most tripodal amido ligands contain a carbon backbone, however, examples of nitrogen, silicon, and phosphorus backbones are also known, as shown in Figure 1.7.[104-106, 118-121]

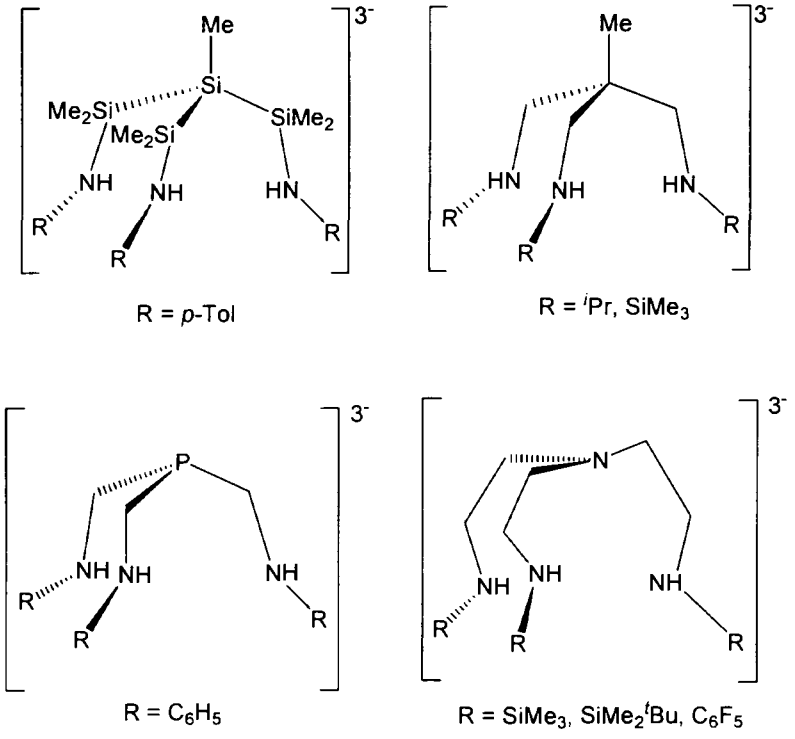

Figure 1.7. Tripodal tridentate amido ligands with different backbones.

Another type of amido ligand that has been utilized greatly in lanthanide chemistry (Figure 1.8) contains a purely carbon back bone with flexible amino phenol arms is H_3tam, where H_3tam= 1,1,1-tris((2-hydroxybenzyl)aminomethyl)ethane. The

References begin on page 30

reported ligand has been used for the syntheses of various *d–f* metal complexes $[LnNi_2(tam)_2)]^+$ (Ln = La, Pr, Nd, Gd, Dy, Ho, Er, Yb) in which phenolic oxygens prefer to bind to the bridging lanthanide metal centre.[122]

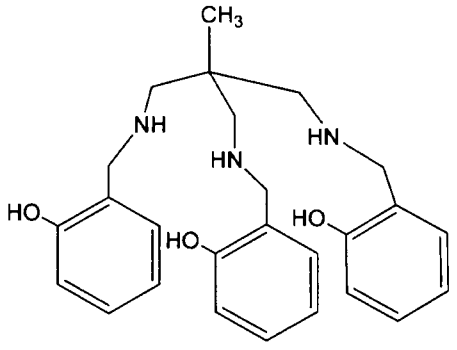

Figure 1.8. Structure of H_3tam (1,1,1-tris(((2-hydroxybenzyl)amino)methyl)ethane).

1.2.1 Syntheses of Complexes Containing Tripodal Amido Ligands

Synthetic routes involving the facile preparation of complexes containing tripodal amido ligands via the metathesis of metal halides with lithium salts of ligands are shown in Scheme 1.1.[106, 123, 124]

References begin on page 30

Scheme 1.1

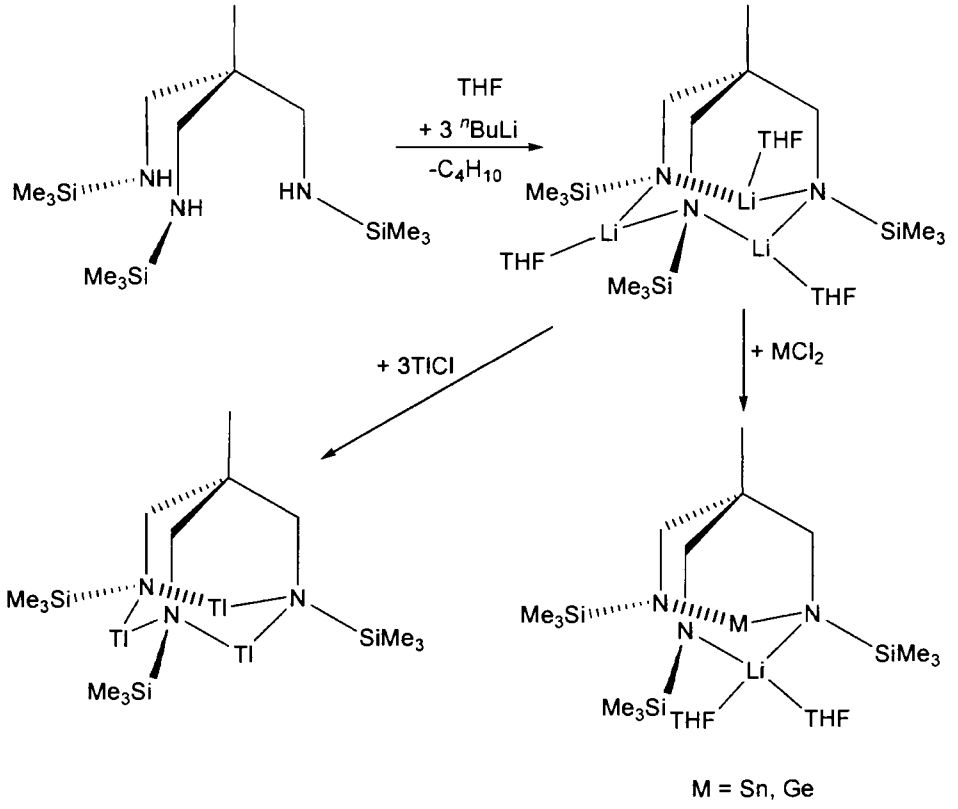

Similar to tripodal amido phosphine ligands, triamidoamine ligands ($[(RNCH_2CH_2)_3N]_3$ where, R = bulky substituent, such as $SiMe_3$) have also been used to stabilize tetravalent transition metals, such as V^{4+}, Ta^{4+} or W^{4+}.[98] These amine ligands are very much related to the neutral tren ligands or tris(pyrazolyl)borate ligands, which have been mostly used with late transition metals.[125, 126] These ligands create a 3-fold-symmetric pocket by coordinating to the transition metal centre in tetradentate manner. As shown in Scheme 1.2, lithium salts of triamidoamine ligands can be used as a starting material to synthesize these pseudo trigonal-bipyramidal complexes. [127, 128]

References begin on page 30

Scheme 1.2

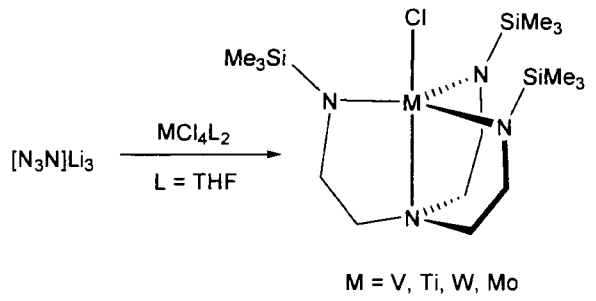

As shown in Scheme 1.3, tripodal amido amine ligands can also be utilized to stabilize the metal-ligand triple bond, for example, alkylation of tungsten chloride by lithium salt generated thermodynamically favorable W≡C bond after the lost of hydrogen gas.[127]

Scheme 1.3

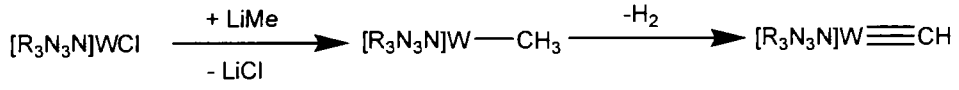

1.2.2 Lanthanide Complexes Supported by Ligands Containing both Phosphorus and Nitrogen Donor Atoms ([P-N] System)

A new class of chelating ligands that has been used in lanthanide chemistry involves ligands containing two different types of donor atoms, such as P-N ligand systems with both phosphorus and nitrogen as donor atoms.[92, 129] The important feature of these ligands is that they have a ability to stabilize metals with various oxidation numbers and geometry. Most of the previously reported ligands that were involved in synthesizing polynuclear complexes or clusters were mainly associated with transition metal or main group elements and not many examples are known for lanthanides.[130] Moreover, these reported ligands are specific for particular metal centers and can only

References begin on page 30

be used for explicit applications. Amido ligands with phosphorus back bones were first synthesized in 1970's but were never used as ligands until recently[86] where they were paired with transition metals to make various types of heteronuclear complexes.[85] Another well known P–N ligand system that has been used for making lanthanide metal complexes is the amino-phosphinate ligand class. A significant amount of research in this area has also been conducted by Roesky and coworkers, which involves the incorporation of P-N ligands (Figure 1.9) in lanthanide chemistry.[92, 93]

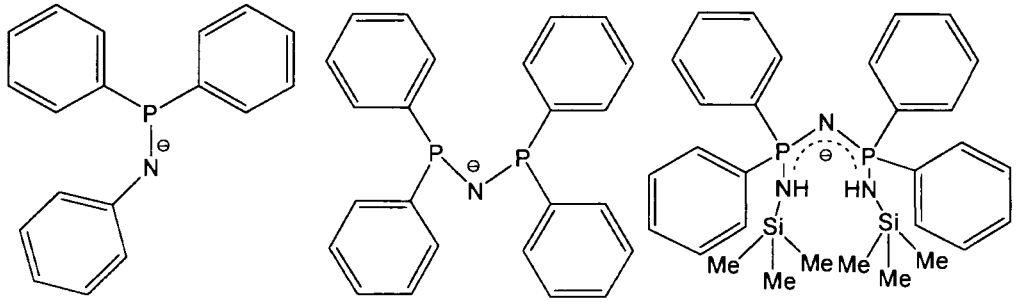

Figure 1.9. Ligands derived from P–N ligand system.

Fryzuk and his group have also greatly contributed to the field of P-N ligand systems and their related complexes.[123, 130] However, these ligands have been mainly utilized in the formation of mononuclear transition metal complexes to study of their coordination chemistry with transition metal ions. As shown in Figure 1.10, depending upon the arrangement of phosphine and amide donors, these ligands are divided into A) [PNP], B) [P_2N_2] and C) [NPN] systems.[131, 132]

References begin on page 30

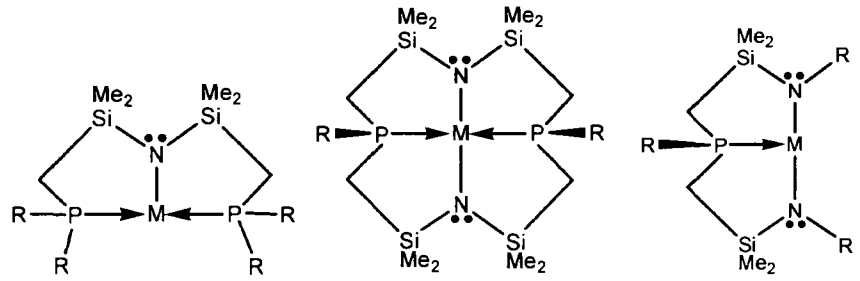

Figure 1.10. Fryzuk motif representing [PN] ligand systems.

Recently, Orvig *et al.* have synthesized numerous varieties of amino-phosphinate ligands used for group 13 metals as well as for lanthanides.[133] These amino-phosphinate ligands can form capped or bicapped complexes depending upon the stoichiometric ratio of ligands to metals (Figure 1.11). It is also reported that these ligands form a coordination sphere around lanthanides with unusual coordination modes.[134] Amino-phosphinate supported lanthanide complexes have been used as catalysts for olefin polymerization.[135] Syntheses of most lanthanide amido complexes involve the reaction of metal halides with appropriate ligands to form complexes coordination numbers of 5-10.[134]

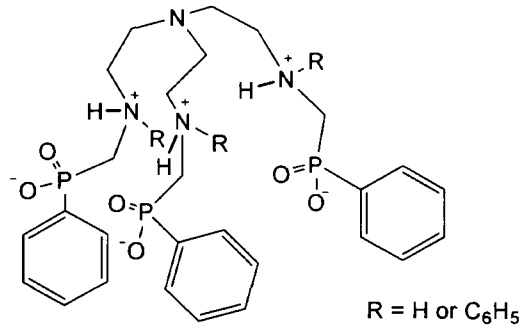

Figure 1.11. Amino-phosphinate ligands.

References begin on page 30

1.2.3 Lanthanide Complexes Supported by Tris(pyrazolyl)borate (Tp) Ligands

Discussion of the chemistry of lanthanide complexes can not be completed without mentioning the contribution of tris(pyrazolyl)borate ligands.[136-140] Due to the large size, ionic bonding nature and tendency to form complexes with high coordination numbers, lanthanides generally prefer to bind with multidentate ligands. Tris(pyrazolyl)borate (Tp) ligands, discovered by Trofimenko, fulfill all these requirements while also providing enough steric bulk that can be tuned by altering the substituents at 3 and 5 positions of pyrazole ring.[126] These ligands have been reported to form stable complexes not only with trivalent lanthanides, but also with bivalent lanthanides; for example Sm^{II} and Yb^{II} complexes using different substituents at 3 and 5 position.[141, 142] Many review articles have also been reported by Takats and Marques which cover the chemical behaviour of Tp ligands associated lanthanide complexes and their applications in catalysis.[136-139, 143] Synthesis of these complexes involve the reaction of metal halides with the sodium or potassium salt of tris(pyrazolyl)borate via salt metathesis as shown in Figure 1.12.[136]

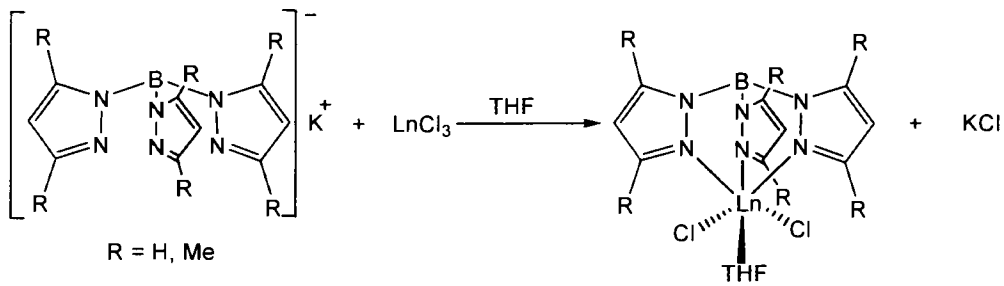

Figure 1.12. Synthesis of tris(pyrazolyl)borate supported trivalent lanthanide complex.

References begin on page 30

Selection or design of appropriate ligands plays an important role in the syntheses as well as the reactivity of heteronuclear complexes. Not many ligands are available with the ability to bind two different metals; surprisingly, there are no tripodal amido ligands reported to date, that contain phosphine, available to bind with another metal. Behaviour of many of these ligands is reserved exclusively for specific metal ions and therefore, they are limited in their potential. The tripodal amido phsophine ligands synthesized in our lab contain desirable properties that other ligands lack; for example, the ability to bind different metal ions in assorted manners, as shown in Figure 1.13.[1, 86,87]

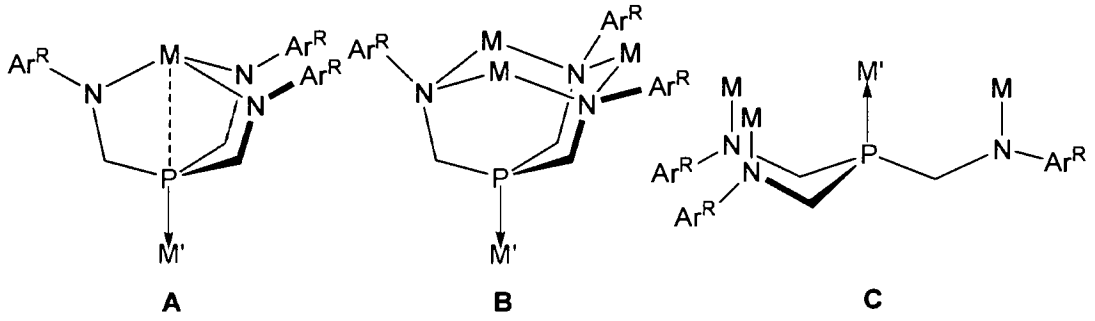

Figure 1.13. Bonding modes of tripodal amido phosphine ligands $P(CH_2NAr^R)_3$ viewing the binding of two different metal ions on two different donor sites.

Other than incorporating these ligands in a variety of multinuclear complexes and clusters, we have also utilized these ligands for the syntheses of magnetic molecules and clusters.[1, 2] Applications of these ligands in multiple areas include: 1) synthesis of polynuclear copper cluster,[87] which contains a total of 8 Cu(I) metal ions, in which center Cu(I) binds to phosphines donor sites of two ligands, and the rest of the Cu(I) metal ions bind to the amido sites; 2) syntheses of heteronuclear complexes containing

References begin on page 30

early and late-transition metals, where the amido sites are capable of binding early transition metals, while the lone pair of phosphorus binds to late metals;[85, 86] 3) introduction of selenium in ligands (tripodal triaminophosphine selenides $Se=P(CH_2NHAr^R)_3$) for stabilizing trinuclear and tetranuclear aluminum complexes and also improving interaction between polynuclear magnetic complexes;[85] and 4) syntheses of trinuclear clusters using only the amido donors, yet leaving the phosphines for binding to other metal centers.[1]

In this thesis, tripodal amido phosphine ligand-supported paramagnetic mononuclear lanthanide complexes and their contribution in heteronuclear *d-f* metal complexes will be discussed. The presence of both hard (N) and soft (P) donor atoms in the ligand systems make these ligands highly appropriate for diamagnetic as well as for paramagnetic heterodinuclear complexes.

1.3 References

1. Hatnean J. A.; Raturi, R.; Lefebvre, J.; Leznoff D. B.; Lawes, G.; Johnson S. A., *J. Am. Chem. Soc.* **2006,** 128, (46), 14992.
2. Raturi, R.; Lefebvre, J.; Leznoff, D. B.; McGarvey, B. R.; Johnson, S. A., *Chem. Eur. J.* **2008,** 14, (2), 721.
3. Hughes, I. D.; Dane, M.; Ernst, A.; Hergert, W.; Luders, M.; Poulters, J.; Staunton, J. B.; Svane, A.; Szotek, Z.; Temmerman, W. M., *Nature* **2007,** 446, 650.
4. Bunzli, J. C. G.; Piguet, C., *Chem. Rev.* **2002,** 102, (6), 1897.
5. Benelli, C.; Gatteschi, D., *Chem. Rev.* **2002,** 102, (6), 2369.
6. Ishikawa, N.; Iino, T.; Kaizu, Y., *J. Am. Chem. Soc.* **2002,** 124, (38), 11440.

References begin on page 30

7. Ishikawa, N.; Iino, T.; Kaizu, Y., *J. Phys. Chem. A* **2003,** 107, (39), 7879.

8. Cheng, H. N.; Gutowsky, H. S., *J. Phys. Chem.* **1978,** 82, (8), 914.

9. Cockeril.A. F.; Davies, G. L. O.; Harden, R. C.; Rackham, D. M., *Chem. Rev.* **1973,** 73, (6), 553.

10. Bleaney, B., *J. Magn. Reson.* **1972,** 8, (1), 91.

11. Mironov, V. S.; Galyametdinov, Y. G.; Ceulemans, A.; Gorller-Walrand, C.; Binnemans, K., *J. Chem. Phys.* **2002,** 116, (11), 4673.

12. Sakamoto, M.; Manseki, K.; Okawa, H., *Coord. Chem. Rev.* **2001,** 219, 379.

13. Wu, B., *J. Coord. Chem.* **2008,** 61, (16), 2558.

14. Bencini, A.; Benelli, C.; Caneschi, A.; Carlin, R. L.; Dei, A.; Gatteschi, D., *J. Am. Chem. Soc.* **1985,** 107, (26), 8128.

15. Costes, J. P.; Dahan, F.; Dupuis, A.; Laurent, J. P., *Inorg. Chem.* **2000,** 39, (2), 169.

16. Wu, B.; Zheng, Y. L.; Ng, S. W., *J. Coord. Chem.* **2008,** 61, (22), 3674.

17. Wickman, H. H.; Merritt, F. R., *Chem. Phys. Lett.* **1967,** 1, (4), 117.

18. Lago, J.; Micotti, E.; Corti, M.; Lascialfari, A.; Bianchi, A.; Carretta, S.; Santini, P.; Procissi, D.; Baek, S. H.; Kogerler, P.; Baines, C.; Amato, A., *Phys. Rev. B* **2007,** 76, (6).

19. Kahn, O., *Molecular Magnetism*. **1993**; p 380.

20. Mito, M.; Iriguchi, K.; Deguchi, H.; Kishine, J.; Kikuchi, K.; Ohsumi, H.; Yoshida, Y.; Inoue, K., *Phys. Rev. B* **2009,** 79, (1).

21. Gatteschi, D.; Bogani, L.; Cornia, A.; Mannini, M.; Sorace, L.; Sessoli, R., *Solid State Sci.* **2008,** 10, (12), 1701.

22. Blundell, S. J., *Contemp. Phys.* **2007,** 48, (5), 275.

References begin on page 30

23. Miller, J. S., *Dalton Trans.* **2006,** (23), 2742.

24. Murugesu, M.; Habrych, M.; Wernsdorfer, W.; Abboud Khalil, A.; Christou, G., *J. Am. Chem. Soc.* **2004,** 126, (15), 4766.

25. Ishikawa, N., *Polyhedron* **2007,** 26, (9-11), 2147.

26. Miyasaka, H.; Saitoh, A.; Abe, S., *Coord. Chem. Rev.* **2007,** 251, (21-24), 2622.

27. Ueki, S.; Sahlan, M.; Ishida, T.; Nogami, T., *Synth. Met.* **2005,** 154, (1-3), 217.

28. Perez, J. M.; Josephson, L.; O'Loughlin, T.; Hogemann, D.; Weissleder, R., *Nature Biotechnol.* **2002,** 20, (8), 816.

29. Jaffer, F. A.; Weissleder, R., *J. Am. Med. Assoc.* **2005,** 293, (7), 855.

30. Bruck, E., *J. Phys. D-App. Phys.* **2005,** 38, (23), R381.

31. Miller, J. S.; Epstein, A. J., *Angew. Chem., Int. Ed.* **1994,** 33, (4), 385.

32. Miyasaka, H.; Nakata, K.; Sugiura, K.-i.; Yamashita, M.; Clerac, R., *Angew. Chem., Int. Ed.* **2004,** 43, (6), 707.

33. Sakamoto, M.; Manseki, K.; Okawa, H., *Coord. Chem. Rev.* **2001,** 219-221, 379.

34. Benelli, C.; Gatteschi, D.; Carnegie, D. W.; Carlin, R. L., *J. Am. Chem. Soc.* **1985,** 107, (8), 2560.

35. Zaleski, C. M.; Depperman, E. C.; Kampf, J. W.; Kirk, M. L.; Pecoraro, V. L., *Angew. Chem., Int. Ed.* **2004,** 43, (30), 3912.

36. Andruh, M.; Ramade, I.; Codjovi, E.; Guillou, O.; Kahn, O.; Trombe, J. C., *J. Am. Chem. Soc.* **1993,** 115, (5), 1822.

37. Benelli, C.; Dei, A.; Gatteschi, D.; Pardi, L., *Inorg. Chem.* **1990,** 29, (18), 3409.

38. Blake, A. J.; Gould, R. O.; Grant, C. M.; Milne, P. E. Y.; Parsons, S.; Winpenny, R. E. P., *J. Chem. Soc., Dalton Trans.* **1997**, (4), 485.

References begin on page 30

39. Costes, J. P.; Auchel, M.; Dahan, F.; Peyrou, V.; Shova, S.; Wernsdorfer, W., *Inorg. Chem.* **2006,** 45, (5), 1924.

40. Costes, J. P.; Dahan, F.; Donnadieu, B.; Garcia-Tojal, J.; Laurent, J. P., *Eur. J. Inorg. Chem.* **2001**, (2), 363.

41. Matsumoto, N.; Sakamoto, M.; Tamaki, H.; Okawa, H.; Kida, S., *Chem. Lett.* **1990**, (6), 853.

42. de Caro, D.; Faulmann, C.; Valade, L., *Chem. Eur. J.* **2007,** 13, (6), 1650.

43. Batten, S. R.; Murray, K. S., *Coord. Chem. Rev.* **2003,** 246, (1-2), 103.

44. Batten, S. R.; Murray, K. S., *Aust. J. Chem.* **2001,** 54, (9 and 10), 605.

45. Goodenough, J. B., *Magnetism and the Chemical Bond; Interscience: New York.* **1963**.

46. Curely, J., *Monatsh. Chem.* **2005,** 136, (6), 987.

47. Tsukerblat, B., *Inorg. Chim. Acta* **2008,** 361, (14-15), 3746.

48. Mrozinski, J., *Coord. Chem. Rev.* **2005,** 249, (21-22), 2534.

49. Tanase, S.; Reedijk, J., *Coord. Chem. Rev.* **2006,** 250, (19-20), 2501.

50. Zhou, Y.; Hong, M.; Wu, X., *Chem. Commun.* **2006**, (2), 135.

51. Sokol, J. J.; Hee, A. G.; Long, J. R., *J. Am. Chem. Soc.* **2002,** 124, (26), 7656.

52. Choukroun, R.; Lorber, C.; de Caro, D.; Vendier, L., *Organometallics* **2006,** 25, (18), 4243.

53. Raebiger, J. W.; Miller, J. S., *Inorg. Chem.* **2002,** 41, (12), 3308.

54. Tanaka, M.; Hosokoshi, Y.; Markosyan, A. S.; Inoue, K.; Iwamura, H., *Synth. Met.* **2001,** 122, (3), 463.

References begin on page 30

55. Kahn, M. L.; Sutter, J.-P.; Golhen, S.; Guionneau, P.; Ouahab, L.; Kahn, O.; Chasseau, D., *J. Am. Chem. Soc.* **2000,** 122, (39), 9566.

56. Lecren, L.; Roubeau, O.; Coulon, C.; Li, Y. G.; Le Goff, X. F.; Wernsdorfer, W.; Miyasaka, H.; Clerac, R., *J. Am. Chem. Soc.* **2005,** 127, (49), 17353.

57. He, F.; Tong, M. L.; Chen, X. M., *Inorg. Chem.* **2005,** 44, (23), 8285.

58. Benmansour, S.; Setifi, F.; Triki, S.; Salaun, J. Y.; Vandevelde, F.; Sala-Pala, J.; Gomez-Garcia, C. J.; Roisnel, T., *Eur. J. Inorg. Chem.* **2007**, (1), 186.

59. Gatteschi, D.; Sessoli, R., *Angew. Chem., Int. Ed.* **2003,** 42, (3), 268.

60. Christou, G.; Gatteschi, D.; Hendrickson, D. N.; Sessoli, R., *MRS Bulletin* **2000,** 25, (11), 66.

61. Waldmann, O., *Inorg. Chem.* **2007,** 46, (24), 10035.

62. Sessoli, R.; Gatteschi, D.; Caneschi, A.; Novak, M. A., *Nature* **1993,** 365, (6442), 141.

63. Yang, C. I.; Wernsdorfer, W.; Lee, G. H.; Tsai, H. L., *J. Am. Chem. Soc.* **2007,** 129, (3), 456.

64. Ishikawa, N.; Sugita, M.; Wernsdorfer, W., *Angew. Chem., Int. Ed.* **2005,** 44, (19), 2931.

65. Zhong, Z. J.; Seino, H.; Mizobe, Y.; Hidai, M.; Fujishima, A.; Ohkoshi, S.; Hashimoto, K., *J. Am. Chem. Soc.* **2000,** 122, (12), 2952.

66. Boudalis, A. K.; Donnadieu, B.; Nastopoulos, V.; Clemente-Juan, J. M.; Mari, A.; Sanakis, Y.; Tuchagues, J. P.; Perlepes, S. P., *Angew. Chem., Int. Ed.* **2004,** 43, (17), 2266.

References begin on page 30

67. Wu, D.; Guo, D.; Song, Y.; Huang, W.; Duan, C. Y.; Meng, O. J.; Sato, O., *Inorg. Chem.* **2009,** 48, (3), 854.

68. Ishikawa, N.; Sugita, M.; Ishikawa, T.; Koshihara, S.-Y.; Kaizu, Y., *J. Am. Chem. Soc.* **2003,** 125, (29), 8694.

69. Osa, S.; Kido, T.; Matsumoto, N.; Re, N.; Pochaba, A.; Mrozinski, J., *J. Am. Chem. Soc.* **2004,** 126, (2), 420.

70. Mishra, A.; Wernsdorfer, W.; Abboud, K. A.; Christou, G., *J. Am. Chem. Soc.* **2004,** 126, (48), 15648.

71. Takamatsu, S.; Ishikawa, N., *Polyhedron* **2007,** 26, (9-11), 1859.

72. Stamatatos, T. C.; Abboud, K. A.; Wernsdorfer, W.; Christou, G., *Inorg. Chem.* **2009,** 48, (3), 807.

73. Coronado, E.; Galan-Mascaros, J. R.; Marti-Gastaldo, C., *J. Am. Chem. Soc.* **2008,** 130, (45), 14987.

74. Bogani, L.; Vindigni, A.; Sessoli, R.; Gatteschi, D., *J. Mater. Chem.* **2008,** 18, (40), 4750.

75. Figuerola, A.; Diaz, C.; El Fallah, M. S.; Ribas, J.; Maestro, M.; Mahia, J. E., *Chem. Commun.* **2001**, (13), 1204.

76. Mariani, M.; Aldrovandi, S.; Corti, M.; Lascialfari, A.; Bogani, L.; Caneschi, A.; Sessoli, R., *Inorg. Chim. Acta* **2008,** 361, (14-15), 4107.

77. Clerac, R.; Miyasaka, H.; Yamashita, M.; Coulon, C., *J. Am. Chem. Soc.* **2002,** 124, (43), 12837.

78. Madalan, A. M.; Bernot, K.; Pointillart, F.; Andruh, M.; Caneschi, A., *Eur. J. Inorg. Chem.* **2007**, (35), 5533.

References begin on page 30

79. Ma, Y. S.; Li, H.; Wang, J. J.; Bao, S. S.; Cao, R.; Li, Y. Z.; Ma, J.; Zheng, L. M., *Chem. Eur. J.* **2007,** 13, (17), 4759.

80. Lefebvre, J.; Callaghan, F.; Katz, M. J.; Sonier, J. E.; Leznoff, D. B., *Chem. Eur. J.* **2006,** 12, (26), 6748.

81. Shi, C. C.; Chen, C. S.; Hsu, S. C. N.; Yeh, W. Y.; Chiang, M. Y.; Kuo, T. S., *Inorg. Chem. Commun.* **2008,** 11, (10), 1264.

82. Dechambenoit, P.; Ferlay, S.; Hosseini, M. W.; Planeix, J. M.; Kyritsakas, N., *New J. Chem.* **2006,** 30, (10), 1403.

83. Buschmann, W. E.; Liable-Sands, L.; Rheingold, I. L.; Miller, J. S., *Inorg. Chim. Acta* **1999,** 284, (2), 175.

84. Cotton, F. A.; Lu, J.; Yokochi, A., *Inorg. Chim. Acta* **1998,** 276, (1-2), 447.

85. Han, H.; Johnson, S. A., *Organometallics* **2006,** 25, (23), 5594.

86. Han, H.; Elsmaili, M.; Johnson, S. A., *Inorg. Chem.* **2006,** 45, (18), 7435.

87. Keen, A. L.; Doster, M.; Han, H.; Johnson, S. A., *Chem. Commun.* **2006**, (11), 1221.

88. Xie, X. M.; Huang, J. L., *Appl. Organomet. Chem.* **2009,** 23, (1), 1.

89. Zimmermann, M.; Tornroos, K. W.; Sitzmann, H.; Anwander, R., *Chem. Eur. J.* **2008,** 14, (24), 7266.

90. Zhou, L. Z.; Wang, Y. M.; Yao, Y. M.; Zharig, Y.; Shen, Q., *J. Rare Earths* **2007,** 25, (5), 544.

91. Jaroschik, F.; Shima, T.; Li, X. F.; Mori, K.; Ricard, L.; Le Goff, X. F.; Nief, F.; Hou, Z. M., *Organometallics* **2007,** 26, (23), 5654.

92. Roesky, P. W., *Heteroat. Chem.* **2002,** 13, (6), 514.

References begin on page 30

93. Roesky, P. W., *Z. Anorg. Allg. Chem.* **2003,** 629, (11), 1881.

94. Roesky, P. W., *Chem. Soc. Rev.* **2000,** 29, (5), 335.

95. Giardello, M. A.; Yamamoto, Y.; Brard, L.; Marks, T. J., *J. Am. Chem. Soc.* **1995,** 117, (11), 3276.

96. Wilson, L. J.; Cagle, D. W.; Thrash, T. P.; Kennel, S. J.; Mirzadeh, S.; Alford, J. M.; Ehrhardt, G. J., *Coord. Chem. Rev.* **1999,** 192, 199.

97. Hermann, P.; Kotek, J.; Kubicek, V.; Lukes, I., *Dalton Trans.* **2008**, (23), 3027.

98. Kanesato, M.; Mizukami, S.; Houjou, H.; Tokuhisa, H.; Koyama, E.; Nagawa, Y., *J. Alloys . Compds.* **2004,** 374, (1-2), 307.

99. Miao, W.; Li, S. H.; Cui, D. M.; Huang, B. T., *J. Organomet. Chem.* **2007,** 692, (17), 3823.

100. Raymond, K. N., *Eur. J. Solid State Inorg. Chem.* **1991,** 28, 225.

101. Aratake, Y.; Okawa, H.; Asato, E.; Sakiyama, H.; Kodera, M.; Kida, S.; Sakamoto, M., *J. Chem. Soc., Dalton Trans.* **1990**, (10), 2941.

102. Chin, J., *Curr. Opin. Chem. Biol.* **1997,** 1, (4), 514.

103. Radecka-Paryzek, W.; Patroniak, V.; Lisowski, J., *Coord. Chem. Rev.* **2005,** 249, (21-22), 2156.

104. Gade, L. H., *Acc. Chem. Res.* **2002,** 35, (7), 575.

105. Findeis, B.; Contel, M.; Gade, L. H.; Laguna, M.; Concepcion, M.; Scowen, I. J.; McPartlin, M., *Inorg. Chem.* **1997,** 36, (11), 2386.

106. Contel, M.; Hellmann, K. W.; Gade, L. H.; Scowen, I. J.; McPartlin, M.; Laguna, M., *Inorg. Chem.* **1996,** 35, (12), 3713.

References begin on page 30

107. Olsher, U.; Elgavish, G. A.; Jagurgrodzinski, J., *J. Am. Chem. Soc.* **1980,** 102, (10), 3338.

108. Zhou, L. Y.; Wang, J. F.; Zhang, Y.; Yao, Y. M.; Shen, Q., *Inorg. Chem.* **2007,** 46, (14), 5763.

109. Liu, B.; Cui, D. M.; Ma, J.; Chen, X. S.; Jing, X. B., *Chem. Eur. J.* **2007,** 13, (3), 834.

110. Kempe, R.; Noss, H.; Irrgang, T., *J. Organomet. Chem.* **2002,** 647, (1-2), 12.

111. Gade, L. H.; Friedrich, S.; Trosch, D. J. M.; Scowen, I. J.; McPartlin, M., *Inorg. Chem.* **1999,** 38, (23), 5295.

112. Hellmann, K. W.; Bergner, A.; Gade, L. H.; Scowen, I. J.; McPartlin, M., *J. Organomet. Chem.* **1999,** 573, (1-2), 156.

113. Friedrich, S.; Memmler, H.; Gade, L. H.; Li, W. S.; McPartlin, M., *Angew. Chem., Int. Ed. Engl.* **1994,** 33, (6), 676.

114. Park, S. H.; Milletti, M. C.; Gardner, N., *Polyhedron* **1998,** 17, (8), 1267.

115. Sun, D. F.; Cao, R.; Sun, Y. Q.; Bi, W. H.; Li, X. J.; Wang, Y. Q.; Shi, Q.; Li, X., *Inorg. Chem.* **2003,** 42, (23), 7512.

116. Tong, M. L.; Lee, H. K.; Chen, X. M.; Huang, R. B.; Mak, T. C. W., *J. Chem. Soc., Dalton Trans.* **1999**, (21), 3657.

117. Tong, M. L.; Chen, X. M.; Ye, B. H.; Ji, L. N., *Angew. Chem., Int. Ed.* **1999,** 38, (15), 2237.

118. Gade, L. H.; Renner, P.; Memmler, H.; Fecher, F.; Galka, C. H.; Laubender, M.; Radojevic, S.; McPartlin, M.; Lauher, J. W., *Chem. Eur. J.* **2001,** 7, (12), 2563.

References begin on page 30

119. Gade, L. H.; Memmler, H.; Kauper, U.; Schneider, A.; Fabre, S.; Bezougli, I.; Lutz, M.; Galka, C.; Scowen, I. J.; McPartlin, M., *Chem. Eur. J.* **2000,** 6, (4), 692.

120. Wang, S. W.; Qian, H. M.; Yao, W.; Zhang, L. J.; Zhou, S. L.; Yang, G. S.; Zhu, X. C.; Fan, J. X.; Liu, Y. Y.; Chen, G. D.; Song, H. B., *Polyhedron* **2008,** 27, (13), 2757.

121. Panda, T. K.; Zulys, A.; Gamer, M. T.; Roesky, P. W., *J. Organomet. Chem.* **2005,** 690, (23), 5078.

122. Xu, Z.; Read, P. W.; Hibbs, D. E.; Hursthouse, M. B.; Abdul Malik, K. M.; Patrick, B. O.; Rettig, S. J.; Seid, M.; Summers, D. A.; Pink, M.; Thompson, R. C.; Orvig, C., *Inorg. Chem.* **2000,** 39, (3), 508.

123. Fryzuk, M. D.; Jafarpour, L.; Kerton, F. M.; Love, J. B.; Patrick, B. O.; Rettig, S. J., *Organometallics* **2001,** 20, (7), 1387.

124. Fryzuk, M. D.; Giesbrecht, G. R.; Johnson, S. A.; Kickham, J. E.; Love, J. B., *Polyhedron* **1998,** 17, (5-6), 947.

125. Trofimenko, S., *Chem. Rev.* **1993,** 93, (3), 943.

126. Trofimenko, S., *J. Am. Chem. Soc.* **1966,** 88, (8), 1842.

127. Schrock, R. R., *Acc. Chem. Res.* **1997,** 30, (1), 9.

128. Cummins, C. C.; Schrock, R. R.; Davis, W. M., *Inorg. Chem.* **1994,** 33, (7), 1448.

129. Huang, R.; Frost, B. J., *Inorg. Chem.* **2007,** 46, (26), 10962.

130. Fryzuk, M. D.; Haddad, T. S.; Berg, D. J., *Coord. Chem. Rev.* **1990,** 99, 137.

131. Fryzuk, M. D.; Jafarpour, L.; Rettig, S. J., *Organometallics* **1999,** 18, (20), 4050.

132. Fryzuk, M. D.; Haddad, T. S.; Berg, D. J.; Rettig, S. J., *Pure Appl. Chem.* **1991,** 63, (6), 845.

References begin on page 30

133. Kovacs, M. S.; Monga, V.; Patrick, B. O.; Orvig, C., *Dalton Trans.* **2006**, (1), 31.

134. Huskowska, E.; Maupin, C. L.; Parker, D.; Williams, J. A. G.; Riehl, J. P., *Enantiomer* **1997,** 2, (5), 381.

135. Gamer, M. T.; Rastatter, M.; Roesky, P. W.; Steffens, A.; Glanz, M., *Chem. Eur. J.* **2005,** 11, (10), 3165.

136. Marques, N.; Sella, A.; Takats, J., *Chem. Rev.* **2002,** 102, (6), 2137.

137. Bell, Z. R.; Motson, G. R.; Jeffery, J. C.; McCleverty, J. A.; Ward, M. D., *Polyhedron* **2001,** 20, (15-16), 2045.

138. Santos, I.; Marques, N., *New J. Chem.* **1995,** 19, (5-6), 551.

139. Takats, J., *J. Alloys . Compds.* **1997,** 249, (1-2), 52.

140. Long, D. P.; Bianconi, P. A., *J. Am. Chem. Soc.* **1996,** 118, (49), 12453.

141. Ferrence, G. M.; McDonald, R.; Morissette, M.; Takats, J., *J. Organomet. Chem.* **2000,** 596, (1-2), 95.

142. Hillier, A. C.; Liu, S. Y.; Sella, A.; Elsegood, M. R. J., *J. Alloys. Compds.* **2000,** 303, 83.

143. Hasinoff, L.; Takats, J.; Zhang, X. W.; Bond, P. H.; Rogers, R. D., *J. Am. Chem. Soc.* **1994,** 116, (19), 8833.

References begin on page 30

CHAPTER-2

Syntheses and Characterization of Trivalent Lanthanide Complexes: A Step Towards Heteronuclear *d-f* Metal Complexes

2.1 Introduction

Heteronuclear complexes containing *d* and *f* block metal ions have been known to possess interesting magnetic properties, which make them desirable to use as building blocks for molecular magnets.[1-5] Due to the increasing demand for new molecular materials, there has been a significant amount of research into the syntheses of *d-f* metal complexes to better understand the magnetic coupling between metal centers. However,

References begin on page 79

designing an appropriate ligand with the ability to chelate *d* and *f* metal ions in order to observe the bonding interaction between the metal centers is still a problem. To date, combinations of various *d-f* metal ions have been used for di-, tri- and polynuclear complexes; the most well known polynuclear complexes are Ln-Co,[6-10] Ln-Cu,[2, 11, 12] Ln-Ni,[13] and Ln-Fe[14-16] (Ln = lanthanides). Most *d-f* magnetic complexes contain Gd(III) and Cu(II) because of the non-degenerate ground state of Gd^{3+}, which simplifies the magnetic analysis.[17] The magnetic interaction between two metal centers in heteronuclear complexes also depends on the binding ability of the supporting ligand. To date, the most common binding modes that have been found in heteronuclear complexes involve: A) binding of two different metal ions at the same coordination site on the ligands, such as bridging amides, phosphides, carbonyl donor ligands; B) binding of two different metals to a ligand that contains two different donor (hard and soft) sites, such as ligands containing phosphorus and nitrogen as soft and hard donor atoms respectively, and C) direct bonding interaction between metal centers. (Figure 2.1)

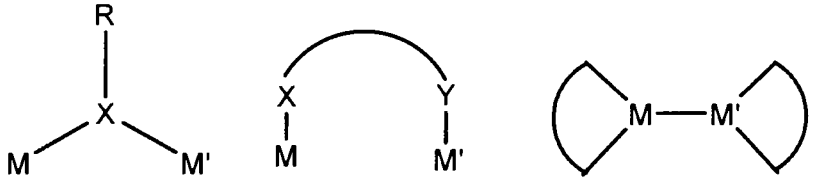

(A) (B) (C)

Figure 2.1. Different types of binding modes in heterodinuclear complexes. Here M and M′ represent two different metal centers, R = substituent attach to the ligand sites, and X and Y are two different sites of the ligand. (A) = ligand with single coordination site, (B) = multidentate bridging ligand, and (C) = metal ions connected to each other without any ligand support.

References begin on page 79

All the heteronuclear *d-f* metal complexes reported in the literature are based on the above described metal-ligand binding modes, which allow both *d* and *f* metal ions to interact with each other. For example, reaction of $Fe_3(CO)_{12}$ with 2 equivalents of $(C_5Me_5)_2Yb(OEt_2)$ formed a carbonyl bridged heteronuclear complex namely, $[(C_5Me_5)_2Yb]_2[Fe_3(CO)_7(\mu\text{-}CO)_4]$.[18] Costes *et al.* have also reported a number of *d-f* heteronuclear complexes bridged by supporting ligands,[19-21] in which the hexadentate 1,2-bis((3-methoxysalicylidene)amino)-ethane ligand acts as a suitable ligand for binding Fe^{3+} and Gd^{3+} via phenolate oxygen atoms.[22] Other *d-f* metal complexes include CuLn(Fsal-3)$(NO_3)_3(CH_3OH)_{0.5}$, (where H_2Fsal-3 is N,N'-bis(3-formyl-5-methylsalicylidene)) and Ln = La, Nd, Eu, Gd, and Ho. In these examples, Cu^{2+} was attached to the $N_2O_2^-$ site, and Ln^{3+} was attached to the O_4^- coordination site of the ligand, showing ferromagnetically coupled metal centers.[23] Heteronuclear $[Sm_6Cu_{24}(\mu\text{-}OH)_{30}(Gly)_{12}(Ac)_{12}(ClO_4)(H_2O)_{16}]\cdot(ClO_4)_9\cdot(OH)_2\cdot(H_2O)_{31}$, (where Gly = glycine and Ac = acetate) possessed an octahedral skeleton, where the glycine ligand chelated copper and samarium ions via carboxyl and amine sites. The complex contained six Sm^{3+} ions at the vertices, twelve Cu^{2+} ions in the middle and the remaining twelve Cu^{2+} ions formed the outer layer.[24]

There are not many examples in the literature that involve direct Ln-M bonds. Among these, the reported Lu-Ru complex [(THF)Cp_2Lu-RuCp$(CO)_2$], (where THF = tetrahydrofuran) displayed the shortest lanthanide-transition metal-metal distance of 2.96 Å known to date.[25] In this metal complex both the metal centers were connected to each other via a metal-metal bond without using any bridging ligand (Figure 2.1 C). Though *d-f* heterometallic complexes have more applications in catalysis, our target applications involve syntheses of magnetic materials or molecule-based magnets. Bencini in 1986,

References begin on page 79

reported two magnetic *d-f* trinuclear metal complexes $Gd\{Cu(Hapen)\}_2(H_2O)_3(ClO_4)_3 \cdot 2Cu(Hapen)$, (where Hapen = *N,N'*-ethylenebis(*o*-hydroxyacetophenoneiminato)) and $Gd\{Cu(Salen)\}_2(H_2O)ClO_4)_3 \cdot 2Cu(Salen) \cdot 0.5C_2H_5NO_2]$, (where Salen = *N,N'*-ethylenebis(salicylaldiminato)*o*-hydroxyacetophenoneiminato)). Both of the metal complexes showed a ferromagnetic interaction between Cu(II) and Gd(III) metal centers.[26]

Ligand design as well as metal selection plays an important role in the chemical and physical behaviour of heteronuclear complexes. Most of the lanthanide complexes that have been used for *d-f* heteronuclear complexes are based on multidentate ligands.[27, 28] Lanthanide ions form high coordination complexes due to their large ionic size and ionic bonding nature, and the ligand design controls coordination chemistry as well as the geometry of these complexes. Although the preferred and the most stable oxidation state for all lanthanide ions is +3, oxidation states such as +2 and +4 are also accessible.[29-33] Syntheses of lanthanide amido complexes involve the reaction of metal halides with the appropriate amido ligands. Lanthanides with amides and other P-N ligand systems, such as phosphinoamides, bis(phosphino)amides, bis(phosphinoamino)methanides, and amino-phosphinate complexes, have been used as catalysts for polymerization.[34, 35]

Lanthanides are also known for their unique magnetic and spectroscopic properties that depend on the surrounding ligands. The purpose of this study is to use the trivalent lanthanide metal ions for the syntheses of heteronuclear complexes supported by tripodal amido-ligands. In this Chapter, we are reporting the syntheses of a series of mononuclear trivalent lanthanide complexes, which were then further utilized to interact

References begin on page 79

with various transition metal complexes for synthesizing heterodinuclear *d-f* metal complexes.

2.2 Results and Discussion

2.2.1 Syntheses of Mononuclear Trivalent Lanthanide Complexes

In this study, diamagnetic yttrium complexes (**2a-c**) were chosen as model compounds and all other lanthanide-based reactions were performed in an analogous manner. Syntheses of mononuclear trivalent yttrium complexes involve the reaction of 1 equivalent of $[P(CH_2NHC_6H_5)_3]$ (**1a**) or $[P(CH_2NH\text{-}3,5\text{-}Me_2C_6H_3)_3]$ (**1b**) with 1 equivalent of $Y[N(SiMe_2)_2]_3$ in THF. The reaction mixture enabled the formation of block-shaped crystals (66-69 %) of the intended product at room temperature after 24 h (equation 2.1). To optimize the process, the same reactions were also tested in different solvents such as toluene, benzene, acetonitrile, and pyridine. These experiments gave inconclusive results and showed the presence of only ligand peaks (**1a-1c**) in $^{31}P\{^1H\}$ NMR spectra. While reactions of $Y[N(SiMe_2)_2]_3$ with **1a** or **1b** required 1 equivalent of $Y[N(SiMe_2)_2]_3$, the same reaction with **1c** required 1.5 equivalents of $Y[N(SiMe_2)_2]_3$ and 8-10 h refluxing. The reaction of equimolar amounts of $Y[N(SiMe_2)_2]_3$ and **1c** showed the presence of excess ligand with the resulting complex in $^{31}P\{^1H\}$ as well as in ^1H NMR spectra and required excess amount of $Y[N(SiMe_2)_2]_3$ for the formation of complex **2c** (yield 97 %). Further addition of $Y[N(SiMe_2)_2]_3$ reacted with the excess amount of ligand and thus increased the formation of **1c** with no sign of ligand peaks, as noticed in NMR spectra.

References begin on page 79

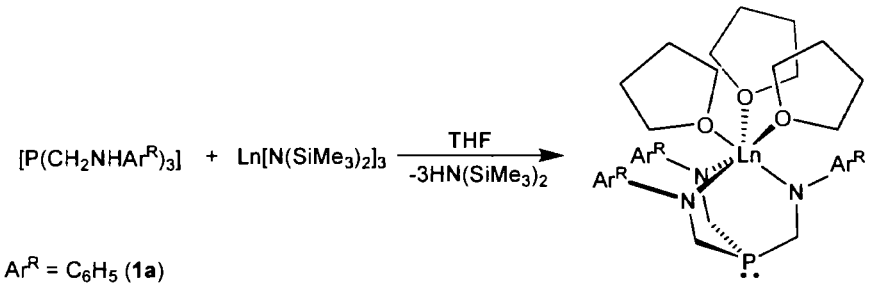

(2.1)

Ar^R = C_6H_5 (**1a**)
3,5-$Me_2C_6H_3$ (**1b**)
3,5-$(CF_3)_2C_6H_3$ (**1c**)

Ln = Y (**2a-c**)
Gd (**3a-c**)
Tb (**4a-c**)
Dy (**5a-c**)
Ho (**6a-c**)
Er (**7a-c**)
Tm (**8a-c**)

The ^{1}H NMR spectra in THF as well as the X-ray crystal structures of complexes **2a, 2b** and **2c** revealed the presence of C_3 symmetry in solution and in the solid state due to the fact that both hydrogen atoms that are attached to the CH_{2s} (CH_2 connected with phosphorus atom) are diastereotopic in solution. A solid-state crystal structure of six coordinate $[P(CH_2NAr^R)_3Y(THF)_3]$ is depicted in Figure 2.2. Crystals of **2a** and **2b** were obtained directly from the reaction mixture, while **2c** was crystallized from a mixture of benzene/hexamethyldisiloxane. Crystalline **2b** contains disordered THF solvent molecules, while **2c** showed rotational disorder of the CF_3 substituents. In all these structures, the lanthanide metal centers are chelated by three ancillary amido donors and capped with three THF molecules. The phosphine lone pair is directed away from the metal and is well suited to interact with another metal. Introduction of a yttrium metal center to the tripodal amido ligand altered the C-P-C angles and showed that the sum of C-P-C angles in **2a**, **2b**, and **2c**, are 316.82(7)°, 318.75(3)° and 320.58(7)° respectively, which are larger than the sum of the ligand precursors; for example, for **1b** the sum of C-P-C angles is 299.5(3)°. For complexes **2b** and **2c,** presence of the methyl and trifluoromethyl substituents on the phenyl ring is responsible for the increase of the C-P-C

References begin on page 79

angle. Comparison of structural data of all the lanthanide metal complexes (**2-8**) showed small difference in bond lengths, bond angles and C-P-C angles. The small difference in C-P-C angles in the lanthanide series (Gd-Yb) is due to the introduction of different sizes metal ions, which should also affect the donor ability. Despite the fact that phosphine lone pair is away from the lanthanide metal center, affect of metal can be noticed on $^{31}P\{^{1}H\}$ NMR shifts, which shifted in the direction of unexpected upfield in comparison to the ligand precursors (**1a-1c**). It has been reported that the increase in C-P-C angles move the chemical shifts towards downfield. For example, $^{31}P\{^{1}H\}$ NMR shifts of alkyl phosphine, such as PMe_3, PEt_3, and P^tBu_3 are −62, −20, and +63 ppm.[36]

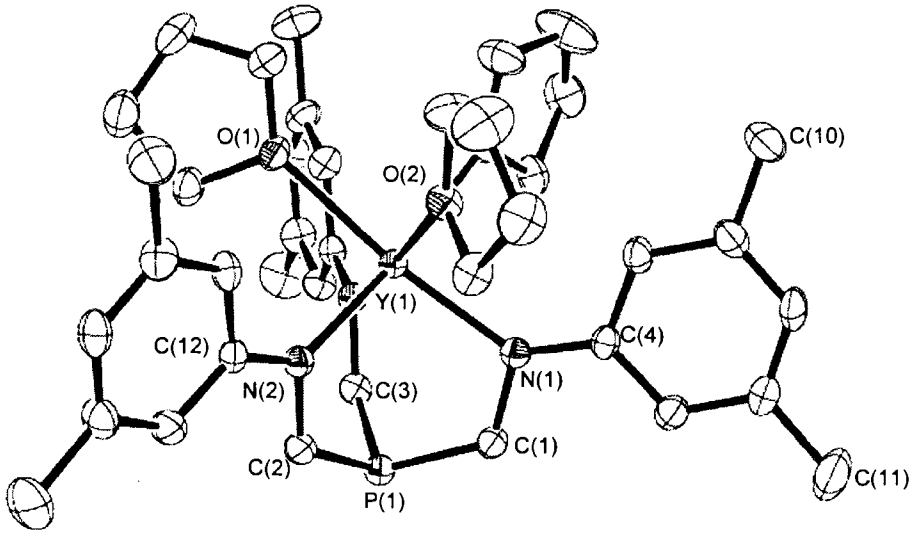

Figure 2.2. An ORTEP depiction of the solid-state molecular structure of $[P(CH_2N\text{-}3,5\text{-}Me_2C_6H_3)_3]Y(THF)_3$ (**2b**). Hydrogen atoms are omitted for clarity. Selected bond lengths or distances (Å): Y(1)---P(1), 3.281(7); Y(1)-N(1), 2.254(4); Y(1)-O(1), 2.444(3); C(1)-N(1), 1.446(6); C(1)-P(1), 1.854(5). Selected angles in deg: N(1)-C(1)-P(1), 121.5(4); C(1)-P(1)-Y(1), 67.47(17); N(1)-Y(1)-N(1), 96.51(12); N(1)-Y(1)-O(1), 89.64(15); N(1)-Y(1)-P(1), 59.49(9).

References begin on page 79

The ^{1}H and $^{31}P\{^{1}H\}$ NMR spectra of complexes **2a** and **2b**, acquired in any solvent (toluene or benzene) other than THF showed the presence of the mixture of two compounds (mononuclear and dinuclear). Variable-temperature NMR confirmed an equilibrium between mononuclear and dinuclear products due to the loss of THF molecules. As shown in Scheme 2.1, high temperature directed the equilibrium towards a dinuclear product after losing two THF molecules. Cooling the sample at room temperature shifted the equilibrium towards mononuclear complex. The ^{1}H NMR spectrum of mononuclear symmetric complex (**2a-2c**) displayed one CH_2, three aromatic (one *o*-H, *m*-H and *p*-H) and two proton environments for three THF molecules bound to the yttrium metal center. However, the ^{1}H NMR spectrum of the dinuclear product showed six CH_2's, nine aromatic environments (six for each *o*-H, *m*-H and *p*-H) and two proton environments for THF molecules. Attempts to isolate the dinuclear complex involved the dissolving of symmetric complex in warm toluene, followed by drying to remove the free THF molecules. The addition of 1-2 drops of THF to the dinuclear complex generated mononuclear yttrium product, which confirmed the formation of the dinuclear product due to the loss of the THF molecule. Several cycles of heating and drying decomposed the product and hence affected the isolated yield of the dinuclear yttrium complex.

References begin on page 79

Scheme 2.1

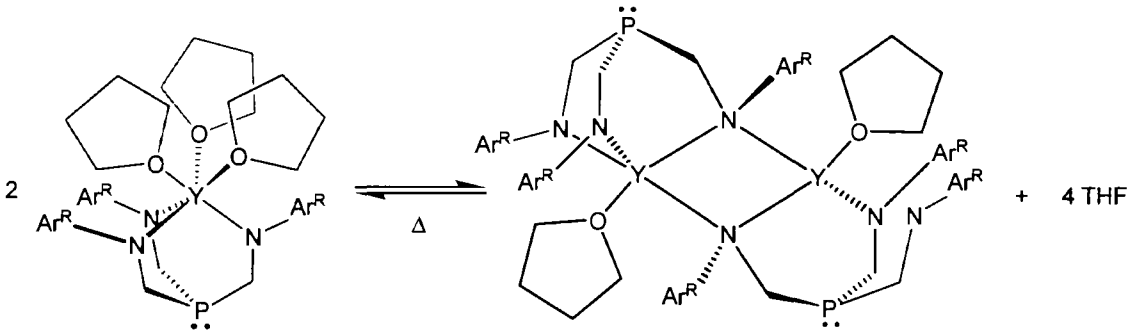

Ar^R = C_6H_5 (**2a**)
= 3,5-$Me_2C_6H_3$ (**2b**)

Ar^R = C_6H_5 (**2a'**)
= 3,5-$Me_2C_6H_3$ (**2b'**)

Various attempts at crystallizing the dinuclear product succeeded in the formation of block shaped off-white crystals, which were obtained from the bromobenzene solution. The X-ray molecular structure shown in Figure 2.3, confirmed the presence of dinuclear yttrium complex in which both yttrium ions are attached to each other by bridging amido nitrogen atoms. Each trivalent yttrium ion is five coordinate and contains one THF molecule. The dinuclear product has C_i symmetry, where both asymmetric units are related to each other. The crystal structure also contained disordered bromobenzene molecules. The yttrium-yttrium distance was found to be 3.808(4) Å, which is ~4 % longer than the distance reported in closely related dimeric yttrium hydro compound (3.672(1) Å) in which both yttrium amido metal ions are bridged by hydrogen atoms.[37]

References begin on page 79

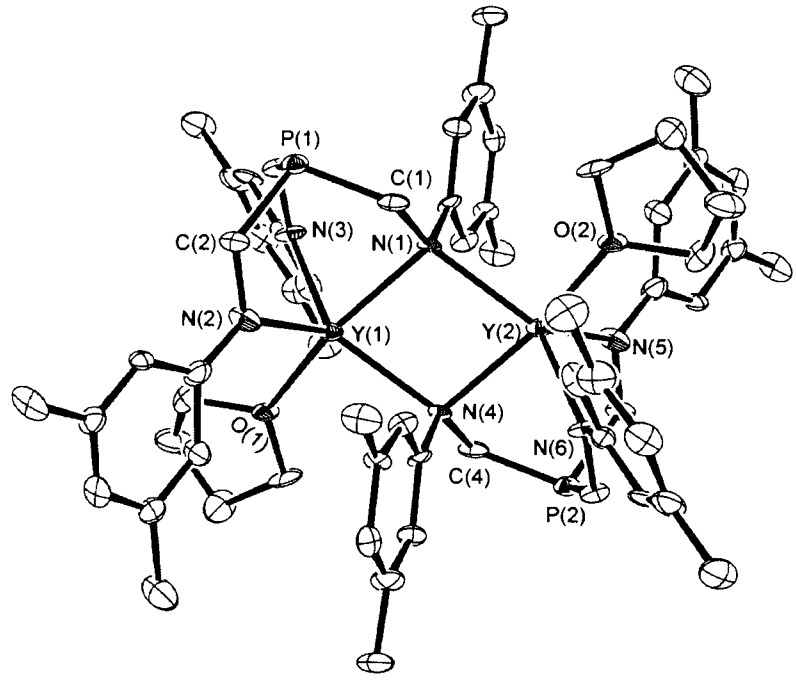

Figure 2.3. An ORTEP depiction of the solid-state molecular structure of $[P(CH_2N\text{-}3,5\text{-}Me_2C_6H_3)_2(\mu\text{-}N\text{-}3,5\text{-}Me_2C_6H_3)Y(THF)]_2$ (**2b'**). Hydrogen atoms are omitted for clarity. Selected bond lengths or distances (Å): Y(1)-N(1), 2.282(14); Y(1)-N(2), 2.305(14); Y(1)-N(3), 2.504(13); Y(1)-Y(2), 3.808(4). Selected angles in deg: N(1)-C(1)-P(1), 118.83(4); N(1)-Y(1)-N(2), 133.83(17); N(1)-Y(1)-N(3), 94.84(13); N(1)-Y(1)-O(1), 98.12(10).

Syntheses of all the paramagnetic trivalent lanthanide complexes (**3a-b** to **8a-b**) were analogous to **2a-b** and involved mixing of equimolar amount of ligand and $Ln[N(SiMe_2)_2]_3$ in THF. Similar to complex **2c**, complexes (**3-8c**) were obtained from refluxing the mixture of 1 equivalent of $[P(CH_2NH\text{-}3,5\text{-}(CF_3)_2C_6H_3)_3]$ (**1c**) and 1.5 equivalents of $Ln[N(SiMe_2)_2]_3$ (where Ln = Gd, Tb, Dy, Ho, Er, and Tm) in THF for 9-10

References begin on page 79

h. Chemical shifts of **4 to 8a-c** were assigned by ^{1}H and $^{31}P\{^{1}H\}$ NMR spectroscopy and all the paramagnetic lanthanide complexes (Table 2.1) except **8a-c** showed a large chemical shift range from −1000 to 1200 ppm in the $^{31}P\{^{1}H\}$ NMR due to dipolar shifts. However, in the case of the thulium complexes (**8a-c**) we were not able to observe the phosphorus NMR shifts because of the larger line width broadening (Experimental Section, Table 2.1).

2.2.1.1 Through-space ^{31}P-^{89}Y Coupling

The $^{31}P\{^{1}H\}$ NMR spectra chemical shifts of the ligand precursors (**1a**, **1b** and **1c**) are –32.1, –29.6 and –32.6 ppm respectively, whereas yttrium complexes (**2a-c**) showed signals at δ –60.6, –61.4 and –62.8 ppm. The coordination of yttrium metal to these ligands causes an upfield shift of the ^{31}P resonances, which is unusual, because increasing C-P-C angles normally shifts the chemical shift towards lower fields.[38] We have previously ascribed this unusual shift in related transition metal complexes by interactions of the minor lobe of the lone pair associated orbital with the adjacent metal centre.[39] All three mononuclear yttrium complexes exhibit 15 Hz couplings between yttrium (^{89}Y, I = ½) and phosphorus in their $^{31}P\{^{1}H\}$ NMR spectra. This $^{3}J_{PY}$ value is large considering that $^{1}J_{PY}$ values are typically in the range of 50-80 Hz, and $^{2}J_{PY}$ values are typically 4 to 6 Hz, though values as large as 11 Hz have been reported in conjugated systems.[40, 41] As expected, $^{3}J_{PY}$ coupling constants should be smaller due to the predominantly ionic nature of bonding in Y^{3+} complexes **2a-c** and thus the smaller Fermi contact terms, but we were unable to uncover any example of $^{3}J_{PY}$ values in the literature for comparison. This suggests that the coupling between Y and P could be mediated by a through-space

References begin on page 79

interaction. The X-ray data demonstrate that the Y-P distance is 3.281(7) Å in complex **2b,** and this proximity of the phosphorus and Y atoms could allow a weak bonding interaction to occur between the minor lobe of the phosphorus lone pair and the metal. A detailed explanation regarding Y-P coupling is provided in Chapter 5.

2.2.1.2 Magnetic Susceptibilities of Trivalent Lanthanides

The molar magnetic susceptibilities χ_m of powdered samples of paramagnetic trivalent lanthanide amides were studied over the temperature range of 300.0-2.0 K. A plot of the product of magnetic susceptibility and temperature ($\chi_m T$) versus temperature (T) for complexes $[P(CH_2N\text{-}3,5\text{-}Me_2C_6H_3)_3]Ln(THF)_3$ (Ln = Er, Dy or Tm) is shown in Figure 2.4. At room temperature complexes **4a**, **7a** and **8a** displayed $\chi_m T$ values of 11.34, 14.17 and 7.11 $cm^3 \cdot K \cdot mol^{-1}$, respectively, which correspond to the previously calculated values of their trivalent free ions at room temperature eg. Er^{3+} (11.48 $cm^3 \cdot K \cdot mol^{-1}$), Dy^{3+} (14.17 $cm^3 \cdot K \cdot mol^{-1}$) and Tm^{3+} (7.15 $cm^3 \cdot K \cdot mol^{-1}$).[42]

References begin on page 79

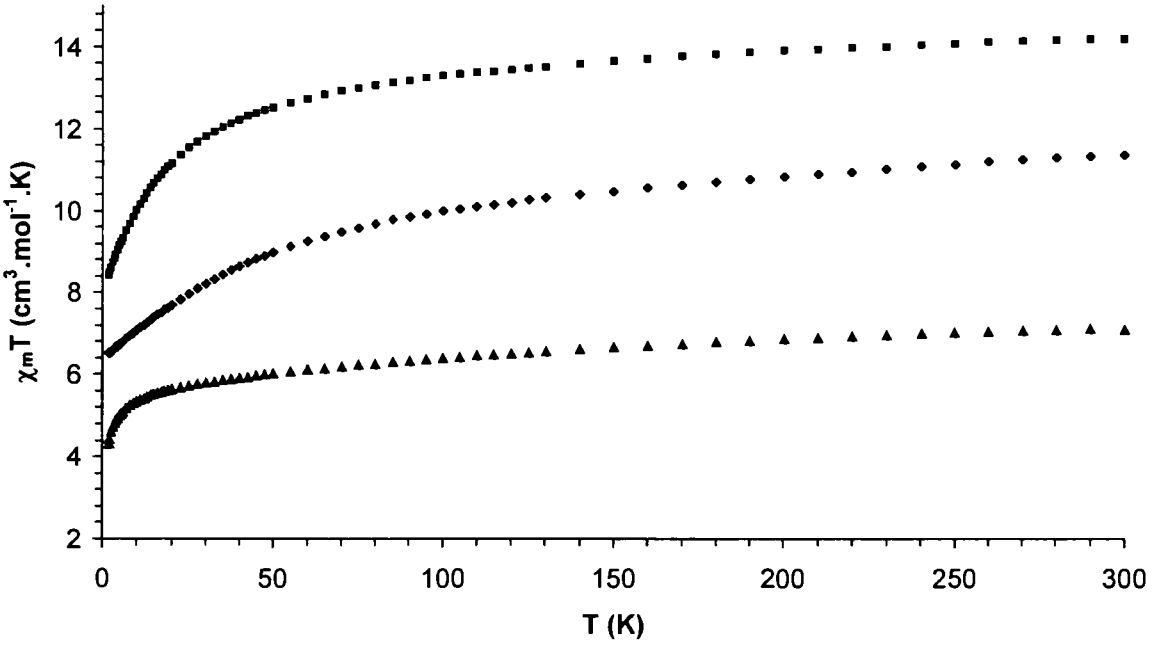

Figure 2.4. Plot of $\chi_m T$ versus temperature for complexes **4a** (squares), **7a** (diamonds) and **8a** (triangles).

2.2.1.3 Electron Paramagnetic Resonance (EPR) Spectrum of Mononuclear Gadolinium Compounds

All the three gadolinium complexes (**3a-c**) were characterized by their EPR spectra and elemental analyses. The solid-state X-ray structure of **3b** confirmed the C_3 symmetry and showed that analogous to other mononuclear lanthanides, complexes **3a-c** also contain six coordinate metal centres chelated by the amido donors. The X-band EPR spectra of powdered Gd complexes (**3a-c**) obtained at 77 K are shown in Figure 2.5 A-C, which display resonances from zero to 14000 G. These gadolinium compounds showed large zero-field splittings, which are larger than the reported anionic bis(phthalocyaninato)gadolinium complex.[43] The spectra were adequately modelled using only B_{20} values from ±0.181 to ±0.197 cm^{-1}, B_{40} values from 1.87 x 10^{-5} to 2.67 x 10^{-5} and

References begin on page 79

the g value of 2.0023. Even after every effort of modelling the EPR spectra of complex **3a** and **c**, we were not able to produce a better model. It can be predicted that the peaks obtained in the experimental spectra might be due to the presence of either a mixture of compounds (mono and dinuclear) or due to the presence of polymorphism. As expected for Gd(III), B_{20} terms were found to be much larger than the B_{40} B_{43}, B_{60}, B_{63} and B_{66} crystal field parameters, and attempts to fit these parameters did not produce a significantly better model of the experimental data. However, modelling of the data using anisotropic line widths made considerable improvement in modelled spectra. The relative sign of B_{20} cannot be determined from this EPR data, and thus it is not clear if the m_s = ±1/2 or m_s = ±7/2 substates are lowest in energy.

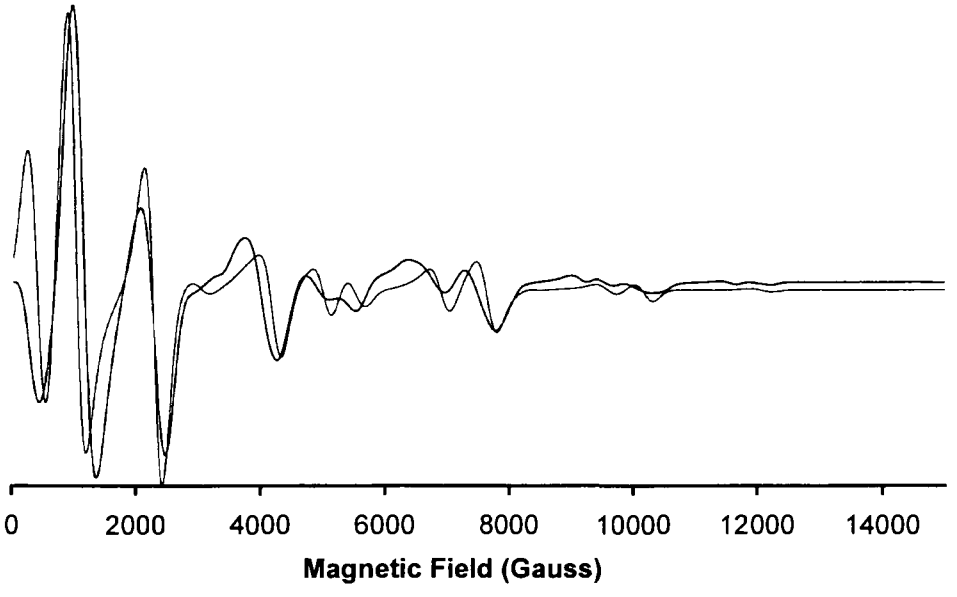

Figure 2.5.A. X-band EPR spectrum of $[P(CH_2NC_6H_5)_3]Gd(THF)_3$ (**3a**) (dark line) and simulated spectrum (grey line) (B_{20} = ±0.189 cm^{-1} (±2025 G), B_{40} = 2.0 x 10^{-5} cm^{-1} (0.21 G), $g_{\|} = g_{\perp}$ = 2.0023 and anisotropic line widths ($\|$ = 160 G, $\perp$ = 200 G)).

References begin on page 79

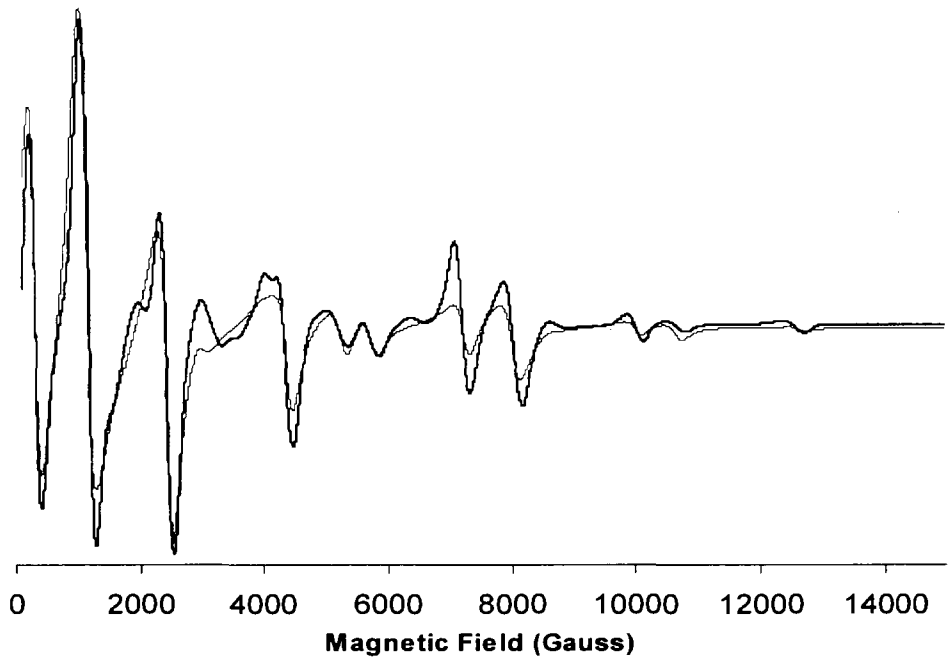

Figure 2.5.B. X-band EPR spectrum of $[P(CH_2N\text{-}3,5\text{-}Me_2C_6H_3)_3]Gd(THF)_3$ **(3b)** (dark line) and simulated spectrum (grey line) ($B_{20} = \pm 0.195$ cm^{-1} (± 2090 G), $B_{40} = 1.87 \times 10^{-5}$ cm^{-1} (0.20 G), $g_{\|} = g_{\perp} = 2.0023$ and anisotropic line widths ($\|$ = 140 G, $\perp$ = 200 G)).

References begin on page 79

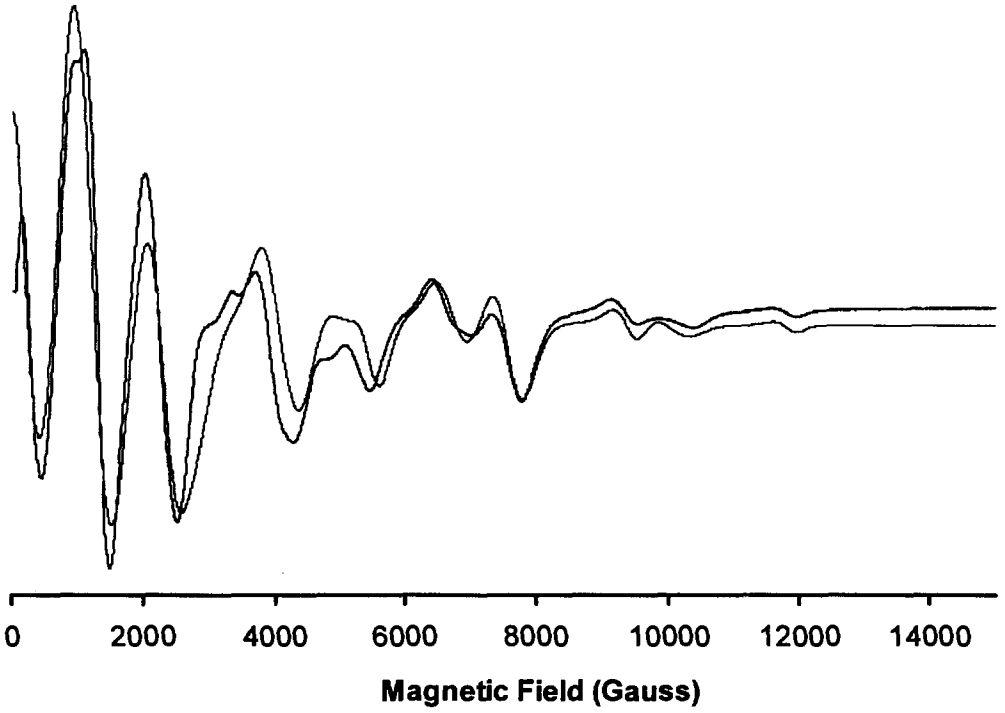

Figure 2.5.C. X-band EPR spectrum of $[P(CH_2N\text{-}3,5\text{-}(CF_3)_2C_6H_3)_3]Gd(THF)_3$ (**3c**) (dark line) and simulated spectrum (grey line) ($B_{20} = \pm 0.182$ cm^{-1} ($\pm$1950 G), $B_{40} = 3 \times 10^{-5}$ cm^{-1} (0.28 G), $g_{\|} = g_{\perp} = 2.0023$ and anisotropic line widths ($\|$ = 160 G, $\perp$ = 270 G)).

2.2.2 Mononuclear Lanthanide Complexes: Building Blocks for Heteronuclear *d–f* Metal Complexes

In these mononuclear lanthanide complexes, the lone pair of the phosphorus atom is directed away from the lanthanide metal centre and acts as a suitable donor for the interaction of another metal centre. In order to build polynuclear complexes where these lanthanide complexes can couple to transition metal complexes via bridging tripodal ligands, these mononuclear lanthanide complexes were used to react with various transition metal complexes. For through-space exchange coupling, the desired transition

References begin on page 79

metal complex must be attached to the phosphine donor and should satisfy two requirements: first, it must direct unpaired electron density towards the mononuclear lanthanide ion; and second, it must have magnetic properties that are easy to model.

To further investigate the possibility of interaction between two metal ions in heterodinuclear complexes, diamagnetic $PtMe_2(COD)$ (where COD = 1,5-cyclooctadiene) was selected and reacted with a two-fold excess of **2c** in the presence of THF, as shown in equation (2.2). The solution was then filtered and layered with pentane, which crystallized in the form of red colour crystals after 5-6 days. The presence of a singlet with ^{195}Pt satellites and 1770 Hz coupling in the phosphorus NMR spectrum provide the evidence of typical *cis*-bis(phosphine)Pt-complexes.[44] The resultant square planar heteronuclear Pt-complex (**9**) showed no sign of Pt-Y coupling in the $^{31}P\{^1H\}$ NMR spectrum.

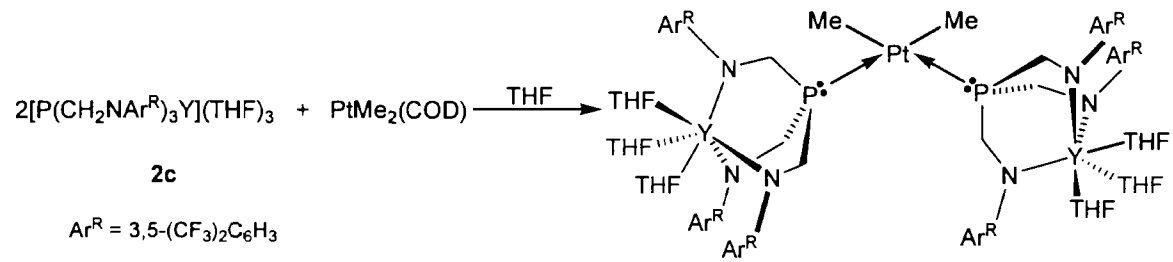

(2.2)

The solid-state molecular structure of complex **9**, as presented in Figure 2.6 shows the presence of two molecules of **2c** attached to a platinum atom, after replacing cyclooctadiene. The lone pairs of both phosphine molecules, which are directed away from yttrium metal, act as donor moeity for platinum metal ions. The distance between the platinum and the yttrium metal center is 5.677(7) Å and between the platinum and phosphorus is 2.287(6) Å. Introduction of platinum metal in the formation of the

References begin on page 79

heteronuclear complex slightly decreased the sum of the P-C-P angles (320.58(7)°) in complex **9**.

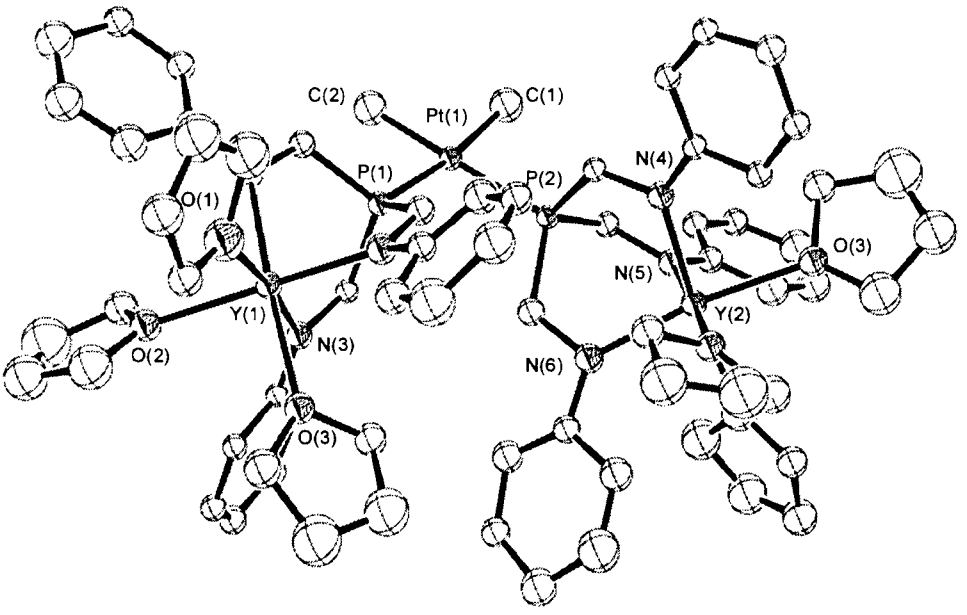

Figure 2.6. An ORTEP depiction of solid state molecular structure of $[P(CH_2N\text{-}3,5\text{-}(CF_3)_2C_6H_3)_3Y(THF)_3]_2PtMe_2$ (**9**). Hydrogen atoms and CF_3 groups are omitted for clarity. Selected bond lengths or distances (Å): Y(1)---P(1), 3.394(10); P(1)-Pt(1), 2.287(7); Y(1)--Pt(1), 5.677(7); Selected angles in deg: P(1)-Pt(1)-P(1), 97.7(3); C(1)-Pt(1)-C(2), 81.8(17).

A second attempt towards the syntheses of heterodinuclear *d-f* metal complexes involved the reaction of 1 equivalent $Ni(acac)_2$ (acac = actylacetonate) with a 2 equivalents of $P(CH_2NHC_6H_5)_3$ followed by its reaction with $Ln[N(SiMe)_2]_3$. The synthesis of the *d-f* metal complex synthesis involve, first mixing of both reactants (**1a** and $Ni(acac)_2$) in THF for 3 h followed by rinsing with pentane before drying for 2 h (equation 2.3). After 2-3 days, a saturated solution in benzene resulted in the formation of violet crystals of

References begin on page 79

$[P(CH_2NHC_6H_5)_3Ni(acac)_2]$ (**10**). The X-ray crystal structure revealed that the product was an octahedral phosphine adduct, which formed upon the addition of two molecules of ligand to the $Ni(acac)_2$. Further reaction of complex **10** with 2 equivalents of $Y[N(SiMe)_2]_3$ did not form the expected *d-f* metal complex, which can be explained on the basis of HSAB (hard- and soft- acid and base) theory. According to this theory, in this reaction, nickel would act as a soft Lewis acid in comparison to the harder yttrium ion and the acac ligand (acetylacetonate) as a hard Lewis base (harder than the amido donor), which would favour the yttrium ion binding to the acac ligand, by replacing the amido donor. Therefore, this theory suggests that transition metal complexes containing soft Lewis bases (softer than the amido donor) will be a better choice for the formation of *d-f* metal complexes.

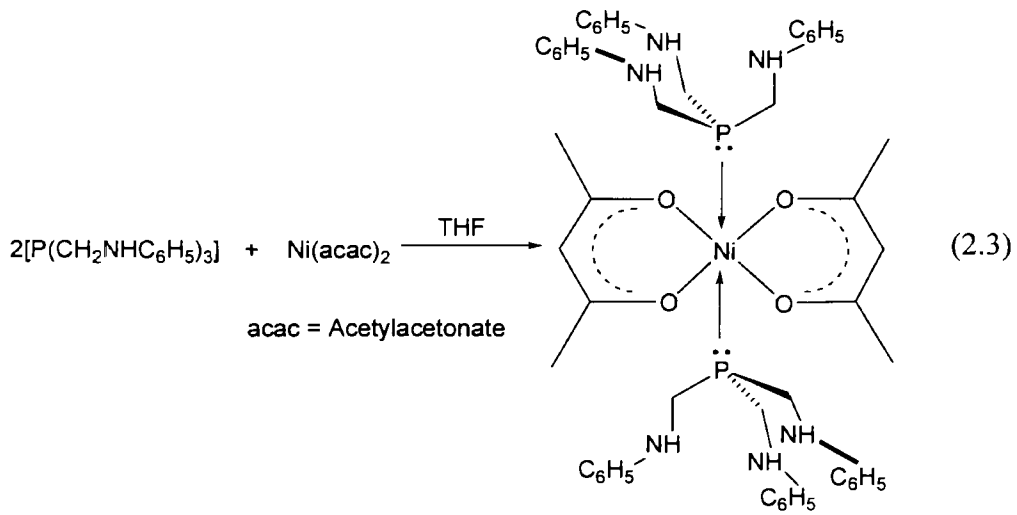

(2.3)

10

The solid-state molecular structure of complex **10**, given in Figure 2.7, shows the octahedral nature of Ni(II) complex in which the nickel metal ion is 2.4617(8) Å apart from phosphorus atom, which is 0.09 Å shorter than the previously reported nickel-

References begin on page 79

phosphine complex.[45] Bonding of the nickel ion in between two molecules of ligand precursor **1a** slightly opens up the C-P-C angle, which then becomes 313.26(5)°.

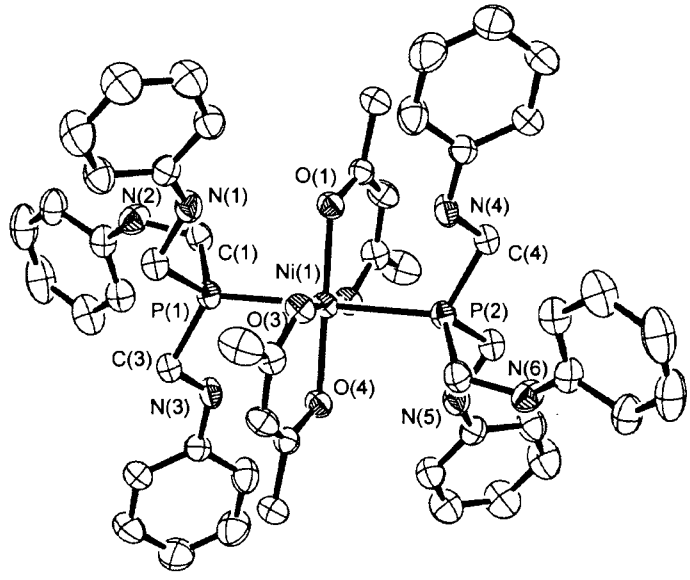

Figure 2.7. An ORTEP depiction of solid state molecular structure of $[P(CH_2NHC_6H_5)_3]_2$ $Ni(acac)_2$ (**10**) showing 30% probability surface . Hydrogen atoms are omitted for clarity. Selected bond lengths or distances (Å): Ni(1)---P(1), 2.4617(8); Ni(1)-O(1), 2.011(2); Ni(1)-O(2), 2.038(2).

One of our attempts to check the possibility of interaction between *d-f* metal ions in heteronuclear complexes also involved the reaction of **2a-c** with [TPP]Co (where TPP = 5,10,15,20–tetrakis(4–methoxyphenyl)porphyrin). To achieve our goal, 1 equivalent of **2c** was reacted with 1 equivalent of [TPP]Co in toluene, which resulted in the formation of the related five-coordinate phosphine adducts of Co(II) porphyrin, as known previously.[46-48] Reddish brown crystals were obtained directly from the toluene solution and the crystal structure (Figure 2.8) revealed that the resultant product is a five

References begin on page 79

coordinate heteronuclear Co–Y complex in which two THF and one DMF (dimethyl formamide) molecules are coordinated to the yttrium metal centre instead of three THF molecules (present in the mononuclear yttrium complex **2a-c**). Further investigation suggested that the presence of a DMF molecule ([TPP]Co purchased from Aldrich was crystallized from DMF) in the resulting five coordinate cobalt phosphine complex was due to the stronger donor ability of DMF. In complex $P(CH_2N\text{-}3,5\text{-}(CF_3)_2C_6H_3)_3Y(THF)_2(DMF)]TPPCo$ (**11**), average Y-N distance is 2.283(2) Å, P(1)---Y(1) distance is 3.305(6) Å and Y(1)---Co(1) are 5.685(10) Å apart from each other. The sum of the C-P-C angles in complex **11** is 325.9(12) Å, which is approximately 28° larger than the sum of C-P-C angles for the ligand precursor, **1c**.

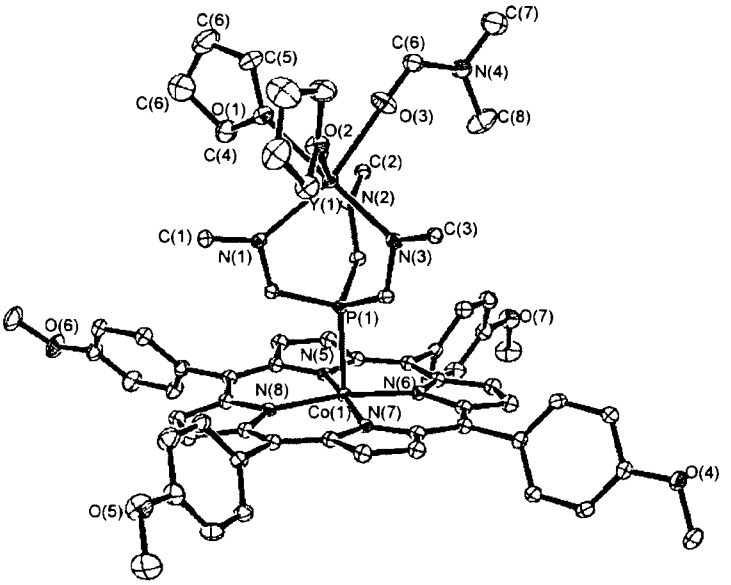

Figure 2.8. An ORTEP depiction of solid state molecular structure of $[P(CH_2N\text{-}3,5\text{-}(CF_3)_2C_6H_3)_3Y(THF)_2(DMF)]TPPCo$ (**11**). Hydrogen and fluorine atoms are omitted for clarity and only the *ipso* carbons of the phenyl substituent on nitrogen are shown. Selected bond lengths or distances (Å): Y(1)---P(1), 3.305(6); P(1)-Co(1), 2.382(9); Y(1)-N(1), 2.279(5); Y(1)-N(2), 2.288(5); Y(1)-N(3), 2.280(5); Y(1)---Co(1), 5.685(10).

References begin on page 79

2.2.3 Introduction of Tris(Pyrazolyl)Borate: A THF Substitute

Due to the weaker donor ability of THF towards our lanthanide complexes, all three THF molecules were easily replaced by the tris(pyrazolyl)borate ligand. A variety of poly(pyrazolyl)borate ligands have been used to study the chemical and photophysical properties of lanthanides.[49-51] It has been reported previously that tris(pyrazolyl)borate ligands control the reactivity as well as the steric bulk of the metal complexes.[52] The number of equivalents of pyrazolyl ligands required to attach to the metal centre depend on the steric bulk of the substituents attached to the 3- and 5- position of the pyrazolyl rings, which also controls the coordination sphere. Depending upon the substituents attached to the pyrazolyl ring, various other Tp ligands have also been studied, such as Tp, $Tp^{Me,Me}$ (methyl group attached in 3 and 5 positions), $Tp^{Me,Me,Et}$ (Me on 3,5 and Et on 4^{th} position), $Tp^{CF3,CF3}$ ($R_3 = R_5 = CF_3$) etc, as shown in Table 2.1. Out of these, $Tp^{Me,Me}$ is the most extensively used, due to the appropriate amount of steric bulk provided by methyl groups.

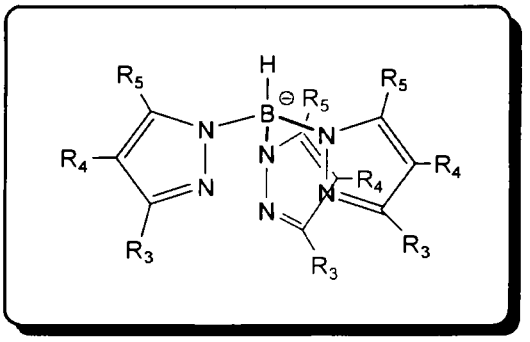

Tris(pyrazolyl)borate ligand

References begin on page 79

Table 2.1. Substituents attached to the pyrazolyl ring

Symbol	R_3	R_4	R_5
Tp	H	H	H
Tp^{Me2}	Me	H	Me
Tp^{Me2Et}	Me	Et	Me
Tp^{tBuMe}	*t*Bu	H	Me
Tp^{Ms}	Mes	H	H
Tp^{MsMe}	Mes	H	Me
$Tp^{(CF3)2}$	CF_3	H	CF_3

To replace the THF donor molecules from complexes **2a-c,** 1 equivalent of yttrium complexes (**2a-c**) were reacted with similar numbers of moles of the tris(pyrazolyl) borate potassium salt (**KTp^{Me}**) in THF (Equation 2.4). Tris(pyrazolyl)borate behaves as a tridentate anionic ligand and has been used earlier for lanthanide complexes.[49] Mixing of both reactants (**2a-c** and **KTp^{Me}**) resulted in the formation of six coordinate lanthanide compounds capped with three nitrogen molecules of the tris(pyrazolyl)borate and chelated with three nitrogen molecules of tripodal amido ligand. Similar to the formation of **2a** and **2b**, **12a** and **12b** required mixing of 1 equivalent of **2a-b** with 1 equivalent of **KTp^{Me}** at room temperature in the presence of THF. Formation of **12c** required reaction of 1.5 equivalents of potassium salt of tris(pyrazolyl) borate with 1 equivalent of **KTp^{Me}** and 10-12 h refluxing in THF.

References begin on page 79

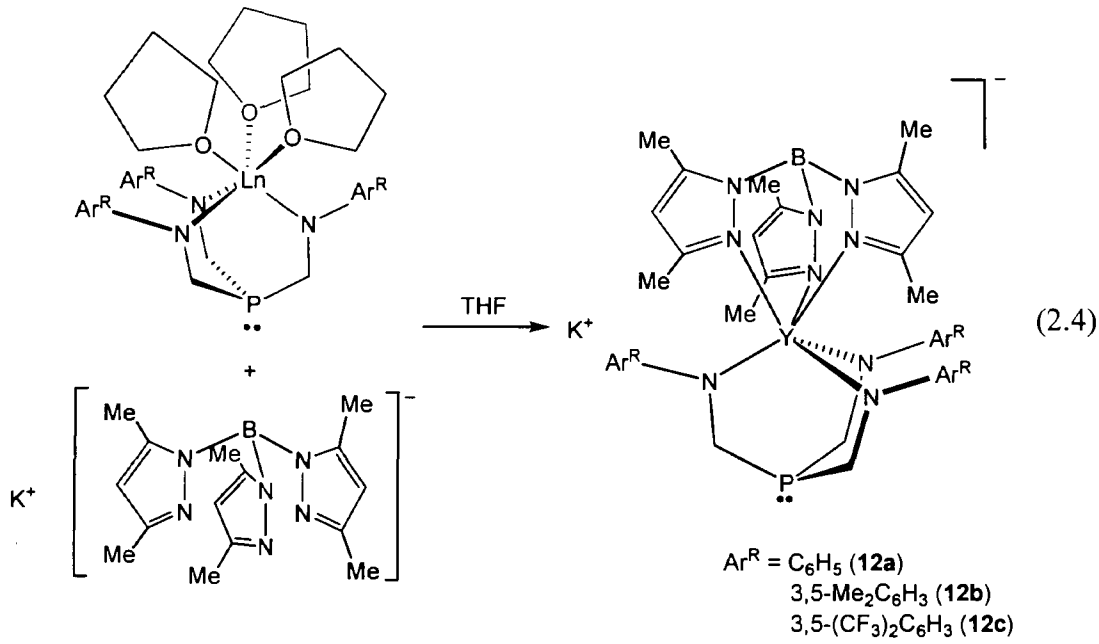

(2.4)

Efforts to obtain X-ray quality crystals of **12a-c,** as well as their further reactions with different metal complexes, revealed that both **12a** and **12b** are less soluble in benzene or toluene than **12c.** It has been reported that most of these LnTp reactions involve the metathesis of lanthanide salts in THF and it was also found that the solubility of these compounds depend on their relative structures (with or without solvent molecules).[51] Block-shaped X-ray quality crystals of **12c** were easily obtained from the mixture of benzene/hexamethyldisiloxane. The ORTEP depiction of the solid state molecular structure of **12c** is given in Figure 2.9. The crystal structure of **12c** displays that the potassium metal ion is coordinated with one molecule of THF and one molecule of benzene. Comparison of bond lengths and angles with **2a-c** showed only small variations due to the replacement of THF molecules by a KTp^{Me} ligand in complex **12c**. There was no significant difference observed in the sum of C-P-C angles in complex **12c** (320.95°(8)) and in complex **2c** (320.58°(7)).

References begin on page 79

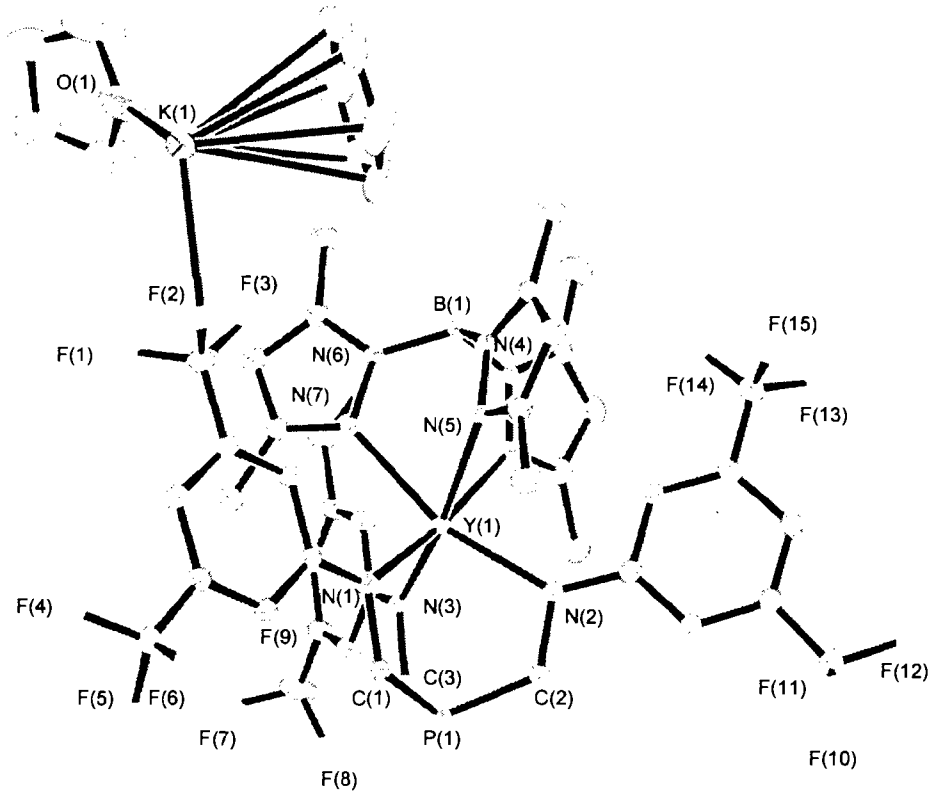

Figure 2.9. An ORTEP depiction of the solid–state molecular structure of $K^+[P(CH_2N\text{-}3,5\text{-}(CF_3)_2C_6H_3)_3YTp^{Me}]^-$ (**12c**) showing potassium attached with cocrystallized benzene and THF. 30% thermal ellipsoids are shown. Hydrogen atoms are omitted for clarity and only the *ipso* carbons of the phenyl substituents on nitrogen are shown. Selected bond lengths or distances (Å): Y(1)---P(1), 3.3173(9); Y(1)---B(1), 3.543(5); Y(1)-N(3), 2.298(3); Y(1)-N(1), 2.292(3); Y(1)-N(2), 2.288(3); Y(1)-N(5) 2.432(3); Y(1)-N(7) 2.452(3); Y(1)-N(9), 2.453(3). Selected angles in degrees: N(7)-Y(1)-N(9), 78.81(9); N(5)-Y(1)-N(9), 74.49(9); N(5)-Y(1)-N(7), 77.61(9); C(3)-P(1)-C(1), 105.87(15); C(3)-P(1)-C(2), 106.96(15); C(1)-P(1)-C(2), 108.12(15).

In order to form the heteronuclear complexes with magnetically coupled *d* and *f* block metals, mononuclear compounds **12a-c** were further reacted with various transition

References begin on page 79

metal halides. Most of these reactions involve the displacement of the yttrium ion from the amido complexes by harder Lewis bases (harder than the amido donors). An example of these reactions involve the reaction of complex **12** with Zr-halides, which resulted in the form of Zr-amido complexes.[53] The $^{31}P\{^{1}H\}$ chemical shifts of the Zr-complexes correspond to the previously reported Zr-amido complexes and showed the shifts ~ −70 ppm.[53] These displacement reactions, where harder Lewis acid (Y^{3+}) was easily displaced by hard chloride ions, suggest that transition metal complexes containing soft Lewis bases (softer than the amido donors) will be a better choice to for the syntheses of *d-f* metal complexes.[54]

$$[P(CH_2NAr^R)_3]YTp^{Me} + ZrCl_4 \xrightarrow{THF} [P(CH_2NAr^R)_3]ZrCl(THF) \quad \text{major product} \qquad (2.5)$$

$$[P(CH_2NAr^R)_3]YTp^{Me} + Cp_2ZrCl_2 \xrightarrow{THF} [P(CH_2NAr^R)_3]ZrCp \quad \text{major product} \qquad (2.6)$$

2.3 Summary and Conclusions

The syntheses and characterization of a series of tripodal amido ligand supported mononuclear lanthanide complexes were carried out using different donor molecules and tripodal amido phosphine ligands. Large zero field splitting was observed in mononuclear gadolinium complexes, which is larger than in the reported anionic bis(phthalocyaninato)gadolinium complex. These mononuclear complexes were then further utilized for the syntheses of heteronuclear *d–f* metal complexes. Preliminary efforts at synthesizing heteronuclear complexes done in this Chapter provided some insight into the importance of ligand design as well as on the selection of appropriate

References begin on page 79

transition metal complexes for *d-f* metal-metal interaction. It can also be concluded that transition metal complexes, which possess large magnetic anisotropy and weaker field ligands will be more appropriate for observing metallic interactions when making complexes with anionic complexes of lanthanide $K^+[P(CH_2NAr^RC_6H_3)_3LnTp^{Me}]^-$.

2.4 Experimental

General Techniques - Unless otherwise stated, all experiments were performed under an inert atmosphere of dinitrogen using either Schlenk techniques, or an MBraun glove box. Dry oxygen free solvents were used throughout. Anhydrous pentane and toluene were purchased from Aldrich, sparged with nitrogen and passed through activated alumina under a positive pressure of nitrogen gas; toluene and hexanes were further deoxygenated using Ridox catalyst columns.[55] Deuterated benzene and toluene were dried by heating at reflux over Na/K in a sealed vessel under partial pressure, then trap-to-trap distilled, and freeze-pump-thaw degassed three times.

Instrumentation - ^1H, $^{13}C\{^1H\}$, $^{19}F\{^1H\}$ and $^{31}P\{^1H\}$ NMR spectra were recorded on Bruker AMX (300 MHz) and Bruker AMX (500 MHz) spectrometers. All chemical shifts are reported in ppm, and all NMR coupling constants (*J*) are in Hz. ^1H NMR spectra were referenced to residual protons (C_6D_5H, δ 7.15, C_7D_7H, δ 2.09, $CHDCl_2$ δ 5.35, and C_4D_7HO δ 1.73) with respect to trimethylsilane at δ 0.0. $^{13}C\{^1H\}$ spectra were referenced relative to solvent resonances (C_6D_6, δ 128.0 and C_7D_8, δ 20.4, CD_2Cl_2 δ 54.0, and C_4D_8O δ 67.4). $^{31}P\{^1H\}$ NMR spectra referenced to external 85 % H_3PO_4 at δ 0.0. For $^{19}F\{^1H\}$ NMR spectra, trifluoroacetic acid was used as the external reference at δ 0.0. Elemental analyses were performed by the Centre for Catalysis and Materials Research (CCMR) at

References begin on page 79

the University of Windsor. Magnetizations were measured with a Quantum Design MPMS-XL system at Simon Fraser University. Samples were run in a PVC holder specially designed to possess a constant cross-sectional area.

EPR Spectroscopy - EPR spectra were collected using an X-band Bruker ESR 300 E spectrometer. The program Spin[56] was used to simulate the Gd^{3+} spectrum using only $B_{20}(D)$ crystal field parameter and the program Sim[57] was used to generate spectra with the B_{20}, B_{40}, B_{43}, B_{60}, B_{63} and B_{66} crystal field parameters.

Chemicals - The compounds tris(hydroxymethyl)phosphine, aniline, 3,5-dimethyl aniline, 3,5-bis(trifluoromethyl)aniline, anhydrous YCl_3, 3,5-dimethyl-1pyrazolyl, $Ni(acac)_2$, $PtMe_2(COD)_2$, potassium borohydride, $LiN(SiMe_2)$, $NaN(SiMe_2)$ and [TPP]Co (where TPP = 5,10,15,20–tetrakis(4–methoxyphenyl)porphyrin) were purchased from Aldrich. Anhydrous $LnCl_3$ (Ln = Gd, Tm, Ho, Tb, Dy and Er) were purchased from Strem. All the reagents were used without further purification. All three tripodal amido-phosphine ligands were synthesized by the method reported previously from our lab.[39] The compounds $Y[N(SiMe_3)_2]_3$ and $Ln[N(SiMe_3)_2]_3$ (Ln = Gd, Tm, Ho, Tb, Dy and Er) were synthesized via the literature methods.[58, 59] Potassium hydrotris(1-pyrazolyl)borate (KTp^{Me}) was synthesized by the method given in the literature.[52] The ligand precursors $P(CH_2NHC_6H_5)_3$, $P(CH_2NH\text{-}3,5\text{-}Me_2C_6H_3)_3$ and $P(CH_2NH\text{-}3,5\text{-}(CF_3)_2C_6H_3)_3$ were prepared by literature methods and will be numbered as **1a**, **1b** and **1c**, respectively.[39]

Synthesis of Symmetric $[P(CH_2NC_6H_5)_3Y(THF)_3]$ (2a). A mixture of $P(CH_2NHC_6H_6)_3$ (500 mg, 1.4 mmol) and $Y[N(SiMe_3)_2]_3$ (798 mg, 1.4 mmol) was stirred in 20 mL of THF at room temperature for 30 min and left overnight for crystallization. The solution was filtered and the remaining white crystalline solid rinsed with 50 mL

References begin on page 79

pentane and dried under vacuum for 3 h (66 %, 600 mg). ^{1}H NMR (C_4D_8O, 300 MHz, 298 K): δ 1.45 (12H, $YOCH_2CH_2$), 3.52 (12H, $YOCH_2$), 4.12 (d, $^2J_{PH}$ = 6.2 Hz, 6H, PCH_2), 7.12 (d, Ar, 6H, *o-H*), 7.24 (m, Ar, 6H, *m* and *p-H*). $^{31}P\{^1H\}$ NMR (C_4D_8O, 121.5 MHz, 298 K): δ –60.6 (d, J_{PY} = 15.1 Hz). Anal. Calcd for $C_{33}H_{45}N_3O_3PY$: C, 60.83; H, 3.95; N, 6.09. Found: C, 60.90; H, 4.01; N, 6.12.

Dinuclear Complex $[P(CH_2NC_6H_5)_2(\mu\text{-}NC_6H_5)Y(THF)]_2$ (2a'). Complex **2a** converts into dinuclear complex **2a'** after losing two THF molecules at high temperatures and in the presence of benzene or toluene. Synthesis of **2a'** involves the redissolving of complex **2a** in warm toluene followed by drying under vacuum. The process was repeated 5-6 times till the resultant product was obtained. ^{1}H NMR (C_6D_6, 300 MHz, 338 K): δ 1.35 (br, 8H, OCH_2CH_2), 3.46 (br, 8H, $YOCH_2$), 3.85 (m, 6H, PCH_2), 3.57 (t, 2H, PCH_2), 4.67 (d, 2H, PCH_2), 4.95 (dd, 2H, PCH_2), 6.42 (d, Ar, 4H, *o-H*), 6.65 (m, Ar, 6H, *o* and *p-H*), 6.73 (d, Ar, 4H, *o-H*), 6.82 (t, Ar, 2H, *p-H*), 7.28 (m, Ar, 6H, *m* and *p-H*), 7.1-7.34(m, Ar, 8H, m-*H*). $^{31}P\{^1H\}$ NMR (C_6D_6, 121.5 MHz, 338 K): δ – 45.2 (d, J_{PY} = 15.1 Hz).

Synthesis of Symmetric $[P(CH_2N\text{-}3,5\text{-}Me_2C_6H_3)_3Y(THF)_3]$ (2b). A mixture of $P(CH_2NH\text{-}3,5\text{-}Me_2C_6H_3)_3$ (500 mg, 1.15 mmol) and $Y[N(SiMe_3)_2]_3$ (657 mg, 1.15 mmol) was stirred in 20 mL of THF at room temperature for 30 min and left overnight for crystallization. The solution was filtered and the remaining white crystalline solid rinsed with 50 mL pentane and dried under vacuum for 3 h (68.5 %, 575 mg). ^{1}H NMR (C_4D_8O, 300 MHz, 298 K): δ 1.45 (b, 12H, $YOCH_2CH_2$), 2.25 (s, 18H, Ar-CH_3), 3.51 (b, 12H, $YOCH_2$), 4.05 (d, 6H, $^2J_{PH}$ = 6.1 Hz, PCH_2), 6.19 (b, Ar, 6H, *o-H)*, 6.23 (s, 3H, *p-H*). $^{31}P\{^1H\}$ NMR (C_4D_8O, 121.5 MHz, 298 K): δ – 61.4 (d, J_{PY} = 15.1 Hz). Anal. Calcd for $C_{39}H_{57}N_3O_3PY$: C, 63.66; H, 7.81; N, 5.71. Found: C, 63.80; H, 7.92; N, 5.73.

References begin on page 79

Dinuclear Complex $[P(CH_2N\text{-}3,5\text{-}Me_2C_6H_3)_2(\mu\text{-}N3,5\text{-}Me_2C_6H_3)Y(THF)]_2$ (2b').

Complex **2b** converts into asymmetric complex **2b'** after losing two THF molecules at high temperatures and in the presence of benzene or toluene. Synthesis of **2b'** involves the redissolving of complex **2b** in warm toluene followed by drying. The process was repeated 5-6 times till the resultant product was obtained. ^1H NMR (C_6D_6, 300 MHz, 338 K): δ 1.47 (b, 8H, OCH_2CH_2), 3.50 (b, 8H, $YOCH_2$), 2.12 (s, 6H, Ar-CH_3), 2.25 (s, 6H, Ar-CH_3), 2.35 (s, 6H, Ar-CH_3) 3.56 (m, 6H, PCH_2), 3.62 (d, 2H, PCH_2), 4.45 (d, 2H, PCH_2), 5.16 (dd, 2H, PCH_2), 5.84 (s, Ar, 4H, *o-H*), 6.14 (s, Ar, 2H, *p-H*), 6.20 (s, Ar, 4H, *o-H*), 6.24 (s, Ar, 2H, *p-H*), 6.34 (s, Ar, 2H, *p*-H), 6.85 (s, Ar, 4H, *o*-H). $^{31}P\{^1H\}$ NMR (C_6D_6, 300 MHz, 338 K): δ – 46.0 (d, J_{PY} = 15.1 Hz).

Synthesis of $[P(CH_2N\text{-}3,5\text{-}(CF_3)_2C_6H_3)_3Y(THF)_3]$ (2c). A mixture of $P(CH_2NH\text{-}3,5\text{-}(CF_3)_2C_6H_3)_3$ (750 mg, 0.993 mmol) and $Y[N(SiMe_3)_2]_3$ (849.10 mg, 1.48 mmol) was refluxed in 20 mL of THF overnight. The solvent was evacuated after cooling the mixture to room temperature yielding an off-white solid. The product was then washed with 50 mL pentane and dried under vacuum for 3 h (97 %, 890 mg). X-ray quality crystals were obtained from benzene/hexamethyldisiloxane mixture. ^1H NMR (C_6D_6, 300 MHz, 298 K): δ 1.72 (b, 12H, $YOCH_2$), 3.58 (d, 6H, $^2J_{PH}$ = 5.8 Hz, PCH_2), 4.13 (b, 12H, $YOCH_2$), 6.81 (s, Ar, 6H, *o-H*), 6.87 (s, Ar, 3H, *p-H*), $^{13}C\{^1H\}$ NMR (C_6D_6, 75.5 MHz, 298 K): δ 26.2 (s, $YOCH_2CH_2$), 44.2 (d, J_{PC} = 17.4 Hz, PCH_2), 68.4 (s, $YOCH_2CH_2$), 106.5 (s, Ar *o-C*), 113.2 (s, Ar *p-C*), and 124.1 (s, Ar *m-C*), 122.9 (q, *J* = 32.9 Hz, $ArCF_3$), 156.8 (d, *J* = 5.5 Hz, *ipso-C*). $^{31}P\{^1H\}$ NMR (C_6D_6, 121.5 MHz, 298 K): δ – 62.8 (d, J_{PY} = 15.1 Hz), $^{19}F\{^1H\}$ NMR (C_6D_6, 282.1 MHz, 298 K): δ 14.71 (s). Anal. Calcd. for $C_{39}H_{39}F_{18}N_3O_3PY$: C, 44.21; H, 3.71; N, 3.97. Found: C, 44.28; H, 3.85; N, 3.84.

References begin on page 79

Syntheses of $[P(CH_2NC_6H_5)_3Ln(THF)_3]$ (Ln = Gd, Tb, Dy, Ho, Er and Tm) (3a-8a). All other lanthanide complexes were also synthesized in an analogous manner to the yttrium complex using 1:1 ratio of ligand and $Ln[N(SiMe_3)_2]_3$. Products were crystallized in the form of white (Gd, Tb, Dy, Ho, Tm and Yb) and pink (Er) coloured crystals (yield 60-70 %). Crystallized products were filtered next day, and then rinsed with pentane followed by drying under vacuum for 2 h.

Syntheses of $[P(CH_2N\text{-}3,5\text{-}Me_2C_6H_3)_3Ln(THF)_3]$ (Ln = Gd, Tb, Dy, Ho, Er and Tm) (3b-8b). A mixture of $P(CH_2NH\text{-}3,5\text{-}Me_2C_6H_3)_3$ and $Ln[N(SiMe_3)_2]_3$ (1:1) was stirred in 20 mL of THF at room temperature for 30 min. After filtration crystallized products were rinsed with pentane and then dried under vacuum for 2h (yield 60-70 %).

Synthesis of $[P(CH_2N\text{-}3,5\text{-}(CF_3)_2C_6H_3)_3Ln(THF)_3]$ (Ln = Gd, Tb, Dy, Ho, Er and Tm) (3c-8c). A mixture of $P(CH_2NH\text{-}3,5\text{-}(CF_3)_2C_6H_3)_3$ and $Ln[N(SiMe_3)_2]_3$ (1:1.5) was refluxed in 20 mL of THF 9-10 h. The solvent was removed under vacuum after cooling the mixture to room temperature leaving an off-white (Gd, Tb, Dy, Ho, and Tm) and pink colour solid (Er). The product was washed with 50 mL pentane and dried under vacuum for 3 h (yield 60-70 %).

^1H (C_6D_6, 300 MHz, 298 K) and $^{31}P\{^1H\}$ (C_6D_6, 121.5 MHz, 298 K) NMR spectrum of $[P(CH_2NAr^R)_3Ln(THF)_3]$ (Ln = Tb, Dy, Ho, Er and Tm) as shown in Table 2.2.

References begin on page 79

Table 2.2. NMR chemical shifts of complexes **4a–c, 5a–c, 6a-c, 7a-c** and **8a–c.**

Compounds	**^{1}H**					**^{31}P{^{1}H}**	**^{19}F{^{1}H}**
$[P(CH_2NC_6H_5)_3Ln(THF)_3]$	CH_2	CH_3	Ar *o-H*	Ar *m-H*	Ar *p-H*		
Tb	–44.5		42.6	54.2	64.3	– 950	
Dy	–322.3		26.2	32.3	48.5	–1017	
Ho	–56.8		20.2	29.6	37.3	– 48	
Er	–210.4		27.5	28.5	25.6	–413	
Tm	415.2		–31.5	–41.3	–48.2		
$[P(CH_2N\text{-}3,5\text{-}Me_2C_6H_3)_3Ln(THF)_3]$							
Tb	–49.2	–30.1	39.2		61.3	– 956	
Dy	–403.4	–289.2	21.2		35.4	–1225	
Ho	–66.4	–42.7	16.4		28.5	–56	
Er	–278.7	–159.3	24.6		20.3	–576	
Tm	508.3	410.2	–27.3		–35.6		
$[P(CH_2N\text{-}3,5\text{-}CF_3)_2C_6H_3)_3Ln(THF)_3]$							
Tb	–40.4		47.7		66.2	– 931	–49
Dy	–275.5		30.2		59.0	–957	–301
Ho	–47.7		26.3		45.2	– 39	–59
Er	–101.4		33.9		27.4	–303	179
Tm	322.2		–43.4		–55.7		514

Synthesis of $[P(CH_2N\text{-}3,5\text{-}(CF_3)_2C_6H_3)_3Y(THF)_3]_2PtMe_2$ (9). In a small flask 1 equivalent of $PtMe_2COD$ (20 mg, 0.0149 mmol) and 2 equivalents of $[P(CH_2N\text{-}3,5\text{-}(CF_3)_2C_6H_3)_3Y(THF)_3]$ (128 mg, 0.0299 mmol) were stirred in 0.7 mL of CH_2Cl_2 for 24 h. After that solution mixture was filtered and layered with pentane which resulted as red coloured crystals of **9**. $^{31}P\{^1H\}$ NMR (CD_2Cl_2, 121.5 MHz, 298 K): δ – 7.58 (s, J_{PtP} = 1770 Hz).

Synthesis of $[P(CH_2NHC_6H_5)_3]_2Ni(acac)_2$ (10). A mixture of 2 equivalents of $P(CH_2NHC_6H_5)_3$ (1.36 g, 3.89 mmol) with $Ni(acac)_2$ (500 mg, 1.94 mmol) was added together in 40 mL of THF and stirred for 4 h at room temperature. After 4 h the solvent was removed under vacuum and the residue was rinsed with pentane and dried under

References begin on page 79

vacuum for 2 h. Evaporation of a saturated solution in benzene provided violet coloured crystals (60 %, 700 mg). Anal. Calcd for $C_{52}H_{64}N_6O_4P_2Ni$: C, 65.21; H, 6.74; N, 8.77. Found: C, 65.50; H, 6.96; N, 8.57.

Synthesis of P(CH$_2$N-3,5-(CF$_3$)$_2$C$_6$H$_3$)$_3$Y(THF)$_2$(DMF)]TPPCo (11). A mixture of **2c** (500 mg, 0.737 mmol) and [5, 10, 15, 20-tetrakis(4-methoxyphenyl)porphinato]cobalt (II), [TPP]Co(II) (584 mg, 0.737 mmol) was stirred in 25 mL of toluene for 30 min. The solution was filtered and the resultant reddish-purple crystalline solid was washed with pentane (50 mL) and dried under vacuum for 4 h (47.5 %, 515 mg). Anal. Calcd for $C_{39}H_{39}F_{18}N_8O_3PYCo$: C, 61.30; H, 4.32; N, 6.67. Found: C, 61.47; H, 4.12; N, 6.54.

Synthesis of K$^+$[P(CH$_2$NC$_6$H$_5$)$_3$YTp^{Me}]$^-$.THF.Benzene (12a). A mixture of [P(CH$_2$NC$_6$H$_5$)$_3$Y(THF)$_3$] (678 mg, 1.04 mmol) and K[HB(C$_3$H$_3$N$_2$)$_3$] (350 mg, 1.04 mmol) was stirred in 20 mL of THF at room temperature for 5 h. The solution was filtered and the remaining white solid was rinsed with 50 mL pentane and dried under vacuum for 3 h (76 %, 615 mg). ^{1}H NMR (C_6D_6, 300 MHz, 298 K): δ 2.76 (s, 9H, TpC*H$_3$*), 2.85 (s, 9H, TpC*H$_3$*), 3.13 (d, 6H, $^2J_{PH}$ = 7.1 Hz, PC*H$_2$*), 4.21 (b, 1H, B*H*), 6.12 (s, 3H, Tp*H*), 6.47 (d, 6H, Ar *o-H*), 6.75 (t, 3H, Ar *p-H*), 7.12 (m, 6H, Ar *m-H*). ^{13}C{^{1}H} NMR (C_6D_6, 75.5 MHz, 298 K): δ 26.1 (d, J_{PC} = 16.2 Hz, P*C*H$_2$), 16.5 (s, Tp*C*H$_3$), 11.2 (s, Tp*C*H$_3$), 112.1, 114.4 and 132.9 (s, Ar, *o-C, p-C* and *m-C*), 153.6 (Ar, *ipso-C*), 146.1 (s, Tp*C*-1), 108.2 (s, Tp*C*-2), 141.4 (s, Tp*C*-3). ^{31}P{^{1}H} NMR (C_6D_6, 121.5 MHz, 298 K): δ –50.5 (d, J_{PY} = 15.1 Hz). Anal. Calcd. for $C_{36}H_{43}N_9BKPY$: C, 56.04; H, 5.62; N, 16.34. Found: C, 56.14; H, 5.72; N, 16.36.

Synthesis of K$^+$[P(CH$_2$N-3,5-Me$_2$C$_6$H$_3$)$_3$YTp^{Me}]$^-$.THF.Benzene (12b). A mixture of [P(CH$_2$N-3,5-Me$_2$C$_6$H$_3$)$_3$Y(THF)$_3$] (653 mg, 0.909 mmol) and

References begin on page 79

$K[HB(C_3H_3N_2)_3]$ (305 mg, 0.909 mmol) was stirred in 20 mL of THF at room temperature for 5 h. The solution was filtered and remaining white solid was rinsed with 50 mL pentane and dried under vacuum for 3 h (77 %, 600 mg). ^1H NMR (C_6D_6, 300 MHz, 298 K): δ 2.32 (s, 18H, Ar C*H*$_3$), 2.68 (s, 9H, TpC*H*$_3$), 2.91 (s, 9H, TpC*H*$_3$), 3.32 (d, 6H, $^2J_{PH}$ = 7.3 Hz, PC*H*$_2$), 4.30 (b, 1H, B*H*), 5.9 (s, 3H, Tp*H*), 6.34 (d, Ar, 6H, *o-H*), 6.45 (s, Ar, 3H, *p-H*). $^{13}C\{^1H\}$ NMR (C_6D_6, 75.5 MHz, 298 K): δ 25.2 (d, J_{PC} = 17.4 Hz, P*C*H$_2$), 17.2 (s, Tp*C*H$_3$), 11.6 (s, Tp*C*H$_3$), 23.1 (s, Ar *C*H$_3$), 109.8, 138.5 and 119.4 (s, Ar, *o-C, p-C* and *m-C*), 142.3 (Ar, *ipso-C*), 144.6 (s, Tp*C*-1), 105.2 (s, Tp*C*-2), 139.1 (s, Tp*C*-3). $^{31}P\{^1H\}$ NMR (C_6D_6, 121.5 MHz, 298 K): δ – 48.6 (d, J_{PY} = 15Hz). Anal. Calcd. for $C_{42}H_{55}N_9BKPY$: C, 58.95; H, 6.48; N, 14.73. Found: C, 58.92; H, 6.37; N, 14.71.

Synthesis of $K^+[P(CH_2N\text{-}3,5\text{-}(CF_3)_2C_6H_3)_3YTp^{Me}]^-$.THF.Benzene (12c). A mixture of $[P(CH_2N\text{-}3,5\text{-}(CF_3)_2C_6H_3)_3Y(THF)_3]$ (608 mg, 0.573 mmol) and $K[HB(C_3H_3N_2)_3]$ (193.3 mg, 0.573 mmol) was refluxed in 20 mL of THF for 6-8 h. The solvent was then removed under vacuum after cooling the mixture to room temperature leaving an off-white solid. The product was washed with ~50 mL pentane and dried under vacuum for 3 h (68 %, 440 mg). ^1H NMR (C_6D_6, 300 MHz, 298 K): δ 1.81 (s, 9H, TpC*H*$_3$), 2.43 (s, 9H, TpC*H*$_3$), 3.83 (d, 6H, $^2J_{PH}$ = 8.1 Hz, PC*H*$_2$), 4.33 (b, 1H, B*H*), 5.61 (s, 3H, Tp*H*), 6.47 (d, Ar, 6H, *o-H*), 6.75 (s, Ar, 3H, *p-H*). $^{13}C\{^1H\}$ NMR (C_6D_6, 75.5 MHz, 298 K): δ 30.8 (d, J_{PC} = 15.4 Hz, P*C*H$_2$), 116.5 and 113.2, 134.1 (s, Ar, *o-C, p-C* and *m-C*), 122.6 (q, *J* = 32.9 Hz, Ar*C*F$_3$), 155.8 (d, *J* = 5.5 Hz, *ipso-C*). $^{31}P\{^1H\}$ NMR (C_6D_6, 121.5 MHz, 298 K) δ: – 49.4 (d, J_{PY} = 15Hz). $^{19}F\{^1H\}$ NMR (C_6D_6, 282.1 MHz, 298 K): δ 14.75 (s). Anal. Calcd for $C_{42}H_{37}F_{18}N_9PBKY$: C, 42.77; H, 3.16; N, 10.69. Found: C, 42.92; H, 3.28; N, 10.63.

References begin on page 79

X-ray Crystallography - Each crystal was covered with paratone, mounted on a glass fibre and rapidly placed into the cold N_2-stream of the Kryo-Flex low temperature device. The X-ray data were collected using the SMART[60] software on a Bruker APEX CCD diffractometer using a graphite monochromator with Mo Kα radiation (λ= 0.71073 Å). Details of crystal data, data collection and structure refinement are listed in Table 2.1, 2.2 and 2.3. Data reduction was performed using SAINTPlus[61] software, and data were corrected for absorption using SADABS.[62] The structures were solved by direct methods using SIR97[63], refined by full-matrix least squares on F^2 using SHELXL-97[64] and the WinGX[65] software package, and the thermal ellipsoid plots were produced using ORTEP32.[66] All non-hydrogen atoms were refined anisotropically and all hydrogen atoms were placed in appropriate geometrically calculated positions.

Details of selected crystallographic data, data collection and structure refinement of compounds **2b, 2b′, 3a**, **5c**, **10, 12c** and **9** are listed in Table 2.3, 2.4 and 2.5.

References begin on page 79

Table 2.3. Selected X-ray Crystallographic Data for Compounds **2b, 2b'**and **3a.**

	2b	**2b′**	**3a**
Empirical formula	$C_{39}H_{57}N_3O_3PY$	$C_{66}H_{83}Br_2N_6O_2P_2Y_2$	$C_{33}H_{45}N_3O_3PGd$
Formula weight	799.80	1391.97	719.94
Crystal system	Trigonal	Cubic	Cubic
a (Å)	12.3093(14)	9.758(4)	19.2900(8)
b (Å)	12.3093(14)	24.918(9)	19.2900(8)
c (Å)	16.548(4)	14.161(5)	19.2900(8)
α (deg)	90	90	90
β (deg)	90	96.894(5)	90
γ (deg)	120	90	90
V (Å^3)	2171.4(6)	3418(2)	7177.9(5)
Space group	$P3_1$/c	$P2_1$/n	*P* a-3
Z	2	4	8
Density (g/cm^3)	1.224	1.430	1.332
μ (Mo Kα) (mm^{-1})	1.421	1.623	1.925
Temperature (K)	293	293	293
Total no. of reflections	24637	29081	77491
Residuals: R_1; wR_2	0.0563; 0.1405	0.0724; 0.1283	0.0604; 0.1483

References begin on page 79

Table 2.4. Selected X-ray Crystallographic Data for Compounds **5c, 10** and **12c.**

	5c	**10**	**12c**
Empirical formula	$C_{39}H_{39}F_{18}N_3O_3PDy$	$C_{52}H_{64}N_6O_4P_2Ni$	$C_{42}H_{37}F_{18}N_9PBKY$
Formula weight	1197.24	1075.2	2869.9
Crystal system	Monoclinic	Trigonal	Triclinic
a (Å)	13.101(3)	34.6050(18)	12.8569(15)
b (Å)	21.381(6)	34.6050(18)	13.5299(16)
c (Å)	17.083(4)	12.1404(13)	18.278(2)
α (deg)	90	90	71.7250(10)
β (deg)	92.847(3)	90.00	72.6370(10)
γ (deg)	90	120	79.9150(10)
V ($Å^3$)	4779(2)	12590.45(16)	2869.9(6)
Space group	*P* 121/n1	*R*-3	*P*-1
Z	4	9	2
Density (g/cm^3)	1.662	1.134	1.539
μ (Mo Kα) (mm^{-1})	1.150	0.449	1.222
Temperature (K)	293	298	293
Total no. of reflections	11074	24637	10101
Residuals: R_1; wR_2	0.0397; 0.114	0.0522; 0.1307	0.0462; 0.1347

References begin on page 79

Table 2.5. Selected X-ray Crystallographic Data for Compound **9**

	9
Empirical formula	$C_{80}H_{78}F_{36}N_9O_6P_2Y_2Pt$
Formula weight	7225.6
Crystal system	Monoclinic
a (Å)	26.998(9)
b (Å)	12.941(4)
c (Å)	28.785(9)
α (deg)	90
β (deg)	92.224(5)
γ (deg)	90
V (Å^3)	10049.36(6)
Space group	*C* 2/c
Z	1
Density (g/cm^3)	1.19
μ (Mo Kα) (mm^{-1})	1.595
Temperature (K)	293
Total no. of reflection	10101
Residuals: R_1; wR_2	0.0624; 0.1012

References begin on page 79

2.5 References

1. Miller, J. S.; Epstein, A. J., *Angew. Chem.* **1994,** 106, (4), 399.
2. Sakamoto, M.; Manseki, K.; Okawa, H., *Coord. Chem. Rev.* **2001,** 219-221, 379.
3. Benelli, C.; Gatteschi, D.; Carnegie, D. W.; Carlin, R. L., *J. Am. Chem. Soc.* **1985,** 107, (8), 2560.
4. Zaleski, C. M.; Depperman, E. C.; Kampf, J. W.; Kirk, M. L.; Pecoraro, V. L., *Angew. Chem., Int. Ed.* **2004,** 43, (30), 3912.
5. Andruh, M.; Ramade, I.; Codjovi, E.; Guillou, O.; Kahn, O.; Trombe, J. C., *J. Am. Chem. Soc.* **1993,** 115, (5), 1822.
6. Chen, F.; Lu, W. M.; Zhu, Y.; Wu, B.; Zheng, X. M., *J. Coord. Chem.* **2009,** 62, (5), 808.
7. Wu, B., *J. Coord. Chem.* **2008,** 61, (16), 2558.
8. Tanase, S.; Reedijk, J., *Coord. Chem. Rev.* **2006,** 250, (19-20), 2501.
9. Li, G. M.; Akitsu, T.; Sato, O.; Einaga, Y., *J. Coord. Chem.* **2004,** 57, (3), 189.
10. Cui, Y.; Zheng, F. K.; Huang, J. S.; Qian, Y. T., *Chin. J. Struct. Chem.* **2001,** 20, (2), 112.
11. Bencini, A.; Benelli, C.; Caneschi, A.; Dei, A.; Gatteschi, D., *Inorg. Chem.* **1986,** 25, (4), 572.
12. Wu, B.; Zheng, Y. L.; Ng, S. W., *J. Coord. Chem.* **2008,** 61, (22), 3674.
13. Seminara, A.; Giuffrida, S.; Musumeci, A.; Fragala, I., *Inorg. Chim. Acta* **1984,** 95, (4), 201.
14. Zhao, H. H.; Lopez, N.; Prosvirin, A.; Chifotides, H. T.; Dunbar, K. R., *Dalton Trans.* **2007**, (8), 878.

References begin on page 79

15. Chen, W. T.; Guo, G. C.; Wang, M. S.; Xu, G.; Cai, L. Z.; Akitsu, T.; Akita-Tanaka, M.; Matsushita, A.; Huang, J. S., *Inorg. Chem.* **2007,** 46, (6), 2105.

16. Murugesu, M.; Mishra, A.; Wernsdorfer, W.; Abboud, K. A.; Christou, G., *Polyhedron* **2006,** 25, (2), 613.

17. Ramade, I.; Kahn, O.; Jeannin, Y.; Robert, F., *Inorg. Chem.* **1997,** 36, (5), 930.

18. Tilley, T. D.; Andersen, R. A., *J. Am. Chem. Soc.* **1982,** 104, (6), 1772.

19. Costes, J. P.; Auchel, M.; Dahan, F.; Peyrou, V.; Shova, S.; Wernsdorfer, W., *Inorg. Chem.* **2006,** 45, (5), 1924.

20. Costes, J. P.; Dahan, F.; Donnadieu, B.; Garcia-Tojal, J.; Laurent, J. P., *Eur. J. Inorg. Chem.* **2001**, (2), 363.

21. Costes, J. P.; Dahan, F.; Dupuis, A.; Laurent, J. P., *Inorg. Chem.* **1997,** 36, (16), 3429.

22. Costes, J.-P.; Dahan, F.; Dumestre, F.; Clemente-Juan, J. M.; Garcia-Tojal, J.; Tuchagues, J.-P., *Dalton Trans.* **2003**, (3), 464.

23. Sakamoto, M.; Kitakami, Y.; Sakiyama, H.; Nishida, Y.; Fukuda, Y.; Sakai, M.; Sadaoka, Y.; Matsumoto, A.; Okawa, H., *Polyhedron* **1997,** 16, (19), 3345.

24. Zhou, Y.; Hong, M.; Wu, X., *Chem. Commun.* **2006**, (2), 135.

25. Beletskaya, I. P.; Voskoboynikov, A. Z.; Chuklanova, E. B.; Kirillova, N. I.; Shestakova, A. K.; Parshina, I. N.; Gusev, A. I.; Magomedov, G. K. I., *J. Am. Chem. Soc.* **1993,** 115, (8), 3156.

26. Bencini, A.; Benelli, C.; Caneschi, A.; Carlin, R. L.; Dei, A.; Gatteschi, D., *J. Am. Chem. Soc.* **1985,** 107, (26), 8128.

References begin on page 79

27. Radecka-Paryzek, W.; Patroniak, V.; Lisowski, J., *Coord. Chem. Rev.* **2005,** 249, (21-22), 2156.

28. Bunzli, J. C. G.; Petoud, S.; Piguet, C.; Renaud, F., *J. Alloys Compd.* **1997,** 249, (1-2), 14.

29. Wiecko, M.; Roesky, P. W., *Organometallics* **2009,** 28, (4), 1266.

30. Meyer, G., *Angew. Chem., Int. Ed.* **2008,** 47, (27), 4962.

31. Noh, W.; Girolami, G. S., *Polyhedron* **2007,** 26, (14), 3865.

32. Avignant, D.; Largeau, E.; Gaumet, V.; Dugat, P.; El-Ghozzi, M., *J. Alloys Compd.* **1998,** 275, 1.

33. Hu, Z. W.; Kaindl, G.; Muller, B. G., *J. Alloys Compd.* **1997,** 246, (1-2), 177.

34. Panda, T. K.; Zulys, A.; Gamer, M. T.; Roesky, P. W., *J. Organomet. Chem.* **2005,** 690, (23), 5078.

35. Gamer, M. T.; Rastatter, M.; Roesky, P. W.; Steffens, A.; Glanz, M., *Chem. Eur. J.* **2005,** 11, (10), 3165.

36. Tolman, C. A., *J. Am. Chem. Soc.* **1970,** 92, (10), 2953.

37. Hultzsch, K. C.; Spaniol, H. P.; Okuda, J., *Angew. Chem., Int. Ed.* **1999,** 38, (1-2), 227.

38. Feindel, K. W.; Wasylishen, R. E., *Can. J. Chem.* **2004,** 82, (1), 27.

39. Han, H.; Elsmaili, M.; Johnson, S. A., *Inorg. Chem.* **2006,** 45, (18), 7435.

40. Grim, S. O.; Sangokoya, S. A., *J. Chem. Soc., Chem. Commun.* **1984,** (23), 1599.

41. Pinkerton, A. A.; Earl, W. L., *J. Chem. Soc., Dalton Trans.* **1979,** (9), 1347.

42. Benelli, C.; Gatteschi, D., *Chem. Rev.* **2002,** 102, (6), 2369.

References begin on page 79

43. Ishikawa, N.; Sugita, M.; Ishikawa, T.; Koshihara, S.; Kaizu, Y., *J. Phys. Chem. B* **2004,** 108, (31), 11265.

44. Harr, C. M.; Nolan, S. P.; Marshall, W. J.; Moloy, K. G.; Prock, A.; Giering, W. P., *Organometallics* **1999,** 18, (4), 474.

45. Dickman, M. H., *Acta Crystallogr. Sec. E* **2001,** 57, m220.

46. Decastro, B.; Rangel, M.; Raynor, J. B., *J.Chem. Soc., Dalton Trans.* **1990**, (11), 3311.

47. Wayland, B. B.; Abdelmag, M. E., *J. Am. Chem. Soc.* **1974,** 96, (15), 4809.

48. Wayland, B. B.; Minkiewi, J. V.; Abdelmag, M. E., *J. Am. Chem. Soc.* **1974,** 96, (9), 2795.

49. Marques, N.; Sella, A.; Takats, J., *Chem. Rev.* **2002,** 102, (6), 2137.

50. Takats, J., *J. Alloys Compd.* **1997,** 249, (1-2), 52.

51. Bell, Z. R.; Motson, G. R.; Jeffery, J. C.; McCleverty, J. A.; Ward, M. D., *Polyhedron* **2001,** 20, (15-16), 2045.

52. Trofimen, S., *J. Am. Chem. Soc.* **1966,** 88, (8), 1842.

53. Han, H.; Johnson, S. A., *Eur. J. Inorg. Chem.* **2008,** (3), 471.

54. Xu, X. P.; Zhang, Z. J.; Yao, Y. M.; Zhang, Y.; Shen, Q., *Inorg. Chem.* **2007,** 46, (22), 9379.

55. Pangborn, A. B.; Giardello, M. A.; Grubbs, R. H.; Rosen, R. K.; Timmers, F. J., *Organometallics* **1996,** 15, (5), 1518.

56. Spin, *EPR simulation program, A. Ozarowski, National High Magnetic Field Laboratory, Florida.*

References begin on page 79

57. Sim, *version 2004-5, An EPR Simulation Program, H. Weihe, Department of Chemistry, University of Copehagen.*

58. Bradley, D. C.; Ghotra, J. S.; Hart, F. A., *J. Chem. Soc., Dalton Trans.* **1973**, (10), 1021.

59. Bradley, D. C.; Ghotra, J. S.; Hart, F. A., *J. Chem. Soc.,Chem. Commun.* **1972**, (6), 349.

60. SMART, *Molecular analysis research tool; Bruker AXS Inc.: Madison, WI.* **2001**.

61. SAINTPlus, *Data reduction and correction program; Bruker AXS Inc.: Madison, WI.*

62. SADABS, *An empirical absorption correction program; Bruker AXS Inc.: Madison, WI,* **2001**.

63. Altomare, A.; Burla, M. C.; Camalli, M.; Cascarano, G. L.; Giacovazzo, C.; Guagliardi, A.; Moliterni, A. G. G.; Polidori, G.; Spagna, R., *J. Appl. Crystallogr.* **1999,** 32, (1), 115.

64. Sheldrick, G. M., *SHELXL-97; Universitat Gottingen: Gottingen.*

65. Farrugia, L. J., *J. Appl. Crystallogr.* **1999,** 32, 837.

66. Farrugia, L. J., *J. Appl. Crystallogr.* **1997,** 30, 565.

References begin on page 79

CHAPTER-3

A Phosphine-Mediated Through-Space Exchange Coupling Pathway for Unpaired Electrons in a Heterobimetallic *d-f* Metal Complexes

3.1 Introduction

In molecular magnets,[1-3] exchange coupling[4,5] between homo or heteronuclear paramagnetic metal ions depend on the electronic and magnetic properties of the participating metal centres. Progress in the field of molecular magnets demands new synthetic approaches to design intricate architectures, which can include macromolecular polynuclear complexes.[6] Typically, the same bonding interactions that assemble these

References begin on page 121

complexes and networks are also responsible for the transmission of exchange coupling by a super-exchange pathway. Single atom bridging metal centres often perform this role, but larger π-conjugated bridging ligands, such as cyano donors and examples of other bridging donors ligands as stated in Chapter 1, are also capable of propagating exchange coupling [7,8]. An appropriate ligand design that could facilitate a building block approach to magnetic materials would be beneficial to this field, and in particular, building blocks with at least axial symmetry would aid in the modelling of magnetically anisotropic systems.

It has been shown earlier that trianionic tripodal triamidophosphine ligands such as $P(CH_2NHPh)_3$ can be used to generate both polynuclear[9,10] as well as heterobimetallic complexes,[11] as depicted in Figure 3.1. In the case of exchange or super-exchange coupling between the two metal centres labelled M and M′ in paramagnetic heterobimetallic analogues, these $P(CH_2NPh)_3M$ moieties could act as valuable building blocks. Due to the ubiquity of phosphine donors in coordination chemistry, it should prove facile to utilize these complexes in the assembly of magnetic polynuclear complexes and modify them to generate extended networks. The tripodal ligands are designed in such a way that separates both metal centres M and M′ from each other by four σ-bonds, which would seem to preclude any significant exchange coupling via this pathway. However, the minor lobe of the lone pair associated orbital extends the phosphine towards the metal centre labelled in M′, which in theory could provide a unique combined through-bond/through-space pathway for exchange coupling. The study of heterodinuclear complexes containing both lanthanides and transition metal ions (*d-f* complexes)[12-22] is of current interest due to the large magnetic anisotropies of the

References begin on page 121

lanthanides.[23] These lanthanide metal ions, mainly heavier lanthanides (f^9-f^{13}), have also been utilized to design single-molecule magnets.[15,20, 24-28] This chapter describes the through-space exchange coupling between *d-f* metal centres (M and M') via a bridging phosphine donor.

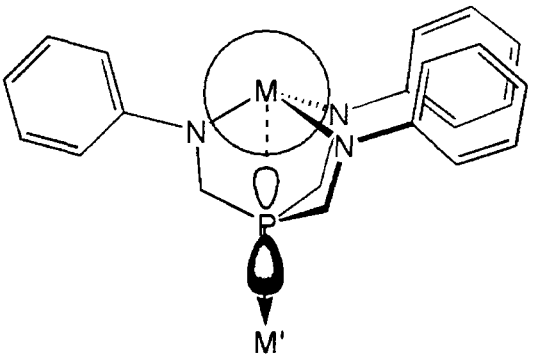

Figure 3.1. Through-space interactions in tripodal complexes of $P(CH_2NPh)_3$ with metal complexes M and M' with the minor and major lobes of lone pair orbital on phosphorus.

3.2. Results and Discussions

3.2.1 Synthesis of the Ligand Precursor

To achieve the goal of stable well-defined lanthanide building blocks, we modified the tripodal triamido donors we had previously used (Chapter 2) to incorporate additional donors and to satisfy the desire of the trivalent lanthanides to form complexes with high coordination numbers (Chapter 2). The target ligand precursor, $P(CH_2NHC_6H_4\text{-}2\text{-}CO_2Me)_3$ (**13**), was synthesized via the reaction of $P(CH_2OH)_3$ with methyl anthranilate, $H_2NC_6H_4\text{-}2\text{-}CO_2Me$, in toluene, as shown in equation 3.1. The water produced in this reaction was removed by azeotropic distillation using a Dean-Stark apparatus.[29] The

References begin on page 121

solution of **13** oxidizes rapidly in air, and thus, the solid product was stored under an inert atmosphere.

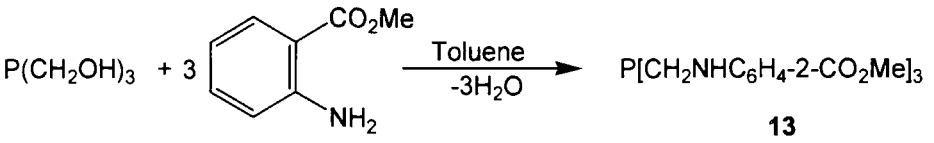

(3.1)

X-ray quality crystals of **13** were obtained by slow evaporation of a benzene/hexamethyldisiloxane solution. An ORTEP depiction of the solid-state molecular structure is shown in Figure 3.2. The structure features intramolecular hydrogen bonding between the carbonyl and amino functionalities. The positions of the three amino hydrogens were refined using isotropic thermal parameters. The sum of C-P-C angles is 298.31(2)°, typical for phosphine donors with C-P-C angles less than the tetrahedral angle (109.5°).[30]

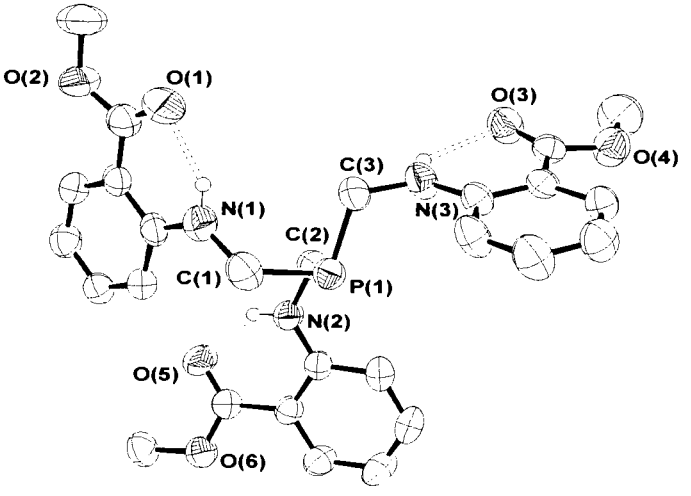

Figure 3.2. Solid-state molecular structure of $[P(CH_2NHC_6H_4\text{-}2\text{-}CO_2Me)_3]$ **(13)** as determined by X-ray crystallography. Hydrogen atoms are omitted for clarity, except those associated with N(1), N(2) and N(3). Hydrogen bonding interactions are shown as dashed lines. Selected bond angles (°): C(1)-P(1)-C(2), 102.62(13); C(1)-P(1)-C(3), 98.44(14); C(1)-P(1)-C(3), 97.25(13).

References begin on page 121

3.2.1 Synthesis of a Mononuclear Yttrium Complex

The similar ionic radius of Y(III) to the ionic radii of the heavier lanthanides, such as Gd(III), prompted us to begin our studies by preparing an yttrium complex of **13** to be used as a diamagnetic model complex. The reaction of **13** with 1 equivalent of $Y[N(SiMe_3)_2]_3$ in toluene at room temperature resulted in the precipitation of orthorhombic yellow crystals of $P(CH_2NC_6H_4\text{-}2\text{-}CO_2Me)_3Y$ (**14**), as shown in equation 3.2. The aromatic region of the ^1H NMR spectrum of **14** features 4 multiplets, assigned by a combination of 2D-COSY and 2D-NOESY spectroscopy. Analysis of the reaction mixture via ^1H and $^{31}P\{^1H\}$ NMR spectroscopy revealed that no side products were formed, other than the byproduct $HN(SiMe_3)_2$.

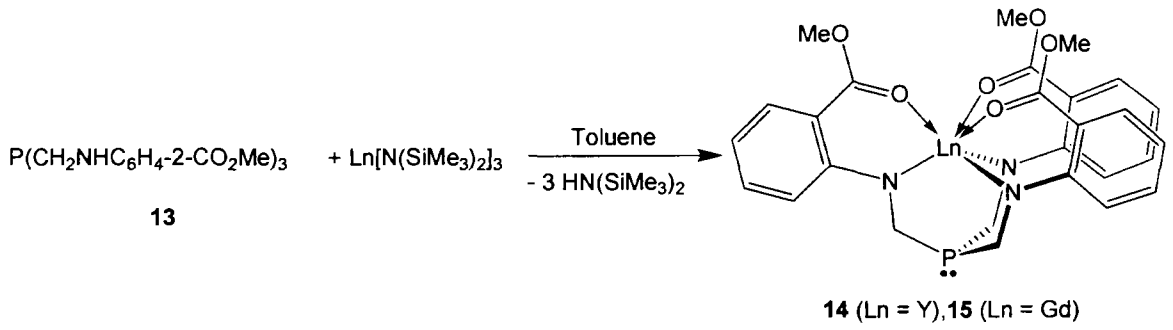

(3.2)

The solid-state molecular structure of **14** was determined by X-ray crystallography, and an ORTEP depiction is shown in Figure 3.3. Despite the collection of X-ray diffraction data on several crystals of **14** that appeared suitable for solid-state structure determination, twinning complicated the solution of this structure. All atoms in the model structure were treated isotropically, and some restraints had to be used, which limited the accuracy of bond lengths and angles. Complex **14** has crystallographic C_3 symmetry, and features a six-coordinate Y centre chelated by the ligand amido donors and

References begin on page 121

the carbonyl oxygens of the ester functionality. The phosphine lone pair is directed away from the metal, and thus, is available for donation to a second metal.

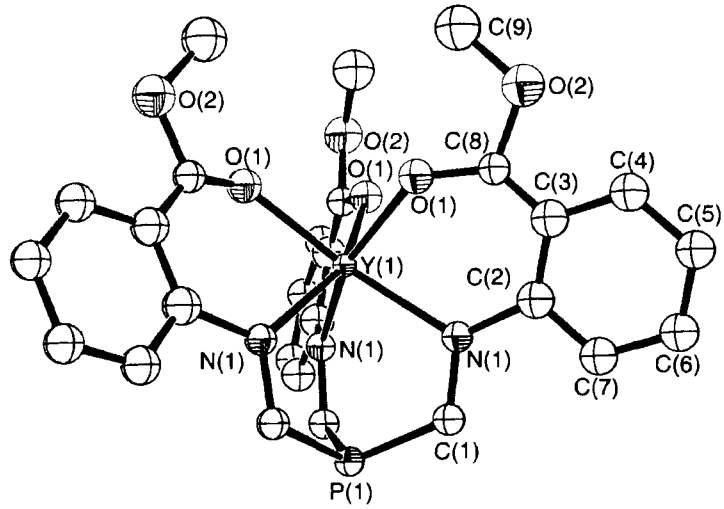

Figure 3.3. Solid-state molecular structure of $[P(CH_2NC_6H_4\text{-}2\text{-}CO_2Me)_3]Y$ (**14**) as determined by X-ray crystallography. Hydrogen atoms are omitted for clarity.

Alternatively, mononuclear trivalent lanthanide complexes (**14** and **15**) could also be prepared via the reaction of 1 equivalent of complex **16** with 1 equivalent of anhydrous lanthanide trichloride in toluene (Scheme 3.1). While NMR scale reactions confirmed the presence of complexes **14** and **15** in both ^{1}H and $^{31}P\{^{1}H\}$ NMR spectra, scaling up the reaction always resulted in the formation of the mixture of compounds, as observed in NMR spectra.

References begin on page 121

Scheme 3.1.

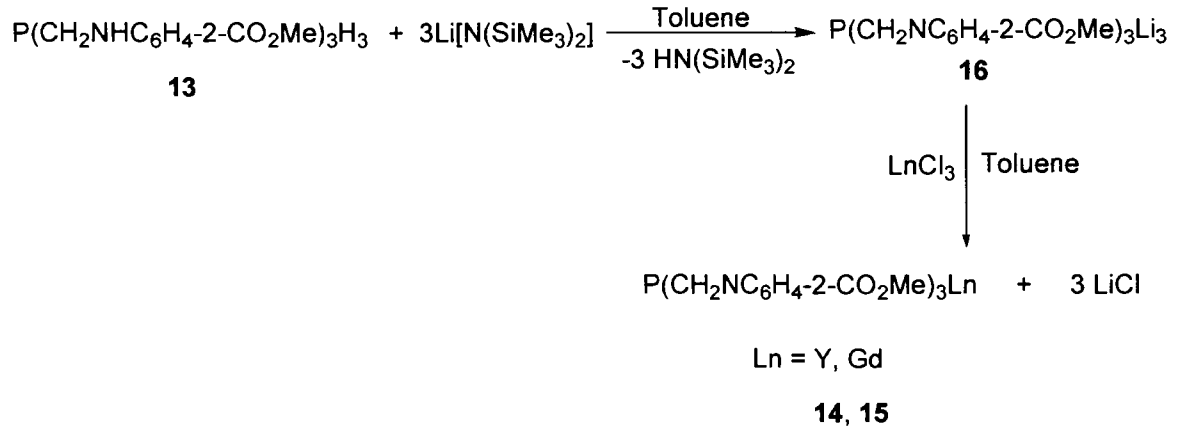

3.2.3 Synthesis of a Li-salt of Ligand Precursor

The lithium salt of ligand precursor (**16**), shown in Scheme 3.1 can be easily produced via the reaction of 3 equivalents of lithium bis(trimethylsilyl) amide with a single equivalent of ligand precursor (**13**) in toluene (Scheme 3.1). Mixing of both reactants at room temperature, with toluene as the solvent, produced yellow X-ray quality crystals of compound **16**. Analysis of the isolated lithium salt by ^{1}H and $^{31}P\{^{1}H\}$NMR spectroscopy proved it to be devoid of any side product.

The solid-state molecular structure of **16** was determined by X-ray crystallography, and an ORTEP depiction is shown in Figure 3.4. The complex displayed approximate C_3 symmetry, with all lithium ions bridged between amido donors. In many of the reported lithium salts of amido ligand, lithium ions require an oxygen containing external donor moiety, such as THF or ether, for stabilization.[17,31] However, the present compound (**16**) contains built-in oxygen atoms within the ester functions of the methyl anthranilate arms. The X-ray data showed the presence of two cocrystallized toluene

References begin on page 121

molecules which were removed from the powder of **16**, after several hours of drying, as confirmed by elemental analysis.

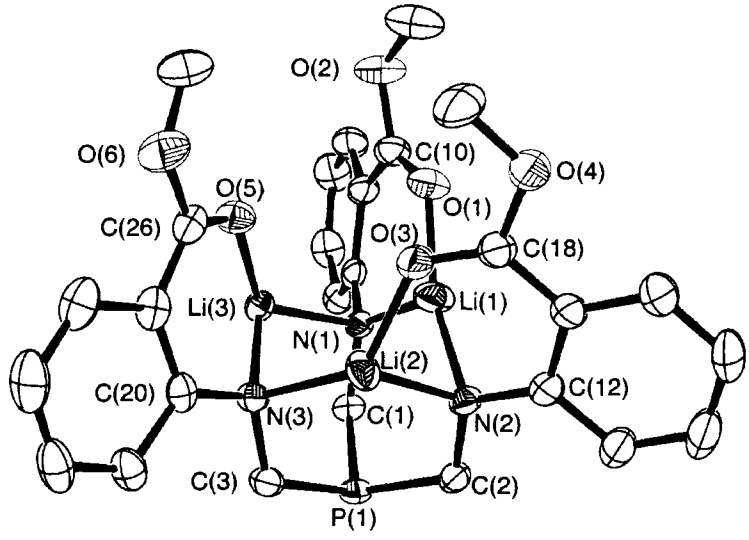

Figure 3.4. Solid-state structure of $[P(CH_2NC_6H_4\text{-}2\text{-}CO_2Me)_3]Li_3$ **(16)** as determined by X-ray crystallography. Hydrogen atoms and co-crystallized toluene molecules are omitted for clarity. Selected bond angles (°): C(1)-P(1)-C(2), 106.48(10); C(1)-P(1)-C(3), 107.85(10); C(2)-P(1)-C(3), 106.56(11). Selected bond distances (Å): Li(1)-N(1), 1.936(5); Li(1)-N(2), 1.996(5); Li(2)-N(2), 1.982(5); Li(2)-N(3), 2.014(4); Li(1)-Li(3), 2.777(6); Li(1)-Li(2), 2.697(7); Li(3)-P(1), 2.575(4).

3.2.4 Through-Space ^{31}P-^{89}Y Coupling

The $^{31}P\{^1H\}$ NMR spectrum chemical shift of **13** is δ –33.6 ppm, whereas in complex **14,** the ^{31}P signal is observed at δ –57.0 ppm. This upfield shift is unusual, since the increase in C-P-C angles upon coordination of a large metal such as Y should induce the opposite effect;[32] we have previously ascribed this unusual shift in related complexes

References begin on page 121

to interactions of the minor lobe of the lone pair with the adjacent metal centre (Figure 3.1).[11]

Also notable in the $^{31}P\{^{1}H\}$ NMR of complex **14** is the observation of a 15 Hz coupling between yttrium (^{89}Y, I = ½) and phosphorus. This $^{3}J_{PY}$ value is large considering that $^{1}J_{PY}$ values are typically in the range of 50-80 Hz,[33, 34] and $^{2}J_{PY}$ values are typically 4 to 6 Hz, though values as large as 11 Hz have been reported in conjugated systems.[34, 35] The largely ionic nature of bonding to Y suggests that $^{3}J_{PY}$ coupling constants should be smaller, due to smaller Fermi contact terms, but we could find no $^{3}J_{PY}$ values in the literature for comparison. This suggests that the coupling between Y and P could be mediated by a through-space interaction. The X-ray data suggest an approximate Y-P distance of 3.36 Å, and the proximity of the phosphorus and Y atoms could allow a formal bonding interaction to occur between the minor lobe of the phosphorus lone pair and the metal.

An ab initio calculation using the density functional theory (DFT) B3YLP method and DGDZVP basis set was used to test this theory. This calculation predicts a J_{PY} value of –11.2 Hz, whose absolute value is close to the –15 Hz observed experimentally, and the Fermi contact term of –10.2 Hz predominates. The sign of this value is consistent with a direct interaction between nuclei mediated by a pair of electrons and the opposite signs of the magnetogyric ratios for ^{31}P and ^{89}Y. The paramagnetic spin-orbit, dipolar, and diamagnetic spin-orbit contributions to the coupling constant are all calculated to be much smaller than the Fermi contact term, with values of –0.8, –0.14 and –0.026 Hz, respectively. An analysis of the molecular orbitals predicted[36] from this calculation determined that only the HOMO-3 has any significant overlap of density between P and

References begin on page 121

Y, as required for a Fermi contact term. A depiction of this molecular orbital, which is primarily associated with the lone pair on phosphorus, is shown in Figure 3.5. The minor lobe of the lone pair orbital clearly extends back towards the Y centre, allowing a through-space interaction.

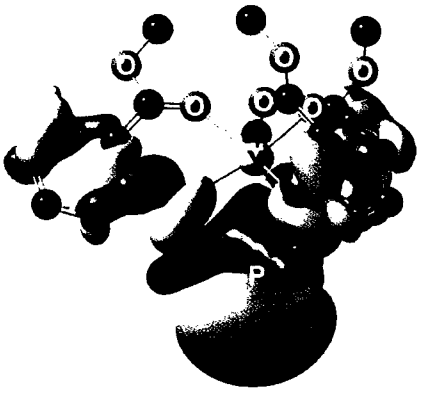

Figure 3.5. Depiction of the HOMO-3 orbital associated with the phosphorus lone pair, obtained from a DFT calculation.

3.2.5 Synthesis of a Mononuclear Gadolinium Complex

The reaction of the ligand precursor **13** with $Gd[N(SiMe_3)_2]_3$ produced the paramagnetic complex $P(CH_2NC_6H_4\text{-}2\text{-}CO_2Me)_3Gd$ (**15**), as shown in equation 3.3. Similar to the synthesis of **14**, yellow orthorhombic X-ray quality crystals precipitated from toluene. The crystal structures of both **14** and **15** are isomorphous, and only small metric differences in the unit cell parameters, due to the slightly larger size of Gd(III), were observed for this complex. As with complex **14**, this C_3 symmetric complex crystallized in a trigonal space group, and difficulties associated with twinning

References begin on page 121

complicated the solution of this structure; therefore connectivity could not be accurately determined.

The X-band EPR spectrum of a powdered sample of complex **15** was obtained at 77 K and is shown in Figure 3.6. The spectrum displays resonances from near zero-field to 12500 G. The spectrum can be adequately modelled using only a B_{20} value of ±0.194 cm^{-1} (±2080 G), and a g value of 1.994.[37] As would be expected for Gd(III), the B_{40} B_{43}, B_{60}, B_{63} and B_{66} crystal field parameters were found to be much smaller than the B_{20} term, and attempts to fit these parameters did not produce a significantly better model of the experimental data; in fact more significant improvements in fit were obtained by modelling the line widths anisotropically. The zero-field splitting in **15** is almost an order of magnitude larger than has been reported for a related anionic bis(phthalocyaninato)gadolinium complex,[38] whose Dy, Tb,[39] and Ho[40] analogues have been shown to behave as mononuclear single-molecule magnets due to the large ligand induced zero-field splitting of their ground states. The approximate energy difference between the lowest and highest sublevels at zero-field for complex **15** is 2.328 cm^{-1}; however, the relative sign of B_{20} cannot be determined from this EPR data, and thus it is not clear if the $S = \pm 1/2$ or $S = \pm 7/2$ substates are lowest in energy.

References begin on page 121

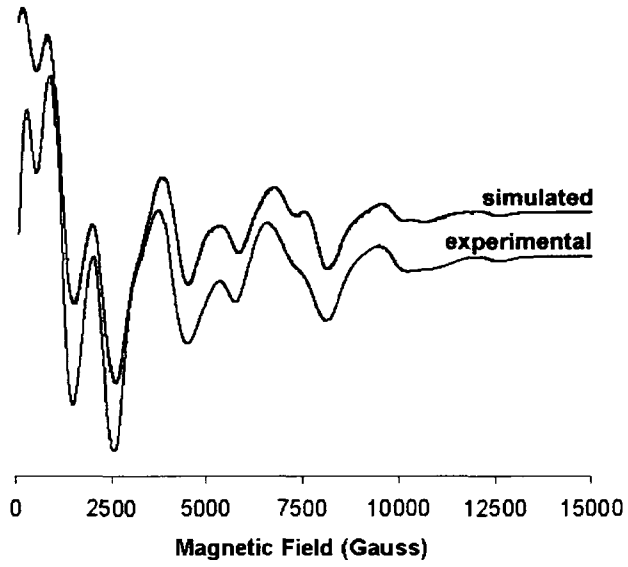

Figure 3.6. X-band EPR spectrum of a powdered sample of **15** at 77 K (lower trace) and a simulated spectrum (upper trace) with $S = 7/2$, $B_{20} = \pm 0.194$ cm^{-1} ($\pm$ 2080 G), $g = 1.994$, and anisotropic line widths ($\parallel$ = 240 G, $\perp$ = 360 G).

3.2.6 Magnetic Susceptibility of Complex 15

The molar magnetic susceptibility χ_m of a powdered sample of complex **15** immobilized in eicosane was studied over the temperature range of 300.0-2.0 K using a SQUID magnetometer. A plot of the product of magnetic susceptibility and temperature ($\chi_m T$) versus temperature for complex **15** is shown in Figure 3.7. The $\chi_m T$ value of **15** at room temperature of 7.82 cm^3·K·mol^{-1} corresponds to the expected value of Gd^{3+} ion at room temperature (7.88 cm^3·K·mol^{-1}), and is also in agreement with the room temperature toluene solution value of 7.8 cm^3·K·mol^{-1} determined using Evans' method. The magnitude of $\chi_m T$ for the powdered sample of **15** decreased slightly below 15 K, and reaches a value of 7.43 cm^3·K·mol^{-1} at 2 K. The modelled temperature dependence of $\chi_m T$ obtained using the negative value of the B_{20} crystal field value, –0.194 cm^{-1}, obtained

References begin on page 121

from the simulation of the EPR data is also shown in Figure 3.7, as a solid line. This model predicts a slight drop in $\chi_m T$ at low temperatures, as is observed, but the fit is not sufficient to determine the sign of B_{20}, because a similar decrease in $\chi_m T$ is predicted using a positive B_{20} value. The calculated magnetic anisotropy at low temperatures for this magnitude of B_{20} is not insignificant at temperatures below 20 K, and the contributions from $\chi_{\parallel m}T$ and $\chi_{\perp m}T$ are shown as dashed lines in Figure 3.7. At 1 K $\chi_{\parallel m}T$ and $\chi_{\perp m}T$ are predicted to be 15.74 and 3.31 $cm^3 \cdot K \cdot mol^{-1}$, respectively, when B_{20} is −0.194 cm^{-1}. For the corresponding positive value of B_{20}, the 1 K, $\chi_{\parallel m}T$ and $\chi_{\perp m}T$ values are 2.60 and 10.07, respectively. For the majority of *d-f* heteronuclear gadolinium complexes studied, exchange coupling is small and only observed at low temperatures, but little consideration has been given to the potential influence of crystal-field induced magnetic anisotropy at Gd^{3+} in the spin-spin coupling pathways that operate in these complexes. Regardless, the nearly temperature independent value of $\chi_m T$ in complex **15** facilitates the observation of spin-spin exchange coupling in heterobimetallic complexes prepared using this precursor.

References begin on page 121

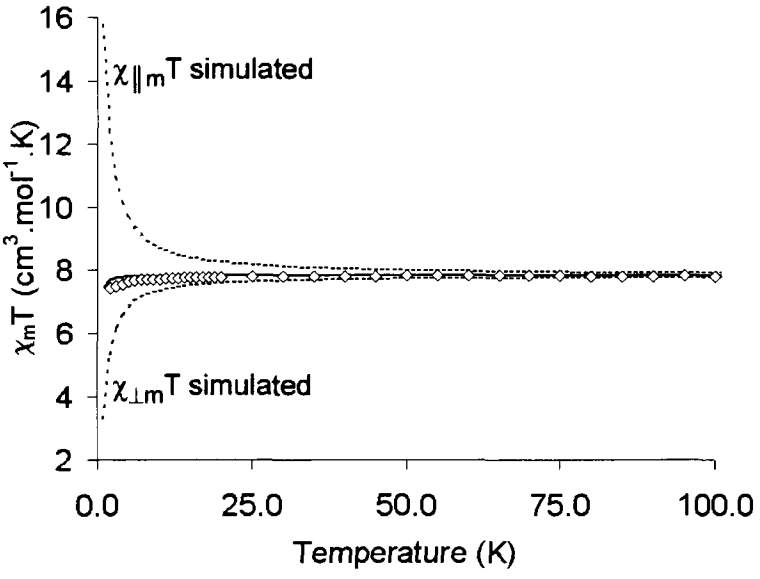

Figure 3.7. Plot of $\chi_m T$ versus temperature for complex **15**, shown as diamonds, along with the simulated fit, obtained using $B_{20} = -0.194$ cm^{-1} and $g = 1.994$, shown as a solid line. The calculated $\chi_{\parallel m}T$ and $\chi_{\perp m}T$ contributions obtained from the simulation are shown as dashed lines. The simulations were performed using the spin Hamiltonians $\hat{H}_z = [B_{20}(\hat{S}_z^2\text{-}21/4)] + gBH_0\hat{S}_z$ for the parallel component and $\hat{H}_{x,y} = [B_{20}(\hat{S}_z^2\text{-}21/4)] + gBH_0\hat{S}_{x,y}$ for the perpendicular component, where B represents the Bohr magneton and H_0 is the applied field.

A DFT geometry optimization calculation was performed on **15**, and the resultant calculated spin-density is shown in Figure 3.8. The unpaired spins are primarily located on the Gd(III) centre, which is expected due to the contracted nature of the *f*-orbitals; however, some spin density of the opposite sign is found on the amido and carbonyl donor atoms. Only a very small contribution from unpaired spin density is found on the phosphorus atom or the adjacent carbon atoms. To use complex **15** as a magnetic building block, it is necessary to observe exchange coupling between the gadolinium centre and a

References begin on page 121

transition metal bound to the available phosphine donor. The localized nature of the unpaired electrons on gadolinium necessitates a careful choice of transition metal to attach to the phosphine; it must be capable of delocalizing its unpaired electron density towards the gadolinium centre.

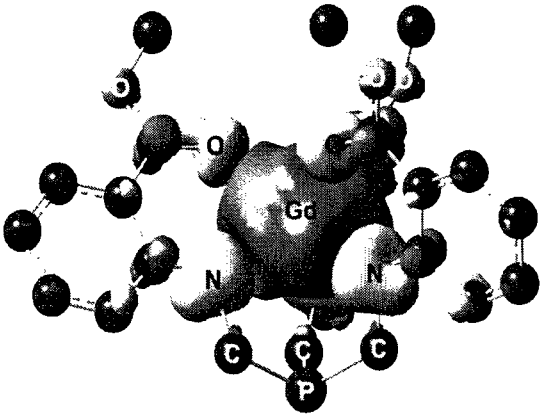

Figure 3.8. An isosurface of the calculated spin density for $P(CH_2NC_6H_4\text{-}2\text{-}CO_2Me)_3Gd$ (**15**).

3.3.7 Determining the Phosphine Donor Ability of Yttrium and Gadolinium Complexes From Their reactions with $[Rh(CO)_2(\mu\text{-}Cl)]_2$

The standard procedure to measure the phosphine donor ability of any carbonyl containing phosphines depends on the carbonyl stretching frequency. Various methods have been used in this regard, in which the reaction of phosphine complexes with *trans*-chloro carbonyl rhodium compound is the most extensively used method. As shown in Scheme 3.2, this method involves the reaction of one equivalent of a rhodium carbonyl compound with four equivalents of phosphine complexes **13**, **14** and **15**.

References begin on page 121

Scheme 3.2

$2\ P(CH_2NHC_6H_4\text{-}2\text{-}CO_2Me)_3$ (**13**) + $1/2\ [Rh(CO)_2(\mu\text{-}Cl)]_2 \longrightarrow$ *trans*-$Cl(CO)Rh[P(CH_2NHC_6H_4\text{-}2\text{-}CO_2Me)_3]_2$ (**17**)

$2\ P(CH_2NC_6H_4\text{-}2\text{-}CO_2Me)_3Y$ (**14**) + $1/2\ [Rh(CO)_2(\mu\text{-}Cl)]_2 \longrightarrow$ *trans*-$Cl(CO)Rh[P(CH_2NC_6H_4\text{-}2\text{-}CO_2Me)_3Y]_2$ (**18**)

$2\ P(CH_2NC_6H_4\text{-}2\text{-}CO_2Me)_3Gd$ (**15**) + $1/2\ [Rh(CO)_2(\mu\text{-}Cl)]_2 \longrightarrow$ *trans*-$Cl(CO)Rh[P(CH_2NC_6H_4\text{-}2\text{-}CO_2Me)_3Gd]_2$ (**19**)

The products precipitated as an orange-yellow powder after mixing the reagents and leaving the reaction mixture at room temperature in dichloromethane. Products were indentify as *trans*-rhodium carbonyl phosphine complexes by ^1H and $^{31}P\{^1H\}$ NMR spectroscopy. Comparison of CO stretching frequencies of all three complexes (**17**, **18** and **19**) revealed that the phosphine ligand (ν_{CO} = 1978.9 cm^{-1}) is less electron donating than the yttrium phosphine complex (ν_{CO} = 1963.4 cm^{-1}), which has a lesser donating ability than gadolinium complex (ν_{CO} = 1954.1 cm^{-1}). Comparison of these complexes with other phosphine donors showed that the strongest phosphine donor ability of complex **16,** has similar donor ability to P^tBu_3,[41, 42] which shows CO stretching frequency of 1954 cm^{-1} with rhodium carbonyl complex. Despite the fact that the phosphine lone pair is directed away from metal centers, the phosphine donor capability of trivalent lanthanide metal complexes affects the syntheses of heteronuclear complex. Introduction of metal ions to the ligand center strengthens the donor capability of metal complexes by increasing the sum of the C-P-C angles, which also depend on the size of the metal ion.

References begin on page 121

3.2.8 Syntheses of Heterobimetallic (*d-f*) Metal Complexes

To demonstrate that through-space exchange coupling is viable in heterobimetallic complexes using these tripodal amidophosphine ligands, a transition metal complex must be attached to the phosphine donor that satisfies two requirements: firstly, it must direct unpaired electron density towards the complexed gadolinium centre; secondly, it must have magnetic properties that are easy to model. We chose to use [TPP]Co (where [TPP] = 5, 10, 15, 20-tetrakis(4-methoxyphenyl)porphine) as the transition metal moiety, because it has a single unpaired electron in a nondegenerate orbital, and thus should exhibit straightforward magnetism. Additionally, the singly occupied molecular orbital (SOMO) in adducts of [TPP]Co is primarily the d_z^2 orbital directed perpendicular to the plane of the [TPP]Co moiety, and thus should directly overlap with the phosphine donor orbital. Related five-coordinate phosphine adducts of Co(II) porphyrins with diamagnetic phosphine donors are known.[43-45]

Complexes **3** and **4** reacted with [TPP]Co in toluene to provide brown-purple crystalline solids, which were identified as the heterobimetallic complexes [TPP]CoP($CH_2NC_6H_4$-2-$CO_2Me)_3$Ln (Ln = Y(**20**) or Gd (**21**)), as shown in equation 3.3.

References begin on page 121

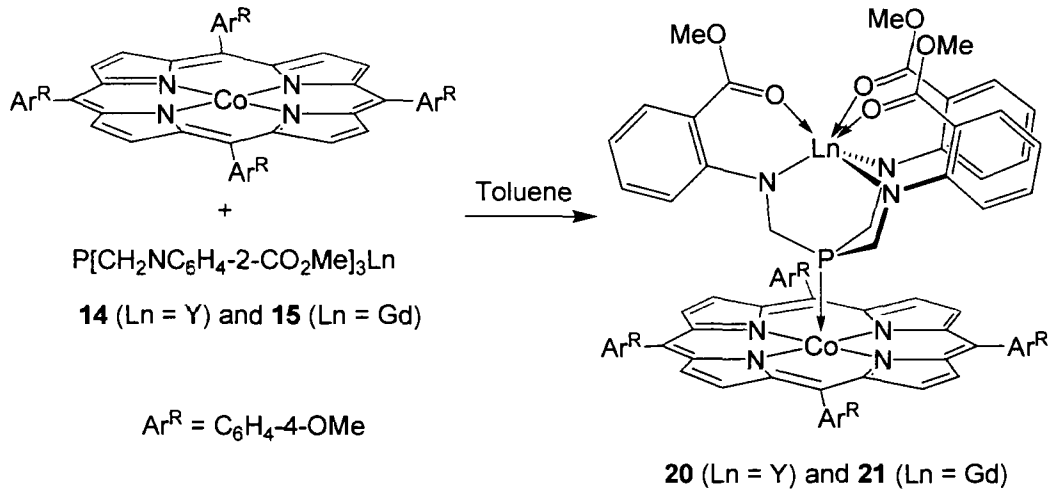

(3.3)

Single crystals of **20** and **21** were obtained from the slow evaporation of saturated toluene solutions. The initial solubility of these complexes in toluene appears kinetic, as the resultant product has only modest solubility. The solid-state molecular structures of **20** and **21** were determined by X-ray crystallography, and an ORTEP depiction of the solid-state molecular structure of **21** is shown in Figure 3.9. As anticipated, the triamido donors chelate the lanthanide centre, and the phosphine lone pair is bound to the [TPP]Co moiety. Although **20** and **21** display slightly different metrical parameters, they are isostructural. These structures further confirm the connectivity determined for the mononuclear complexes **15** and **16**; the tripodal ligand chelates via the amido donors and the carbonyl oxygens to the lanthanide metals. The Co-P bond length in complex **21** is 2.4128(9) Å; there is a large range of reported Co(II)-phosphine distances, which can be as short as 2.2127(8) Å[46] and as long as 2.479(5) Å.[47] The relatively elongated Co-P bond length in complex **21** can be rationalized from a crystal-field theory argument that the lone unpaired electron in this d^7 species occupies the d_z^2 orbital, which is directed towards the phosphine donor.

References begin on page 121

The ionic radius of Gd(III) is approximately 0.04 Å larger than the ionic radius of Y(III),[48] and this results in slightly different bond lengths between complexes **20** and **21**. In complex **21**, the average Gd-N distance is 2.330(2) Å and the average Gd-O bond length is 2.315(2) Å, whereas in complex **21** the average Y-N and Y-O bond lengths are 2.299(1) and 2.2771(9) Å, respectively. The P(1)···Y(1) distance of 3.2575(6) Å in **20** is less than 7 % longer than the longest reported Y-P bond length of 3.045(2) Å,[49] although shorter Y-P bond lengths are more typical.[33, 50] In comparison, the P(1)···Gd(1) distance of 3.2440(9) Å in **21** is actually shorter than the P(1)···Y(1) distance in **20**, which can be rationalized by the slightly larger size of the Gd(III) ion requiring a greater strain in the ancillary ligand to accommodate this large metal. This assertion is confirmed by the slightly smaller sum of C-P-C angles in **20** than in **21**, which are 324.69(17)°, and 326.70(26)° respectively. These values are approximately 28° larger than the sum of C-P-C angles for the ligand precursor, **13**, which can be attributed primarily to the coordination of the large lanthanide.[11]

References begin on page 121

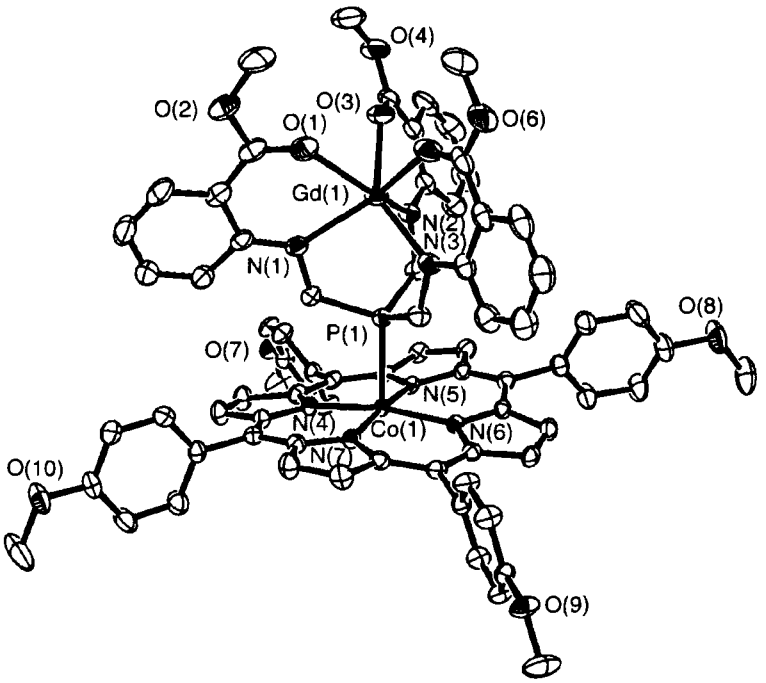

Figure 3.9. Solid-state molecular structure of [TPP]CoP($CH_2NC_6H_4$-2-$CO_2Me)_3$Gd **(21)** as determined by X-ray crystallography. Hydrogen atoms are omitted for clarity. Selected distances (Å): P(1)-Co(1), 2.4128(9); Gd(1)-N(1), 2.325(3); Gd(1)-N(2), 2.332(3); Gd(1)-N(3), 2.336(3); Gd(1)···P(1), 3.2440(9).

3.2.9 EPR Spectra of Complexes 20 and 21

The X-band EPR spectrum of a frozen toluene solution of [TPP]CoP($CH_2NC_6H_4$-2-$CO_2Me)_3$Y was obtained at 77 K and is shown in Figure 3.10. The EPR spectrum of **20** confirms the low spin S = ½ nature of the complex and that the complex remains a 1:1 adduct of **14** and [TPP]Co in solution. A simulated spectrum was obtained by considering the cobalt centre in **20** to have approximate axial symmetry and was fitted using anisotropic $g_{\|}$ and $g_{\perp}$ values of 1.98 and 2.21, respectively. The simulation revealed that the phosphorus superhyperfine coupling constants $A_{P\|}$ and $A_{P\perp}$ of 176 and 144 G,

References begin on page 121

respectively are larger than the cobalt (^{59}Co, I = 7/2) hyperfine coupling constants $A_{Co\|}$ and $A_{Co\perp}$ of 50 and 63 G, respectively. The simulated spectrum is also shown in Figure 3.10. In the room-temperature solution EPR spectra, the signal is a doublet due to superhyperfine coupling to ^{31}P, and A_{Co} cannot be resolved, which further confirms that in these adducts have considerable unpaired electron density residing on the phosphine donor.

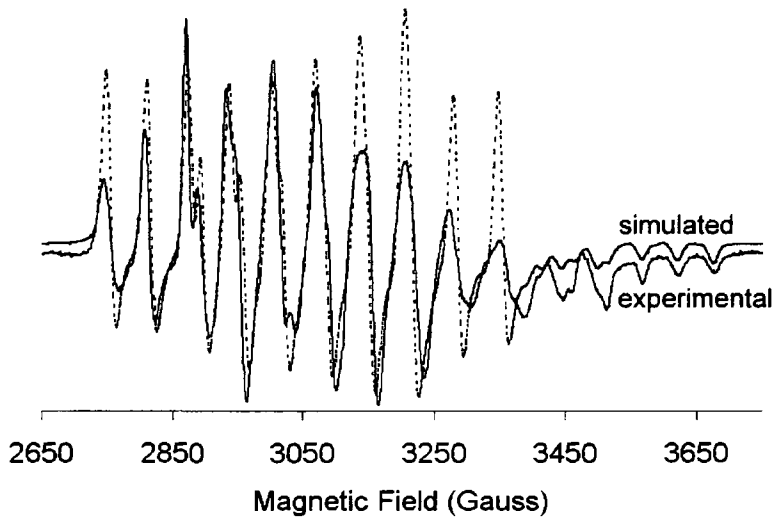

Figure 3.10. X-band EPR spectrum of a powdered sample of **20** at 77 K (solid line) and a simulated spectrum (dotted line, offset above) obtained using $g_{\|}$ = 1.98, $g_{\perp}$ = 2.21, $A_{P\|}$ = 176 G, $A_{P\perp}$= 144 G, $A_{Co\|}$ = 50 G, $A_{Co\perp}$ = 63 G.

It has previously been shown[51] in related complexes that, by using third order perturbation theory, the g values can be used to determine the energy separation of the $^2A_1$ ground state and the ^2E, $^4A_2$, and ^4E excited states in phosphine adducts of cobalt porphyrins. In this complex, the lowest energy d-orbitals should be the degenerate d_{xz} and d_{yz} orbitals, followed by the d_{xy} orbital and the singly occupied d_{z^2} orbital. The $d_{x^2-y^2}$

References begin on page 121

orbital is highest in energy and is unoccupied in the ground state. The c_1, c_3 and c_5 parameters are related to the $g_{\|}$ and $g_{\perp}$ values as shown in equation 3.5 and 3.6. Here $c_1 = \xi/(E[^2E]-E[^2A_1])$, where E[state] represents the energy of a given state and ξ is the one electron spin-orbit coupling constant. The ^2E excited configuration results from an electron from the doubly degenerate d_{xy} and d_{yz} orbitals being promoted to the d_{z2} orbital. Similarly, $c_3 = \xi/(E[^4E]-E[^2A_1])$ and $c_5 = \xi/(E[^4A_2]-E[^2A_1])$ are parameters corresponding to the $^4A_2$ and ^4E configurations. With strong-field donors such as phosphines, the $^4A_2$ configuration, which results from the promotion of an electron from the d_{xy} orbital to the d_{x2-y2} orbital is similar in energy to the ^4E state, which results from the promotion of an electron from the doubly degenerate d_{xy} and d_{yz} orbitals to the d_{x2-y2} orbital. This is because the d_{xz} and d_{yz} orbitals are relatively close in energy to the d_{xy} orbital, whereas the d_{x2-y2} orbital is significantly higher in energy. The approximation that $c_3 \cong c_5$ is therefore reasonable,[52, 53] and a simplified expression for $g_{\perp}$ is obtained, as shown in equation 3.7. For complex **20** this analysis results in the values $c_1 = 0.039$ MHz and $c_3 = 0.11$ MHz, which is consistent with previously reported data for related complexes.[53]

$$g_{\|} = 2.0023 + 2c_3^2 - 3c_1^2 \qquad (3.5)$$

$$g_{\perp} = 2.0023 + 6c_1 - 6c_1^2 + (2/3)c_3^2 + (8/3)c_5^2 - (4/3)c_3c_5 \qquad (3.6)$$

$$g_{\perp} \cong 2.0023 + 6c_1 - 6c_1^2 + 2c_3^2 \quad (c_3 \cong c_5) \qquad (3.7)$$

This analysis can be extended to the evaluation of the hyperfine and superhyperfine coupling constants.[59] The expressions for the hyperfine coupling constants $A_{Co\|}$ and $A_{Co\perp}$ are given in equations 3.8 and 3.9 and can be used to estimate the values of

References begin on page 121

P, which is the dipolar term for the hyperfine coupling constant, and K, which is the Fermi contact term. An equation for P using the assumption $c_3 \cong c_5$ is shown in equation 3.10. The value for P for complex **8** was determined to be 683 MHz, which is very close to the value for the free ion, which is 689 MHz,[54] and is indicative of primarily large d_{z^2} spin density on the Co(II) centre, as was anticipated. The value of K is –187 MHz. It should be noted that this analysis predicts that the sign of $A_{Co\perp}$ is negative.[59] An analysis of the superhyperfine coupling constants to ^{31}P allows for a evaluation of the contribution of the phosphine 3s and 3p orbitals to the unpaired spin density on the phosphine donor.[53] This breakdown estimates that 12% of the unpaired spin density resides on the phosphine donor, with 4.5% associated with the phosphorus 3s orbital and 4.9% residing in the phosphorus 3p orbital.

$$A_{Co\parallel} = K + P[4/7 - (4/7)c_3 - (6/7)c_1 + (2/63)c_3^2 - (64/63)c_5^2 + (30/14)c_1^2 + (8/21)c_5c_3] \quad (3.8)$$

$$A_{Co\perp} = K + P[-2/7 + (2/7)c_3 + (45/7)c_1 + (12/63)c_3^2 + (40/63)c_5^2 - (57/14)c_1^2 - (34/21)c_5c_3] \quad (3.9)$$

$$P \cong (A_{Co\parallel} - A_{Co\perp}) / [(6/7) - (6/7)c_3 - (51/7)c_1 + (12/63)c_3^2 + (87/14)c_1^2] \quad (3.10)$$

A DFT calculation was performed on complex **20** using the solid-state structural coordinates obtained by X-ray crystallography. The spin-density predicted from this calculation is shown as an isosurface depiction in Figure 3.11 (left). Consistent with the EPR spectrum of **20**, this analysis reveals that considerable unpaired electron density resides on the phosphorus atom. Notably, this unpaired electron density extends back towards the Y centre, which should allow for through-space exchange coupling in complexes where Y is replaced by a paramagnetic lanthanide. The extensive delocalization of the unpaired electron density onto the phosphorus atom and towards the yttrium centre can be rationalized by considering the nature of the SOMO, which can be

References begin on page 121

approximated as an antibonding interaction between the phosphine lone-pair, which has contributions from both the 3s and 3p orbital of the phosphorus atom, and the d_{z2} orbital of the cobalt centre. A simplified depiction of this interaction is also shown in Figure 3.11(right).

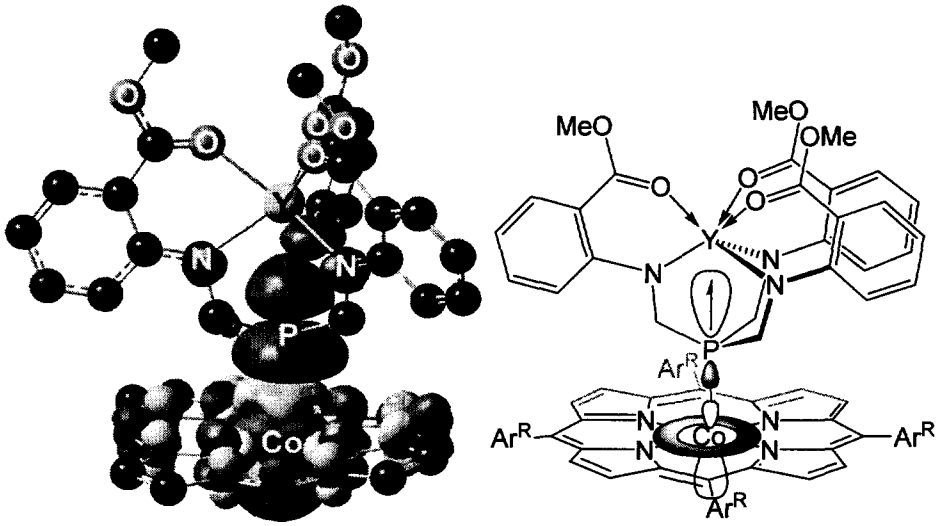

Figure 3.11. A depiction of an isosurface of the calculated spin density for heterodinuclear yttrium-cobalt complex **20** (left) and a simplification of the antibonding interaction associated with the SOMO (right).

The 77 K X-band EPR spectrum of a powdered sample of complex **21** is shown in Figure 3.12. The spectrum cannot be modelled to a reasonable fit by assuming no interaction between the Co(II) and Gd(III) centre using any combination of the B_{20} and B_{22} crystal field parameters. The complete spin Hamiltonian for complex **21** would have to take into account the crystal field splitting of the Stark substates as well as the exchange coupling between the two metal centres. This is complicated by the presence of only pseudo-axial symmetry in complex **21**, as well as the significant exchange coupling

References begin on page 121

interaction between the unpaired electrons associated with Co(II) and Gd(III). The exchange interaction is more easily estimated from the magnetic susceptibility data.

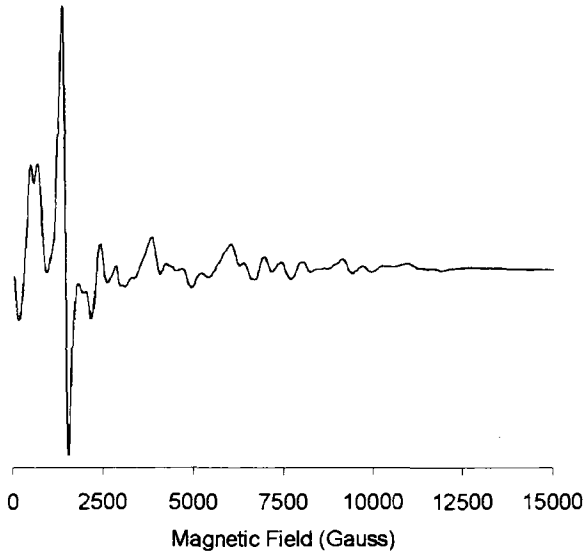

Figure 3.12. X-band EPR spectrum of a powdered sample of **21** at 77 K.

3.2.10 Magnetic Properties of Complexes 20 and 21

The Evans' method value of $\chi_m T$ for a 298 K toluene solution of complex **20** was difficult to measure, due to the low solubility of **20** and the significant diamagnetic contribution cancelling the majority of the paramagnetic contribution to the susceptibility. The uncorrected value was determined to be 0.36 $cm^3 \cdot K \cdot mol^{-1}$, which is close to the value of 0.375 $cm^3 \cdot K \cdot mol^{-1}$ expected for a species bearing a single unpaired electron in a nondegenerate orbital[12] but after subtraction of the diamagnetic contribution a corrected value of $\chi_m T$ of 0.59 $cm^3 \cdot K \cdot mol^{-1}$ was obtained. The molar magnetic susceptibility of complex **20** was measured over the temperature range of 300-1.8 K in an applied magnetic field of 1 T, and $\chi_m T$ (corrected for a slight temperature-independent

References begin on page 121

paramagnetism of 1.38×10^{-3} $cm^3 \cdot K \cdot mol^{-1}$) was found to be independent of temperature, with a value of 0.39 $cm^3 \cdot K \cdot mol^{-1}$ at 1.8 K. The simplicity of the magnetism of this species renders the observation of exchange coupling in species **21** facile, because in the absence of coupling a negligible temperature dependence of $\chi_m T$ with temperature is predicted.

At room temperature, the anticipated value of $\chi_m T$ for complex **21** is 8.26 $cm^3 \cdot K \cdot mol^{-1}$. This value corresponds to the value of two uncoupled isolated ions Gd(III), (S = 7/2, $\chi_m T$ = 7.88 $cm^3 \cdot K \cdot mol^{-1}$) and Co(II), ($S$ = 1/2, $\chi_m T$ = 0.375 $cm^3 \cdot K \cdot mol^{-1}$). The Evans' method value of $\chi_m T$ for a 298 K toluene solution of complex **21** was determined to be 8.40 $cm^3 \cdot K \cdot mol^{-1}$, which is approximately the value anticipated in the absence of coupling. The molar magnetic susceptibility of a powdered sample of complex **21** was measured over the temperature range of 300-1.8 K in an applied magnetic field of 0.01 T. The plot of the product of susceptibility and temperature ($\chi_m T$) versus temperature for complex **21** is shown in Figure 3.13. At room temperature, the experimental value of $\chi_m T$ is close to the value 8.26 $cm^3 \cdot K \cdot mol^{-1}$ predicted in the absence of significant coupling. This value decreases at low temperatures, to a value of 6.20 $cm^3 \cdot K \cdot mol^{-1}$ at 1.8 K, suggesting a weak antiferromagnetic coupling between the S = 1/2 and S = 7/2 centres that result in an S = 3 ground state, which should have a $\chi_m T$ value of 6.0 $cm^3 \cdot K \cdot mol^{-1}$.

References begin on page 121

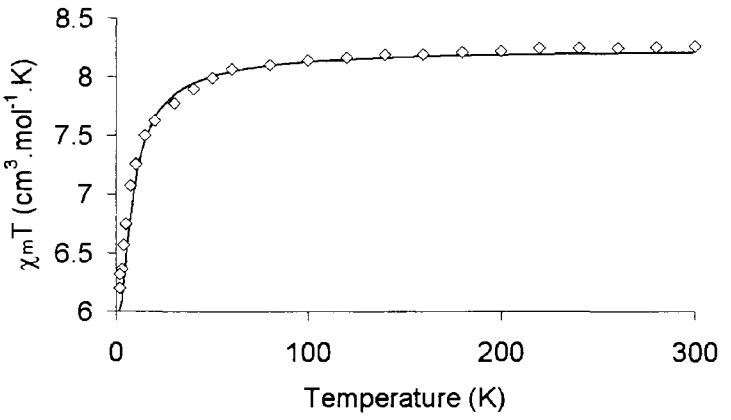

Figure 3.13. Plots of $\chi_m T$ versus T for complex **21** (◊), and the simulated fit obtained using $J = -2.1$ cm^{-1}, shown as a solid line.

This data was modelled using the simplified spin Hamiltonian given in equation 3.11, where $\boldsymbol{S}_{Gd}$ and $\boldsymbol{S}_{Co}$ are the spin-operators associated with Gd(III) and Co(II), and J is the magnetic exchange constant. The simplified Hamiltonian results in an expression that can be used to fit the temperature dependence of $\chi_m T$ using the coupling constant J, as shown in equation 3.12.

$$\hat{H}_{ex} = -J\, S_{Gd} \cdot S_{Co} \qquad (3.11)$$

$$\chi_m T = \frac{4N\beta^2 g^2}{k}\left[\frac{15 + 7e^{-4J/kT}}{9 + 7e^{-4J/kT}}\right] \qquad (3.12)$$

N = Avogadro's number

β = Bohr Magneton & k = Boltzman constant

A J value of -2.1 cm^{-1} was determined from this analysis, and the modelled fit is included as a solid line in Figure 3.13. This J value corresponds to an 8.4 cm^{-1} separation of the S = 3 ground state and the S = 4 state. The antiferromagnetic nature of the interaction is opposite to that most typically observed,[12, 14, 16, 17, 20, 31, 55] and provides

References begin on page 121

support for the suggestion that the exchange mechanism involves the direct overlap of the magnetic orbitals which contain the unpaired electrons associated with the Co(II) and Gd(III) centres, primarily due the extensive delocalization of the magnetic orbitals associated with the Co(II) over the phosphorus donor. The magnitude of *J* found here is comparable to the values that have been determined for other *d-f* heterobimetallics,[56] which demonstrates that the through-space exchange-coupling between transition metal and lanthanides mediated by these tripodal ligand is equally as effective as the superexchange mechanism which commonly operates in *d-f* complexes that utilize bridging donor atoms shared by the transition metal and lanthanide. This result suggests that paramagnetic tripodal complexes of the transition metals or lanthanides using analogous supporting ligands should be effective as magnetic building blocks.

3.3 Summary and Conclusions

The ligand precursor $P(CH_2NHC_6H_4\text{-}2\text{-}CO_2Me)_3$ (**13**) was used to synthesize six coordinate lanthanide complexes $P(CH_2NC_6H_4\text{-}2\text{-}CO_2Me)_3Ln$ (Ln = Y(**15**), Gd (**16**)) where both metals are attached with amido donors. The lithium salt of ligands precursor (**14**) was generated after the reaction of one equivalent of **13** with three equivalents of $LiN(SiMe_3)_2$ in toluene, and was also used to make complexes **15** and **16** via an alternative method.

In order to make heterobimetallic *d-f* metal complexes, the phosphorus lone pair was utilized to bind to a transition metal complex. Effects of both lanthanide metals (Y and Gd) on the donor capability of phosphine was extrapolated from the CO stretching frequencies of *trans*-$Rh(CO)ClL_2$ (L = **13**, **15** and **16**) and the result suggested that the

References begin on page 121

heavier gadolinium metal increases the donor ability of phosphine to a greater degree than yttrium metal due to increased C-P-C angles. Even though calculations suggest that the Gd(III) complex $P(CH_2NC_6H_4\text{-}2\text{-}CO_2Me)_3Gd$ (**15**) has negligible spin density on the phosphorus atom, with the appropriate choice of transition metal complex it proved possible to observe magnetic exchange coupling in the heterobimetallic complex $[TPP]CoP(CH_2NC_6H_4\text{-}2\text{-}CO_2Me)_3Gd$ (**21**). This coupling is mediated by the delocalization of the spin-density of the cobalt centre onto the phosphine donor, which allows direct overlap of the magnetic orbital associated with Co(II) with the *f*-electrons on the Gd(III) centre. Contrary to what is typically observed in *d-f* complexes, where more ligand mediated super-exchange pathways operate, this through-space interaction results in weak antiferromagnetic coupling. The magnitude of this exchange coupling is of an equal magnitude to other *d-f* complexes, which bodes well for the potential use of the mononuclear lanthanide complexes of this ligand as building blocks for larger polymetallic complexes where through-space interactions yield magnetically ordered systems or single-molecule magnet behaviour.

3.4 Experimental

General Techniques - Unless otherwise stated, all experiments were performed under an inert atmosphere of dinitrogen using either using Schlenk techniques or an MBraun glove box. Dry oxygen-free solvents were used throughout. Anhydrous pentane and toluene were purchased from Aldrich, sparged with nitrogen and passed through activated alumina under a positive pressure of nitrogen gas; toluene and hexanes were further deoxygenated using Ridox catalyst columns.[57] Deuterated benzene was dried by

References begin on page 121

heating at reflux over sodium/potassium in a sealed vessel under partial pressure, then trap-to-trap distilled, and freeze-pump-thaw degassed three times.

Instrumentation - ^{1}H, $^{13}C\{^{1}H\}$ and $^{31}P\{^{1}H\}$ NMR spectra were recorded from Bruker AMX (300 MHz) or Bruker AMX (500 MHz) spectrometer. All chemical shifts are reported in ppm, and all NMR coupling constants (*J*) are in Hz. ^{1}H NMR spectra were referenced to residual protons (C_6D_5H, δ 7.15 and $CDHCl_2$, δ 5.32) with respect to trimethylsilane at δ 0.0. $^{13}C\{^{1}H\}$ spectra were referenced relative to solvent resonances (C_6D_6, δ 128.0 and CD_2Cl_2, δ 54.0, 298 K). $^{31}P\{^{1}H\}$ NMR spectra referenced to external 85% H_3PO_4 at δ 0.0. EPR spectra of all solid samples were collected using an X-band Bruker ESR 300E spectrometer. Unless otherwise noted, magnetizations were measured at 100 G with a Quantum Design Evercool MPMS-XL system. Corrections for the diamagnetic contributions of compounds were made using Pascal's constants. Samples were run in a PVC holder specially designed to possess a constant cross-sectional area. Elemental analyses were performed by the Centre for Catalysis and Materials Research (CCMR) at the University of Windsor.

Computer Programmes - The program Simpip[58] was used to model the Co(II) spectra of complex **20**. The program Spin[59] was used to simulate the Gd^{3+} spectrum of **16** using only the B_{20} crystal field parameter and the program Sim[60] was used to generate spectra with the B_{20}, B_{40} B_{43}, B_{60}, B_{63} and B_{66} crystal field parameters.

Calculations - Ab inito DFT calculations were performed using the hybrid functional B3LYP or UB3LYP[61] method with the Gaussian 03 package.[62] The basis functions used were the DGDZVP set for complex **15** and the CEP-31G for complex **16**. Both were optimized with C_3 symmetry. For the model complex for species **20** the CEP-

References begin on page 121

121G* basis set was used on all atoms except for Y and Co, for which the CEP-121G basis set was used. All these basis sets are provided in the Gaussian 03 program.

Chemicals - The compounds tris(hydroxymethyl)phosphine, methyl anthranilate, 5, 10, 15, 20-tetrakis(4-methoxyphenyl)-21*H*,23*H*-porphine cobalt(II), lithium bis(trimethylsilyl)amide, $[(CO)Rh(\mu\text{-}Cl)]_2$ and anhydrous YCl_3 were purchased from Sigma Aldrich. Anhydrous $GdCl_3$ was purchased from Strem. All the reagents were used without further purification. The compounds $Y[N(SiMe_3)_2]_3$ and $Gd[N(SiMe_3)_2]_3$ were synthesized via the literature methods.[63, 64]

Synthesis of $P(CH_2NHC_6H_4\text{-}2\text{-}CO_2Me)_3$ (13). A mixture of $P(CH_2OH)_3$ (5 g, 0.040 mol) methyl anthranilate (30.45 g, 0.20 mol) and 70 mL of toluene were combined in a 250 mL three neck flask equationuipped with Dean-Stark trap and a condenser. The solution was heated to reflux for 1 h and the water produced was removed azeotropically. After cooling to room temperature the solvent was evaporated to dryness under vacuum, and the creamy white residue was rinsed with diethyl ether 2-3 times to remove excess methyl anthranilate. The product was then collected by filtration and dried under vacuum (20 g, 95 % yield). X-ray quality crystals were obtained by slow evaporation of a benzene and hexamethyldisiloxane solution. ^{1}H NMR (C_6D_6, 300 MHz, 298 K): δ 3.36 (d, $^2J_{PH}$ = 5.1 Hz, 6H, PC*H*$_2$), 3.46 (s, 9H, C*H*$_3$), 6.49 (dd, 3H, Ar-*H*), 6.71(d, 3H, Ar-*H*), 7.15 (ddd, 3H, Ar-*H*), 7.96 (dd, 3H, Ar-*H*), 8.29 (br, 3H, N*H*). ^{13}C{^{1}H} NMR (C_6D_6, 75.5 MHz, 298 K): δ 38.1 (d, J_{PC} = 15.4 Hz, P*C*H$_2$), 51.1 (s, *C*H$_3$), 110.9, 112.1, 115.3, 131.9 and 134.8 (s, Ar-*C*), 151.6 (d, J = 2.7 Hz *ipso-C*), 169.1 (s, *C*O$_2$).^{31}P{^{1}H} NMR (C_6D_6, 121.5 MHz, 298 K): δ −33.6 (s). Anal. Calcd for $C_{27}H_{30}N_3O_6P$: C, 61.94; H, 5.78; N, 8.03. Found: C, 61.90; H, 5.68; N 8.13.

References begin on page 121

Synthesis of $P(CH_2NC_6H_4\text{-}2\text{-}CO_2Me)_3Y$ (14). A mixture of **13** (1 g, 1.91 mmol) and $Y[N(SiMe_3)_2]_3$ (1.633 g, 2.86 mmol) was stirred in 70 mL of toluene for 5 h. The resultant yellow crystalline precipitate was isolated by filtration, rinsed with 50 mL pentane and dried for 4 h (77 %, 1.45 g). ^1H NMR (C_6D_6, 300 MHz, 298 K): δ 3.25 (s, 9H, C*H*$_3$), 3.92 (d, $^2J_{PH}$ = 7.1 Hz, 6H, PC*H*$_2$), 6.46 (dd, $^3J_{HH}$ = 8.1, 6.6 Hz, 3H, C_6H_4-5-C*H*), 6.78 (d, $^3J_{HH}$ = 8.8 Hz, 3H, C_6H_4-3-C_5*H*), 7.27 (ddd, $^3J_{HH}$ = 8.8, 6.6 Hz, $^4J_{HH}$ = 1.8 Hz, 3H, C_6H_4-4-C*H*), 8.10 (dd, $^3J_{HH}$ = 8.1 Hz, $^4J_{HH}$ = 1.8 Hz, 3H, C_6H_4-6-C*H*). $^{13}C\{^1H\}$ NMR (C_6D_6, 75.5 MHz, 298 K) δ: 38.1 (d, J_{PC} = 15.4 Hz, P*C*H$_2$), 51.5 (s, *C*H$_3$), 172.1 (s, *C*O$_2$), 108.7, 112.1, 114.4, 132.9 and 136.6 (s, Ar-*C*), 153.6 (*ipso-C*). $^{31}P\{^1H\}$ NMR (C_6D_6, 121.5 MHz, 298 K) δ: −57.0 (d, J_{PY} = 15.1 Hz). Anal. Calcd for $C_{27}H_{27}N_3O_6PY$: C, 53.21; H, 4.47; N, 6.90. Found: C, 53.10; H, 4.45; N, 6.96.

Alternative method to prepare complex **14** in NMR scale involve, the mixing of complex **16** (15 mg, 0.028 mmol) and YCl_3 (5.5 mg, 0.028 mmol) in 2 mL of toluene.

Synthesis of $P(CH_2NC_6H_4\text{-}2\text{-}CO_2Me)_3Gd$ (15). A mixture of **13** (500 mg, 0.938 mmol) and $Gd[N(SiMe_3)_2]_3$ (600 mg, 0.938 mmol) was stirred in 20 mL of toluene for 30 min. The solution was filtered and remaining yellow crystalline solid was rinsed with 50 mL pentane and dried for 4 h (67 %, 425 mg). Anal. Calcd for $C_{27}H_{27}N_3O_6PGd$: C, 47.04; H, 3.95; N, 6.09. Found: C, 47.28; H, 4.02; N, 6.24.

Synthesis of $P(CH_2NC_6H_4\text{-}2\text{-}CO_2Me)_3Li_3$ (16). A mixture of **13** (1.06 g, 1.99 mmol) and $LiN(SiMe_3)_2$ (1 g, 5.98 mmol) was stirred in 40 mL of toluene for 30 min. The solution was filtered and remaining yellow crystalline solid was rinsed with 50 mL of pentane and dried for 4 h (68 %, 975 mg). A second crop of the product was obtained from the mother liquor in the form of yellow powder (15 % 210 mg), which make the

References begin on page 121

total yield of 83 %. ^{1}H NMR (C_6D_6, 300 MHz, 298 K): δ 1.19 (b, $LiOCH_2CH_2$), 3.17 (b, $LiOCH_2$), 3.33 (d, $^2J_{PH}$ = 7.7 Hz, 6H, PCH_2), 3.52 (s, 9H, OCH_3), 6.35 (dd, $^3J_{HH}$ = 8.1, 6.8 Hz, 3H, C_6H_4-5-C*H*), 7.27 (ddd, $^3J_{HH}$ = 8.8, 6.6 Hz, $^4J_{HH}$ = 1.8 Hz, 3H, C_6H_4-4-C*H*), 7.5 (d, $^3J_{HH}$ = 9.8 Hz, 3H, C_6H_4-3-C_5*H*), 8.10 (dd, $^3J_{HH}$ = 8.1 Hz, $^4J_{HH}$ = 1.8 Hz, 3H, C_6H_4-6-C*H*).^{13}C{^{1}H} NMR (C_6D_6, 75.5 MHz, 298 K) δ: 38.1 (d, J_{PC} = 15.4 Hz, PCH_2), 51.5 (s, CH_3), 172.1 (s, CO_2), 108.7, 112.1, 114.4, 132.9 and 136.6 (s, Ar-*C*), 153.6 (*ipso-C*). ^{31}P{^{1}H} NMR (C_6D_6, 121.5 MHz, 298 K) δ: −22.5 (s). Anal. Calcd for $C_{27}H_{27}N_3Li_3O_6P$: C, 59.91; H, 5.03; N, 7.76. Found: C, 60.01; H, 5.12; N, 7.60.

Synthesis of [*trans*-RhCl(CO)[P($CH_2NHC_6H_4$-2-$CO_2Me)_3$)]$_2$ (17). A mixture of **13** (54.8 mg, 0.102 mmol) and [Rh(CO)$_2$(μ-Cl)]$_2$ (10 mg, 0.026 mmol) was stirred in 5 mL of toluene for 30 min. The orange-yellow precipitate was filtered and dried for 2 h. ^{1}H NMR (CD_2Cl_2, 300 MHz, 298 K): δ 3.47 (s, 9H, CH_3), 3.55 (s, 6H, PCH_2), 6.42 (t, 3H, $^3J_{HH}$ = 13.6 Hz, Ar-*H*), 7.03 (d, 3H, $^2J_{HH}$ = 7.9 Hz, Ar-*H*), 7.41 (td, 3H, Ar-*H*), 8.1 (dd, 3H, Ar-*H*), 8.5 (br, 3H, N*H*.^{13}C{^{1}H} NMR (CD_2Cl_2, 75.5 MHz, 298 K), δ: 43.2 (d, J_{PC} = 15.4 Hz, PCH_2), 52.5 (s, CH_3), 112.1, 113.2, 116.2, 133.1 and 135.9 (s, Ar-*C*), 153.6 (d, *J* = 2.7 Hz *ipso-C*), 171.1 (s, CO_2).^{31}P{^{1}H} NMR (CD_2Cl_2, 121.5 MHz, 298 K) δ: 24.8 (d, J_{PRh} = 122.07 Hz). IR: υ = 1978.9 cm^{-1}.

Synthesis of [*trans*-RhCl(CO)[P($CH_2NC_6H_4$-2-$CO_2Me)_3$Y]$_2$ (18). A mixture of **14** (62.68 mg, 0.102 mmol) and [Rh(CO)$_2$(μ-Cl)]$_2$ (10 mg, 0.0257 mmol) was stirred in 5 mL of toluene for 30 min. Crystallized orange-yellow product was filtered and dried for 2 h. ^{1}H NMR (CD_2Cl_2, 300 MHz, 298 K): δ 3.96 (s, 9H, CH_3), 4.34 (s, 6H, PCH_2), 6.4 (t, 3H, $^3J_{HH}$ = 14.7 Hz, Ar-*H*), 6.9 (d, 3H, $^2J_{HH}$ = 9.0 Hz, Ar-*H*), 7.37 (td, 3H, Ar-*H*), 7.9 (dd,

References begin on page 121

3H, Ar-*H*). $^{13}C\{^1H\}$ NMR (CD_2Cl_2, 75.5 MHz, 298 K), δ: 172.9 (s, *C*O_2), 160.8 (*ipso-C*), 136.9, 133.0, 114.6, 112.5, 108.9 (s, Ar-*C*), 120.1 (s, *C*O) 52.6 (s, *C*H_3), 48.2 (s, P*C*H_2). $^{31}P\{^1H\}$ NMR (CD_2Cl_2, 121.5 MHz, 298 K) δ: 4.0 (d, J_{PRh} = 123.6 Hz). IR: υ = 1963.6 cm^{-1}.

Synthesis of [*trans*-RhCl(CO)[P($CH_2NC_6H_4$-2-$CO_2Me)_3Gd]_2$ (19). A mixture of **15** (69.71 mg, 0.025 mmol) and [Rh(CO)$_2$(μ-Cl)]$_2$ (10 mg, 0.0257 mmol) was stirred in 5 mL of toluene for 30 min. Crystalline orange-yellow product was filtered and dried for 2 h. IR: υ = 1954.2 cm^{-1}.

Synthesis of [TPP]CoP($CH_2NC_6H_4$-2-$CO_2Me)_3Y$ (20). A mixture of **14** (450 mg, 0.738 mmol) and [5, 10, 15, 20-tetrakis(4-methoxyphenyl)porphinato]cobalt(II) (584.67 mg, 0.737 mmol) was stirred in 25 mL of toluene for 30 min. The solution was filtered and the resultant reddish-purple crystalline solid was washed with pentane (50 mL) and dried for 4 h (65.2 %, 675 mg). X-ray quality crystals were obtained by performing the reaction without stirring, and the structure contains 2 equationuivalents of cocrystallized toluene. The complex is sparingly soluble in toluene and benzene. ^1H NMR (C_6D_6, 300 MHz, 298 K): δ 3.2 (br, 9H, CO_2CH_3), 4.4 (br, 18 H total,-O*C*H_3 and P*C*H_2), 5.8 (br, 3H, C_6H_4), 6.9 (br, 3H, C_6H_4), 7.3 (br, 3H, C_6H_4), 8.2 (br, 3H, C_6H_4), 8.8 (br, 8H, TPP-*m-H*), 11.5 (v br, 8H, TPP-*o-H*), 15.1 (v br, 8H, pyrrole-*H*). Anal. Calcd for $C_{75}H_{63}N_7O_{10}$PYCo: C, 64.29; H, 4.53; N, 7.00. Found: C, 64.23; H, 4.82; N, 6.81.

Synthesis of [TPP]CoP($CH_2NC_6H_4$-2-$CO_2Me)_3Gd$ (21). A mixture of **15** (500 mg, 0.737 mmol) and [5, 10, 15, 20-tetrakis(4-methoxyphenyl)porphinato]cobalt (II), [TPP]Co(II) (584 mg, 0.737 mmol) was stirred in 25 mL of toluene for 30 min. The

References begin on page 121

solution was filtered and the resultant reddish-purple crystalline solid was washed with pentane (50 mL) and dried for 4 h (47.5%, 515 mg). Anal. Calcd for $C_{75}H_{63}N_7O_{10}PGdCo$: C, 61.30; H, 4.32; N, 6.67. Found: C, 61.47; H, 4.12; N, 6.54.

X–ray Crystallography. Each crystal was covered with Paratone, mounted on a glass fibre and rapidly placed into the cold N_2 stream of the Kryo-Flex low-temperature device. The data were collected using the SMART[65] software on a Bruker APEX CCD diffractometer using a graphite monochromator with Mo Kα radiation (λ = 0.71073 Å). Data reduction was performed using SAINT[66] software, and the data were corrected for absorption using SADABS.[67] The structures were solved by direct methods using SIR97[68] and refined by full-matrix least-squares on F^2 using SHELXL-97[69] and the WinGX[70] software package, and the thermal ellipsoid plots were produced using ORTEP32.[71] In general, thermal parameters for non-hydrogen atoms were treated anisotropically, and all hydrogens were placed in idealized locations. The co-crystallized benzene solvent in complex **13** was modelled as an idealized hexagon, with equationual isotropic thermal parameters on the six carbon atoms, and the hydrogens associated with this disordered moiety were omitted. The hydrogen atoms associated with the three amine functionalities that were involved in hydrogen bonding in complex **13** were located in an electron-density difference map and their positions and isotropic thermal parameters were refined. Multiple data sets were acquired for complexes **15** and **16**, but all suffered from twinning.

References begin on page 121

Details of selected crystallographic data, data collection and structure refinement of compounds **13, 14, 15, 16, 20** and **21** are listed in Table 3.1 and 3.2.

Table 3.1. Selected X-ray Crystallographic Data for Compounds **13, 14** and **15.**

	13	**14**	**15**
Empirical formula	$C_{27}H_{30}N_3O_6P$	$C_{27}H_{27}N_3O_6PLi_3$	$C_{27}H_{27}N_3O_6PY$
Formula weight	562.56	725.6	609.40
Crystal system	Triclinic	Tetragonal	Trigonal
a (Å)	10.8108(17)	24.3430(14)	14.6660(3)
b (Å)	11.3382(18)	24.3430(14)	14.6660(3)
c (Å)	12.513(2)	13.2326(15)	20.9460(9)
α (deg)	104.725(2)	90	90
β (deg)	104.725(2)	90	90
γ (deg)	90.718(2)	90	120
V ($Å^3$)	1429.3(4)	7841.40(11)	3905.06(20)
Space group	*P*-1	*I*-4	*R*3c
Z	2	8	6
Density (g/cm^3)	1.31	1.23	1.56
μ (Mo Kα) (mm^{-1})	0.144	0.119	2.349
Temperature (K)	173	173	173
Total no. of reflections	16454	43927	13993
Residuals: R_1; wR_2 (all data)	0.0624; 0.1800	0.0582; 0.1434	0.1372; 0.4167

References begin on page 121

Table 3.2. Selected X-ray Crystallographic Data for Compounds **16, 20** and **21.**

	16	**20**	**21**
Empirical formula	$C_{27}H_{27}N_3O_6PGd$	$C_{89}H_{79}N_7O_{10}PCoY$	$C_{89}H_{79}N_7O_{10}PCoGd$
Formula weight	708.7	1585.46	1653.74
Crystal system	Trigonal	Triclinic	Triclinic
a (Å)	14.6765(11)	14.4404(19)	14.442(2)
b (Å)	14.6660(11)	15.509(2)	15.495(2)
c (Å)	21.2161(3)	18.736(2)	18.737(3)
α (deg)	90.00	90.2840(10)	90.6480(2)
β (deg)	90.00	112.6130(10)	112.571(2)
γ (deg)	120.00	90.1050(10)	89.894(2)
V ($Å^3$)	3957.7(7)	3873.5(10)	3871.5(10)
Space group	*R*3c	*P*-1	*P*-1
Z	6	2	2
Density (g/cm^3)	1.70	1.42	1.36
μ (Mo Kα) (mm^{-1})	2.684	1.046	1.150
Temperature (K)	173	173	173
Total no. of reflections	13580	44292	43148
Residuals: R_1; wR_2 (all data)	Not fully solved[(a)]	0.0397; 0.1041	0.0397; 0.1115

[(a)] twinning complicated the solution of structures for complexes **15** and **16**

References begin on page 121

3.5 References

1. Itoh, K.; Kinoshita, M., *Molecular Magnetism: New Magnetic Materials*. **2002**.
2. Kahn, O., *Molecular Magnetism*. **1993**, p 380.
3. Miller, J. S., *Dalton Trans.* **2006**, (23), 2742.
4. Li, D.; Parkin, S.; Wang, G.; Yee, G. T.; Clerac, R.; Wernsdorfer, W.; Holmes, S. M., *J. Am. Chem. Soc.* **2006,** 128, (13), 4214.
5. Berlinguette, C. P.; Vaughn, D.; Canada-Vilalta, C.; Galan-Mascaros, J. R.; Dunbar, K. R., *Angew. Chem. Int. Ed.* **2003,** 42, (13), 1523.
6. Mrozinski, J., *Coord. Chem. Rev.* **2005,** 249, (21-22), 2534.
7. Batten, S. R.; Murray, K. S., *Coord. Chem. Rev.* **2003,** 246, (1-2), 103.
8. Batten, S. R.; Murray, K. S., *Aust. J. Chem.* **2001,** 54, (9-10), 605.
9. Hatnean J. A.; Raturi, R.; Lefebvre, J.; Leznoff D. B.; Lawes, G.; Johnson S. A., *J. Am. Chem. Soc.* **2006,** 128, (46), 14992.
10. Keen, A. L.; Doster, M.; Han, H.; Johnson, S. A., *Chem. Commun.* **2006**, (11), 1221.
11. Han, H.; Elsmaili, M.; Johnson, S. A., *Inorg. Chem.* **2006,** 45, (18), 7435.
12. Sakamoto, M.; Manseki, K.; Okawa, H., *Coord. Chem. Rev.* **2001,** 219, 379.
13. Benelli, C.; Gatteschi, D.; Carnegie, D. W.; Carlin, R. L., *J. Am. Chem. Soc.* **1985,** 107, (8), 2560.
14. Benelli, C.; Dei, A.; Gatteschi, D.; Pardi, L., *Inorg. Chem.* **1990,** 29, (18), 3409.
15. Zaleski, C. M.; Depperman, E. C.; Kampf, J. W.; Kirk, M. L.; Pecoraro, V. L., *Angew. Chem., Int. Ed.* **2004,** 43, (30), 3912.
16. Costes, J. P.; Dahan, F.; Donnadieu, B.; Garcia-Tojal, J.; Laurent, J. P., *Eur. J. Inorg. Chem.* **2001**, (2), 363.

References begin on page 121

17. Matsumoto, N.; Sakamoto, M.; Tamaki, H.; Okawa, H.; Kida, S., *Chem. Lett.* **1990**, (6), 853.

18. Andruh, M.; Ramade, I.; Codjovi, E.; Guillou, O.; Kahn, O.; Trombe, J. C., *J. Am. Chem. Soc.* **1993,** 115, (5), 1822.

19. Blake, A. J.; Gould, R. O.; Grant, C. M.; Milne, P. E. Y.; Parsons, S.; Winpenny, R. E. P., *J. Chem. Soc., Dalton Trans.* **1997**, (4), 485.

20. Costes, J. P.; Auchel, M.; Dahan, F.; Peyrou, V.; Shova, S.; Wernsdorfer, W., *Inorg. Chem.* **2006,** 45, (5), 1924.

21. Benelli, C.; Blake, A. J.; Milne, P. E. Y.; Rawson, J. M.; Winpenny, R. E. P., *Chem. Eur. J.* **1995,** 1, (9), 614.

22. Kempe, R.; Noss, H.; Irrgang, T., *J. Organomet. Chem.* **2002,** 647, (1-2), 12.

23. Mironov, V. S.; Galyametdinov, Y. G.; Ceulemans, A.; Gorller-Walrand, C.; Binnemans, K., *J. Chem. Phys.* **2002,** 116, (11), 4673.

24. Mishra, A.; Wernsdorfer, W.; Parsons, S.; Christou, G.; Brechin, E. K., *Chem. Commun.* **2005**, (16), 2086.

25. Mishra, A.; Wernsdorfer, W.; Abboud, K. A.; Christou, G., *J. Am. Chem. Soc.* **2004,** 126, (48), 15648.

26. Osa, S.; Kido, T.; Matsumoto, N.; Re, N.; Pochaba, A.; Mrozinski, J., *J. Am. Chem. Soc.* **2004,** 126, (2), 420.

27. Tang, J.; Hewitt, I.; Madhu, N. T.; Chastanet, G.; Wernsdorfer, W.; Anson, C. E.; Benelli, C.; Sessoli, R.; Powell, A. K., *Angew. Chem., Int. Ed.* **2006,** 45, 1729.

28. Christou, G.; Gatteschi, D.; Hendrickson, D. N.; Sessoli, R., *MRS Bulletin* **2000,** 25, (11), 66.

References begin on page 121

29. Frank, A. W.; Drake, G. L., *J. Org. Chem.* **1972,** 37, (17), 2752.

30. Tolman, C. A., *J. Am. Chem. Soc.* **1970,** 92, (10), 2953.

31. Schumann, H.; Winterfeld, J.; Rosenthal, E. C. E.; Hemling, H.; Esser, L., *Z. Anorg. Allg. Chem.* **1995,** 621, (1), 122.

32. Feindel, K. W.; Wasylishen, R. E., *Can. J. Chem.* **2004,** 82, (1), 27.

33. Fryzuk, M. D.; Haddad, T. S.; Berg, D. J., *Coord. Chem. Rev.* **1990,** 99, 137.

34. Grim, S. O.; Sangokoya, S. A., *J. Chem. Soc.,Chem. Commun.* **1984,** (23), 1599.

35. Pinkerton, A. A.; Rossier, M.; Spiliadis, S., *J. Magn. Reson.* **1985,** 64, (3), 420.

36. Stowasser, R.; Hoffmann, R., *J. Am. Chem. Soc.* **1999,** 121, (14), 3414.

37. Hutchison, C. A.; Judd, J. B. R.; Pope, D. F. D., *Proc. Phys. Soc.* **1957,** 70B, 514.

38. Ishikawa, N.; Sugita, M.; Ishikawa, T.; Koshihara, S.; Kaizu, Y., *J. Phys. Chem. B* **2004,** 108, (31), 11265.

39. Ishikawa, N.; Sugita, M.; Wernsdorfer, W., *Angew. Chem., Int. Ed.* **2005,** 44, (19), 2931.

40. Ishikawa, N.; Sugita, M.; Wernsdorfer, W., *J. Am. Chem. Soc.* **2005,** 127, (11), 3650.

41. Fey, N.; Tsipis, A. C.; Harris, S. E.; Harvey, J. N.; Orpen, A. G.; Mansson, R. A., *Chem. Eur. J.* **2006,** 12, (1), 291.

42. Cooney, K. D.; Cundari, T. R.; Hoffman, N. W.; Pittard, K. A.; Temple, M. D.; Zhao, Y., *J. Am. Chem. Soc.* **2003,** 125, (14), 4318.

43. Decastro, B.; Rangel, M.; Raynor, J. B., *J. Chem. Soc., Dalton Trans.* **1990,** (11), 3311.

44. Wayland, B. B.; Abdelmag.Me, *J. Am. Chem. Soc.* **1974,** 96, (15), 4809.

References begin on page 121

45. Wayland, B. B.; Minkiewi, J. V.; Abd-Elmageed, M. E., *J. Am. Chem. Soc.* **1974,** 96, (9), 2795.

46. Fryzuk, M. D.; Leznoff, D. B.; Thompson, R. C.; Rettig, S. J., *J. Am. Chem. Soc.* **1998,** 120, (39), 10126.

47. Bradley, D. C.; Welch, A. J.; Smallwoo, R. J.; Hursthou, M. B., *J. Chem. Soc.,Chem. Commun.* **1972,** (15), 872.

48. Shannon, R. D., *Acta Crystallogr. Sec. A* **1976,** 32, (1), 751.

49. Hitchcock, P. B.; Lappert, M. F.; Mackinnon, I. A., *J. Chem. Soc.,Chem. Commun.* **1988**, (23), 1557.

50. Roesky, P. W., *Heteroatom Chem.* **2002,** 13, (6), 514.

51. McGarvey, B. R., *Can. J. Chem.* **1975,** 53, (16), 2498.

52. Lin, W. C., *Inorg. Chem.* **1976,** 15, (5), 1114.

53. Wayland, B. B.; Sherry, A. E.; Bunn, A. G., *J. Am. Chem. Soc.* **1993,** 115, (17), 7675.

54. McGarvey, B. R., *J. Phys. Chem.* **1967,** 71, (1), 51.

55. Bencini, A.; Benelli, C.; Caneschi, A.; Carlin, R. L.; Dei, A.; Gatteschi, D., *J. Am. Chem. Soc.* **1985,** 107, (26), 8128.

56. Sakamoto, M.; Manseki, K.; Okawa, H., *Coord. Chem. Rev.* **2001,** 219, 379.

57. Pangborn, A. B.; Giardello, M. A.; Grubbs, R. H.; Rosen, R. K.; Timmers, F. J., *Organometallics* **1996,** 15, (5), 1518.

58. Simpip, *An EPR simulation program, M. Nilges, Illinois EPR Research Centre.*

59. Spin, *EPR simulation program, A. Ozarowski, National High Magnetic Field Laboratory, Florida.*

References begin on page 121

60. Sim, *version 2004-5, An EPR Simulation Program, H. Weihe, Department of Chemistry, University of Copehagen.*

61. Becke, A. D., *J. Chem. Phys.* **1993,** 98, 5648.

62. Gaussian 03, Revision C.01, M. J. Frisch, G. W. Trucks, H. B. Schlegel, G. E. Scuseria, M. A. Robb, J. R. Cheeseman, J. A. Montgomery, Jr., T. Vreven, K. N. Kudin, J. C. Burant, J. M. Millam, S. S. Iyengar, J. Tomasi, V. Barone, B. Mennucci, M. Cossi, G. Scalmani, N. Rega, G. A. Petersson, H. Nakatsuji, M. Hada, M. Ehara, K. Toyota, R. Fukuda, J. Hasegawa, M. Ishida, T. Nakajima, Y. Honda, O. Kitao, H. Nakai, M. Klene, X. Li, J. E. Knox, H. P. Hratchian, J. B. Cross, V. Bakken, C. Adamo, J. Jaramillo, R. Gomperts, R. E. Stratmann, O. Yazyev, A. J. Austin, R. Cammi, C. Pomelli, J. W. Ochterski, P. Y. Ayala, K. Morokuma, G. A. Voth, P. Salvador, J. J. Dannenberg, V. G. Zakrzewski, S. Dapprich, A. D. Daniels, M. C. Strain, O. Farkas, D. K. Malick, A. D. Rabuck, K. Raghavachari, J. B. Foresman, J. V. Ortiz, Q. Cui, A. G. Baboul, S. Clifford, J. Cioslowski, B. B. Stefanov, G. Liu, A. Liashenko, P. Piskorz, I. Komaromi, R. L. Martin, D. J. Fox, T. Keith, M. A. Al-Laham, C. Y. Peng, A. Nanayakkara, M. Challacombe, P. M. W. Gill, B. Johnson, W. Chen, M. W. Wong, C. Gonzalez, J. A. Pople, Gaussian, Inc., Wallingford CT, ***2004***.

63. Bradley, D. C.; Ghotra, J. S.; Hart, F. A., *J. Chem. Soc., Chem. Commun.* **1972**, (6), 349.

64. Bradley, D. C.; Ghotra, J. S.; Hart, F. A., *J. Chem. Soc., Dalton Trans.* **1973**, (10), 1021.

65. SMART, *Molecular analysis research tool; Bruker AXS Inc.: Madison, WI.* **2001**.

References begin on page 121

66. SAINTPlus, *Data reduction and correction program; Bruker AXS Inc.: Madison, WI.*

67. SADABS, *An empirical absorption correction program; Bruker AXS Inc.: Madison, WI,* **2001**.

68. Altomare, A.; Burla, M. C.; Camalli, M.; Cascarano, G. L.; Giacovazzo, C.; Guagliardi, A.; Moliterni, A. G. G.; Polidori, G.; Spagna, R., *J. Appl. Crystallogr.* **1999,** 32, (1), 115.

69. Sheldrick, G. M., *SHELXL-97; Universitat Gottingen: Gottingen.*

70. Farrugia, L. J., *J. Appl. Crystallogr.* **1999,** 32, 837.

71. Farrugia, L. J., *J. Appl. Crystallogr.* **1997,** 30, 565.

References begin on page 121

CHAPTER-4

Effect of Temperature on Pseudocontact Shifts of Paramagnetic Lanthanide Complexes

4.1 Introduction

For lanthanides, crystal field parameters play an important role in describing the magnetic properties and hence, the direction of the magnetization i.e. magnetic anisotropy in magnetic molecules. The unique magnetic properties of the lanthanides enables them to be used as magnetic materials and single molecule magnets (SMMs).[1-3] In magnetic materials such as SMMs, large magnetic moment and large magnetic anisotropy are the two important features, and are responsible for the through-space coupling between metal ions.[4, 5] The magnitude as well as the sign of the magnetic

References begin on page 170

anisotropy depends on the nature of the lanthanide ion, crystal field splitting strength and the molecular geometry of the compound. Depending upon the sign of anisotropy, trivalent lanthanide ions are divided into two categories: the first group involves Ce^{3+}, Sm^{3+}, Tb^{3+}, Dy^{3+} and Ho^{3+}, with positive anisotropy and the second group involves late lanthanides such as Er^{3+}, Tm^{3+} and Yb^{3+} with negative anisotropy. It is reported that lanthanide ions from the two different categories can not have the same sign for anisotropy. Among all the trivalent lanthanide ions, Dy^{3+}, Tb^{3+}, and Tm^{3+} show high magnetic anisotropy, with Tb^{3+} being the highest.[4, 6, 7] Magnetic anisotropy also induces pseudocontact (dipolar) shifts in lanthanide complexes and thus can be measured by NMR spectroscopy as described in Chapter 1 (Section 1.1, equation 1.9).

The paramagnetic shifts of lanthanide complexes are the combination of isotropic contact (δ_C) and anisotropic pseudocontact (δ_{PC}) shifts (equation (4.1)). In principle, the separation of these two terms is based on their temperature dependence and requires the chemical shifts of a single lanthanide complex. It has been reported earlier that in ^1H NMR spectra pseudocontact contribution dominates over the contact contribution, whereas in ^{13}C and ^{31}P spectra, the contact contribution plays an important role.[8]

$$\Delta\delta = \delta_C + \delta_{PC} = F\langle S_z\rangle + G\{B_{20}\}CT^{-2} \qquad (4.1)$$

S_z = projection of the total electron spin magnetization of the lanthanide on the direction of the external magnetic field

C = magnetic constant at given temperature T

B_{20} = second order crystal field parameter

F = contact shift (depends on the delocalization of the metal spin density on sustrate nuclei)

G = pseudocontact shift (depends on the geometry of the complex)

References begin on page 170

The large pseudocontact shifts, which are due to the dipolar contribution, enables lanthanide complexes to be used as lanthanide shift reagents (LSR) and contrast agents in structural biology[9, 10] and in magnetic resonance imaging (MRI) respectively.[11, 12] The pseudocontact contribution of lanthanide complexes increases the separation between the closely related NMR signals, which simplifies the complex NMR spectra of organic compounds in solution NMR-spectroscopy.[13-15] The magnetic anisotropy of lanthanides also allows them to align the related complex in an external magnetic field. This tendency of lanthanide complexes allows them to be used as magnetically active liquid crystals for the alignment of the protein molecules in magnetic fields.[16-18] Lanthanide liquid crystals are easier to magnetize by weak external fields than the conventional diamagnetic liquid crystals.

The paramagnetic properties of the lanthanides permit them not only to be used for spectral simplification of low-molecular weight complexes but also as biological probes for determining protein and peptide structures.[19-25] Heptadentate water soluble lanthanide complexes have been reported to act as multiple probes (luminescent, NMR and chiroptical) for bioactive species.[26-28] Paramagnetic lanthanide ions can also be used for NMR studies of biological membranes such as phospholipids-bilayered micelles, by changing their magnetic alignment.[29, 30] Bicelles, a mixture of long and short-chain phospholipids offer an environment for membrane proteins. Whereas similar to micelles, small bicelles can be used for the solution NMR study of membrane proteins,[31] larger bicelles are use for the alignment of membrane proteins in the solid-state NMR spectroscopy. Although the structural study of proteins by solution NMR is much more complicated than solving their crystal structures, small structural changes due to

References begin on page 170

temperature or pH can be easily detected by solution NMR. Due to the paramagnetic properties of lanthanides, their attachment to proteins facilitates the determination of protein solution structures and dynamics.

In the protein structure study, calcium ions bound to protein molecules can be replaced by lanthanide ions, because of the similarity between calcium and lanthanide ions.[10, 19, 32] Both divalent Ca^{2+} and trivalent Ln^{3+} share similar ionic radii (Ca^{2+} = 1-1.18 Å and Ln^{3+} = 0.86-1.22 Å) and form the same type of bonds in biological systems. Other than sharing these properties with the calcium ion, lanthanides also possess some characteristic features, such as colour, magnetism and luminescence, which also favour them for use in biochemical investigations. Recently Bertini et al reported the structural characterization of the metalloprotein (calbindin D_{9k}) by replacing the Ca^{2+} with trivalent cerium (Ce^{3+}).[33] Introduction of lanthanides in proteins changes the chemical shifts and line broadening and thus provide important information regarding protein structure or protein encounter complexes.[24, 25, 34] Sykes and coworkers have used trivalent lanthanides such as Yb^{3+} to bind with the EF site of parvalbumin for determining the protein structure.[24, 35] They have also proposed a new method for separating the contact and pseudocontact shifts of late lanthanide ions (Dy-Yb) without the knowledge of the structural symmetry of the lanthanide binding protein complexes. Other than replacing Ca^{2+}, lanthanides also act as binding tags for specific sites of proteins and peptides. It has been reported recently that a lanthanide-binding peptide tag with a Cysteine residue can also be used to study the protein in different magnetic anisotropy tensor orientations.[36]

References begin on page 170

As reported earlier, contact and pseudocontact shifts of an isostructural series of lanthanide complexes can be separated from each other on the basis of their temperature dependence.[7] To date, several methods have been developed to calculate the pseudocontact shifts of lanthanides. McGarvey and Kurland first verified the relationship between the pseudocontact shifts and the magnetic susceptibility of the anisotropic portion of the shifts.[37] Later, Bleaney expanded the isotropic portion of the shifts using a temperature dependent term and magnetic anisotropy.[7] Bleaney's theory is based upon the high temperature magnetic anisotropy. As shown in equation (4.2), Bleaney described the magnetic anisotropy of a lanthanide complex using the second order crystal field parameter (a_{20}) and has T^{-2} temperature dependence. Here, K_0 is a constant, which depends on the lanthanide.[7]

$$\chi_{\parallel} - \chi_{\perp} = \frac{K_0}{T^2} a_{20} \qquad (4.2)$$

The above equation (4.2) can also be written as equation (4.3):

$$\chi_{\parallel} - \chi_{\perp} = \frac{C_2}{T^2} \qquad (4.3)$$

Where,

$$C_2 = \frac{g_J^2 \beta_e^2 J(J+1)(2J+3)(J-1)\sqrt{2/3}(a_{20}{}^k{}_{J2} < r^2 >)}{30k^2} \qquad (4.4)$$

k_{J2} = constant with different values for each lanthanide with different J states

g_J = Landé factor

B_e = Bohr magneton

C_2 can be calculated by using g_J, β_e and k_{J2} values given in the literature.[7]

References begin on page 170

Bleaney's theory is based on the hypothesis that the overall crystal field splitting (ΔE_{CF}) of the lanthanides should not be larger than their thermal energy (kT). Therefore, only second-rank crystal-field parameters such as B_{20} and B_{22} can be used for the calculation of magnetic anisotropy. For example, lanthanide complexes, where thermal energy is lower than the crystal field splitting, particularly for those complexes that exhibit large magnetic anisotropy and have the ratio of $\Delta E_{CF}/k$T greater than one, T^{-2} term does not provide enough information about the magnetic anisotropy. Bleaney's theory does not fit with these complexes because it completely ignores the higher crystal field parameters and higher temperature dependent terms (T^{-3}, T^{-4}... T^{-n}).

Reilley and coworkers supported this theory and proved experimentally that pseudocontact shifts depend only on T^{-2}.[38] However, Wong and Horrocks[39] and Horrocks independently[40] later supported the dependency of pseudocontact shift on T^{-1} rather than on T^{-2}. Golding and Pyykko extended Bleaney's theory and reported small deviations in lanthanide shifts using higher crystal field parameters.[41] While Cheng and Gutowsky showed that paramagnetic shifts depend on either T^{-1} or T^{-2}, Gutowsky and Stout extended Bleaney's theory using a T^{-3} term and concluded that contribution of this term is very small (~10 %), and that T^{-2} is the only important term for most of the lanthanide complexes.[42, 43] McGarvey also supported Gutowsky and Stout's theory using additional higher temperature dependent terms such as T^{-3}, and concluded that these terms also make significant contributions in pseudocontact shifts and require additional crystal field parameters, including rank four and six ($B_{40's}$ and $B_{60's}$).[44] An expansion of equations 4.3 (equation 4.5) using higher term such as T^{-3} shows that the T^{-3} temperature dependence of the magnetic anisotropy requires additional crystal field

References begin on page 170

parameters. The presence of additional crystal field parameters, such as L = 2, 4 and 6 complicate the calculation and result in the expression of the magnetic anisotropy as shown in equation (4.5).

$$\chi_{\parallel} - \chi_{\perp} = C_2 T^{-2} + C_3 T^{-3} \tag{4.5}$$

For the lanthanide complexes that require more than 6 crystal-field parameters, the equation for the T^{-3} temperature dependent term can be written as given below (equation 4.6):

$$C_3 = -(2/315)g_J^2\beta_e^2 k^{-3} J(J+1)(2J-1)(2J+3)(J-1)(J+2)k_1 a_{20}^2 + 6k_2 a_{20}a_{40} + k_3(10a_{40}^2 - 7a_{43}^2) + k_4(30a_{40}a_{60} + 12\sqrt{3}a_{63}a_{43}) + k_5(7a_{60}^2 - 5a_{63}^2 - 22a_{66}^2) \tag{4.6}$$

Here, $k_{J's}$ are the constants and depend on the lanthanides. McGarvey expressed the crystal field parameters as a_{LM}[41, 44] (Stevens formulation) and reported that a contribution of the T^{-3} term can not be ignored for the calculation of magnetic anisotropies because it contributes ~10-20 % at room temperature. Conversion of a_{LM} to B's can be done using another operator, A_L^M, given in the literature.[44, 45]

In this Chapter we are reinvestigating the importance of higher temperature dependent terms and their significant contribution in pseudocontact shifts and magnetic anisotropy at room temperature. In our study we calculated the magnetic anisotropies of the given crystal field parameters over the range of 100-500 K using McGarvey's and Bleaney's methods and then compared them with the values obtained from the computational program employing full quantum mechanical treatment (CONDON).[46]

References begin on page 170

4.2 Results and Discussion

4.2.1 Temperature Dependent Magnetic Anisotropy

In order to determine the consequence of T^{-3} and higher terms on pseudocontact shifts, a series of earlier reported isostructural lanthanide complexes were selected. The given crystal field parameters ($B_{2's}$, $B_{4's}$ and $B_{6's}$) of these chosen complexes were used to calculate the temperature dependent magnetic anisotropy using Bleaney's and McGarvey's equations (4.1 and 4.4).[7, 44] Other than calculating the magnetic anisotropies of the paramagnetic lanthanides, these methods can also be used to express the magnitude and the sign of the pseudocontact shifts. Contribution of both T^{-2} and T^{-3} terms on lanthanide's pseudocontact shifts were calculated over the temperature range from 100 to 500 K at 10 K intervals. All the crystal field parameters used in this study were obtained from the literature.[47-53]

Bis(phthalocyaninato)lanthanide complexes $[Pc_2Ln]^-TBA^+$ - The first example (Figure 4.1) chosen in this study is a set of anionic bis(phthalocyaninato)lanthanide complexes $[Pc_2Ln]^-TBA^+$ (where Pc = dianion of phthalocyanin, and Ln = Tb^{3+}, Dy^{3+}, Ho^{3+}, Er^{3+}, Tm^{3+} and Yb^{3+}; TBA = tetra(*n*-butyl)ammonium). Crystal field parameters of these fully characterized compounds have been reported earlier.[47] These double-decker phthalocyanine complexes contain eight-coordinate lanthanide metal center sandwiched between two π-conjugate planar ligands. These complexes have D_{4d} symmetry, which requires only three major crystal field parameters (B_{20}, B_{40} and B_{60}). The solid-state molecular structures of these isostructural complexes,[47] as determined by X-ray crystallography, showed a slight decrease in skew

References begin on page 170

angle and distance between both ligands, with increase in lanthanide atomic number, due to the lanthanide contraction.

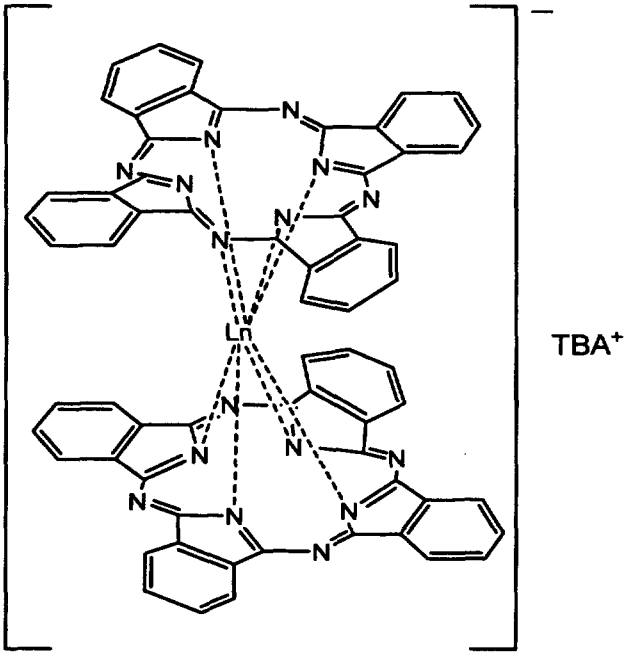

Figure 4.1. Diagram of $[Pc_2Ln]^-TBA^+$, showing lanthanide ion (Ln = Tb^{3+}, Dy^{3+}, Ho^{3+}, Er^{3+} Tm^{3+} and Yb^{3+}) sandwiched between two phthalocyanine ligands.

The comparison of the two approaches (Bleaney's equation 4.3 and McGarvey's equation 4.5) to estimate the magnetic anisotropy using the reported crystal field parameters are plotted, along with the full quantum mechanical treatment (CONDON) and is shown in Figure 4.2 & 4.3. It was reported earlier that the T^{-2} term is an important factor and plays as a major component in pseudocontact shifts at room temperature, where other terms are less than 10 %.[7] Our results suggest that the contribution of the T^{-3} and other higher order terms is also noteworthy at room temperature and can be neglected only at extremely high temperatures (>500 K).

References begin on page 170

Anisotropy versus temperature graphs in Figure 4.2, show that at temperature range from 300-500 K, anisotropies calculated from equation 4.5 (including T^{-3} term) is closer to the CONDON values than the anisotropies calculated from equation 4.3 (only T^{-2} term).

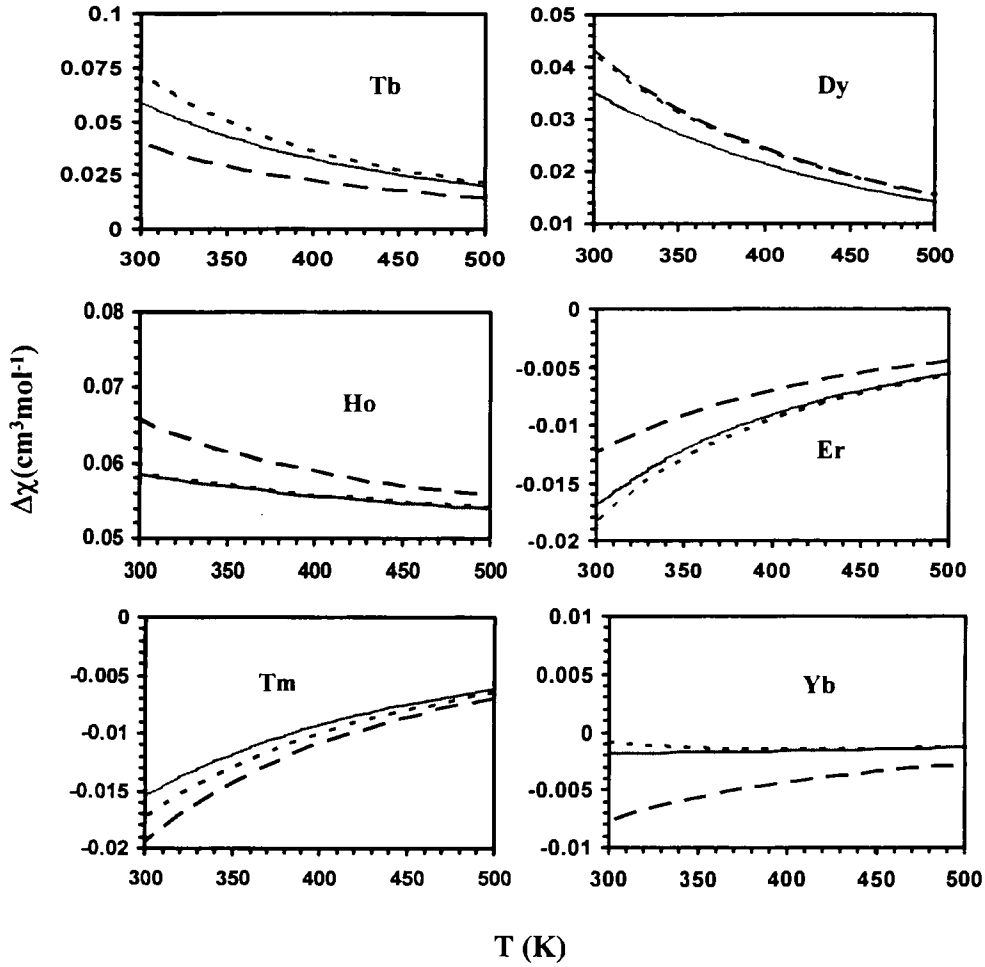

Figure 4.2. Comparison plots of temperature dependent magnetic anisotropies ($\Delta\chi$) calculated from Bleaney's equation 4.3 (big dash), McGarvey's equation 4.5 (small dash) and a complete quantum mechanical treatment (CONDON) (grey line) vs temperature (T) for $[Pc_2Ln]^-TBA^+$. Deviation in anisotropy at temperature ranges from 300-500 K.

References begin on page 170

Data calculated in the temperature range from 300-500 K revealed the importance of higher terms such as T^{-3}, which suggested that higher terms contributed almost 2-48 % of the T^{-2} term. However, in the case of Tb and Yb-complexes the T^{-3} contribution is around 85-90 % of the T^{-2} term. It is noticeable from the graphs shown in Figure 4.1 that the T^{-2} term alone does not provide sufficient magnitude for anisotropy to match up with the CONDON values. This error between CONDON values and T^{-2} values become less after including the T^{-3} term. In this example, the T^{-3} term is more important than the T^{-2} term over the temperature range from 300-500 K for calculating anisotropies, however, no obvious trend was observed among the lanthanide series. Although, including the T^{-3} term gives the results closer to CONDON, it also shows the presence of other higher terms below 250 K, which deviate the magnetic anisotropy from the anisotropy obtained from CONDON (Figure 4.3). Comparison of magnetic anisotropy calculations also showed that the magnitude of the C_2 term is proportional to the second order crystal field (L = 2), and the magnitude as well as the sign of the C_3 term is proportional to the higher crystal field parameters such as L = 2, 4 and 6. Although B_{20} and other second order crystal field parameters play major roles in temperature dependent magnetic anisotropy, other crystal field terms also have significant contributions and hence these cannot be ignored.

References begin on page 170

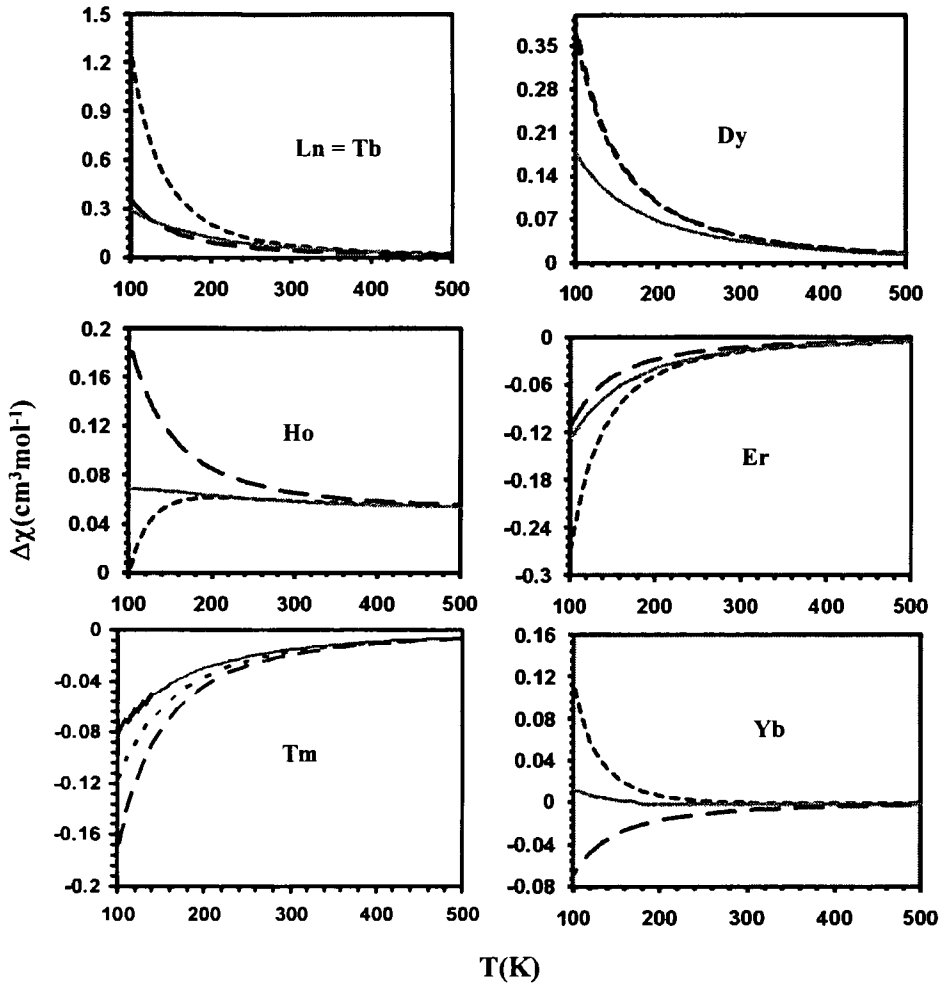

Figure 4.3. Comparison plots of temperature dependent magnetic anisotropies ($\Delta\chi$) calculated from Bleaney's equation 4.3 (big dash), McGarvey's equation 4.5 (small dash) and a complete quantum mechanical treatment (CONDON) (grey line) vs temperature (T) for $[Pc_2Ln]^-TBA^+$ at temperature ranges from 100-500 K.

To analyse the contribution of the T^{-3} relative to the T^{-2} term, the ratio of C_3/C_2T was calculated as shown in Table 4.1. The results showed that variation (2-90 % of the C_2 term) in the contribution of the C_3 term can be noticed through out the lanthanide series.

References begin on page 170

Table 4.1. Ratio of (C_3/C_2T)x100 at 300 K in $[LnPc_2]^-TBA^+$

Ln	B_{20}[(a)]	B_{40}[(a)]	B_{60}[(a)]	Ratio (C_3/C_2T)x100	%Errors Relative to CONDON	
					C_2	C_3
Tb^{3+}	840	−1840	592	84.06	67.5	10.9
Dy^{3+}	800	−1760	640	−1.62	23.7	21.2
Ho^{3+}	740	−1600	720	−45.59	267	5.6
Er^{3+}	700	−1480	752	47.59	27.3	7.3
Tm^{3+}	676	−1200	800	−10.71	24.2	10.9
Yb^{3+}	650	−1200	960	−89.06	300	44.6

[(a)] Crystal field parameters are expressed in Wybourne's formulation (cm^{-1})

Since we are emphasising the importance of the T^{-3} and other higher temperature dependent terms on pseudocontact shifts, the relative % errors (% error of C_2 and C_3 relative to CONDON) were also calculated over the temperature range of 100-500 K. As shown from Table 4.1, comparison of the magnetic susceptibilities calculated from CONDON and the C_3 term showed less difference and closer values than obtained by comparing CONDON values with the C_2 term.

Not only the overall magnetic susceptibility but both the key components (χ_{xx}/χ_{yy} and χ_{zz}) of the magnetic susceptibility also show their temperature dependency. The change in the product of susceptibility and temperature ($\chi_{xx}T$ and $\chi_{zz}T$) can be noticed in Figure 4.4. Of all these lanthanide complexes, Tb and Dy complexes show the decrease in $\chi_{zz}T$ and increase in $\chi_{xx}T$, starting above 100 K. The difference in both components at low temperature is due to the higher energy gap between the ground substates. In case of $[Pc_2Ho]^-$, the rapid change in $\chi_{xx}T$ and $\chi_{zz}T$ values at low temperatures are the result of a strong temperature dependency. In case of $[Pc_2Yb]^-$, the $\chi_{xx}T$ value starts to increase at low temperature and at 270 K shows a higher value than $\chi_{zz}T$. This change in anisotropy is due to the increase in the population in the higher energy states. These results also

References begin on page 170

suggest a clear division between metal ions on the basis of axial and planar magnetic anisotropies, in which Tb, Dy and Ho-complexes show a higher value of $\chi_{zz}T$ and Er, Tm and Yb-complexes show a higher value of $\chi_{xx}T$ at room temperature.

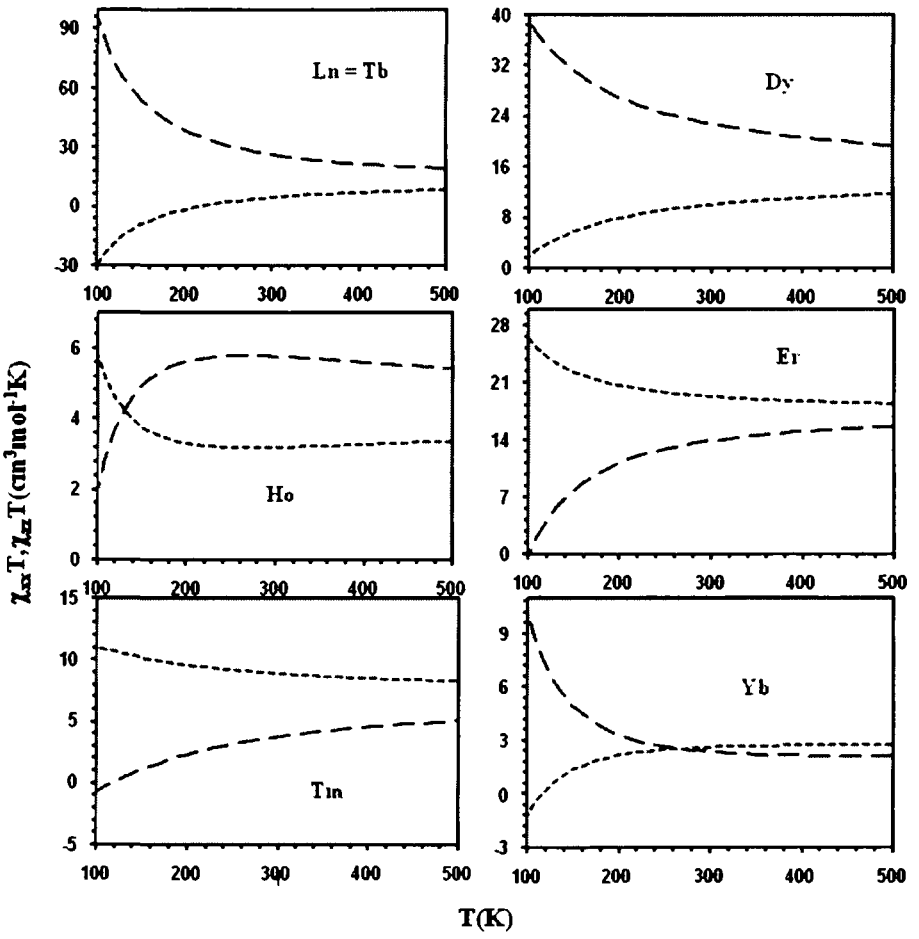

Figure 4.4. Temperature dependence of the products of the magnetic susceptibilities and temperature $\chi_{xx}T$ (small dash), $\chi_{zz}T$ (big dash) of $[Pc_2Ln]^-TBA^+$ for C_3 and higher terms using only McGarvey's equation.

References begin on page 170

As mentioned earlier, lanthanide induced shifts (LIS) are the combination of contact and pseudocontact shifts, which depend on T^{-1} and T^{-2} respectively (equation (4.7)).[7, 38, 42] Thus, in principle, the individual contribution of these terms on LIS can be easily measured and both T^{-1} and T^{-2} can be separated by plotting a graph between $\delta_{LIS}\cdot T$ vs T^{-1}.

$$\delta_{LIS}T = \delta_{CS} + \frac{\delta_{PCS}}{T} \qquad (4.7)$$

However, according to our calculations, due to the considerable involvement of other higher terms such as T^{-3} in pseudocontact shifts, separation of the two shifts on the basis of temperature dependence is unfeasible. On the basis of our theory that pseudocontact shifts are the combination of multiple temperature dependent terms in which not only T^{-2} but T^{-3} and higher terms are also important, paramagnetic shifts of $[LnPc_2]^-$ were calculated using C_2 and C_3 terms. The calculated shifts obtained from both terms were then compared to the reported chemical shifts of $[LnPc_2]^-$.[47] Depending upon the position of the protons from the metal center as given in Table 4.2, δ_α and δ_β represent the chemical shifts of the closer and farther protons respectively. The results as given Table 4.2, show the remarkable similarities between experimental and calculated values $\Delta\delta_{calcd}$ (C_3 term) than $\Delta\delta_{calcd}$ (C_2 term). Similar to the constant value of the ratios ($\Delta\delta_\beta/\Delta\delta_\alpha$) given in the paper,[47] calculations using C_2 and C_3 terms also gave a constant chemical shift ratio ($\Delta\delta_\beta/\Delta\delta_\alpha$), and hence verified the presence of a negligible contact term in paramagnetic NMR shifts. The difference in the chemical shifts of paramagnetic lanthanide complexes with respect to the diamagnetic yttrium complex is represented by $\Delta\delta$.

References begin on page 170

Table 4.2. Comparison of calculated chemical shifts using Bleaney's and McGarvey's (equation 4.3 &equation 4.5) approaches and the experimental chemical shifts (δ) of $[LnPc_2]^-$

Ln	$\Delta\delta_\alpha$(obs)	$\Delta\delta_\alpha(C_2)$	$\Delta\delta_\alpha(C_3)$	$\Delta\delta_\beta$(obs)	$\Delta\delta_\beta(C_2)$	$\Delta\delta_\beta(C_3)$	$\Delta\delta_\beta/\Delta\delta_\alpha$ (obs)	$\Delta\delta_\beta/\Delta\delta_\alpha$ (C_3)	$\Delta\delta_\beta/\Delta\delta_\alpha$ (C_3)
Tb^{3+}	−94.2	−57.7	−106.0	−48.71	−29.2	−53.8	0.52	0.51	0.51
Dy^{3+}	−51.06	−63.23	−62.24	−26.71	−32.05	−31.55	0.52	0.51	0.51
Ho^{3+}	−14.53	−23.0	−12.5	−7.81	−11.7	−6.34	0.54	0.51	0.51
Er^{3+}	26.21	17.9	26.50	13.04	9.09	13.4	0.50	0.51	0.51
Tm^{3+}	25.99	28.07	25.07	13.07	14.23	12.70	0.50	0.51	0.51
Yb^{3+}	3.05	11.10	1.21	1.56	5.62	0.615	0.51	0.51	0.51

Though the C_2 term is important at extremely high temperatures (>500 K), higher terms are important at room temperature and contribute ~30-40 % of the C_2 term. The absence of the higher terms can be easily predicted from Figure 4.5, where chemical shift calculations using only the C_2 term showed larger errors than the chemical shifts calculated using the C_3 term. As reported by Ishikawa and coworkers,[47] calculations for the magnetic anisotropy of $[YbPc_2]^-$ using both Bleaney's and McGarvey's methods also showed change in the anisotropy's sign in between 180-190 K, where planar anisotropy dominates axial anisotropy.

References begin on page 170

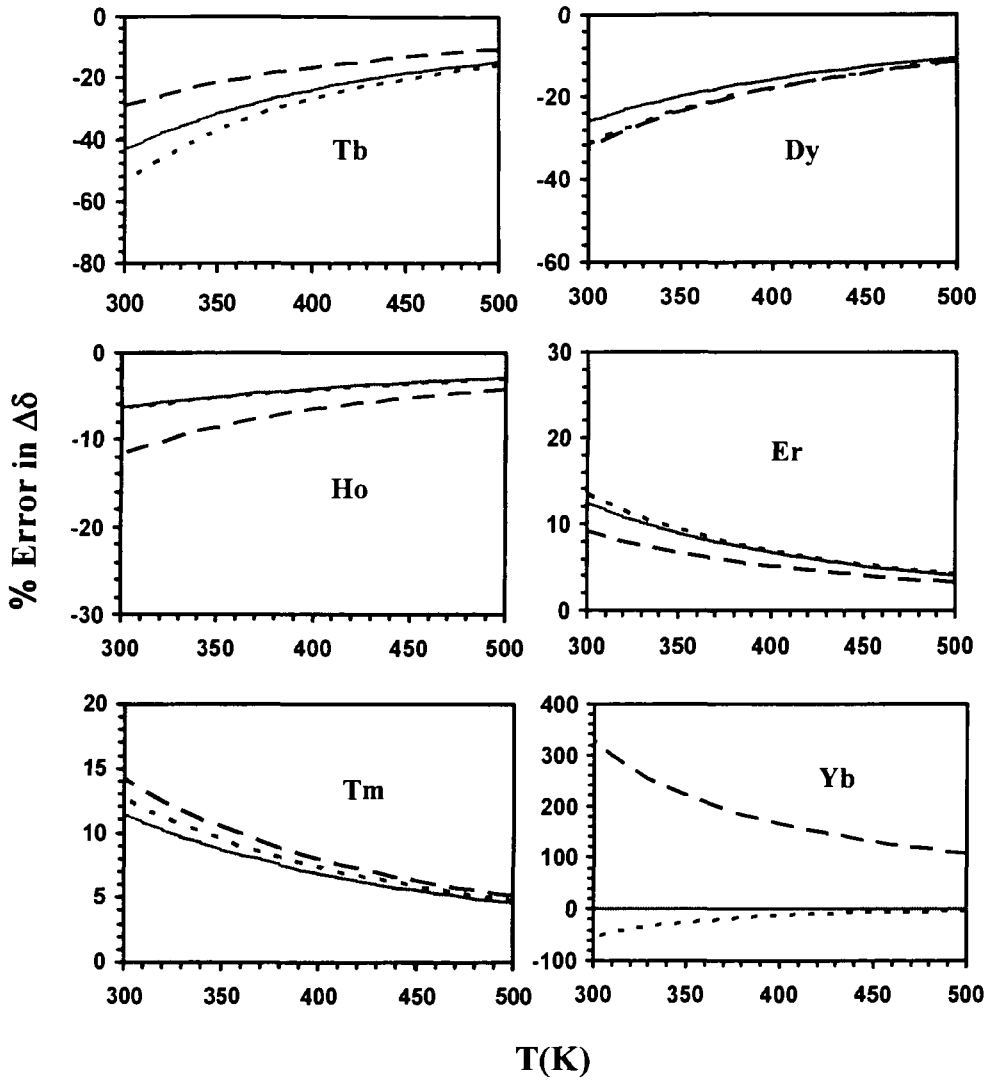

Figure 4.5. Plots of ^{1}H NMR shifts % error vs temperature showing the importance of higher terms in $[Pc_2Ln]^-TBA$. Each grey line, small dash and big dash represents the chemical shift calculated from CONDON, % error in chemical shifts using C_3 and C_2 terms respectively relative to CONDON values at temperature range from 300-500 K.

References begin on page 170

Ln(trensal) - Another example, which was selected to verify our approach towards the T^{-3} term is a set of Ln(trensal) (where trensal = 2,2',2''-tris(salicylideneimino)triethylamine) with known crystal field parameters as shown in Figure 4.6.[48] Syntheses and X-ray details of these compounds were reported earlier.[54, 55] The trensal ligand is a tripodal heptadentate ligand, which forms a isomorphous and isostructural series of trivalent lanthanide complexes using trivalent lanthanide metal ions (Ce-Yb). All these Ln(trensal) compounds have C_3 symmetry, and except for the Ce, Gd and Yb compounds all require B_{20}, B_{40}, B_{43}, B_{60}, B_{63} and B_{66}. While the Gd complex showed no absorption bands in IR-spectra in 0-25000 cm^{-1}, the Ce and Yb complexes showed small number of transitions, which could not be used to generate the parameters required for C_3 symmetry complexes.

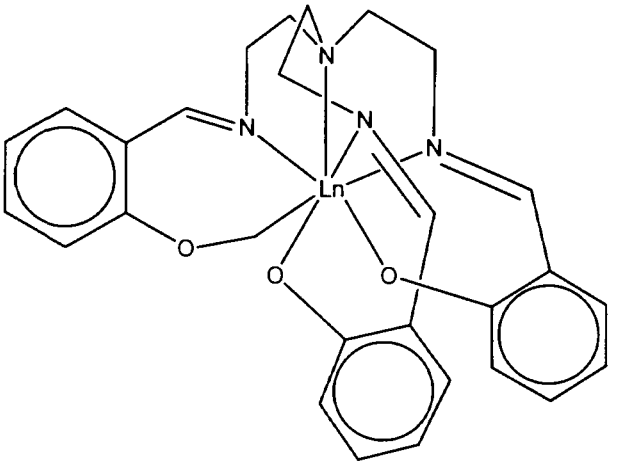

Figure 4.6. Schematic diagram of Ln(trensal) where Ln = Ce-Yb.

As in the first example, the Ln(trensal) complexes also displayed a strong dependence of the pseudocontact shifts on the T^{-3} and other higher temperature dependent terms. The results demonstrated that, for a series of isostructural trivalent lanthanide complexes with larger than C_2 molecular symmetry, higher rank crystal field

References begin on page 170

parameters ($B_{4's}$ and $B_{6's}$) are also require to determine the magnetic anisotropy. The graphical representations shown in Figure 4.7 reveal that the presence of the T^{-2} term alone gave an enormous error in calculating magnetic anisotropy, which can be reduced by the introduction of the T^{-3} and sometimes higher terms. These results also confirmed the contribution of the T^{-3} and higher order terms to around 14-82 % of the T^{-2} term at room temperature. The trivalent Ho(trensal) complex show an exceptionally high percentage of higher temperature dependent terms (146-245 %) of the T^{-2} term.

References begin on page 170

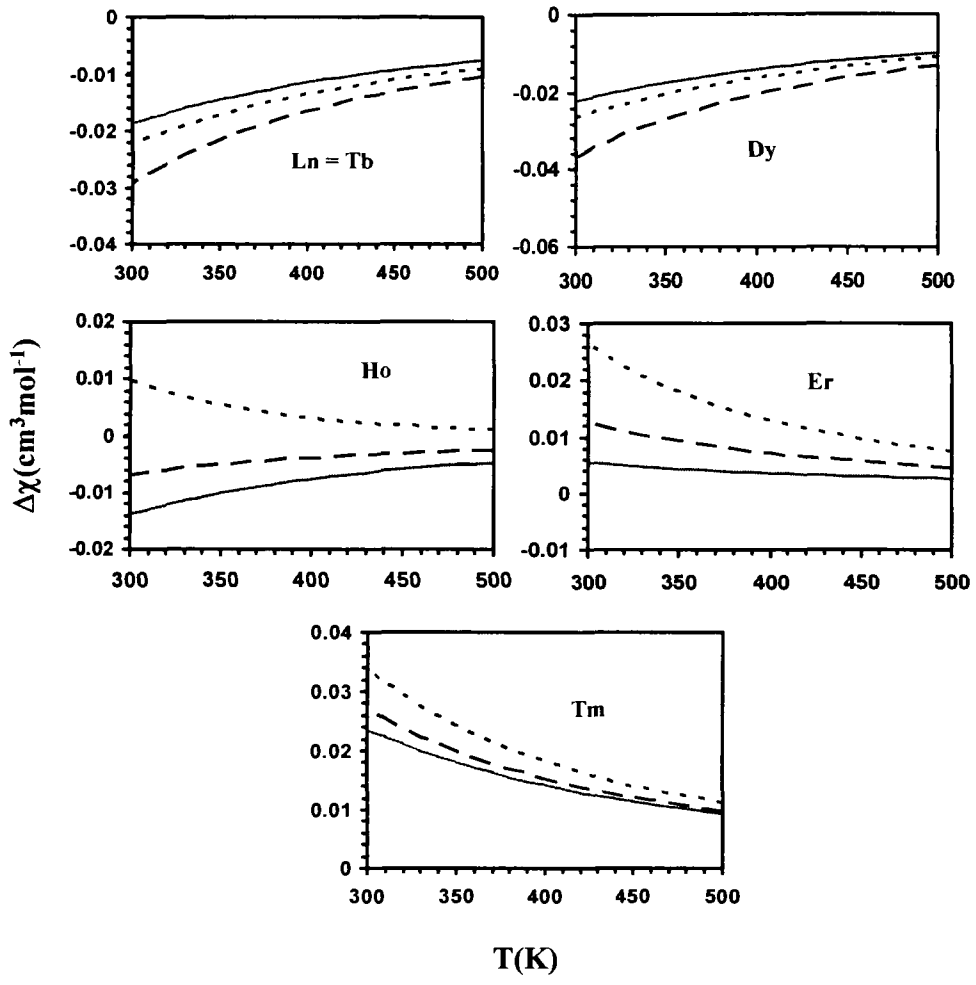

Figure 4.7. Comparison plot of temperature dependent magnetic anisotropies ($\Delta\chi$) calculated from Bleaney's (big dashed line), McGarvey's equation's (small dashed line) and CONDON (grey line) vs temperature (T) for Ln(trensal) from temperature 300-500 K.

Results obtained by calculating (C_3/C_2T) as shown in Table 4.3 reveal that at room temperature the magnitude of the C_3 and higher terms are almost 25-244 % of the C_2 term, which also proves their significant contribution in pseudocontact shifts. However, Ho(trensal) showed an exceptionally high contribution of higher terms due to the result of a higher C_3 and a very low C_2 value.

References begin on page 170

Table 4.3. For Ln^{3+} in Ln(trensal), calculated C_3/C_2T for the given crystal field parameters at 300 K.

Ln	B_{20}	B_{40}	B_{43}	B_{60}	B_{63}	B_{66}	%Ratio (C_3/C_2T)x100	% Error Relative to CONDON	
								C_2	C_3
Tb^{3+}	−617	92	−1928	1582	719	1103	−23.38	6.5	16
Dy^{3+}	−671	−186	−2153	1241	439	660	−27.75	60.8	17.3
Ho^{3+}	−316	−186	−1910	1146	732	460	−243.97	51	168
Er^{3+}	−720	−44	−2121	988	353	545	80.96	132	320
Tm^{3+}	−952	86	−1780	1168	143	801	25.60	15	43

Calculations for % error between the computational values and the anisotropies calculated from Bleaney's and McGarvey's methods, showed the closer correspondence of the values calculated using additional higher terms (C_3 term) with the computational values. The dependency of temperature on anisotropic components (Figure 4.8) shows that in case of Tb(trensal) and Dy(trensal), planar anisotropy dominates over axial anisotropy at room temperature, whereas Er(trensal) and Tm(trensal) show higher axial anisotropy at room temperature. Although Ho(trensal) also shows the greater value of axial anisotropy at room temperature, the difference between the value of χ_{zz} and χ_{xx} is very small.

References begin on page 170

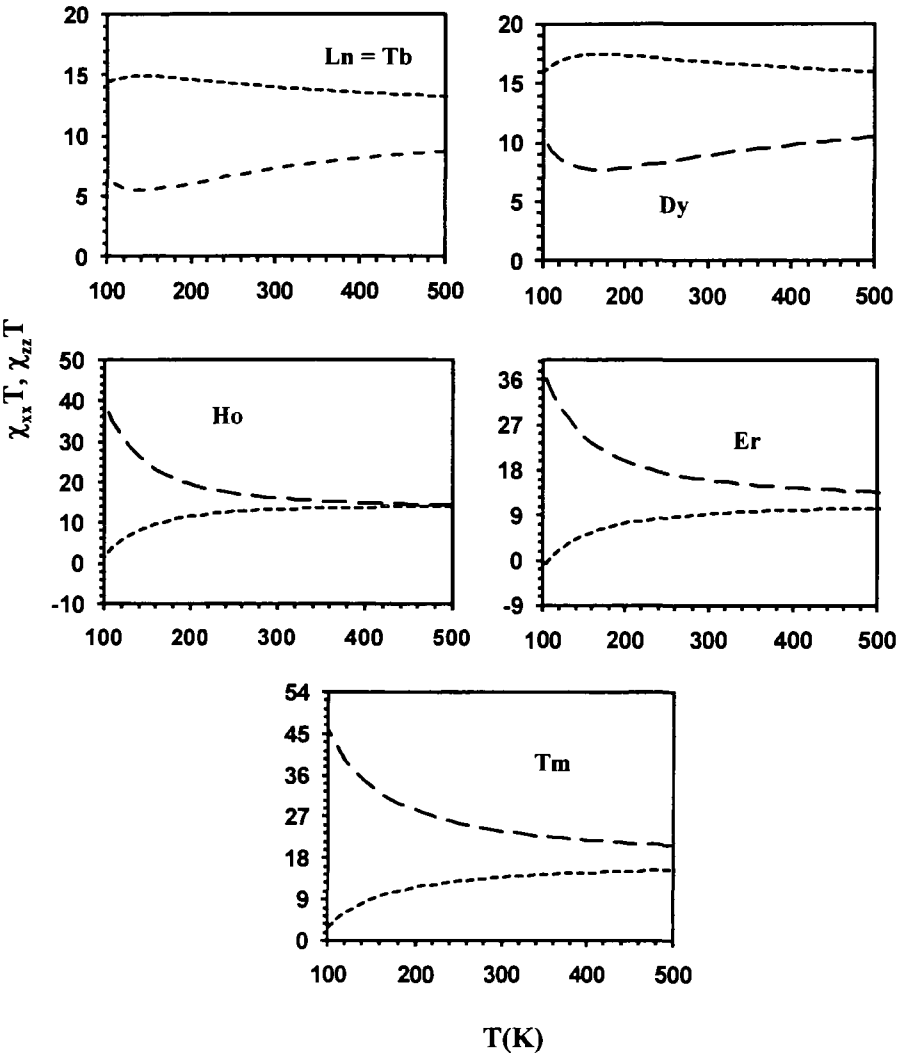

Figure 4.8. Plots of temperature dependent anisotropic components ($\chi_{xx}T/\chi_{zz}T$) versus temperature for Ln(trensal) using C_3 and higher terms, where $\chi_{xx}T$ (small dash), $\chi_{zz}T$ (big dash).

$[Ln(dipic)_3]^{3-}$ - The example of recently reported isostructural lanthanide complexes $[N(C_2H_5)_4]_3[Ln(dipic)_3]\cdot nH_2O$, where Ln = Tb, Dy, Ho, Er, Tm or Yb and dipic = pyridine-2,6-dicarboxylate, were also used in this study to verify the importance of McGarvey's higher terms.[49] As shown in Figure 4.9, the isostructural nine coordinate

References begin on page 170

complexes exhibit D_3 symmetry, which contain six crystal field parameters covering the second, third and forth rank ($B_{2's}$, $B_{4's}$ and $B_{6's}$).

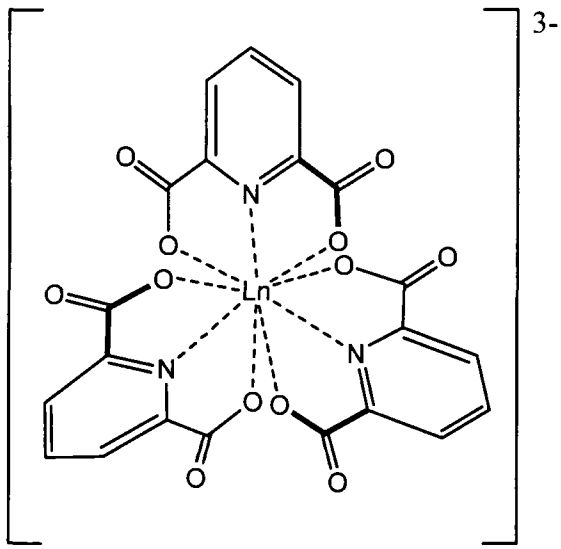

Figure 4.9. Nine coordinate $[Ln(dipic)_3]^{3-}$, where Ln = Tb, Dy, Ho, Er, Tm or Yb.

Magnetic anisotropy calculations for all the metal complexes using T^{-2}, T^{-3} and CONDON, as shown in Figure 4.10, illustrate that the higher order temperature dependent terms are important and give values closer to the CONDON values. While the T^{-2} term is important at extremely high temperatures (above 500 K), significant contribution of the higher terms can be observed at low temperatures (300-500 K). Similar to $[Pc_2Yb]^-$, $[Yb(dipic)_3]^{-3}$ also shows a change in the direction of magnetic susceptibility at room temperature.

The detailed study of the importance of higher terms over the T^{-2} revealed that except for the Dy complex, all other complexes show the presence of additional higher temperature terms such as T^{-4} and higher at low temperatures (below 300 K). To check the significance of each crystal field parameter on the magnetic anisotropy, calculations

References begin on page 170

were done using each parameter independently, which resulted in the finding that similar to second order crystal field, higher crystal field parameters such as fourth and sixth rank are also important.

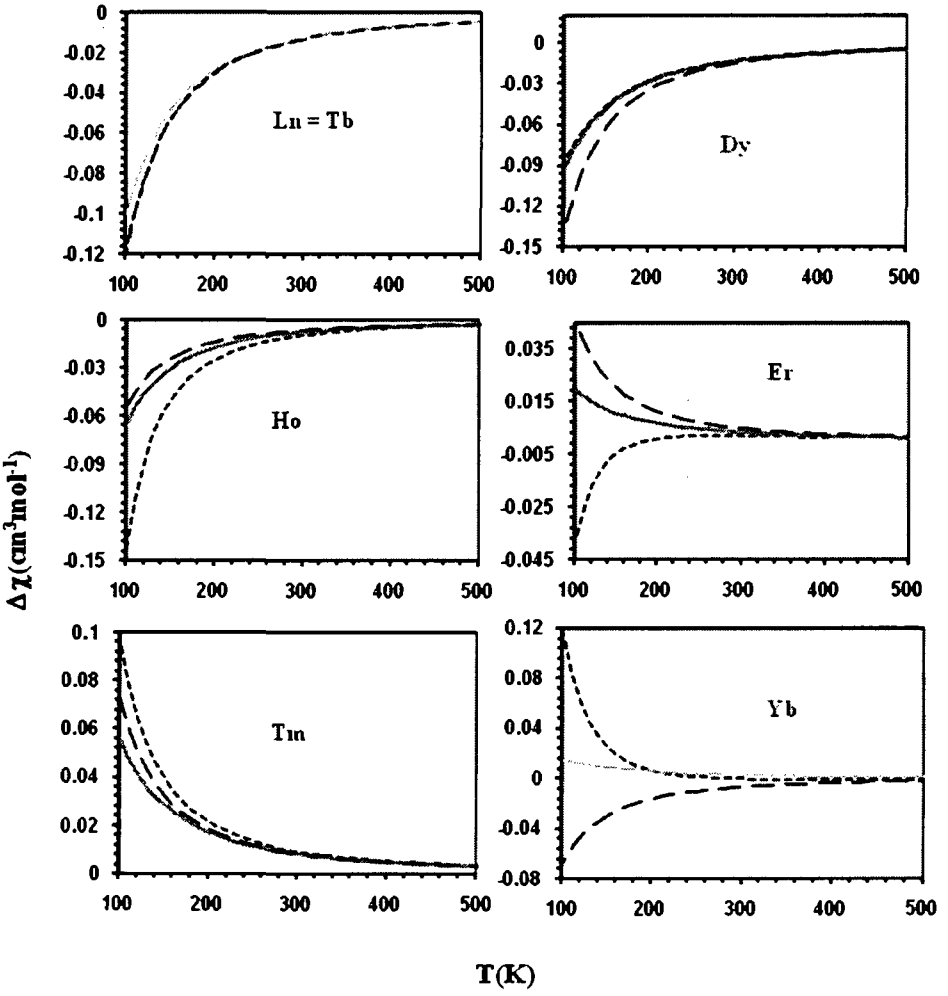

Figure 4.10. Comparison plot of temperature dependent magnetic anisotropies ($\Delta\chi$) calculated from Bleaney's equation (big dashed line), McGarvey's equation (small dashed line) and CONDON (grey line) vs temperature (T) for $[Ln(dipic)_3]^{-3}$.

References begin on page 170

Ln(btmsa)$_3$– It has been reported earlier that tris(bis(trimethylsilyl)amido)lanthanide complexes (Ln(btmsa)$_3$, where Ln = Dy, Ho, Er and Yb) showed C_{3v} symmetry and required B_{20}, B_{40}, B_{43}, B_{60} B_{63} and B_{66}.[50, 56] Crystal field parameters of these complexes were obtained from the low and room temperature absorption and luminescence spectra.[56] As reported earlier, crystal structures of these complexes showed the center metal ion surrounded by three nitrogen atoms of the amido ligand. Calculated values of (C_3/C_2T)x100 for these systems showed that the magnitude of higher terms, mainly T^{-3}, is with in the range from 9-80 % of the T^{-2} term at room temperature. Similar to other examples, these complexes also verified the presence of other higher terms, such as T^{-4}, below 250 K (Figure 4.11).

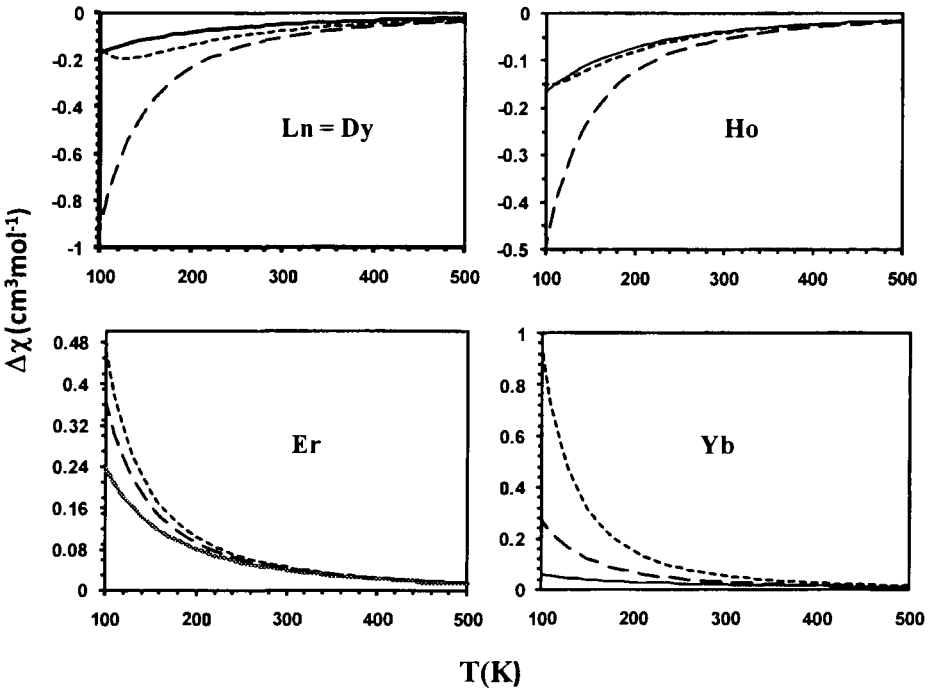

Figure 4.11. Comparison plot of temperature dependent magnetic anisotropies ($\Delta\chi$) calculated from Bleaney's (big dashed line), McGarvey's methods (small dashed line) and CONDON (grey line) vs temperature (T) for [Ln(btmsa)$_3$].

References begin on page 170

LnOCl - The present example is based on the crystal field parameters of axial symmetric lanthanide complexes given in the literature, which were used for the calculation of magnetic anisotropies using C_2 and C_3 terms.[57] Reported lanthanide oxychlorides are a set of the complexes that contain C_{4v} symmetry and posses five non-zero crystal field parameters (B_{20}, B_{40}, B_{44}, B_{60} and B_{64}) obtained from their optical spectra.[57] Unlike compounds with C_{3v} symmetry, C_{4v} systems require additional B_{44} and B_{64} parameters instead of B_{43} and B_{63} crystal field parameters. As shown in Figure 4.12, all four complexes show the dominating higher temperature dependent terms below 250 K and the major contribution of T^{-2} term at relatively high temperature (Figure 4.13). Below 300 K, T^{-4} and higher terms contributions are also noticeable in all these complexes. Study of individual parameters showed the negligible contribution of B_{64} term in these complexes.

References begin on page 170

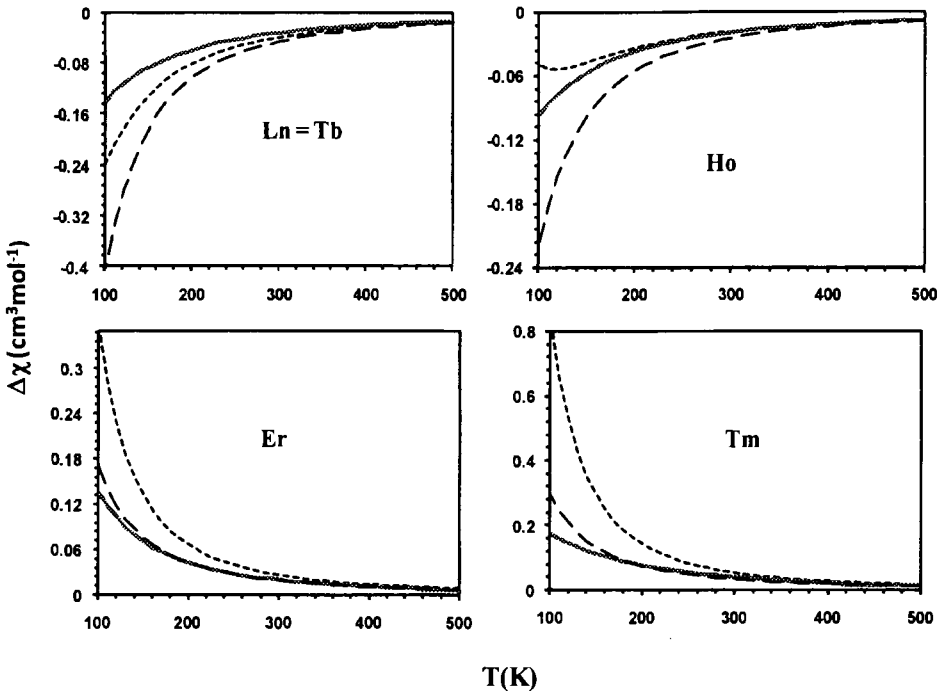

Figure 4.12. Comparison plot of temperature dependent magnetic anisotropies ($\Delta\chi$) calculated from Bleaney's (big dashed line), McGarvey's methods (small dashed line) and CONDON (grey line) vs temperature (T) for LnOCl (Ln = Tb, Ho, Er or Tm).

References begin on page 170

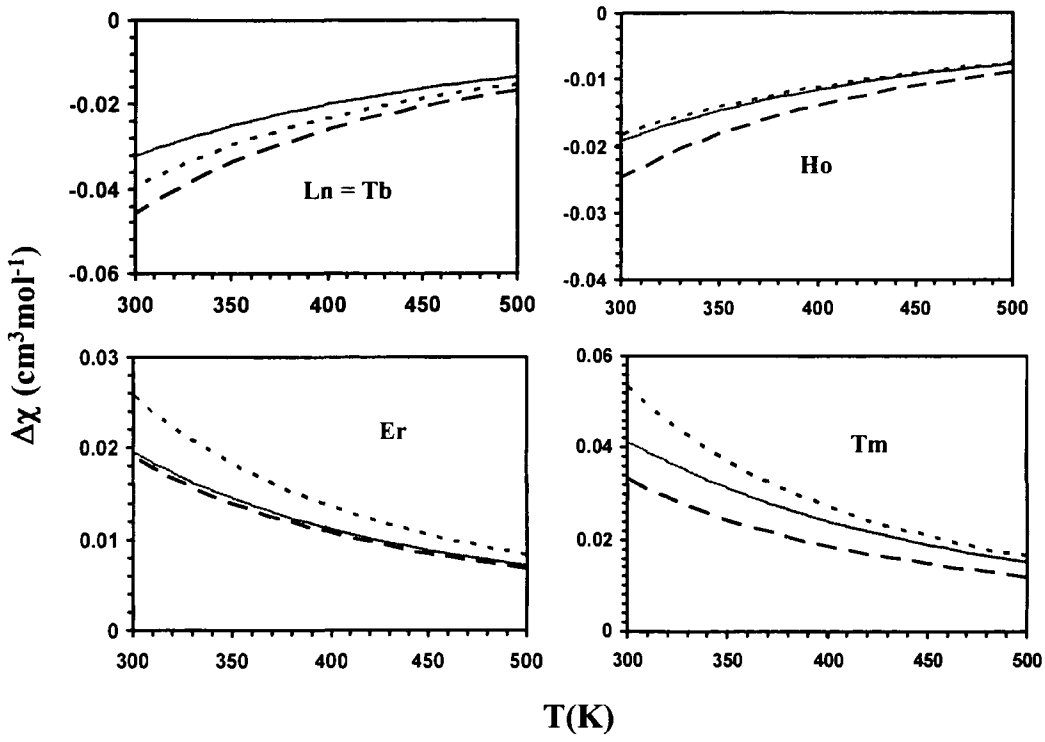

Figure 4.13. Comparison plot of temperature dependent magnetic anisotropies ($\Delta\chi$) calculated from Bleaney's (big dashed line), McGarvey's methods (small dashed line) and CONDON (grey line) vs temperature (T) for LnOCl (Ln = Tb, Ho, Er or Tm) at temperature range from 300-500 K.

References begin on page 170

R_2Fe_{17} - A system containing lanthanide complexes of type R_2Fe_{17} (R = lanthanides) crystallized in two different manners, i.e., hexagonal and rhombohedral, after their crystallization in Th_2Ni_{17} and in Th_2Zn_{17}, respectively.[51] Four crystal field parameters (B_{20}, B_{40}, B_{60} and B_{66}) were obtained for the reported complexes. The complexes showed weaker R-R (*f-f*) interactions related to Fe-Ln (*d-f*) metal interactions. As shown in Figure 4.14, except Er_2Fe_{17} and Tm_2Fe_{17}, all other metal complexes show the presence of the T^{-4} and higher terms at low temperature, due to relatively lower B_{40}, B_{66} values.

References begin on page 170

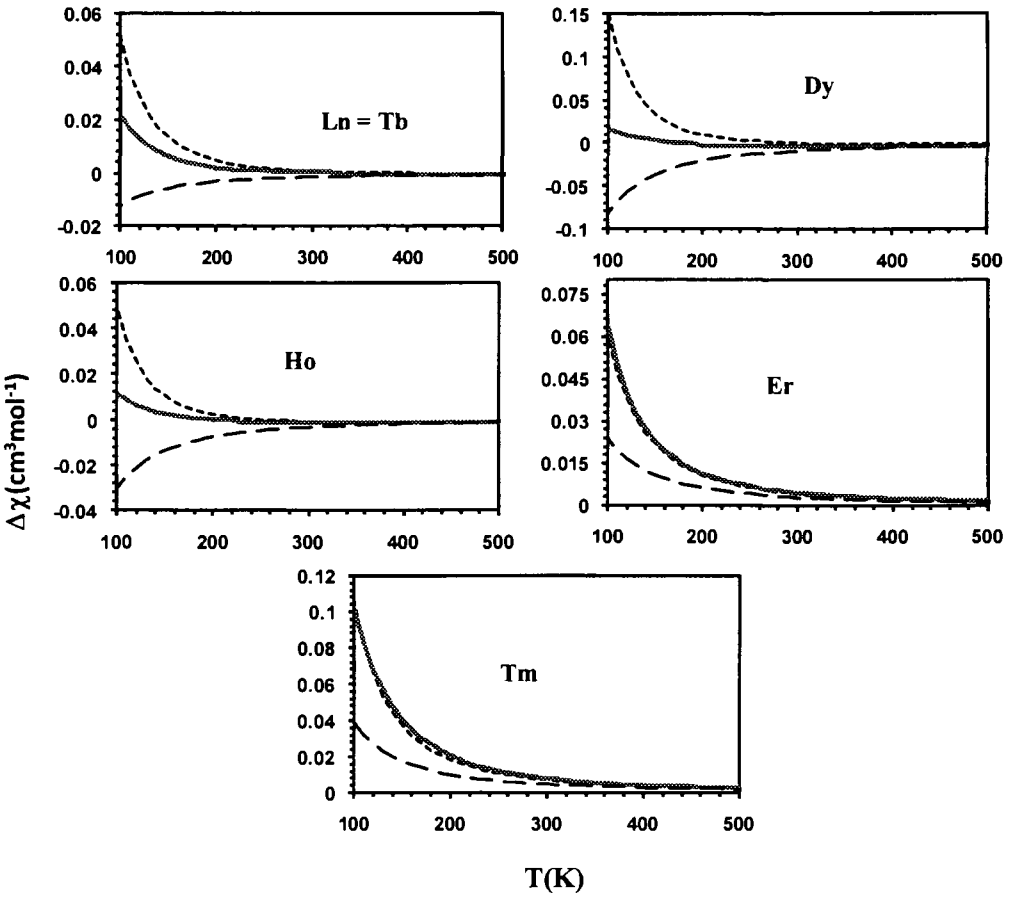

Figure 4.14. Comparison plot of temperature dependent magnetic anisotropies ($\Delta\chi$) calculated from Bleaney's (big dashed line), McGarvey's methods (small dashed line) and CONDON (grey line) vs temperature (T) for R_2Fe_{17} (R = Tb, Dy, Ho, Er or Tm).

***C_{3h}* symmetric lanthanide systems-** Another system reported earlier with C_{3h} symmetry consist of the examples of Tb, Dy, Er and Tm-complexes, which posses four crystal field parameters, including B_{20}, B_{40}, B_{60} and B_{66}.[52, 58] The graphical representation, shown in Figure 4.15, demonstrates that higher order temperature terms make a significant contribution in magnetic anisotropies, which make the calculated values closer to the values obtained from CONDON around 300-500 K. The diversion of

References begin on page 170

the magnetic anisotropy calculated from McGarvey's method below 250 K predicts the presence of other higher terms, contribution of which create a difference between CONDON values and the values calculated from McGarvey's method. While contribution of the T^{-4} and higher terms can be noticed in the Tb and Er complexes below 250 K, the Dy and Tm complexes provide evidence for negligible T^{-4} contribution.

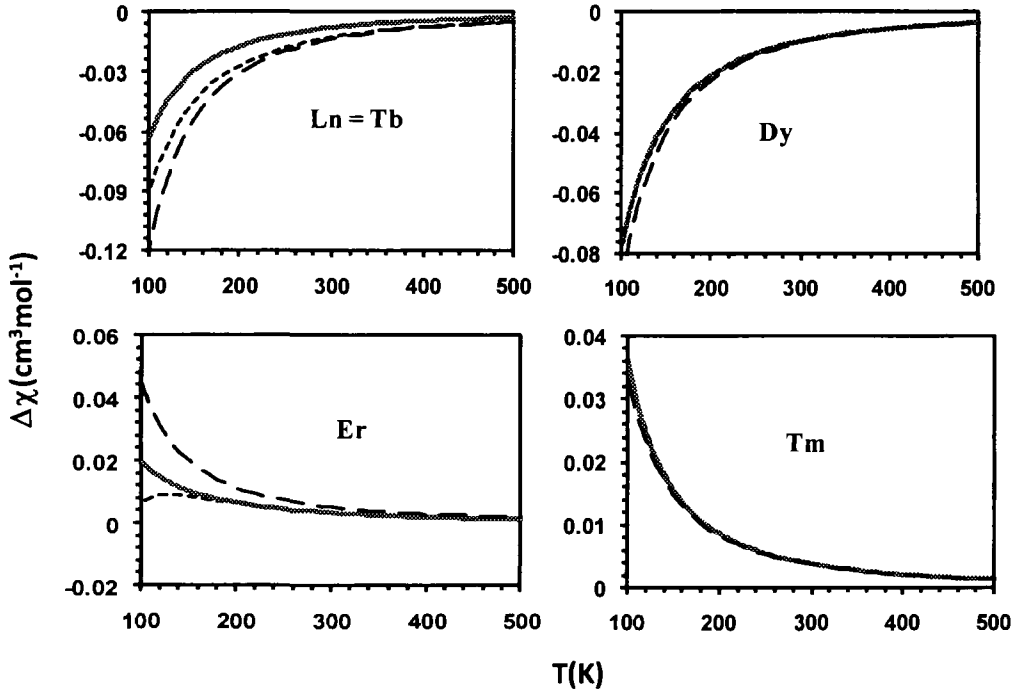

Figure 4.15. Comparison plot of temperature dependent magnetic anisotropies ($\Delta\chi$) calculated from Bleaney's (big dashed line), McGarvey's methods (small dashed line) and CONDON (grey line) vs temperature (T) for the C_{3h} symmetric lanthanide system.

References begin on page 170

Ln^{3+} doped in $LaCl_3$ - Most of the lanthanide complexes reported in the literature for determining the crystal field parameters are trivalent lanthanide ions doped either in ethyl sulfates, nitrates or in $LaCl_3$.[44] Study of these complexes also verified the presence of higher temperature dependent terms such as T^{-3} in between 300-500 K, and in case of Er-complexes, significant contribution of the T^{-4} term, which was completely neglected earlier (Figure 4.16).

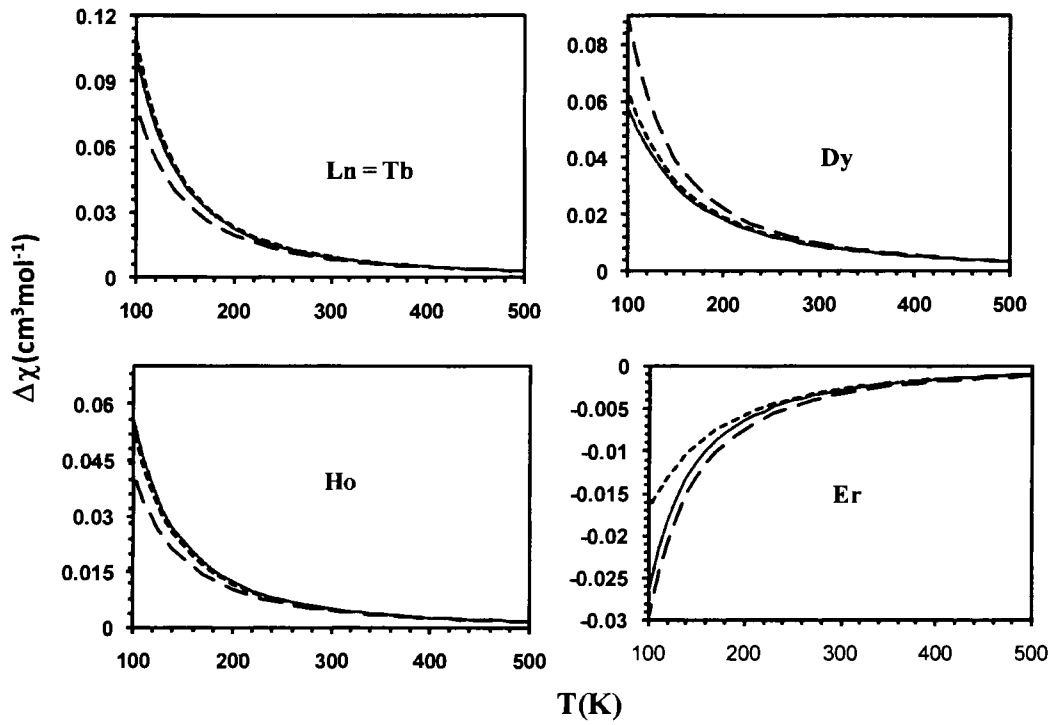

Figure 4.16. Comparison plot of temperature dependent magnetic anisotropies ($\Delta\chi$) calculated from Bleaney's (big dashed line), McGarvey's methods (small dashed line) and CONDON (grey line) vs temperature (T) for Ln^{3+} doped in $LaCl_3$.

References begin on page 170

For the ethyl sulfates doped lanthanide ions, reported crystal field parameters produced the values of $(C_3/C_2T)x100$ = 13-26 %, which confirmed the importance of C_3 and higher terms at room temperature (Table 4.4).

Table 4.4. For Ln^{3+} doped in $La(C_2H_5SO_4)_3(H_2O)_9$ crystals, calculated C_3/C_2T for the given crystal field parameters at 300 K.

Ln	B_{20}	B_{40}	B_{60}	B_{66}	%Ratio $(C_3/C_2T)x100$	% Error Relative to CONDON	
						C_2	C_3
Tb^{3+}	−220	−600	−544	490	22.5	16.9	1.8
Dy^{3+}	240	−632	−480	526	−23.80	43.5	9.3
Ho^{3+}	250	−632	−480	412	13.16	13.7	2.3
Er^{3+}	238	−592	−480	396	−16.00	13.5	4.7
Tm^{3+}	259.6	−568	−457.6	455.6	25.95	14.9	7.2
Yb^{3+}	200	−440	−560	537	−18.62	28.5	4.6

Ln^{3+} at S_4 symmetry sites in $LiYF_4$ - Crystal field parameters of trivalent lanthanide complexes containing tetragonal S_4 symmetry sites in $LiYF_4$ were also used to examine the effect of T^{-2} and higher terms on anisotropies. [53] These complexes were principally studied for the *fd* energy levels of heavy lanthanide complexes and showed the presence of both spin-forbidden and spin-allowed *fd* transitions. For this study trivalent lanthanide ions were incorporated in a $LiYF_4$ host lattice to observe the higher energy *fd* excitation bands. Among all the examples used in this study, the present set of lanthanide complexes exhibit low symmetry features and also require imaginary terms in crystal field parameters. Due to inadequate absorption data, no crystal field parameters were reported for the Yb-complex.

References begin on page 170

The results shown in Table 4.5 represent the anisotropies calculated by temperature dependencies in equation (4.3) and (4.5). These anisotropies were then compared with the calculated values obtained from CONDON to show the relative errors or difference between the T^{-2} and higher terms. The calculated values of C_3/C_2T given in Table 4.5 illustrate that the magnitude of the T^{-3} term is between 5-36 % of the T^{-2} term at room temperature.

Table 4.5. For Ln^{3+} at S_4 symmetry sites in $LiYF_4$, calculated C_3/C_2T and relative anisotropies for the given crystal field parameters at 300 K using CONDON, McGarvey's (C_3) and Bleaney's (C_2) terms.

Ln	B_{20}	B_{40}	B_{60}	%Ratio (C_3/C_2T)	($\Delta\chi$) CONDON	($\Delta\chi$) C_2	($\Delta\chi$) C_3
Tb^{3+}	400	−802	−57	36.64	0.024740	0.018891	0.025811
Dy^{3+}	340	−784	−7	−6.51	0.016172	0.018487	0.017283
Ho^{3+}	408	−629	−18	−5.47	0.008282	0.008717	0.008239
Er^{3+}	352	−820	−134	−9.54	-0.005597	-0.006201	-0.005609
Tm^{3+}	348	−639	−182	−9.79	-0.0104918	-0.0099424	-0.010916

Trivalent Lanthanide Complexes Containing Lighter Lanthanide Metal Ions - Other than heavy lanthanide complexes, examples of lighter lanthanide (Ce, Pr and Nd) complexes [44] were also studied to examine the contributions of the C_3 term on magnetic anisotropy calculation or in pseudocontact shifts. Results obtained from the graphs given in Figure 4.17 suggest that calculation for magnetic anisotropies cannot be

References begin on page 170

obtained without including higher temperature dependent terms, which at room temperature contributed 13-25% of the C_2 term.

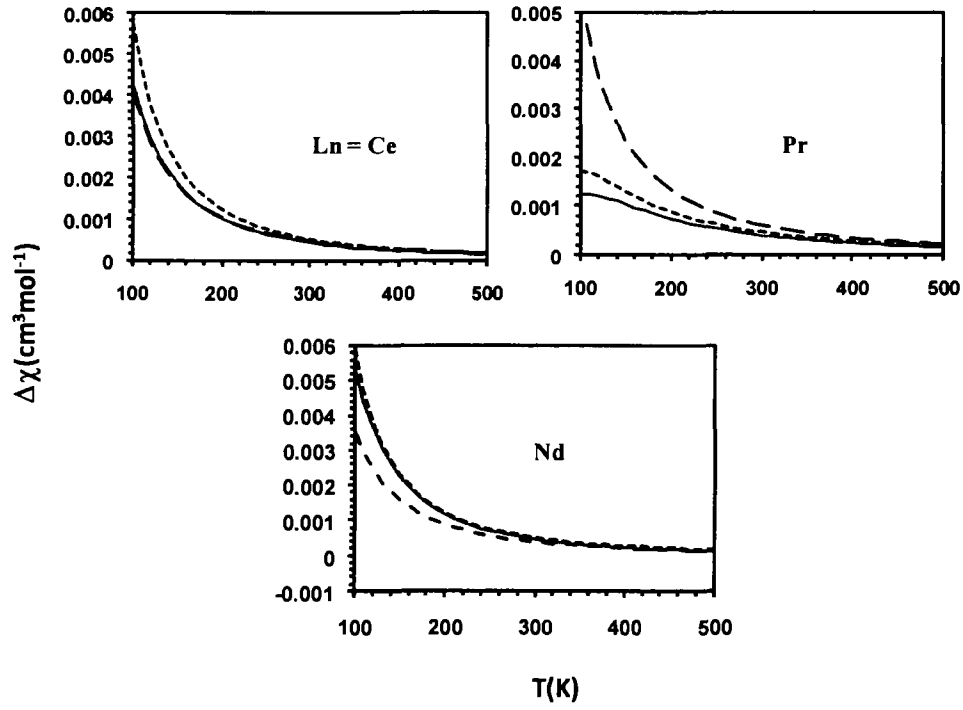

Figure 4.17. Comparison plot of temperature dependent magnetic anisotropies ($\Delta\chi$) calculated from Bleaney's (big dashed line), McGarvey's methods (small dashed line) and CONDON (grey line) vs temperature (T) for Ln^{3+} (Ln = Ce, Pr or Nd) doped in $LaCl_3$.

Another example of early lanthanide ions (Ce^{3+}, Pr^{3+} and Nd^{3+}) was a set of early lanthanide ions doped in ethyl sulfate crystals.[44] These reported trivalent lanthanide ions contain D_{3h} symmetry with four crystal field parameters, such as B_{20}, B_{40}, B_{60} and B_{66}. Calculations of anisotropies using these parameters show the presence of significant amounts of the C_3 and higher terms (Figure 4.18). While interference of the T^{-4} term can

References begin on page 170

be noticed in both Ce and Pr-complexes, no sign of higher temperature dependent terms such as T^{-4} was observed in Nd-complexes below 250 K.

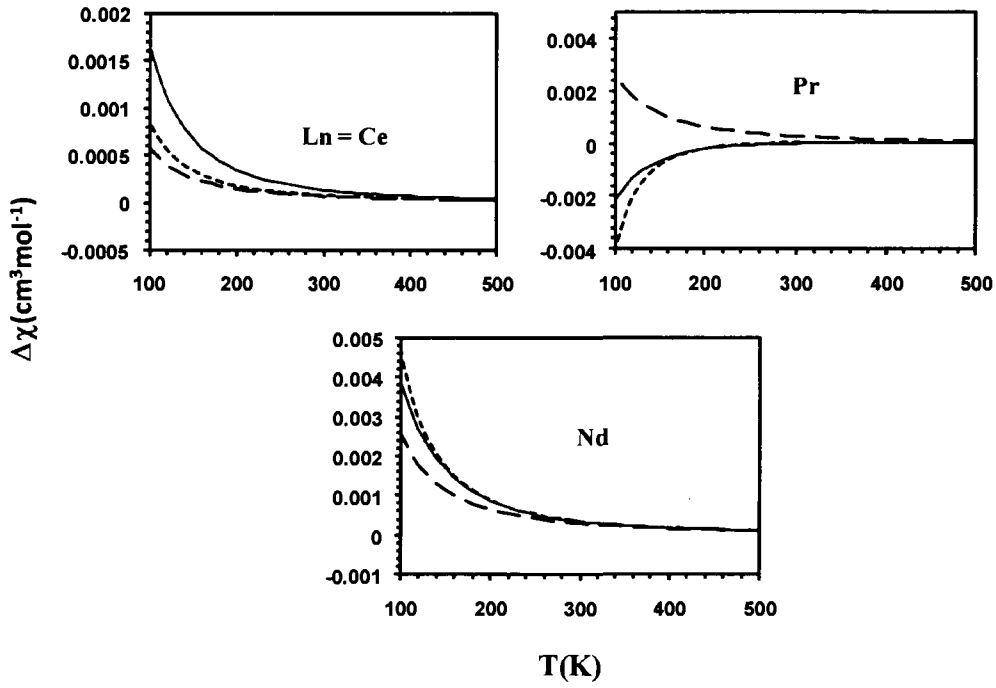

Figure 4.18. Comparison plot of temperature dependent magnetic anisotropies ($\Delta\chi$) calculated from Bleaney's (big dashed line), McGarvey's methods (small dashed line) and CONDON (grey line) vs temperature (T) for Ln^{3+} (Ln = Ce, Pr or Nd) doped in $La(C_2H_5SO_4)_3(H_2O)_9$.

The overall study of these complexes revealed that the ratio of $(C_3/C_2T)x100$, which calculated the importance of the higher terms, increased with the decrease in temperature. At low temperatures a higher percentage ratio sometimes also represents the presence of T^{-4} and higher terms. Although no trend was observed in the lanthanide series, it was found that at low temperatures, larger C_3 is due to the contribution of T^{-4} and higher terms (Table 4.6).

References begin on page 170

Table 4.6. Effect of different C_3 and C_2 terms (calculated from different crystal field parameters) on the ratio of (C_3/C_2T)x100 at different temperatures for Ln^{3+} (Tb-Yb).

Ln	C_3	C_2	T (K)											
			320	**300**	**280**	**260**	**240**	**220**	**200**	**180**	**160**	**140**	**120**	**100**
Tb	−10034.9	402.4	−7.8	−8.3	−8.9	−9.6	−10.4	−11.4	−12.5	−13.9	−15.6	−17.8	−20.8	−24.9
	−34419.7	1374.3	−7.8	−8.3	−8.9	−9.6	−10.4	−11.4	−12.5	−13.9	−15.7	−17.9	−20.9	−25.0
	−448.1	402.4	−0.3	−0.4	−0.4	−0.4	−0.5	−0.5	−0.6	−0.6	−0.7	−0.8	−0.9	−1.1
	−300151.2	−1190.2	78.8	84.1	90.1	97.0	105.1	114.6	126.1	140.1	157.6	180.1	210.2	252.2
	−21048.7	−311.7	21.1	22.5	24.1	26.0	28.1	30.7	33.8	37.5	42.2	48.2	56.3	67.5
	−10178.5	−260.7	12.2	13.0	13.9	15.0	16.3	17.7	19.5	21.7	24.4	27.9	32.5	39.0
	−61317.1	874.2	−21.9	−23.4	−25.1	−27.0	−29.2	−31.9	−35.1	−39.0	−43.8	−50.1	−58.5	−70.1
	−21414.1	42.5	−157.4	−167.9	−179.9	−193.8	−209.9	−229.0	−251.9	−279.9	−314.9	−359.9	−419.8	−503.8

References begin on page 170

Ln	C_3	C_2	T (K)											
			320	**300**	**280**	**260**	**240**	**220**	**200**	**180**	**160**	**140**	**120**	**100**
Dy	−4094.4	303.4	−4.2	−4.5	−4.8	−5.2	−5.6	−6.1	−6.7	−7.5	−8.4	−9.6	−11.2	−13.5
	−255944.8	3050.4	−26.2	−28.0	−30.0	−32.3	−35.0	−38.1	−42.0	−46.6	−52.4	−59.9	−69.9	−83.9
	−17489.3	463.3	−11.8	−12.6	−13.5	−14.5	−15.7	−17.2	−18.9	−21.0	−23.6	−27.0	−31.5	−37.8
	−6122.8	−1305.0	−1.5	−1.6	−1.7	−1.8	−2.0	−2.1	−2.3	−2.6	−2.9	−3.4	−3.9	−4.7
	27953.7	−391.5	−22.3	−23.8	−25.5	−27.5	−29.8	−32.5	−35.7	−39.7	−44.6	−51.0	−59.5	−71.4
	8499.8	−297.9	−8.9	−9.5	−10.2	−11.0	−11.9	−13.0	−14.3	−15.9	−17.8	−20.4	−23.8	−28.5
	−91132.1	1094.6	−26.0	−27.8	−29.7	−32.0	−34.7	−37.8	−41.6	−46.3	−52.0	−59.5	−69.4	−83.3
	−78756.1	277.3	−88.7	−94.7	−101.4	−109.2	−118.3	−129.1	−142.0	−157.8	−177.5	−202.9	−236.7	−284.0

References begin on page 170

Ln	C_3	C_2	T (K)											
			320	**300**	**280**	**260**	**240**	**220**	**200**	**180**	**160**	**140**	**120**	**100**
Ho	−57784.3	740.3	−24.4	−24.4	−27.9	−30.0	−32.5	−35.5	−39.0	−43.4	−48.8	−55.8	−65.0	−78.1
	29290.1	182.0	50.3	53.6	57.5	61.9	67.0	73.1	80.5	89.4	100.6	114.9	134.1	160.9
	64827.8	−474.3	−42.7	−45.6	−48.8	−52.6	−56.9	−62.1	−68.3	−75.9	−85.4	−97.6	−113.9	−136.7
	−6329.8	−160.2	12.3	13.2	14.1	15.2	16.5	18.0	19.8	21.9	24.7	28.2	32.9	39.5
	−4080.3	−138.4	9.2	9.8	10.5	11.3	12.3	13.4	14.7	16.4	18.4	21.1	24.6	29.5
	−148229.1	202.5	−228.7	−243.9	−261.4	−281.5	−304.9	−332.7	−365.9	−406.6	−457.4	−522.7	−609.9	−731.8
	−114664.9	1645.3	−21.8	−23.2	−24.9	−26.8	−29.0	−31.7	−34.8	−38.7	−43.6	−49.8	−58.1	−69.7
	−26894.3	102.6	−82.0	−87.4	−93.7	−100.9	−109.3	−31.7	−131.1	−145.7	−163.9	−187.3	−218.5	−262.2

References begin on page 170

Ln	C_3	C_2	T (K)											
			320	**300**	**280**	**260**	**240**	**220**	**200**	**180**	**160**	**140**	**120**	**100**
Er	−3459.1	114.2	0.0	0.0	0.0	0.0	0.0	0.0	0.0	0.0	0.0	0.0	0.0	0.0
	−62421.7	−570.8	34.2	36.5	39.1	42.1	45.6	49.7	54.7	60.8	68.3	78.1	91.1	109.4
	−24513.6	−1048.1	7.3	7.8	8.4	9.0	9.7	10.6	11.7	13.0	14.6	16.7	19.5	23.4
	27644.5	−150.1	−57.6	−61.4	−65.8	−70.8	−76.7	−83.7	−92.1	−102.3	−115.1	−131.6	−153.5	−184.2
	52825.3	370.0	44.6	47.6	51.0	54.9	59.5	64.9	71.4	79.3	89.2	102.0	119.0	142.8
	−6041.5	125.8	−15.0	−16.0	−17.2	−18.5	−20.0	−21.8	−24.0	−26.7	−30.0	−34.3	−40.0	−48.0
	−4379.4	99.3	−13.8	−14.7	−15.8	−17.0	−18.4	−20.1	−22.1	−24.5	−27.6	−31.5	−36.8	−44.1
	−92435.8	−380.5	75.9	81.0	86.8	93.4	101.2	110.4	121.5	134.9	151.8	173.5	202.4	242.9
	−32778.8	−1214.0	8.4	9.0	9.6	10.4	11.3	12.3	13.5	15.0	16.9	19.3	22.5	27.0
	−12261.7	−79.3	48.3	51.6	55.2	59.5	64.4	70.3	77.3	85.9	96.7	110.5	128.9	154.7

References begin on page 170

Ln	C_3	C_2	T (K)											
			320	**300**	**280**	**260**	**240**	**220**	**200**	**180**	**160**	**140**	**120**	**100**
Tm	−22421.8	−128.6	54.5	58.1	62.3	67.1	72.7	79.3	87.2	96.9	109.0	124.6	145.3	174.4
	−62667.1	−816.0	24.0	25.6	27.4	29.5	32.0	34.9	38.4	42.7	48.0	54.9	64.0	76.8
	17327.7	222.5	24.3	26.0	27.8	30.0	32.4	35.4	38.9	43.3	48.7	55.6	64.9	77.9
	−18620.4	579.4	−10.0	−10.7	−11.5	−12.4	−13.4	−14.6	−16.1	−17.9	−20.1	−23.0	−26.8	−32.1
	−7968.8	−243.4	10.2	10.9	11.7	12.6	13.6	14.9	16.4	18.2	20.5	23.4	27.3	32.7
	−183295.6	−996.8	57.5	61.3	65.7	70.7	76.6	83.6	91.9	102.2	114.9	131.3	153.2	183.9
	−1089.3	−111.4	3.1	3.3	3.5	3.8	4.1	4.4	4.9	5.4	6.1	7.0	8.1	9.8

References begin on page 170

Ln	C_3	C_2	T (K) 320	300	280	260	240	220	200	180	160	140	120	120
Yb	−62288.2	229.1	−85.0	−90.6	−97.1	−104.6	−113.3	−123.6	−135.9	−151.0	−169.9	−194.2	−226.5	−227.9
	−61218.1	229.1	−83.5	−89.1	−95.4	−102.8	−111.3	−121.4	−133.6	−148.4	−167.0	−190.8	−222.7	−267.2
	−3939.1	70.5	−17.5	−18.6	−20.0	−21.5	−23.3	−25.4	−27.9	−31.0	−34.9	−39.9	−46.6	−55.9
	−21609.4	−913.7	75.8	80.9	86.6	93.3	101.1	110.3	121.3	134.8	151.6	173.3	202.1	242.6

References begin on page 170

4.3 Summary and Conclusions

The crystal field parameters of a series of isostructural trivalent lanthanide complexes reported in the literature were used to demonstrate the temperature dependencies of pseudocontact shifts. It has been reported earlier that the pseudocontact shifts depend only on the T^{-2} term with second rank crystal field parameters (L = 2). While McGarvey reported that for pseudocontact shifts the T^{-3} term contributed 10-20 % of the T^{-2} term, our study underlines the importance of the higher temperature dependent terms showing that at room temperature these terms contribute from 20-90 % of the T^{-2} term. We also demonstrated that not only the T^{-3} term but contribution of the T^{-4} and higher terms can also be noticed at low temperatures (below 250 K); these terms have been completely ignored. Change in the sign of anisotropy observed in $[Pn_2Yb]^-$ using the C_3 term supported Ishikawa's results and revealed the importance of higher terms. Similar to McGarvey's prediction, it can also be concluded that the four and six term crystal field parameters are also important to predict the sign as well as the magnitude of higher temperature terms; this is impossible using only second term crystal field parameters. Magnetic anisotropies calculated over 100-500 K provide evidence of the major participation of the T^{-2} term at extremely high temperature (>500 K) rather than at room temperature. Thus, the current study confirms that McGarvey's higher terms, such as T^{-3} and T^{-4}, play significant roles in pseudocontact shifts of paramagnetic lanthanide complexes.

References begin on page 170

4.4 References

1. Ishikawa, N., *Polyhedron* **2007,** 26, (9-11), 2147.
2. Ishikawa, N.; Sugita, M.; Wernsdorfer, W., *J. Am. Chem. Soc.* **2005,** 127, (11), 3650.
3. Zaleski, C. M.; Depperman, E. C.; Kampf, J. W.; Kirk, M. L.; Pecoraro, V. L., *Angew. Chem., Int. Ed.* **2004,** 43, (30), 3912.
4. Ishikawa, N.; Iino, T.; Kaizu, Y., *J. Am. Chem. Soc.* **2002,** 124, (38), 11440.
5. Mironov, V. S.; Galyametdinov, Y. G.; Ceulemans, A.; Gorller-Walrand, C.; Binnemans, K., *J. Chem. Phys.* **2002,** 116, (11), 4673.
6. Ishikawa, N.; Iino, T.; Kaizu, Y., *J. Phys. Chem. A* **2003,** 107, (39), 7879.
7. Bleaney, B., *J. Magn. Reson.* **1972,** 8, (1), 91.
8. Reilley, C. N.; Good, B. W.; Allendoerfer, R. D., *Anal. Chem.* **1976,** 48, (11), 1446.
9. Corson, D. C.; Williams, T. C.; Sykes, B. D., *Biochemistry* **1983,** 22, (25), 5882.
10. Shelling, J. G.; Bjornson, M. E.; Hodges, R. S.; Taneja, A. K.; Sykes, B. D., *J. Magn. Reson.* **1984,** 57, (1), 99.
11. Caravan, P.; Ellison, J. J.; McMurry, T. J.; Lauffer, R. B., *Chem. Rev.* **1999,** 99, (9), 2293.
12. Peters, J. A.; Huskens, J.; Raber, D. J., *Prog. Nucl. Magn. Reson. Spectrosc.* **1996,** 28, (3-4), 283.
13. Cockeril.A. F.; Davies, G. L. O.; Harden, R. C.; Rackham, D. M., *Chem. Rev.* **1973,** 73, (6), 553.
14. Mayo, B. C., *Chem. Soc. Rev.* **1973,** 2, (1), 49.
15. Rondeau, R. E.; Sievers, R. E., *J. Am. Chem. Soc.* **1971,** 93, (6), 1522.

References begin on page 170

16. Bikchantaev, I.; Galyametdinov, Y. G.; Kharitonova, O.; Ovchinnikov, I. V.; Bruce, D. W.; Dunmur, D. A.; Guillon, D.; Heinrich, B., *Liq. Cryst.* **1996,** 20, (4), 489.

17. Binnemans, K.; Galyametdinov, Y. G.; Van Deun, R.; Bruce, D. W.; Collinson, S. R.; Polishchuk, A. P.; Bikchantaev, I.; Haase, W.; Prosvirin, A. V.; Tinchurina, L.; Litvinov, I.; Gubajdullin, A.; Rakhmatullin, A.; Uytterhoeven, K.; Van Meervelt, L., *J. Am. Chem. Soc.* **2000,** 122, (18), 4335.

18. Binnemans, K.; Malykhina, L.; Mironov, V. S.; Haase, W.; Driesen, K.; Van Deun, R.; Fluyt, L.; Gorller-Walrand, C.; Galyametdinov, Y. G., *ChemPhysChem* **2001,** 2, (11), 680.

19. Brittain, H. G.; Richardson, F. S.; Martin, R. B., *J. Am. Chem. Soc.* **1976,** 98, (25), 8255.

20. Pintacuda, G.; John, M.; Su, X. C.; Otting, G., *Acc. Chem. Res.* **2007,** 40, (3), 206.

21. Pintacuda, G.; Park, A. Y.; Keniry, M. A.; Dixon, N. E.; Otting, G., *J. Am. Chem. Soc.* **2006,** 128, (11), 3696.

22. Song, Y. Y.; Xu, Y. Z.; Weng, S. F.; Wang, L. B.; Li, X. F.; Zhang, T. F.; Wu, J. G., *Biospectroscopy* **1999,** 5, (6), 371.

23. Prosser, R. S.; Vold, R. R., *Biophys. J.* **1997,** 72, (2), WPMC4.

24. Lee, L.; Sykes, B. D., *Biochemistry* **1983,** 22, (19), 4366.

25. Lee, L.; Sykes, B. D., *Biophys. J.* **1980,** 32, (1), 193.

26. Dickins, R. S.; Badari, A., *Dalton Trans.* **2006**, (25), 3088.

27. Dickins, R. S.; Parker, D.; Bruce, J. I.; Tozer, D. J., *Dalton Trans.* **2003**, (7), 1264.

28. Piguet, C.; Bunzli, J. C. G.; Bernardinelli, G.; Hopfgartner, G.; Petoud, S.; Schaad, O., *J. Am. Chem. Soc.* **1996,** 118, (28), 6681.

References begin on page 170

29. Prosser, R. S.; Shiyanovskaya, I. V., *Concepts Magn. Reson.* **2001,** 13, (1), 19.

30. Vold, R. R.; Prosser, R. S., *J. Magn. Reson. Ser. B* **1996,** 113, (3), 267.

31. Park, S. H.; Loudet, C.; Marassi, F. M.; Dufourc, E. J.; Opella, S. J., *J. Magn. Reson.* **2008,** 193, (1), 133.

32. Bertini, I.; Luchinat, C.; Aime, S., *Coord. Chem. Rev.* **1996,** 150, R7.

33. Allegrozzi, M.; Bertini, I.; Choi, S. N.; Lee, Y. M.; Luchinat, C., *Eur. J. Inorg. Chem.* **2002**, (8), 2121.

34. Lee, L.; Corson, D. C.; Sykes, B. D., *Biophys. J.* **1985,** 47, (2), 139.

35. Bertini, I.; Janik, M. B. L.; Lee, Y. M.; Luchinat, C.; Rosato, A., *J. Am. Chem. Soc.* **2001,** 123, (18), 4181.

36. Su, X. C.; McAndrew, K.; Huber, T.; Otting, G., *J. Am. Chem. Soc.* **2008,** 130, (5), 1681.

37. Kurland, R. J.; Mcgarvey, B. R., *J. Magn. Reson.* **1970,** 2, 286.

38. C.N. Reilley; B.W. Good; Allendoerfer, R. D., *Anal. Chem.* **1976,** 48, (11), 1446.

39. Horrocks, W. D.; Wong, C. P., *J. Am. Chem. Soc.* **1976,** 98, (23), 7157.

40. Horrocks, W. D., *J. Magn. Reson.* **1977,** 26, (2), 333.

41. Golding, R. M.; Pyykko, P., *Mol. Phys.* **1973,** 26, (6), 1389.

42. Cheng, H. N.; Gutowsky, H. S., *J. Phys. Chem.* **1978,** 82, (8), 914.

43. Stout, E. W.; Gutowsky, H. S., *J. Magn. Reson.* **1976,** 24, (3), 389.

44. McGarvey, B. R., *J. Magn. Reson.* **1979,** 33, (2), 445.

45. Wybourne, B. G., *Spectroscopic Properties of Rare Earths (New York: Wiley)* **1965**.

46. CONDON, *Magnetic Susceptibility Simulation Program, Helmut SCHILDER, Fachhochschule Aachen Germany,* **2000**.

References begin on page 170

47. Ishikawa, N.; Sugita, M.; Okubo, T.; Tanaka, N.; Lino, T.; Kaizu, Y., *Inorg. Chem.* **2003,** 42, (7), 2440.

48. Flanagan, B. M.; Bernhardt, P. V.; Krausz, E. R.; Luthi, S. R.; Riley, M. J., *Inorg. Chem.* **2002,** 41, (20), 5024.

49. Sugita, M.; Ishikawa, N.; Ishikawa, T.; Koshihara, S.; Kaizu, Y., *Inorg. Chem.* **2006,** 45, (3), 1299.

50. Jank, S.; Reddmann, H.; Amberger, H. D., *Inorg. Chim. Acta* **2008,** 361, (7), 2154.

51. Han, X. F.; Jin, H. M.; Zhao, T. S.; Sun, C. C., *J. Phys.: Condens. Matter* **1993,** 5, (45), 8603.

52. Edelstein, N. M., *J. Alloys Compd.* **1995,** 223, (2), 197.

53. van Pieterson, L.; Reid, M. F.; Burdick, G. W.; Meijerink, A., *Phys. Rev. B* **2002,** 65, (4), 045114.

54. Bernhardt, P. V.; Flanagan, B. M.; Riley, M. J., *Aus. J. Chem.* **2001,** 54, (4), 229.

55. Bernhardt, P. V.; Flanagan, B. M.; Riley, M. J., *Aus. J. Chem.* **2000,** 53, (3), 229.

56. Jank, S.; Reddmann, H.; Apostolidis, C.; Amberger, H. D., *Z. Anorg. Allg. Chem.* **2007,** 633, (3), 398.

57. Holsa, J.; Lamminmaki, R.-J., *J. Lumin.* **1996,** 69, (5-6), 311.

58. Buck, S.; Fahnle, M., *J. J. Magn. Magn. Mater.* **1997,** 166, (3), 297.

References begin on page 170

CHAPTER-5

Determination of Crystal Field Parameters of Trivalent Lanthanide Amido Complexes by Variable Temperature NMR Spectroscopy

5.1 Introduction

Paramagnetic lanthanide complexes have become an essential tool in a variety of chemical and biochemical applications due to their unique magnetic properties, such as large magnetic moments and large magnetic anisotropies.[1-4] Magnetic properties of lanthanide complexes depend on their large unquenched orbital angular momentum. Other than gadolinium, the rest of the lanthanides possess orbitally degenerate ground states, which can be raised up to 10^1-10^2 cm^{-1} by the supporting ligands. These

References begin on page 193

supporting ligands are also responsible for crystal field splitting and therefore their selection plays a significant role in the applications of lanthanide complexes. Although the sublevel structure of ground state multiplets of the lanthanide complexes is an important feature in understanding the magnetic properties of lanthanides, the lack of information makes it difficult to determine these sublevel states.

One of the traditional ways to determine these crystal field parameters is via optical spectroscopy methods, such as low-temperature absorption and luminescence.[5-7] A few of these methods involve the doping of trivalent lanthanides into single crystal ions exhibiting a narrow band structure to show the transitions between ground and excited state multiplets. Due to the insufficient participation from the $4f^n$ electrons in chemical bonding, each *f-f* spectral band appears as sharp lines, which can be differentiated from each other. Although these lines are considered as the ligand field splitting between the ground state and the upper state energy levels, in cases where there are no line-like absorption and emission, determining sublevel structure information is an impossible task. In the past decades, the interactions between the energy levels of the *f*-block elements have been studied by optical spectroscopic methods using a Hamiltonian model. In general, the crystal field parametric Hamiltonian H can be expressed by equation (5.1) as given below.

$$H = H_F + \mathrm{V} \qquad (5.1)$$

H_F = Hamiltonian for free lanthanide ions

V = Potential provided by crystal environment

References begin on page 193

Depending upon the symmetry of the complex, the crystal field Hamiltonians of lanthanide ions contain up to 27 crystal field parameters. For unperturbed free ions and symmetrical complexes, the expansion of potential V caused by crystal fields can be written as shown in equation (5.2). In the literature, these parameters are denoted by different numerical factors and Wybourne expressed them using B_{kq}'s as in equation (5.2), where the crystal field Hamiltonian can be expanded using tensor operator C_{kq}.[8]

$$V = \sum B_{kq} (C_{kq})_i \tag{5.2}$$

Lanthanide complexes containing C_{3v} symmetry require a total of six crystal field parameters and, according to Wybourne, their crystal field potential can be expressed as shown in equation (5.3). The crystal field parameters of the lanthanides can also be used to generate the paramagnetic NMR shift and the temperature dependent magnetic anisotropy.[9, 10]

$$V = B_{20}C_{20} + B_{40}C_{40} + B_{43}(C_{4-3} - C_{43}) + B_{60}C_{60} + B_3(C_{6-3} - C_{63}) + B_{66}(C_{6-6} + C_{66}) \tag{5.3}$$

$B_{2's}$, $B_{4's}$ and $B_{6's}$ = crystal field parameters of rank 2, 4 and 6 respectively

NMR shifts obtained from paramagnetic lanthanide complexes are the combined effect of contact and pseudocontact shifts (equation 5.4). While the contact shift is due to the delocalization of metal unpaired electron density to the ligand nuclei (contact or Fermi-contact), the pseudocontact shift is due to the through-space coupling between the metal centre and each nucleus of the participating ligand.

$$\Delta\delta = \delta_C + \delta_{PC} \tag{5.4}$$

References begin on page 193

The pseudocontact shifts in paramagnetic lanthanides are also responsible for the large chemical shifts due to the dipolar contribution, and provide the structural information of the related lanthanide complex. This information can be utilized to calculate the magnetic anisotropy of the corresponding complex, as given in equation (5.5).

$$\Delta\delta = \frac{(3\cos^2\theta - 1)}{2R^3}(\chi_{\parallel} - \chi_{\perp}) \qquad (5.5)$$

$\Delta\delta$ = chemical shifts
R = distance between lanthanide metal and substrate nuclei
θ = angle between lanthanide metal and substrate nuclei

The presence of certain unique magnetic properties have increased the demand of trivalent lanthanide complexes in the application of magnetic materials.[1, 11] They have been used for synthesizing single molecule magnets (SMM) such as mononuclear bis(phthalocyanato)Tb^- and bis(phthalocyanato)Dy^- complexes, which behave as SMM above 20 K.[12] In paramagnetic lanthanide complexes, the large orbital momentum and weak crystal field splitting are responsible for the larger magnetic anisotropy, which allows the alignment of the related complex in the external magnetic field.[13] The pseudocontact shift induced from the large magnetic anisotropy make these complexes useful as shift reagents and contrast agents for the study of protein structures and in MRI, respectively.[14-16] In protein structure studies, calcium ions bound to the protein molecule are replaced by paramagnetic lanthanides due to the similar ionic radii and similar nature of bonding in biological systems.[17, 18] In addition , lanthanide complexes

References begin on page 193

have been used as luminescent probes for the study of various biochemical systems in plants and animal tissues.[19] Large magnetic anisotropy also depends on the ligand field strength and crystal-field splitting of the compound's ground state multiplets. In the case of dinuclear lanthanide complexes, large magnetic anisotropy is a desirable property because it increases the possibilities of through-space metal-metal coupling and thus is useful for molecular wires and molecular chains. In *f*-block systems, crystal field or exchange interactions are usually very strong and thus play an important role in the physical properties of lanthanide complexes.

Crystal field parameters of lanthanide complexes are generally studied at low temperatures using optical spectroscopic methods due to the presence of only a few thermally populated crystal-field levels, which are responsible for an increase in magnetic anisotropy. Low temperature optical studies provide the information about the *f-f* bands, which can be used to determine the crystal field splitting of ground and excited state multiplets. Excluding the special cases, where these bands are sharp enough to separate from each other, obtaining information regarding the crystal-field splitting is not an easy task. Recently, Ishikawa provided a new method to calculate the crystal-field parameters and the electronic structures of lanthanide complexes.[10, 20, 21]

As mentioned earlier, the chemical shifts of paramagnetic lanthanide complexes are comprised of an isotropic contact term and the anisotropic pseudocontact term, and the contribution of these terms depends on the spin state and magnetic anisotropy of the metal ions. In principle, separation of contact and pseudocontact terms are based on their dependency on temperature, and hence on magnetic anisotropy. As explained in Chapter 4, Bleaney proposed that the anisotropy of the lanthanide complexes containing a second

References begin on page 193

term crystal field parameter and the T^{-2} temperature dependent term can be calculated, as shown in equation (5.6).[9, 22]

$$\chi_{\parallel} - \chi_{\perp} = \frac{K_0}{T^2} a_{20} \qquad (5.6)$$

Later, McGarvey expanded temperature dependent magnetic anisotropy using higher terms such as T^{-3}, T^{-4} with all other crystal field parameters.[9] Compounds with C_3 symmetry require six crystal field parameters and according to McGarvey magnetic anisotropy of C_3 symmetry complexes can be written as given in equation (5.7).

$$C_3 = -(2/315)g_J^2\beta_e^2k^{-3}J(J+1)(2J-1)(2J+3)(J-1)(J+2)k_1a_{20}^2 + 6k_2a_{20}a_{40} + k_3(10a_{40}^2 - 7a_{43}^2) \qquad (5.7)$$
$$+k_4(30a_{40}a_{60} + 12\sqrt{3}a_{63}a_{43}) + k_5(7a_{60}^2 - 5a_{63}^2 - 22a_{66}^2)$$

In the above equation k_n represents the constants with different values for each lanthanide and thus verify the dependencies of magnetic anisotropy of each lanthanide on different crystal field parameters. The sign of any two different trivalent lanthanide ions from these two groups can not be the same (as described earlier in Chapter 4). Based on the assumption that in the case of higher lanthanides (Tb^{3+} to Yb^{3+}), crystal field parameters vary linearly, it should be possible to utilize the variable temperature NMR shifts to determine the crystal field parameters. Thus for the C_3 symmetric complexes, it should be possible to fit all the variable temperature NMR shifts of the entire series of heavy lanthanides to 12 variables.

As NMR spectroscopy is an important tool for the characterization of chemical and biochemical compounds, magnetic analysis based on NMR data will be a boon to synthetic chemists, who do not have access to low temperature optical spectroscopy or

References begin on page 193

SQUID (superconducting quantum interference device) magnetometers to determine the crystal-field parameters/magnetic susceptibility. In this chapter, we are proposing a new method, which can be used to determine the crystal field parameters using only variable temperature NMR data. Magnetic anisotropy of lanthanide complexes containing more than C_2 symmetry can also be measured from their pseudocontact shifts. In addition, we are introducing a series of isostructural trivalent lanthanide complexes [$P(CH_2NC_6H_4$-2-$CO_2Me)_3Ln$] with C_3 molecular symmetry and utilizing their chemical shifts for the calculation of crystal field parameters. The mononuclear trivalent lanthanide complexes described in this chapter possess four different proton environments that were observed in ^1H NMR spectra and require six crystal field parameters, denoted as B_{20}, B_{40}, B_{60}, B_{43}, B_{63} and B_{66}.

5.2 Result and Discussion

5.2.1 Syntheses of Trivalent Lanthanide Complexes

All the trivalent lanthanide complexes were prepared in a similar manner, which involve the mixing of 1 equivalent of ligand precursor (**13**) with 1 equivalent of $Ln[N(SiMe_3)_2]_3$ (Ln = Tb, Dy, Ho, Er and Tm) in toluene solution. After 5 h, the solution mixture was precipitated in the form of a yellow crystalline solid as shown in equation (5.8).

References begin on page 193

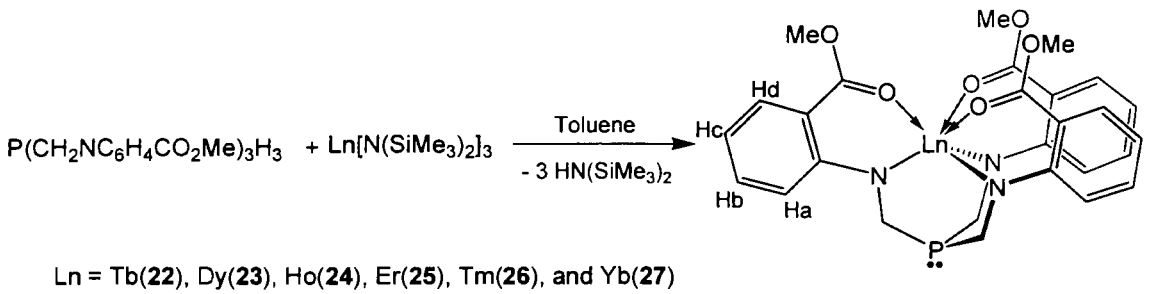

(5.8)

Ln = Tb(**22**), Dy(**23**), Ho(**24**), Er(**25**), Tm(**26**), and Yb(**27**)

The resultant trivalent lanthanide complexes contain C_3 symmetry in solid as well as in solution form, in which each metal center is chelated by three amido nitrogen donors and three ester functionality oxygens. Despite getting X-ray quality crystals, the molecular structure of these trivalent lanthanide complexes (**22-26**) could not be solved because of the difficulties in solving the twinned structures.

5.2.2 Magnetic Studies of Trivalent Lanthanide Complexes

Magnetic susceptibilities of these complexes (**22-26**) were measured over the temperature range of 300 to 2 K using the powdered sample immobilized in eicosane ($C_{20}H_{42}$, chemically inactive, part of paraffin group, and use to cover air-sensitive samples) . The room temperature $\chi_M T$ values (product of magnetic susceptibility and temperature) of these complexes (**22-26**) correspond to the expected value of their free ions at room temperature as shown in Figure 5.1. For example $\chi_M T$ = 11.81 cm^3 K mol^{-1} for Tb^{3+}, 14.18 cm^3 K mol^{-1} for Dy^{3+}, 14.07 cm^3 K mol^{-1} for Ho^{3+}, 11.48 cm^3 K mol^{-1} for Er^{3+} and 7.15 cm^3 K mol^{-1} for Tm^{3+}.[11] In the case of complex **22**, lowering the temperature to 2 K, decreases the magnitude of $\chi_M T$ to 4.93 cm^3 K mol^{-1}. The $\chi_M T$ values of complex **23** and **24** also decrease to 9.17 cm^3 K mol^{-1} and 6.10 cm^3 K mol^{-1}, respectively. While lowering the temperature to 40 K decreases the $\chi_M T$ value of

References begin on page 193

complex **25** to 8.88 cm^3 K mol^{-1}, further decrease in the temperature to 2 K increases the value to 9.91 cm^3 K mol^{-1}. Similar to the other complexes, complex **26** also shows a decrease of $\chi_M T$ value to 3.84 cm^3 K mol^{-1} at 2 K.

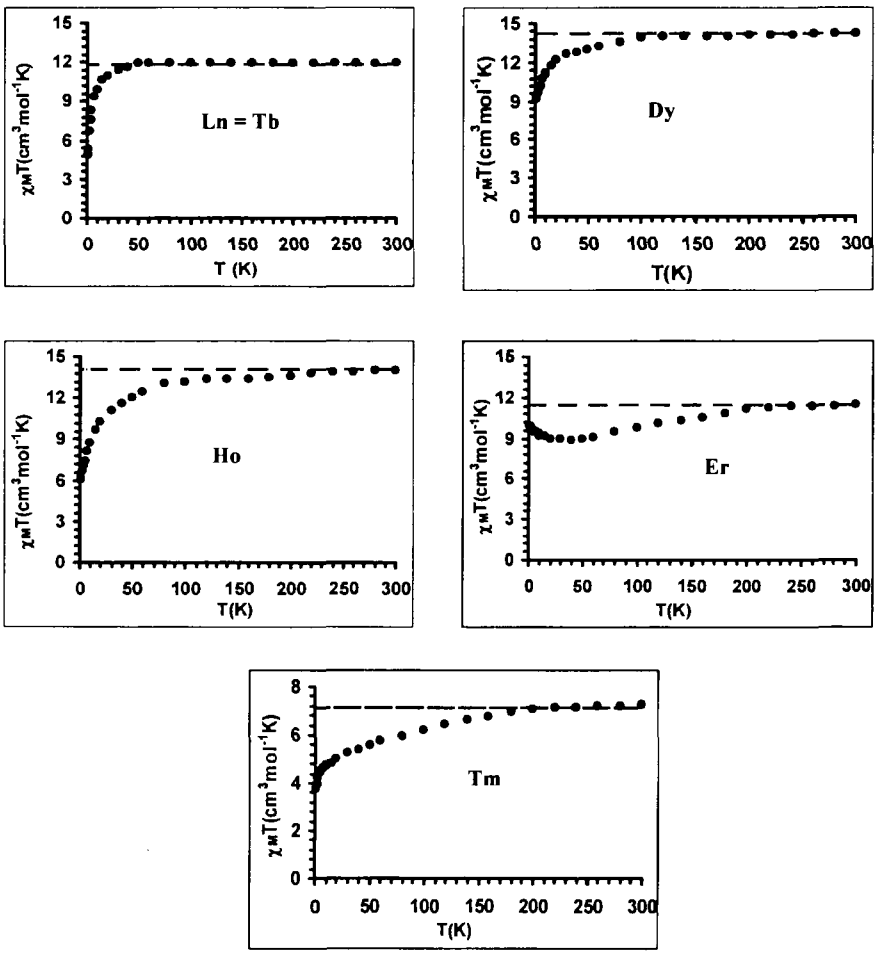

Figure 5.1. Plots of $\chi_m T$ versus T for $P[CH_2NC_6H_4\text{-}2\text{-}CO_2Me]_3Ln$ (Ln = Tb, Dy, Ho, Er and Tm) (•), and the broken line is the $\chi_m T$ value of the corresponding free ion at room temperature.

References begin on page 193

5.2.3 NMR Spectra of Trivalent Lanthanide complexes

As given in Table 5.1, trivalent lanthanide complexes showed large paramagnetic shifts (δ) in $^{31}P\{^{1}H\}$NMR with the chemical shift range from −700 to 700 ppm, due to the dipolar shifts. In this study NMR chemical shifts (Δδ) are the relative shifts of paramagnetic lanthanides with respect to the diamagnetic yttrium complex. As also stated in Chapter 3, each lanthanide complex contains four proton environments, which were assigned by ^{1}H NMR spectra. Depending upon the closeness of these four protons to the center metal ion, they were labelled as Ha, Hb, Hc and Hd, respectively. On the basis of the sign of $^{31}P\{^{1}H\}$NMR shifts, all the trivalent lanthanides complexes were divided into two categories, according to which Tb, Dy and Ho showed negative shifts in phosphorus NMR (−δ), whereas Er, Tm, and Yb showed positive NMR shifts (+δ). Complex **22** showed the largest paramagnetic shift with a negative sign in $^{31}P\{^{1}H\}$ NMR. Failed attempts of finding the phosphorus shift of $P[CH_2NC_6H_4CO_2Me]_3Tm$ (**26**) could be due to the result of the large line broadening or relaxation time.

Table 5.1. $^{31}P\{^{1}H\}$NMR shifts of $P[CH_2NC_6H_4CO_2Me]_3Ln$ (Ln = Y, Tb, Dy, Ho, Er, Tm and Yb)

Ln^{3+}	$^{31}P\{^{1}H\}$NMR shifts (ppm)
Y(**14**)	−57.0
Tb(**22**)	−689.3
Dy(**23**)	−581.0
Ho(**24**)	−375.0
Er(**25**)	322.3
Tm(**26**)	Non-observable
Yb(**27**)	191.7

References begin on page 193

One of the approaches to check the nature of the chemical shifts involves the constant ratio of different shifts of the same lanthanide complex over the range of temperature using equation (5.5). The required bond distance (R), and bond angle required can be calculated from the crystal structures. The constant ratio thus obtained from the chemical shifts implies the presence of dipolar shifts with no contribution of the contact term in the paramagnetic shift.[10] Another approach to calculate the constant ratio involves the $\Delta\delta$ ratios of the similar peaks of different lanthanide complexes. The constant value obtained from these ratios also confirms the presence of only dipolar contributions. As shown in Table 5.2, due to the largest chemical shift in each lanthanide complex, Hd was selected as a reference for calculating the shift ratios. The constant ratio (1.29) was obtained from $\Delta\delta$Hd and $\Delta\delta$Hc in an isostructural lanthanide series at all temperatures, confirming the presence of a dipolar contribution to paramagnetic shifts.

Table 5.2. Assignments of ^{1}H NMR shifts (δ) and paramagnetic shifts ($\Delta\delta$) for $[PN_3]^{CO2Me}Ln$

Ln	δ(Ha)	δ(Hb)	δ(Hc)	δ(Hd)	Δδ(Ha)	Δδ(Hb)	Δδ(Hc)	Δδ(Hd)	Δδ(Hd)/ Δδ(Hc)
Y(14)	6.78	7.27	6.48	8.11					
Tb(22)	26.28	32.37	49.28	63.54	19.5	25.1	42.8	55.5	1.29
Dy(23)	24.88	24.97	46.41	54.62	18.1	17.7	35.2	46.51	1.29
Ho(24)	18.88	19.47	27.28	35.21	12.1	12.2	20.8	27.1	1.30
Er(25)	−7.80	−8.13	−8.22	−11.19	−14.58	−15.4	−14.7	−19.3	1.31
Tm(26)	−7.62	−31.23	−37.62	−48.29	−14.4	−38.5	−44.1	−56.5	1.29
Yb(27)	−4.23	−7.27	−8.92	−10.67	−11.01	−14.54	−15.4	−18.78	1.22

References begin on page 193

5.2.4 Determination of Crystal Field Parameters

To determine the set of crystal field parameters for each complex, ranges of earlier reported crystal parameters given for C_{3v} symmetric trivalent lanthanide complexes were used. Based on the assumption that for the isostructural series of trivalent lanthanide complexes, crystal field parameters vary linearly with the atomic number, crystal field parameters (CFP's) were used with the set of slopes, which can be expressed as written in equation 5.9.

$$\text{CFP's} = B_{20}\boldsymbol{B_{20}s} + B_{40}\boldsymbol{B_{40}s} + B_{43}\boldsymbol{B_{43}s} + B_{60}\boldsymbol{B_{60}s} + B_{63}\boldsymbol{B_{63}s} + B_{66}\boldsymbol{B_{66}s} \quad (5.9)$$

These ranges of parameters were then used to search for the best set of crystal field parameters for the present lanthanide complexes using magnetic anisotropy calculated from the ^{1}H NMR paramagnetic shifts. To this end we have so far developed a method in which a computer program called DLAN was used for the optimization of set of the crystal-field parameters. The best set of crystal field parameters was selected on the basis of their ability to reproduce the temperature dependent magnetic anisotropy (Figure 5.2).

References begin on page 193

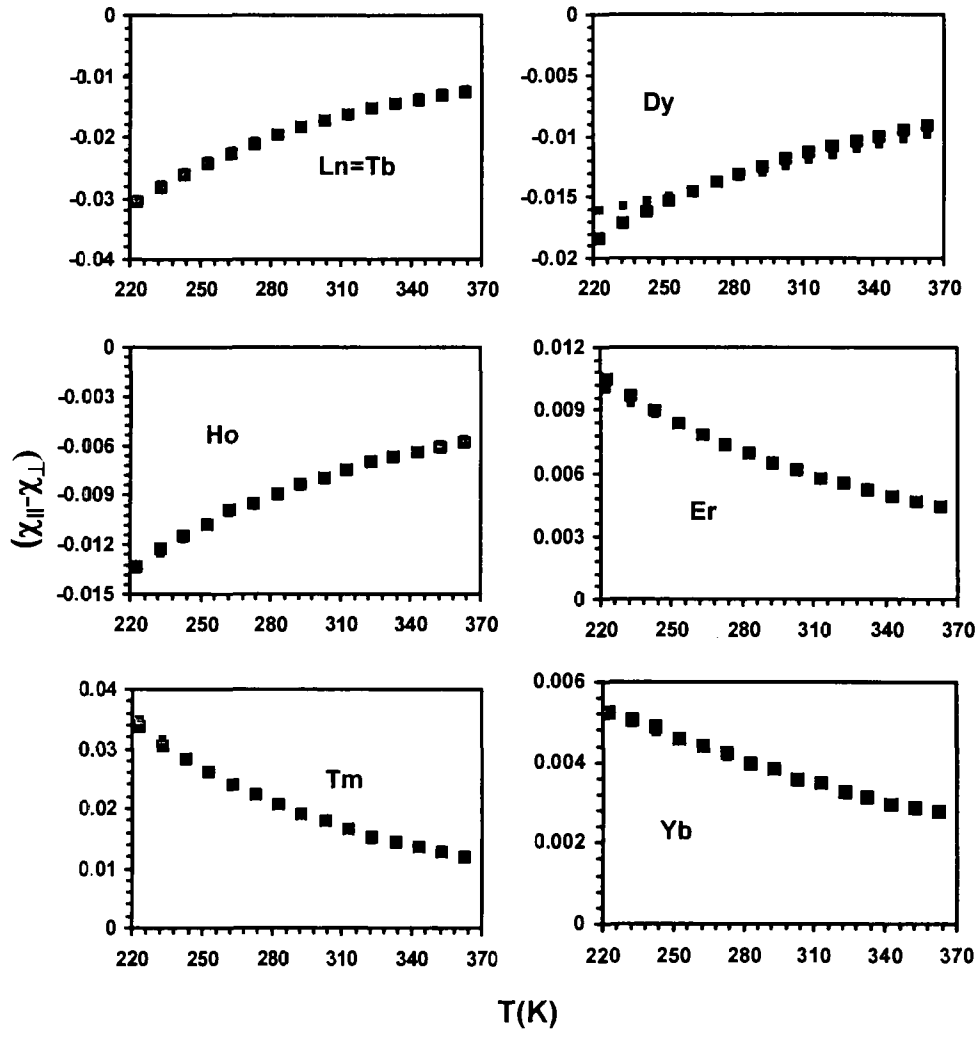

Figure 5.2. Comparison of temperature dependent magnetic anisotropies (grey squares) obtained from calculated crystal field parameters and the experimental data (black squares) obtained from ^{1}H NMR spectra.

To check the linearity assumption, a separate calculation was done without using any slopes (Figure 5.3). The results acquired from the calculation suggested that crystal field parameters vary linearly with *f*-electrons in lanthanide series.

References begin on page 193

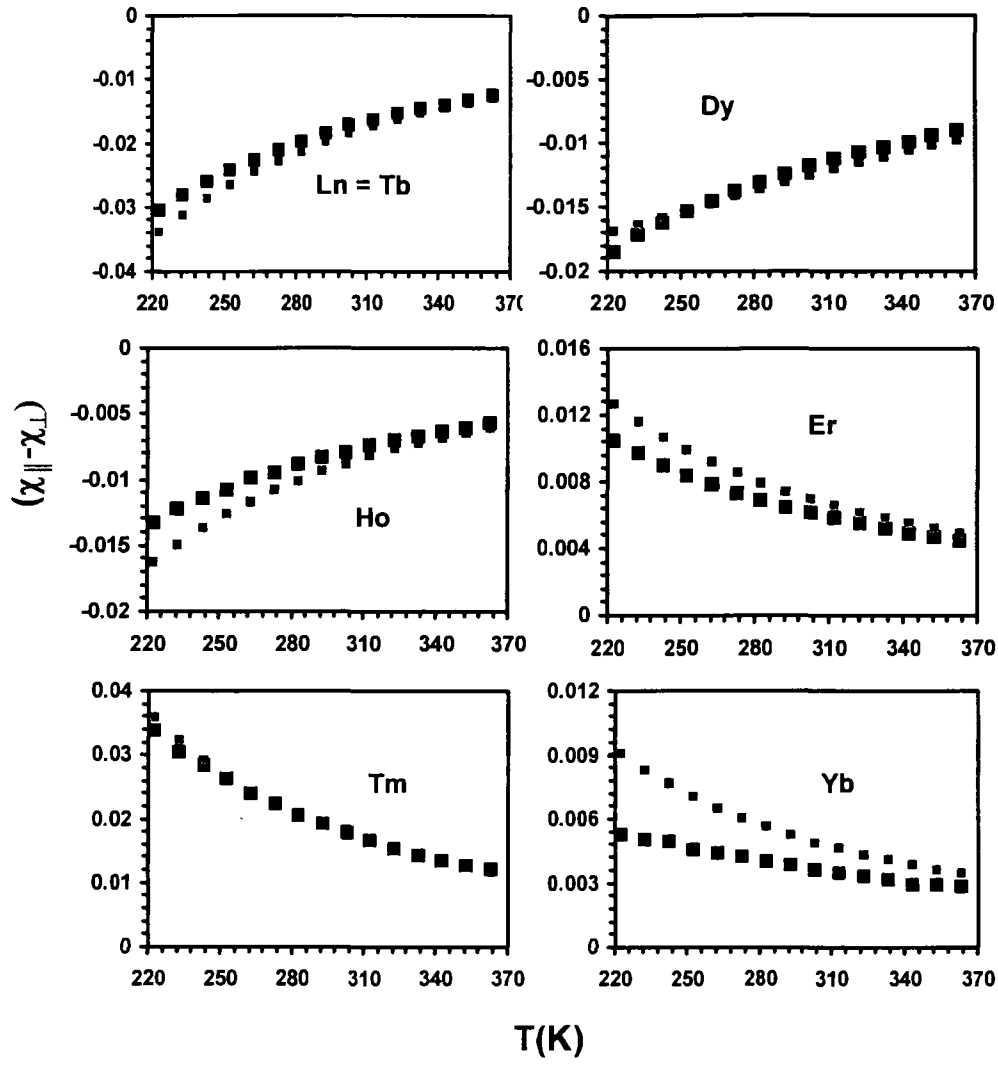

Figure 5.3. Test for the trend in crystal field parameters showing relative magnetic anisotropies obtained from the non-linearity assumption (without slopes). Experimental magnetic anisotropy represented in black squares and the calculated anisotropy in grey squares.

Results obtained from the calculations suggested the dominating contribution of the second term crystal field parameter, i.e., B_{20}, with a negative value. In addition, results also revealed that although signs of B_{43}, B_{60}, B_{63} and B_{66} are not important, the

References begin on page 193

signs of B_{20} and B_{40} make a significant change in the calculation of crystal field parameters. For the current trivalent lanthanide complexes B_{20} and B_{40} required the negative values. Authenticity of these calculated parameters can also be further tested by using them for the calculation of magnetic susceptibility. A computer program called CONDON can be used for such calculations as well as for the calculation of electronic structure of the trivalent lanthanide complexes.[23]

Crystal field parameters given in Table 5.3 are the best fit parameters obtained from NMR data. These parameters can be further used to determine the electronic structure of the present trivalent lanthanide complexes and thus the magnetic properties of these complexes.

Table 5.3 Crystal-field Parameters for $P[CH_2NC_6H_4CO_2Me]_3Ln$

Ln	B_{20}	B_{40}	B_{43}	B_{60}	B_{63}	B_{66}
Tb	−312	−37.12	1200	28.57	133.33	300
Dy	−324	−42.85	1011.11	119.52	633.33	400
Ho	−336	−151.42	1422.22	42.85	400	−371.42
Er	−348	24.28	1500	−24.28	−500	−371.42
Tm	−360	−44.28	1900	−60.95	−66.67	−200
Yb	−372	−405.71	888.89	−64.28	3366.36	−500

5.3 Summary and Conclusions

The reactions of equivalent amounts of tripodal amido ligand $P[CH_2NHC_6H_4CO_2Me]_3$ and $Ln[N(SiMe_3)_2]_3$ (Ln^{3+} = Tb-Yb) afford the trivalent hexadentate lanthanide complexes ($P[CH_2NC_6H_4CO_2Me]_3Ln$). Calculations from the

References begin on page 193

large ^{1}H NMR shifts of these complexes verified the presence of only dipolar (pseudocontact) contributions. These chemical shifts, were used to estimate the magnetic anisotropies using geometrical parameters obtained from the crystal structures of the present trivalent complexes. A set of crystal-field parameters for the isostructural trivalent lanthanide complexes were determined from these anisotropies. The best set of the parameters were chosen by comparing the modelled anisotropy with the experimental anisotropy.

5.4 Experimental

General Techniques- Unless otherwise stated, all experiments were performed under an inert atmosphere of nitrogen using either using Schlenk techniques or an MBraun glove box. Dry oxygen-free solvents were used throughout. Anhydrous pentane and toluene were purchased from Sigma Aldrich, sparged with nitrogen and passed through activated alumina under a positive pressure of nitrogen gas; toluene and pentanes were further deoxygenated using Ridox catalyst columns.[24] Deuterated toluene was dried by heating at reflux over Na/K in a sealed vessel under partial pressure, then trap-to-trap distilled, and freeze-pump-thaw degassed three times.

Instrumentation- ^{1}H and $^{31}P\{^{1}H\}$NMR spectra were recorded from Bruker AMX (300 MHz) or Bruker AMX (500 MHz) spectrometer. All chemical shifts are reported in ppm, and all NMR coupling constants (*J*) are in Hz. ^{1}H NMR spectra were referenced to residual protons (C_7D_7H, δ 2.09) with respect to trimethylsilane at δ 0.0. $^{13}C\{^{1}H\}$ spectra were referenced relative to solvent resonances (C_7D_8, δ 20.4).$^{31}P\{^{1}H\}$

References begin on page 193

NMR spectra referenced to external 85 % H_3PO_4 at δ 0.0. Magnetizations were measured with a Quantum Design MPMS-XL system at Simon Fraser University. Unless otherwise noted, magnetizations were measured at 100 G with a Quantum Design Evercool MPMS-XL system. Corrections for the diamagnetic contributions of compounds were made using Pascal's constants. Samples were run in a PVC holder specially designed to possess a constant cross-sectional area. Elemental analyses were performed by the Centre for Catalysis and Materials Research (CCMR) at the University of Windsor.

Computer Programme- The program Dlan was used to determine the crystal field parameters.

Chemicals- The compounds tris(hydroxymethyl)phosphine and methyl anthranilate, were purchased from Aldrich. Anhydrous $TbCl_3$, $DyCl_3$, $TmCl_3$, $ErCl_3$, $YbCl_3$ and $HoCl_3$ were purchased from Strem. All the reagents were used without further purification and all lanthanide amides ($Ln[N(SiMe_3)_2]_3$) {Ln = Tb, Dy, Ho, Er, Tm, and Yb} were synthesized via literature method.[25,26] Ligand precursor $P(CH_2NHC_6H_4\text{-}2\text{-}CO_2Me)_3$ was prepared according to the method described in Chapter 3 and will be labelled as **13**.

Synthesis of $P[CH_2NC_6H_4CO_2Me]_3Tb$ (22). A mixture of **13** (600 mg, 0.955 mmol) and $Tb[N(SiMe_3)_2]_3$ (720 mg, 0.955 mmol) was stirred in 30 mL of toluene for 5 h. The resultant yellow crystalline precipitate was isolated by filtration, rinsed with 50 mL pentane and dried for 4 h (500 mg, 73 %). X-ray quality crystals were obtained from slow evaporation of toluene at room temperature. ^1H NMR (C_7D_7H, 300 MHz, 298 K): δ

References begin on page 193

26.28 (s, 3H, Ar-*H*), 32.37 (s, 3H, Ar-*H*), 49.28 (s, 3H, Ar-*H*), 63.54 (s, 3H, Ar-*H*), −129.91 (s, 9H, C*H*$_3$), −234.18 (s, 6H, P-C*H*$_2$). ^{31}P{^{1}H} NMR (C_7D_7H, 121.5 MHz, 298 K): δ −689.26. Anal. Calcd. for $C_{27}H_{27}N_3O_6PTb$: C, 47.73; H, 4.01; N, 6.18 Found: C, 47.42; H, 3.99; N, 6.22.

Synthesis of P[CH$_2$NC$_6$H$_4$-2-CO$_2$Me]$_3$Dy (23). A mixture of **13** (600 mg, 0.955 mmol) and Dy[N(SiMe$_3$)$_2$]$_3$ (724 mg, 0.955 mmol) was stirred in 30 mL of toluene for 5 h. The resultant yellow crystalline precipitate was isolated by filtration, rinsed with 50 mL pentane and dried for 4 h (500 mg, 70 %). X-ray quality crystals were obtained from slow evaporation of toluene at room temperature. ^{1}H NMR (C_7D_7H, 300 MHz, 298 K): δ 24.88 (s, 3H, Ar-*H*), 24.97 (s, 3H, Ar-*H*), 54.6 (s, 3H, Ar-*H*), 46.41 (s, 3H, Ar-*H*), −77 (s, 9H, C*H*$_3$), −145 (s, 6H, P-C*H*$_2$). ^{31}P{^{1}H} NMR (C_7D_7H, 121.5 MHz, 298 K): δ −581. Anal. Calcd. for $C_{27}H_{27}N_3O_6PDy$: C, 47.48; H, 3.98; N, 6.15 Found: C, 47.21; H, 3.74; N, 6.19.

Synthesis of P[CH$_2$NC$_6$H$_4$-2-CO$_2$Me]$_3$Ho (24). A mixture of **13** (700 mg, 1.33 mmol) and Ho[N(SiMe$_3$)$_2$]$_3$ (862 mg, 1.33 mmol) was stirred in 70 mL of toluene for 5 h. The resultant yellow crystalline precipitate was isolated by filtration, rinsed with 50 mL pentane and dried for 4 h (620 mg, 67 %). X-ray quality crystals were obtained from slow evaporation of toluene at room temperature. ^{1}H NMR (C_7D_7H, 300 MHz, 298 K): δ 18.88 (s, 3H, Ar-*H*), 19.47 (s, 3H, Ar-*H*), 27.28 (s, 3H, Ar-*H*), 35.21 (s, 3H, Ar-*H*), −57.15 (s, 6H, P-C*H*$_2$), −102.5 (s, 9H, C*H*$_3$). ^{31}P {^{1}H} NMR (C_7D_7H, 121.5 MHz, 298 K): δ −375.0. Anal. Calcd. for $C_{27}H_{27}N_3O_6PHo$: C, 47.31; H, 3.97; N, 6.13, Found: C, 47.33; H, 4.01; N, 6.08.

References begin on page 193

Synthesis of P[$CH_2NC_6H_4$-2-CO_2Me]$_3$Er (25). A mixture of **13**(600 mg, 1.14 mmol) and Er[$N(SiMe_3)_2$]$_3$ (740.8 mg, 1.14 mmol) was stirred in 70 mL of toluene for 5 h. The resultant yellow crystalline precipitate was isolated by filtration, rinsed with 50 mL pentane and dried for 4 h (532 mg, 67 %). X-ray quality crystals were obtained from slow evaporation of toluene at room temperature. ^{1}H NMR (C_7D_7H, 300 MHz, 298K): δ −7.8 (s, 3H, Ar-*H*), −8.13 (s, 3H, Ar-*H*), −8.22 (s, 3H, Ar-*H*), −11.19 (s, 3H, Ar-*H*), 51.2 (s, 6H, P-CH_2), 322.25 (s, 9H, CH_3). ^{31}P{^{1}H} NMR (C_7D_7H, 121.5 MHz, 298K): δ 322.25. Anal. Calcd. for $C_{27}H_{27}N_3O_6PEr$: C, 47.15; H, 3.96; N, 6.11 Found: C, 47.10; H, 3.93; N, 6.20.

Synthesis of P[$CH_2NC_6H_4$-2-CO_2Me]$_3$Tm (26). A mixture of **13** (500 mg, 0.955 mmol) and Tm[$N(SiMe_3)_2$]$_3$ (620 mg, 0.955 mmol) was stirred in 70 mL of toluene for 5 h. The resultant yellow crystalline precipitate was isolated by filtration, rinsed with 50 mL pentane and dried for 4 h (650 mg, 66 %). X-ray quality crystals were obtained from slow evaporation of toluene at room temperature. ^{1}H NMR (C_7D_7H, 300 MHz, 298 K): δ −7.62 (s, 3H, Ar-*H*), −31.23 (s, 3H, Ar-*H*), −37.92 (s, 3H, Ar-*H*), −48.29 (s, 3H, Ar-*H*), 150.16 (s, 9H, CH_3), 255 (s, 6H, P-CH_2). Anal. Calcd. for $C_{27}H_{27}N_3O_6PTm$: C, 47.04; H, 3.95; N, 6.09 Found: C, 46.98; H, 3.94; N, 6.06.

Synthesis of P[$CH_2NC_6H_4$-2-CO_2Me]$_3$Yb (27). A mixture of **13** (600 mg, 1.02 mmol) and Yb[$N(SiMe_3)_2$]$_3$ (745 mg, 1.02 mmol) was stirred in 70 mL of toluene for 5 h. The resultant yellow crystalline precipitate was isolated by filtration, rinsed with 50 mL pentane and dried for 4 h (638 mg, 68 %). X-ray quality crystals were obtained from slow evaporation of toluene at room temperature. ^{1}H NMR (C_7D_7H, 300 MHz, 298 K): δ

References begin on page 193

−4.23 (s, 3H, Ar-*H*), −7.27 (s, 3H, Ar-*H*), −8.92 (s, 3H, Ar-*H*), −10.67 (s, 3H, Ar-*H*), 27.8 (s, 9H, CH_3), 50.71 (s, 6H, P-CH_2). $^{31}P\{^1H\}$ NMR (C_7D_7H, 121.5 MHz, 298K): δ 191.7. Anal. Calcd. for $C_{27}H_{27}N_3O_6PYb$: C, 46.76; H, 3.92; N, 6.06 Found: C, 46.52; H, 3.76; N, 6.01.

5.5 References

1. Zaleski, C. M.; Depperman, E. C.; Kampf, J. W.; Kirk, M. L.; Pecoraro, V. L., *Angew. Chem., In. Ed.* **2004**, 43, (30), 3912.
2. Andruh, M.; Ramade, I.; Codjovi, E.; Guillou, O.; Kahn, O.; Trombe, J. C., *J. Am. Chem. Soc.* **1993,** 115, (5), 1822.
3. Miller, J. S.; Epstein, A. J., *Angew. Chem.* **1994,** 106, (4), 399.
4. Sakamoto, M.; Manseki, K.; Okawa, H., *Coord. Chem. Rev.* **2001,** 219-221, 379.
5. Rudowicz, C.; Qin, J., *J. Alloys Compd.* **2004,** 385, (1-2), 238.
6. van Pieterson, L.; Reid, M. F.; Burdick, G. W.; Meijerink, A., *Phys. Rev. B* **2002,** 65, (4), 045113.
7. Holsa, J.; Lamminmaki, R. J., *J. Lumin.* **1996,** 69, (5-6), 311.
8. Wybourne, B. G., *Spectroscopic Properties of Rare Earths (New York: Wiley)* **1965.**
9. McGarvey, B. R., *J. Magn. Reson.* **1979,** 33, (2), 445.
10. Ishikawa, N.; Sugita, M.; Okubo, T.; Tanaka, N.; Lino, T.; Kaizu, Y., *Inorg. Chem.* **2003,** 42, (7), 2440.
11. Benelli, C.; Gatteschi, D., *Chem. Rev.* **2002**, 102, (6), 2369.

References begin on page 193

12. Ishikawa, N.; Sugita, M.; Ishikawa, T.; Koshihara, S.-Y.; Kaizu, Y., *J. Am. Chem. Soc.* **2003,** 125, (29), 8694.

13. Binnemans, K.; Galyametdinov, Y. G.; Van Deun, R.; Bruce, D. W.; Collinson, S. R.; Polishchuk, A. P.; Bikchantaev, I.; Haase, W.; Prosvirin, A. V.; Tinchurina, L.; Litvinov, I.; Gubajdullin, A.; Rakhmatullin, A.; Uytterhoeven, K.; Van Meervelt, L., *J. Am. Chem. Soc.* **2000,** 122, (18), 4335.

14. Caravan, P.; Ellison, J. J.; McMurry, T. J.; Lauffer, R. B., *Chem. Rev.* **1999,** 99, (9), 2293.

15. Peters, J. A.; Huskens, J.; Raber, D. J., *Prog. Nucl. Magn. Reson. Spectrosc.* **1996,** 28, (3-4), 283.

16. Shelling, J. G.; Bjornson, M. E.; Hodges, R. S.; Taneja, A. K.; Sykes, B. D., *J. Magn. Reson.* **1984,** 57, (1), 99.

17. Brittain, H. G.; Richardson, F. S.; Martin, R. B., *J. Am. Chem. Soc.* **1976,** 98, (25), 8255.

18. Bertini, I.; Luchinat, C.; Aime, S., *Coord. Chem.Rev.* **1996,** 150, R7.

19. Elbanowski, M.; Makowsaka, B., *J. Photochem. Photobiol., A* **1996,** 99, (2-3), 85.

20. Ishikawa, N., *J. Phys. Chem. A* **2003,** 107, (30), 5831.

21. Ishikawa, N.; Iino, T.; Kaizu, Y., *J. Phys. Chem. A* **2002,** 106, (41), 9543.

22. Bleaney, B., *J. Magn. Reson.* **1972,** 8, (1), 91.

23. CONDON, *Magnetic Susceptibility Simulation Program, Helmut SCHILDER, Fachhochschule Aachen Germany,* **2000**.

24. Pangborn, A. B.; Giardello, M. A.; Grubbs, R. H.; Rosen, R. K.; Timmers, F. J., *Organometallics* **1996,** 15, (5), 1518.

References begin on page 193

25. Bradley, D. C.; Ghotra, J. S.; Hart, F. A., *J. Chem. Soc., Chem. Commun.* **1972**, (6), 349.

26. Bradley, D. C.; Ghotra, J. S.; Hart, F. A., *J. Chem. Soc., Dalton Trans.* **1973**, (10), 1021.

References begin on page 193

CHAPTER-6

Summary, Preliminary Results and Future Work

6.1 Summary

In summary, this PhD thesis makes a significant contribution to the study and characterization of the trivalent lanthanide complexes and their heteronuclear magnetic complexes. Due to the advantages of the magnetic properties of lanthanides, their complexes have been utilized for heterodinuclear complexes or clusters, where two metal centers can couple to each other magnetically.[1-12] While the first half of the thesis emphasized on the through-space exchange-coupling between two metal ions in heterodinuclear *d-f* metal complexes, the later chapters examine the details of crystal field dependent magnetic properties, which also depend on the temperature dependent pseudocontact shifts of lanthanides. Although

References begin on page 211

the magnetic properties of lanthanide complexes are theoretically very well understood, in practice it is not an easy task and requires a low temperature optical spectrometer. Using variable temperature NMR spectra, we are proposing a method, which would be helpful to determine the crystal field parameters without the use of the expensive optical instruments and SQUID magnetometer.

6.1.1 Syntheses and Characterization of Heterodinuclear (*d-f*) Complexes

This thesis work started with the syntheses of mononuclear trivalent lanthanide complexes prepared by using tripodal amido-phosphine ligands $P(CH_2NHAr^R)_3$ [Ar^R = C_6H_5, 3,5-$Me_2C_6H_3$ and 3,5-$(CF_3)_2C_6H_3$]. These ligands contain two binding sites suitable to bind two different types of metal ions (*d-f*) in order to make heterodinuclear complexes. Due to the tendency of making higher coordination compounds, the six coordinate trivalent lanthanide complexes used in Chapter 2 required external donor molecules such as THF or a tris(pyrazolyl)borate salt.[13-21] To observe the metal-metal interaction between *d* and *f* metals, initially, varieties of late transition metal complexes such as $PtMe_2(COD)$ (where COD = cyclooctadiene), $Ni(acac)_2$ (where $(acac)_2$ = acetylacetonate), and TPPcobalt(II) (where TPP = 5, 10, 15, 20-tetrakis(4-methoxyphenyl)porphinato) were used to bind the phosphine donor site of the tripodal amido donor ligands as shown Scheme 6.1.

References begin on page 211

Scheme 6.1

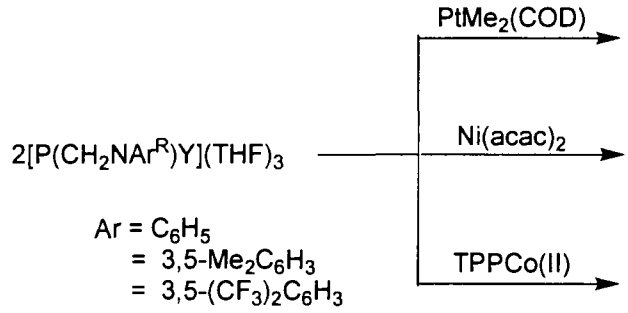

As shown in Scheme 6.2, the TPPCo(II) complex was further used in Chapter 3 where, after reaction with mononuclear trivalent yttrium and gadolinium complexes, heterodinuclear complexes $P(CH_2NC_6H_4\text{-}2\text{-}CO_2Me)_3LnTPPCo$ (Ln = Y, Gd) were produced. The phosphine donor abilities of these complexes were measured by the reaction of 4 equivalents of mononuclear trivalent lanthanides with 1 equivalent of $[Rh(\mu\text{-}Cl(CO)_2]_2$. Although the phosphine lone pair is directing away from the mononuclear metal centre the results showed that the large gadolinium metal possess stronger donor ability than the smaller yttrium metal.

Magnetic and EPR studies of $P(CH_2NC_6H_4\text{-}2\text{-}CO_2Me)_3Ln$ (Ln = Y, Gd) demonstrated the through-space antiferromagnetic coupling between Gd and Co metal ions, which is contrary to what is typically observed in *d-f* metal complexes. This coupling is mediated by the delocalization of the spin-density of the cobalt centre onto the phosphine donor, which allows direct overlap of the magnetic orbital associated with Co(II) with the *f*-electrons on the Gd(III) centre.

References begin on page 211

Scheme 6.2

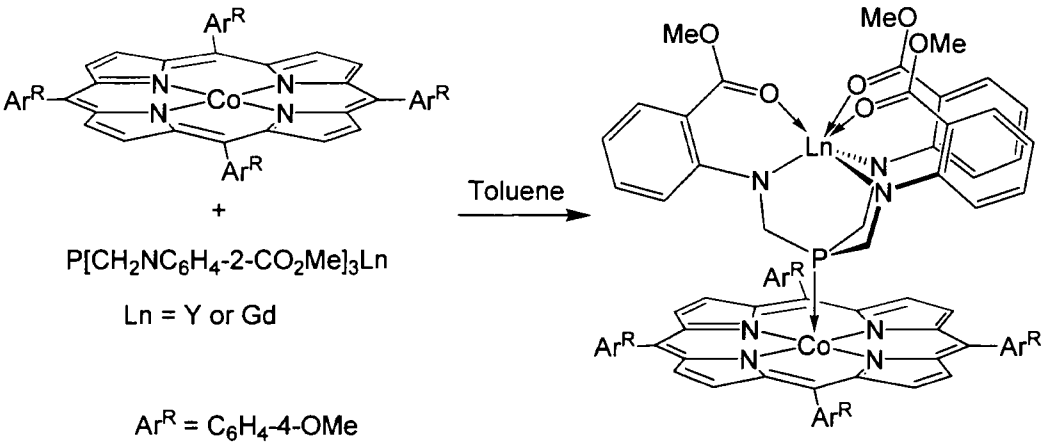

6.1.2 Temperature Dependent Pseudocontact Shifts and Crystal Field Parameters of Paramagnetic Lanthanides

It has been reported earlier that the pseudocontact shifts of lanthanide complexes are temperature dependent and required only second term crystal field parameters for the calculation of magnetic anisotropy as shown in equation (6.1).[7] While the T^{-2} term is the major temperature dependent term in pseudocontact shifts, additional term such as T^{-3} also contribute 10-20 % of the T^{-2} term.[8] In our studies, we have provided the evidence that not only fourth and sixth rank crystal field parameters ($B_{4's}$ and $B_{6's}$) but higher temperature dependent terms (T^{-3},T^{-4}) are also required in addition to the B_{20} and T^{-2} temperature dependent terms for pseudocontact shifts (equation 6.2).

$$\chi_{\parallel} - \chi_{\perp} = \frac{K_0}{T^2} B_{20} \qquad (6.1)$$

$$\chi\parallel\text{-}\chi\perp = C_1T^{-1} + C_2T^{-2} + C_3T^{-3} \qquad (6.2)$$

References begin on page 211

To determine the crystal field parameters of trivalent lanthanides complexes, we have synthesized a series of isostructural lanthanide complexes $P(CH_2NC_6H_4\text{-}2\text{-}CO_2Me)_3Ln$ (Ln = Tb, Dy, Ho, Er and Tm) which contain C_3 symmetry. These complexes are based on a new tripodal amido ligand, which includes ester functionality oxygen atoms and showed rigid chelate rings with four proton environments observed in the ^1H NMR spectra. Using only variable temperature NMR data, we have proposed a method to determine the crystal field parameters of lanthanide complexes. $^{31}P\{^1H\}$ NMR spectra of these complexes showed that the large chemical shifts from 700 to −1200 ppm due to the dipolar shift and can be used to measure the magnetic anisotropy as shown in equation (6.3).[9]

$$\Delta\delta = \frac{(3\mathrm{Cos}^2\theta\text{-}1)}{2R^3}(\chi_{zz}-\bar{\chi}) \qquad (6.3)$$

As shown in equation (6.4), according to Wybourne, C_3 symmetric complexes require 6 crystal field parameters, which can be written as B_{20}, B_{40}, B_{43}, B_{60}, B_{63} and B_{66}.[10] In future the crystal parameters resolved by using NMR spectra can be further utilized to obtain energies of the m_J substates.

$$V = B_{20}C_{20} + B_{40}C_{40} + B_{43}(C_{4-3} - C_{43}) + B_{60}C_{60} + B_3(C_{6-3} - C_{63}) + B_{66}(C_{6-6} + C_{66}) \quad (6.4)$$

References begin on page 211

6.2 Future Work

6.2.1 Future Study of Anionic $K^+\{[(CH_2NAr^R)_3YTp^{Me}]^-$ Complexes

Mononuclear trivalent lanthanide complexes, which are based on tripodal amido phosphine ligands can also be used as building blocks for multinuclear complexes or clusters.[22] Therefore, mononuclear trivalent lanthanide complexes $K^+[P(CH_2NAr^R)_3YTp^{Me}]^-$ (where Ar^R = C_6H_5, 3,5-$Me_2C_6H_3$ and 3,5-$(CF_3)_2C_6H_3$ and Tp = Tris(pyrazolyl)borate potassium salt) synthesized in Chapter 2 can be further used to react with transition metal complexes, to form polynuclear clusters or complexes. The preliminary experiments performed in Chapter 2 suggested that only ligand-exchange resistant transitional metal complexes, which have a tendency to accept phosphine as a donor molecule, can be used to react with these trivalent lanthanide complexes. For example, as shown in Scheme 6.3, paramagnetic $(Mes)_2Cr(PR_3)_2$ can be used to react with $K^+[(P(CH_2NAr^R)_3YTp^{Me}]^-$ to form dinuclear (1:1) or trinuclear (2:1) complexes. In the trinuclear complex, $(Mes)_2Cr(PR_3)_2$ can act as bridging complex between two lanthanide complexes $K^+[P(CH_2NAr^R)_3YTp]^-$.

References begin on page 211

Scheme 6.3

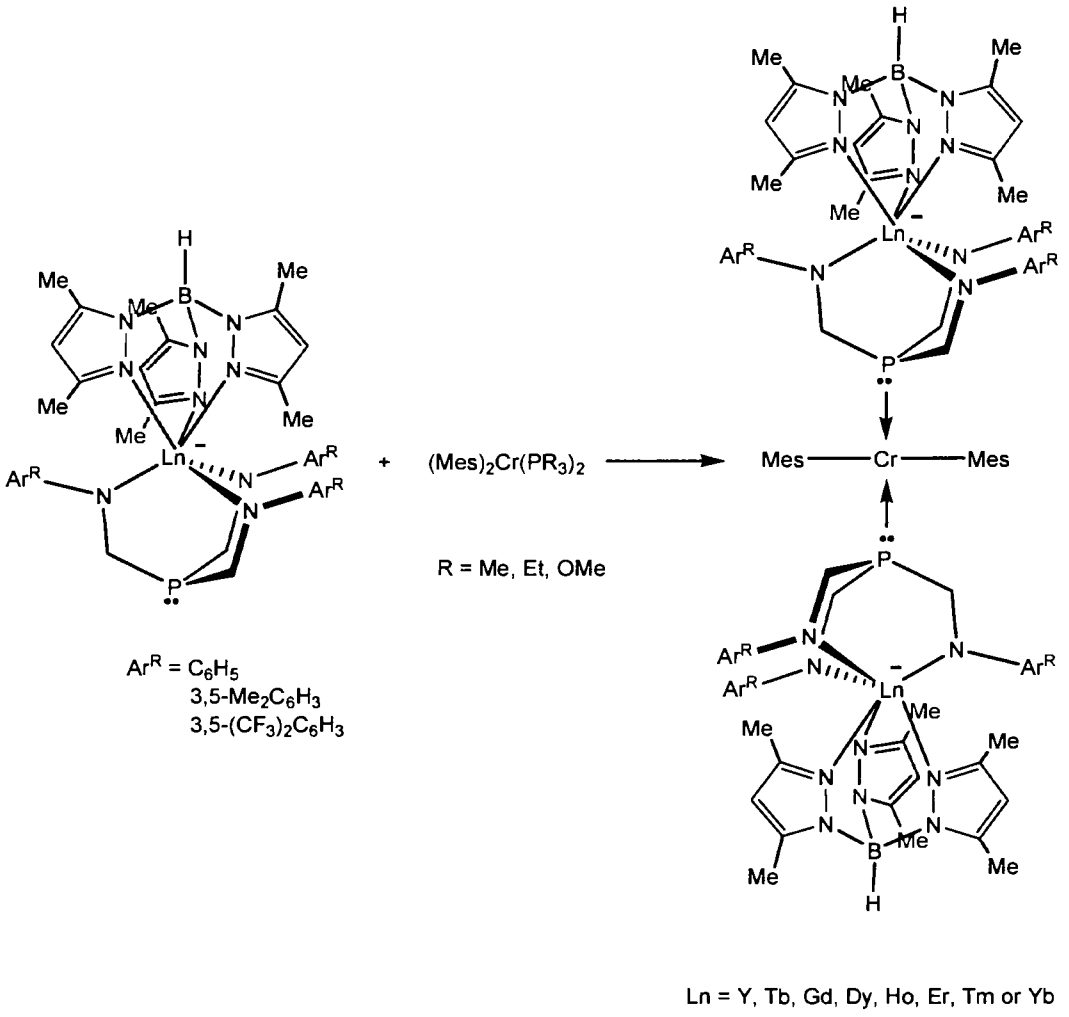

Another example of trinuclear M`-M-M` species involve the reaction of 1 equivalent of tris(pyrazolyl)phosphine ($Tp^{Me}P$) with a similar amount of $P(CH_2NAr^R)_3Ln(THF)_3$ (Ln = Y, Tb, Dy, Gd, Ho, Er, Tm or Yb) followed by their reaction with 2 equivalents of TPPCo(II), as shown in Scheme 6.4. As a long term goal, these heteronuclear complexes can be utilized for magnetic materials, or wires, or 2-D and 3-D networks, due to through-space exchange coupling or metallic interactions.[1, 23, 24]

References begin on page 211

Scheme 6.4

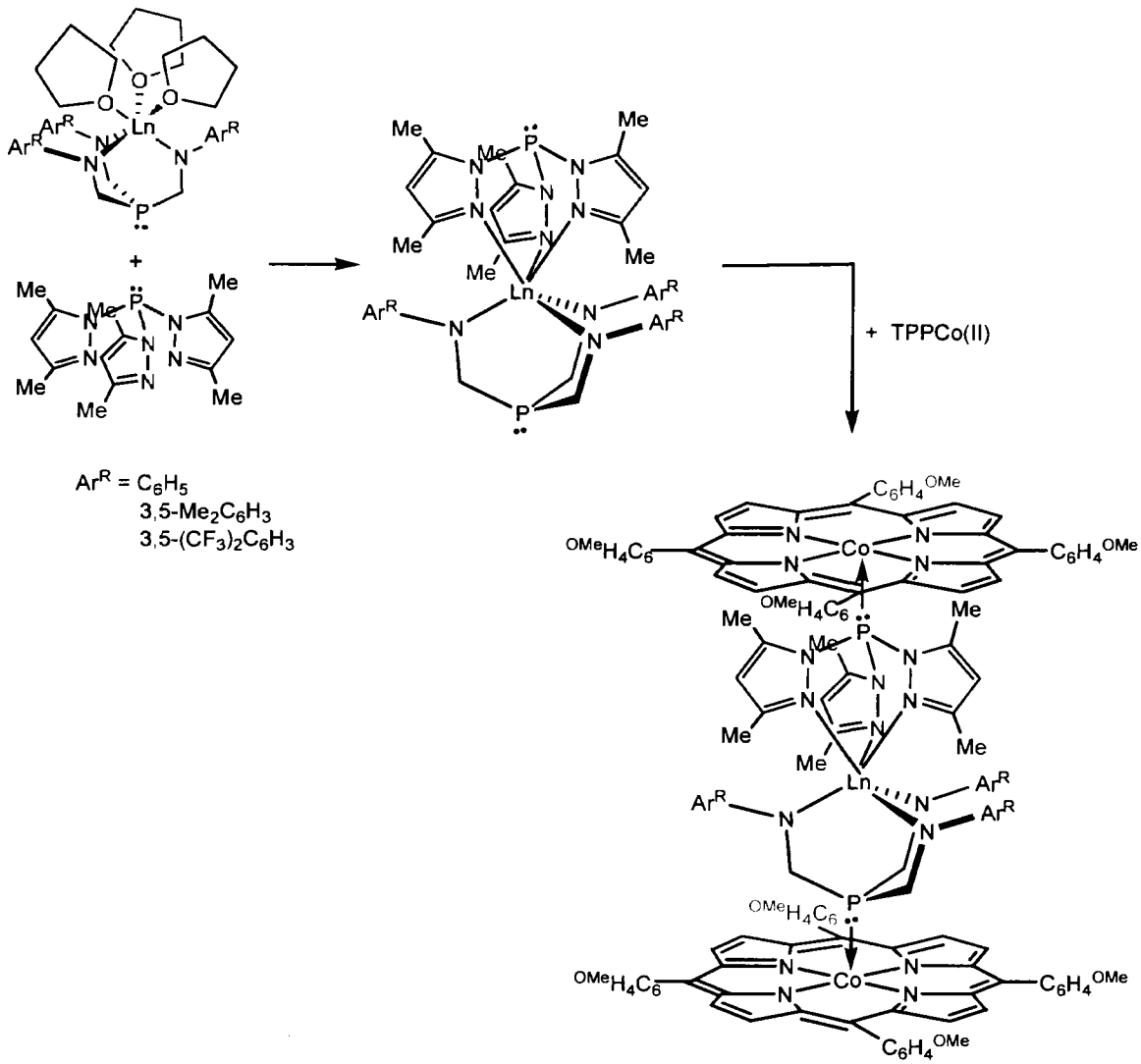

6.2.2 Study of Heterodinuclear Complexes Containing *d-d* Metal Complexes

Similar to paramagnetic heterodinuclear (*d-f*) complexes reported in this thesis, these tripodal amido-phosphine ligands can be also utilized to form heterodinuclear complexes containing *d-d* metal ions.[15] Some preliminary reactions performed in this manner involve the formation of mononuclear paramagnetic vanadium complexes, followed by their reactions with TPPCo(II).

References begin on page 211

Paramagnetic tetravalent vanadium complexes (**28-30**) (Scheme 6.5) were prepared by mixing equivalent amount of ligand precursors (**1a-1c**) and $V(N(Me_2)_4$ in toluene solution. Violet color crystals of the resultant complexes $[P(CH_2NAr^R]_3VNMe_2$ were obtained after cooling the saturated toluene solution. As reported in the literature, dark violet color crystals confirm the synthesis of tetravalent vanadium associated phosphine donors.[25] Formation of the ligand associated tetravalent vanadium complexes were confirmed by their crystal structures, EPR spectra and elemental analysis.

Scheme 6.5

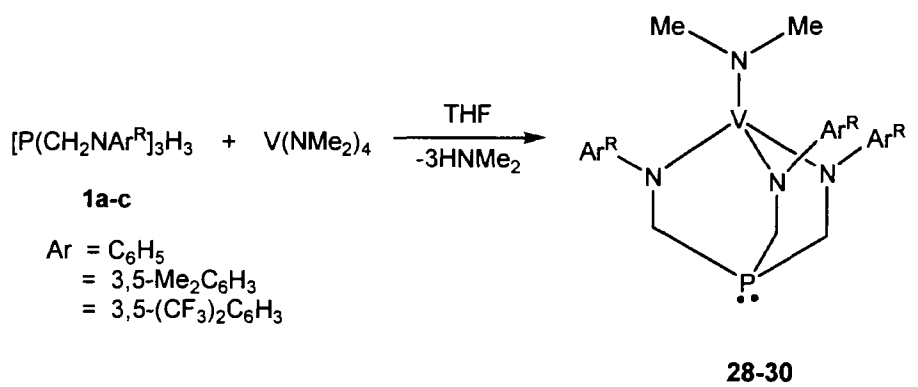

28-30

The solid-state molecular structure of $[P(CH_2NC_6H_5]_3VNMe_2$ was determined by X-ray crystallography and the ORTEP depiction of the molecular structure is given in Figure 6.1. As anticipated, the structure shows the amido nitrogen chelated vanadium center and the phosphine donor pointing away from the metal ion. The sum of C-P-C angles is 311.58(10)°, which is slightly smaller than what was observed in the case of complex **2a**. The sum of C-P-C angles of complex **1a** (299.5(2)°) increased after introducing the vanadium metal ion, which should also affect the donor ability of the corresponding phosphine complex. Although the typical V-P bond distances are 2.5-2.7 Å, the distance between V(1)-P(1) as shown in Figure 6.1, is 2.8646(8) Å,

References begin on page 211

which is almost 9 % larger than the average reported vanadium-phosphorus bond length (2.622(2) Å).[26]

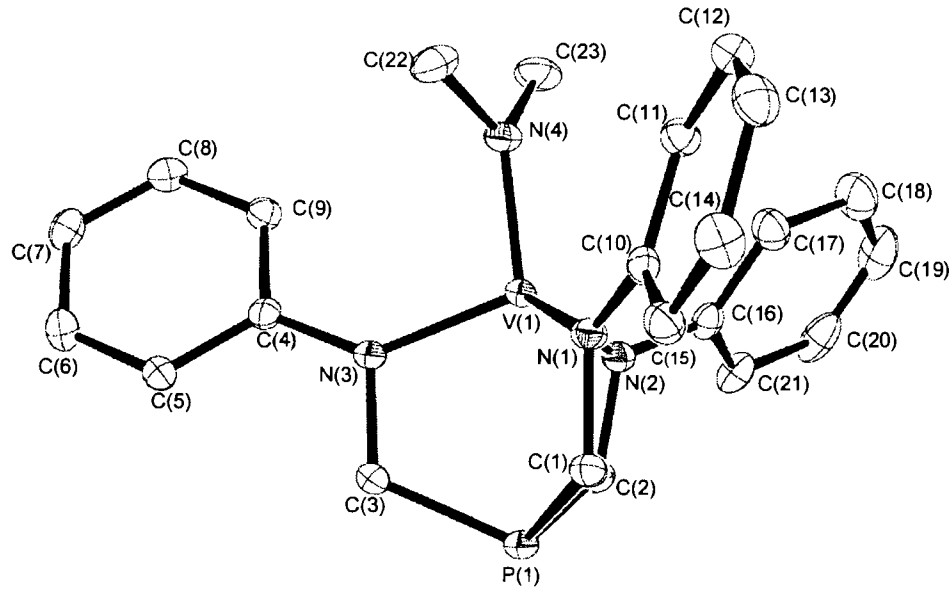

Figure 6.1. ORTEP depiction of the solid-state molecular structure of $[P(CH_2NC_6H_5]_3VNMe_2$ (**28**). Hydrogen atoms are omitted for clarity. Selected distances (Å): V(1)-N(4), 1.9054(18); V(1)-N(1), 1.8184(19); V(1)-N(2), 1.8834(18); V(1)-N(3), 1.9054(18); V(1)-P(1), 2.8646(8). Selected bond angles (°): C(1)-P(1)-C(2), 103.18(10); C(1)-P(1)-C(3), 103.02(10); C(2)-P(1)-C(3), 105.38(10).

The X-band EPR spectra of liquid samples of vanadium complexes (**28-30**) (I = 7/2) were obtained at room temperature as well as at 77 K. While the spectra acquired at room temperature provided the equally spaced eight line pattern, anisotropy was observed in the spectra of frozen samples (Figure 6.2, complex **28**). The EPR spectra of the frozen samples showed the overlapping of two sets of eight lines in which one set refers to the parallel and the other set refers the perpendicular direction. The EPR spectra as well as the crystal structure

References begin on page 211

confirmed the presence of mononuclear vanadium molecule. The spectrum of complex **28**, also confirms the presence of axial symmetry with $g_{\perp} > g_{\parallel}$. The spectrum was adequately modeled using $A_{\parallel}$ value of 134 G, and $A_{\perp}$ of 21 G with the g values of $g_{\parallel} = 1.955$ and $g_{\perp} = 1.989$. The g values are close to the values reported in the literature for $V(NEt_2)_4$.[27] The parameters were obtained from the experimental EPR spectra by comparing the distances between the adjacent parallel or perpendicular lines, where these can be easily differentiated from each other. However, the middle region where both lines overlap each other, calculation for the parameters is trivial. The g values and the hyperfine coupling constant provide the information related to the energy levels. It has been shown earlier for the related tetravalent vanadium complexes that the lowest energy d orbital can not be d_{z2} due to the fact that $g_{\parallel}$ is not close to 2.0023.[27] Thus for square planar vanadium amide complex ($[P(CH_2NC_6H_5]_3VNMe_2$), d_{x2-y2} will act as a ground state orbital.

Due to the overlapping of the two sets of eight lines mainly in the middle region, the attempts to fit these parameters did not produce a significantly better model of the experimental data. More significant improvements in fit were obtained by modeling the line widths anisotropically.

References begin on page 211

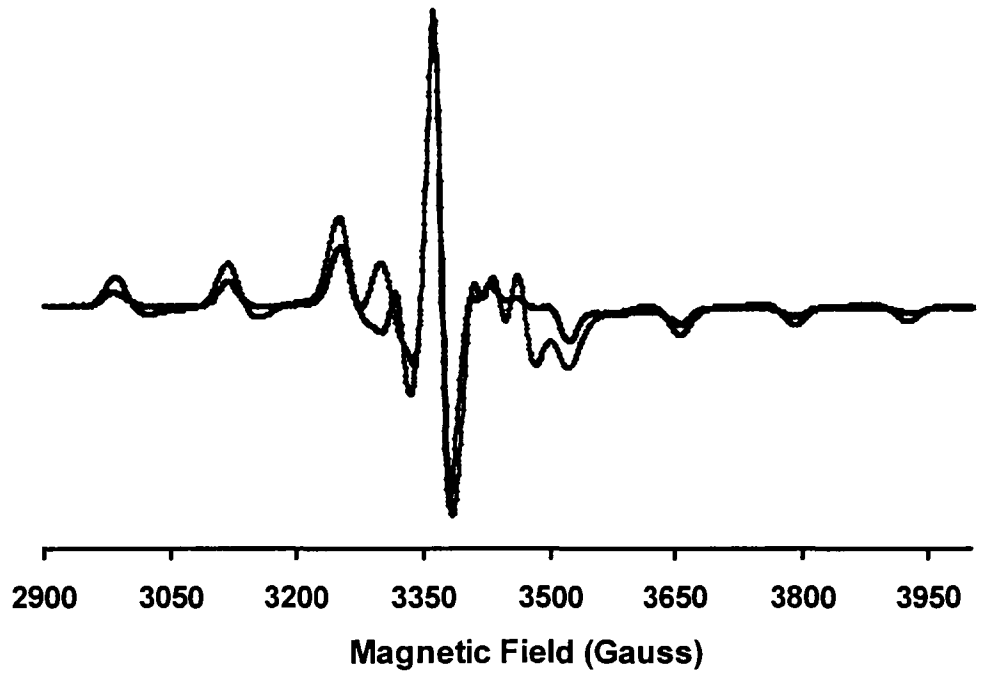

Figure 6.2 EPR spectrum of frozen ($[P(CH_2NAr^R)_3VNMe_2]$ (**28**) sample at 77 K (solid line) and a simulated spectrum (dotted grey line) obtained using $g_{\|} = 1.955$, $g_{\perp} = 1.989$, $A_{\|} = 134$ G, $A_{\perp} = 21$ G.

It is expected that similar to lanthanide complexes, after the reaction with TPPCo(II), mononuclear tetravalent vanadium complexes should also generate heterodinuclear *d-d* complexes. Diamagnetic Ti-complex $[P(CH_2NC_6H_5)_3TiNMe_2]$ was selected as a model for this study and reacted with one equivalent of TPPCo(II). The preliminary results obtained from ^1H NMR spectra verified the presence of a heterodinuclear (*d-d*) complex (Scheme 6.6).

References begin on page 211

Scheme 6.6

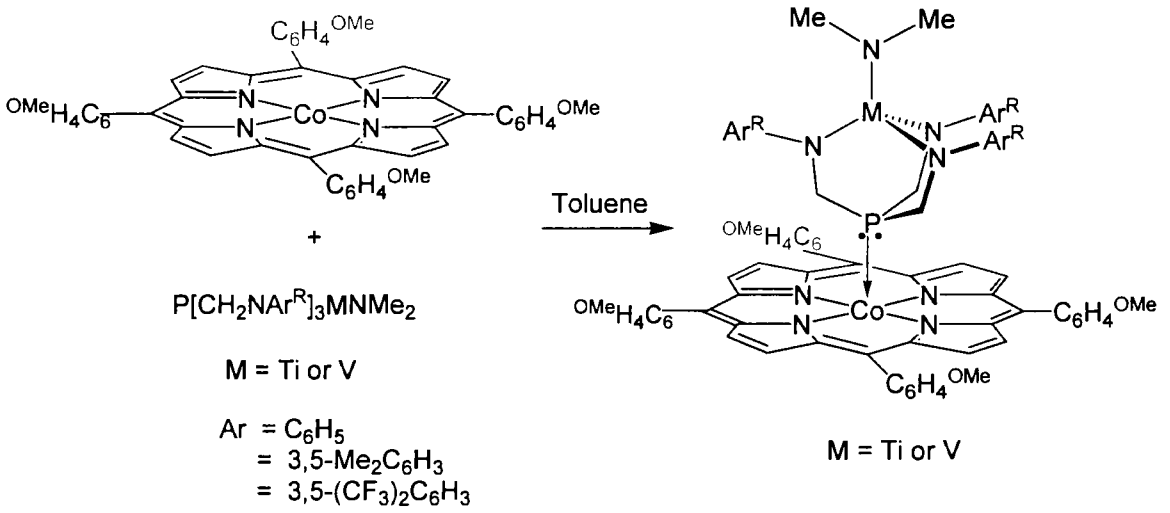

For future studies, these paramagnetic mononuclear vanadium complexes ($[P(CH_2NAr^R)_3VNMe_2]$ will be reacted with another transition metal complex such as TPPCO(II), to form heterdinuclear *d-d* complex $[P(CH_2NAr^R)_3VNMe_2TPPCo]$. These heteronuclear complexes will be further used for polynuclear complexes or magnetic materials.[16,17]

6.3 Experimental

Unless otherwise stated, all experiments were performed under an inert atmosphere of nitrogen using either using Schlenk techniques or an MBraun glove box according to Section 2.4. The compounds anhydrous VCl_4 and $TiCl_4$ were purchased from Aldrich used without further purification. The compound $V(NMe_2)_4$ was prepared from VCl_4 and $LiNMe_2$ and sublimed prior to the use.[28] The complex $[P(CH_2NC_6H_5)_3TiNMe_2]$ was prepared from the reaction of $Ti(NMe_2)_4$ and $[P(CH_2NHC_6H_5)_3$, as reported earlier.[29]

References begin on page 211

Synthesis of $P(CH_2NC_6H_5)_3VNMe_2$ (28). Small portions of $V(NMe_2)_4$ (478 mg, 0.00215 mol) were added to the solution of $P(CH_2NHC_6H_6)_3$ (750 mg, 0.00215 mol) in 20 mL of toluene at –78 °C and stirred for 30 min. stirring the solution for 24 h at room temperature, solvent was evaporated to dryness and the residue was rinsed with pentane (67 %, 635 mg). The violet colour crystals were obtained from the saturated toluene solution kept in the for 2 days overnight. Anal. Calcd for $C_{23}H_{27}N_4PV$: C, 62.58; H, 6.17; N, 12.69. Found: C, 62.54; H, 6.47; N, 12.60.

Synthesis of $P(CH_2N\text{-}3,5\text{-}Me_2C_6H_3)_3VNMe_2$ (29). Small portions of $V(NMe_2)_4$ (522 mg, 0.0023 mol) was added slowly to the solution of $P(CH_2NH\text{-}3,5\text{-}Me_2C_6H_3)_3$ (1 g, 0.0023 mol) in 20 mL of toluene at –78 °C and stirred for 30 min. After stirring the solution for 24 h at room temperature, solvent was evaporated to dryness and the residue was rinsed with pentane (65 %, 785 mg). Anal. Calcd for $C_{29}H_{39}N_4PV$: C, 66.27; H, 7.48; N, 10.66. Found: C, 66.00; H, 7.47; N, 10.69.

Synthesis of $P(CH_2N\text{-}3,5\text{-}(CF_3)_2C_6H_3)_3VNMe_2$ (30). Small portions of $V(NMe_2)_4$ (600 mg, 0.00938 mol) was added slowly to the solution $P(CH_2NH\text{-}3,5\text{-}Me_2C_6H_3)_3$ (500 mg, 0.938 mmol) in 20 mL of toluene at –78 °C and stirred for 30 min. After stirring the solution for 24 h at room temperature, solvent was evaporated to dryness and the residue was rinsed with pentane (65 %, 625 mg). Anal. Calcd for $C_{29}H_{21}F_{18}N_4PV$: C, 41.01; H, 2.49; N, 6.60. Found: C, 40.7 H, 2.47; N, 6.67.

Synthesis of $\{P(CH_2NC_6H_5)_3TiNMe_2\}\cdot$TPPCo(II) (31). Mixture of $P(CH_2NC_6H_6)_3TiNMe_2$ (300 mg, 0.684 mmol) and TPPCo(II) (460 mg, 0.684 mmol) was stirred in toluene for 2 h. The solvent was then dried under vacuum and the reddish purple residue was rinsed with 10 mL of pentane and further dried for 3 h (70 %, 385 mg). ^1H NMR

References begin on page 211

(C_6D_6, 300 MHz, 298 K): δ 3.32 (br, 15 H total, TiN(CH_3)$_2$ and CO_2CH_3), 4.21 (br, 18 H total,-OCH_3 and PCH_2), 6.82 (br, 6H, *o*-Ph), 6.91 (br, 3H, *p*-Ph), 7.26 (br, 6H, *m*-Ph), 8.85 (br, 8H, TPP-*m*-*H*), 11.54 (v br, 8H, TPP-*o*-*H*), 15.23 (v br, 8H, pyrrole-*H*).

Selected crystallographic data of $P(CH_2NC_6H_6)_3VNMe_2$ are shown in Table 6.1.

Table 6.1. Selected X-ray Crystallographic Data of **$P(CH_2NC_6H_6)_3VNMe_2$ (28)**

Empirical formula	$C_{23}H_{27}N_4PV$
ssFormula weight	441.40
Crystal system	Monoclinic
a (Å)	12.153(2)
b (Å)	14.282(2)
c (Å)	12.654(2)
α (deg)	90.00
β (deg)	92.24(2)
γ (deg)	90.00
V (Å^3)	2194.9(6)
Space group	*P2(1)/n*
Z	4
Density (g/cm3)	1.336
μ (Mo Kα) (mm^{-1})	0.541
Temperature (K)	173
Total no. of reflection	4966
Residuals: R_1; wR_2	0.0476; 0.1116

References begin on page 211

6.4 References

1. Mrozinski, J., *Coord. Chem. Rev.* **2005,** 249, (21-22), 2534.
2. Benelli, C.; Dei, A.; Gatteschi, D.; Pardi, L., *Inorg. Chem.* **1990,** 29, (18), 3409.
3. Benelli, C.; Gatteschi, D.; Carnegie, D. W.; Carlin, R. L., *J. Am. Chem. Soc.* **1985,** 107, (8), 2560.
4. Sakamoto, M.; Manseki, K.; Okawa, H., *Coord. Chem. Rev.* **2001,** 219, 379.
5. Costes, J. P.; Dahan, F.; Donnadieu, B.; Garcia-Tojal, J.; Laurent, J. P., *Eur. J. Inorg. Chem.* **2001**, (2), 363.
6. Zaleski, C. M.; Depperman, E. C.; Kampf, J. W.; Kirk, M. L.; Pecoraro, V. L., *Angew. Chem., Int. Edit.* **2004,** 43, (30), 3912.
7. Andruh, M.; Ramade, I.; Codjovi, E.; Guillou, O.; Kahn, O.; Trombe, J. C., *J. Am. Chem. Soc.* **1993,** 115, (5), 1822.
8. Matsumoto, N.; Sakamoto, M.; Tamaki, H.; Okawa, H.; Kida, S., *Chem. Lett.* **1990**, (6), 853.
9. Blake, A. J.; Gould, R. O.; Grant, C. M.; Milne, P. E. Y.; Parsons, S.; Winpenny, R. E. P., *J. Chem. Soc., Dalton Trans.* **1997**, (4), 485.
10. Costes, J. P.; Auchel, M.; Dahan, F.; Peyrou, V.; Shova, S.; Wernsdorfer, W., *Inorg. Chem.* **2006,** 45, (5), 1924.
11. Benelli, C.; Blake, A. J.; Milne, P. E. Y.; Rawson, J. M.; Winpenny, R. E. P., *Chem. Eur. J.* **1995,** 1, (9), 614.
12. Kempe, R.; Noss, H.; Irrgang, T., *J. Organomet. Chem.* **2002,** 647, (1-2), 12.
13. Kanesato, M.; Mizukami, S.; Houjou, H.; Tokuhisa, H.; Koyama, E.; Nagawa, Y., *J. Alloys Compds.* **2004,** 374, (1-2), 307.

References begin on page 211

14. Miao, W.; Li, S. H.; Cui, D. M.; Huang, B. T., *J. Organomet. Chem.* **2007,** 692, (17), 3823.

15. Raymond, K. N., *Eur. J. Solid State . Inorg. Chem.* **1991,** 28, 225.

16. Huskowska, E.; Maupin, C. L.; Parker, D.; Williams, J. A. G.; Riehl, J. P., *Enantiomer* **1997,** 2, (5), 381.

17. Takats, J., *J. Alloys Compds.* **1997,** 249, (1-2), 52.

18. Marques, N.; Sella, A.; Takats, J., *Chem. Rev.* **2002,** 102, (6), 2137.

19. Santos, I.; Marques, N., *New J. Chem.* **1995,** 19, (5-6), 551.

20. Trofimen.S, *J. Am. Chem. Soc.* **1966,** 88, (8), 1842.

21. Ferrence, G. M.; McDonald, R.; Morissette, M.; Takats, J., *J. Organomet. Chem.* **2000,** 596, (1-2), 95.

22. Raturi, R.; Lefebvre, J.; Leznoff, D. B.; McGarvey, B. R.; Johnson, S. A., *Chem. Eur. J.* **2008,** 14, (2), 721.

23. Itoh, K.; Kinoshita, M., *Molecular Magnetism: New Magnetic Materials.* **2002**.

24. Miller, J. S., *Dalton Trans.* **2006**, (23), 2742.

25. Zahletho, J.; Samuel, E.; Livage, J., *Inorg. Chem.* **1988,** 27, (13), 2233.

26. Cotton, F. A.; Lu, J., *Inorg. Chem.* **1995,** 34, (10), 2639.

27. Holloway, C. E.; Mabbs, F. E.; Smail, W. R., *J. Chem. Soc., A-Inorg. Phys. Theor.* **1968**, (12), 2980.

28. Bradley, D. C.; Gitlitz, M. H., *J. Chem.l Soc., A-Inorg. Phys. Theor.* **1969**, (6), 980.

29. Han, H.; Elsmaili, M.; Johnson, S. A., *Inorg. Chem.* **2006,** 45, (18), 7435.

References begin on page 211

Appendix One: X-ray Crystal Structure Data

Table A 1.1. Positional parameters and U(eq) for $[P(CH_2N\text{-}3,5\text{-}Me_2C_6H_3)_3]Y(THF)_3$ (**2b**)

	x	y	z	U(eq)
O(1)	5367(3)	1597(3)	29(2)	62(1)
C(1)	5161(5)	3066(5)	-2434(3)	58(1)
C(8)	1878(7)	2114(8)	612(4)	107(2)
C(13)	4500(5)	427(5)	-376(4)	73(2)
C(11)	4151(11)	149(8)	1007(5)	148(4)
C(12)	3991(7)	-549(7)	283(5)	106(2)
C(10)	5186(8)	1431(7)	872(4)	103(2)
O(2)	3333	-3333	-2515(11)	187(6)
C(14)	3810(30)	-2200(30)	-1980(18)	228(9)
C(15)	4150(20)	-2800(30)	-1330(12)	205(9)
P(1)	6667	3333	-2863(1)	54(1)
Y(1)	6667	3333	-881(1)	45(1)
C(2)	3752(4)	2725(4)	-1361(3)	50(1)
C(6)	1649(5)	2374(6)	-1641(4)	74(2)
C(3)	3404(5)	2548(5)	-540(3)	62(1)
N(1)	4934(4)	2954(4)	-1572(2)	51(1)
C(9)	690(7)	2268(10)	-2271(6)	129(3)
C(7)	2836(5)	2648(5)	-1902(3)	65(1)
C(5)	1346(5)	2192(5)	-838(4)	76(2)
C(4)	2214(6)	2277(5)	-286(4)	74(2)

Table A 1.2. Positional parameters and U(eq) for $[P(CH_2N\text{-}3,5\text{-}Me_2C_6H_3)_2(\mu\text{-}N\text{-}3,5\text{-}Me_2\text{-}C_6H_3)Y(THF)]_2$ (**2b'**)

	x	y	z	U(eq)
Y(001)	5846(2)	9837(1)	6249(1)	26(1)
P(002)	1044(5)	9593(2)	3958(4)	34(1)
O(004)	4696(11)	9517(5)	7518(9)	38(3)
N(002)	3758(14)	9608(5)	5114(10)	22(3)
N(003)	7876(15)	9386(6)	6612(12)	40(4)
N(001)	6584(15)	10603(6)	7068(11)	36(4)
C(030)	4370(20)	10834(8)	7680(13)	38(5)
C(010)	2217(17)	9689(7)	5111(14)	33(5)
C(03)	3960(20)	8075(7)	5046(16)	51(6)
C(06)	5531(17)	8984(8)	4784(13)	33(4)
C(01)	4187(18)	9071(6)	5013(12)	27(4)
C(012)	6978(19)	8499(8)	7143(15)	44(5)
C(024)	7924(17)	10796(7)	6919(12)	30(4)
C(015)	9669(19)	8057(8)	7431(14)	38(5)
C(025)	5870(20)	10915(7)	7667(13)	37(5)
C(09)	9108(17)	9698(7)	6504(14)	33(5)
C(019)	5352(18)	9539(9)	8593(14)	44(5)
C(020)	3310(20)	9282(10)	7552(17)	67(8)
C(011)	8140(20)	8856(8)	6923(15)	43(5)
C(04)	5390(20)	8026(8)	4828(11)	36(5)
C(02)	3413(19)	8600(7)	5140(12)	32(4)
C(013)	7130(20)	7976(8)	7463(14)	43(5)

C(018)	11090(20)	7819(8)	7630(16)	52(6)
C(08)	3140(20)	7598(8)	5247(17)	53(6)
C(016)	9438(18)	8613(7)	7129(12)	30(4)
C(029)	3560(20)	11090(9)	8291(18)	57(6)
C(05)	6190(20)	8484(6)	4678(14)	36(5)
C(028)	4190(20)	11470(8)	8906(15)	52(6)
C(026)	6390(20)	11331(7)	8271(14)	39(5)
C(07)	7620(20)	8427(9)	4400(17)	57(6)
C(014)	8540(20)	7775(7)	7623(15)	49(6)
C(023)	3250(30)	9094(13)	8552(15)	93(11)
C(032)	2060(20)	10990(10)	8270(17)	61(7)
C(027)	5700(30)	11593(8)	8897(16)	56(6)
C(017)	5870(20)	7609(9)	7592(18)	69(7)
C(022)	4240(30)	9488(10)	9194(18)	67(7)
C(031)	6350(30)	12024(9)	9554(15)	62(7)
Br(1)	10180(50)	187(14)	7840(50)	1320(40)
C(102)	9120(30)	206(11)	9395(19)	64(7)
C(100)	9160(50)	-320(20)	9200(40)	150(16)
C(101)	9900(200)	-1060(100)	9750(190)	200(200)

Table A 1.3. Positional parameters and U(eq) for $[P(CH_2N\text{-}3,5\text{-}(CF_3)_2C_6H_3)_3Y(THF)_3]_2PtMe_2$ (**9**)

	x	y	z	U(eq)
P(1)	4649(1)	10119(1)	6355(1)	26(1)
Y(1)	6647(1)	9331(1)	7268(1)	24(1)
N(1)	6740(2)	8881(2)	6132(2)	28(1)
N(2)	4909(2)	8849(2)	7902(2)	29(1)
N(3)	6173(2)	11076(2)	6751(2)	29(1)
N(4)	8281(2)	7684(2)	8338(2)	29(1)
N(5)	7540(2)	7696(2)	7925(2)	29(1)
N(6)	7751(2)	9389(2)	8723(2)	30(1)
N(7)	6815(2)	9696(2)	8458(2)	30(1)
N(8)	9188(2)	9344(2)	7450(2)	27(1)
N(9)	8594(2)	9608(2)	6887(2)	27(1)
C(1)	5788(2)	9364(2)	5823(2)	27(1)
C(2)	4165(3)	9304(3)	7388(2)	29(1)
C(3)	5246(3)	11226(2)	6409(2)	28(1)
C(4)	7432(2)	8243(2)	5716(2)	27(1)
C(5)	7297(2)	8053(2)	5034(2)	27(1)
C(6)	7986(3)	7315(2)	4692(2)	29(1)
C(7)	8855(3)	6753(3)	4972(2)	34(1)
C(8)	9025(3)	6969(3)	5626(2)	34(1)
C(9)	8355(3)	7690(3)	5984(2)	32(1)
C(10)	7763(3)	7140(3)	3988(2)	34(1)
C(11)	9940(3)	6352(3)	5955(3)	48(1)
C(12)	4422(3)	8231(3)	8643(2)	30(1)

C(13)	3321(3)	8030(3)	8905(2)	33(1)
C(14)	2899(3)	7365(3)	9652(2)	39(1)
C(15)	3527(3)	6879(3)	10176(2)	40(1)
C(16)	4623(3)	7095(3)	9930(2)	35(1)
C(17)	5054(3)	7751(3)	9200(2)	33(1)
C(18)	1738(3)	7152(4)	9881(2)	59(1)
C(19)	5329(3)	6555(3)	10477(2)	49(1)
C(20)	6520(3)	11994(2)	6719(2)	29(1)
C(21)	6081(3)	12990(3)	6356(2)	33(1)
C(22)	6477(3)	13896(3)	6345(2)	36(1)
C(23)	7304(3)	13861(3)	6685(2)	38(1)
C(24)	7742(3)	12872(3)	7056(2)	34(1)
C(25)	7370(3)	11970(3)	7072(2)	32(1)
C(26)	5982(4)	14902(3)	5924(3)	50(1)
C(27)	8635(3)	12817(3)	7431(2)	42(1)
C(28)	9266(4)	6405(3)	9290(3)	63(1)
C(29)	8515(3)	6692(3)	8750(2)	40(1)
C(30)	7940(3)	6054(3)	8595(2)	45(1)
C(31)	7335(3)	6701(3)	8085(2)	33(1)
C(32)	6545(3)	6414(3)	7751(2)	44(1)
C(33)	8611(4)	9729(4)	9679(3)	62(1)
C(34)	7699(3)	9853(3)	9288(2)	40(1)
C(35)	6717(3)	10451(3)	9403(2)	45(1)
C(36)	6188(3)	10336(3)	8878(2)	36(1)
C(37)	5100(3)	10834(3)	8748(2)	47(1)
C(38)	10932(3)	9742(3)	7601(2)	47(1)

C(39)	10126(3)	9819(3)	7138(2)	33(1)
C(40)	10156(3)	10381(3)	6363(2)	37(1)
C(41)	9198(3)	10234(3)	6232(2)	31(1)
C(42)	8792(3)	10695(3)	5496(2)	40(1)
B(1)	8697(3)	8700(3)	8316(2)	29(1)
F(1)	8282(2)	6253(2)	3828(1)	51(1)
F(2)	6697(2)	7066(2)	4087(1)	46(1)
F(3)	8049(2)	7908(2)	3321(1)	56(1)
F(4)	9864(3)	5343(2)	6179(3)	117(2)
F(5)	10909(2)	6444(3)	5440(2)	109(1)
F(6)	10048(3)	6556(3)	6582(2)	113(2)
F(7)	1326(2)	6741(4)	10617(2)	124(2)
F(8)	1106(2)	7847(3)	9535(2)	105(1)
F(9)	1645(3)	6307(3)	9634(3)	132(2)
F(10)	5647(3)	5568(2)	10470(2)	90(1)
F(11)	4830(2)	6518(3)	11239(1)	79(1)
F(12)	6245(2)	7015(2)	10306(2)	67(1)
F(13)	4881(2)	14971(2)	6138(2)	72(1)
F(14)	6246(3)	15046(2)	5129(2)	82(1)
F(15)	6266(2)	15735(2)	6029(2)	66(1)
F(16)	9586(2)	13000(3)	6895(2)	96(1)
F(17)	8815(3)	11916(2)	7929(2)	92(1)
F(18)	8484(3)	13535(3)	7807(2)	89(1)
O(1)	12225(3)	4136(3)	7604(2)	91(1)
C(43)	13003(5)	3447(6)	7986(4)	121(3)
C(44)	12500(5)	2481(6)	8394(5)	101(2)

C(45)	11303(5)	2741(6)	8471(4)	92(2)
C(46)	11150(5)	3857(6)	8126(4)	98(2)
C(47)	11811(5)	7297(5)	7224(4)	79(2)
C(48)	12043(5)	7863(4)	6467(4)	81(2)
C(49)	13081(6)	7858(5)	6008(5)	113(3)
C(50)	13889(7)	7291(6)	6283(8)	139(4)
C(51)	13729(9)	6724(7)	7051(8)	137(5)
C(52)	12642(9)	6717(6)	7548(5)	113(3)
K(1)	12581(1)	5490(1)	6253(1)	62(1)

Table A 1.4. Positional parameters and U(eq) for $[P(CH_2NHC_6H_5)_3]_2 Ni(acac)_2$ (**10**)

	x	y	z	U(eq)
C(1)	5761(1)	475(1)	7740(3)	61(1)
C(2)	5050(1)	682(1)	7719(3)	62(1)
C(3)	4878(1)	-190(1)	6998(2)	55(1)
C(4)	6017(1)	522(1)	5781(3)	62(1)
C(5)	6298(1)	810(2)	4964(3)	79(1)
C(6)	5952(2)	-96(2)	4717(3)	93(1)
C(7)	6237(2)	200(2)	3935(4)	110(2)
C(8)	6405(2)	644(2)	4068(4)	103(2)
C(9)	5850(1)	70(1)	5648(3)	70(1)
C(10)	5197(1)	1379(1)	8690(3)	58(1)
C(11)	5327(1)	1622(1)	9672(3)	70(1)
C(12)	5311(1)	2006(1)	9799(3)	84(1)
C(13)	5162(2)	2163(2)	8969(4)	97(1)
C(14)	5026(2)	1924(2)	8009(4)	98(1)
C(15)	5046(1)	1541(1)	7852(3)	75(1)
C(16)	4445(1)	-1382(2)	5060(3)	88(1)
C(17)	4772(1)	-949(1)	6676(3)	54(1)
C(18)	4608(1)	-984(1)	5614(3)	67(1)
C(19)	4434(2)	-1749(2)	5502(4)	102(1)
C(20)	4597(2)	-1712(1)	6549(4)	99(1)
C(21)	4765(1)	-1321(1)	7131(3)	79(1)
C(23)	4205(1)	70(1)	9648(3)	60(1)
C(24)	3987(1)	-352(1)	9161(3)	63(1)

C(22)	3992(1)	357(1)	9625(4)	96(1)
C(25)	4129(1)	-662(1)	9125(2)	51(1)
C(26)	3841(1)	-1103(1)	8549(3)	70(1)
N(1)	5911(1)	702(1)	6683(3)	71(1)
N(2)	5246(1)	1011(1)	8592(3)	65(1)
N(3)	4949(1)	-558(1)	7279(3)	61(1)
O(1)	4581(1)	243(1)	10117(2)	56(1)
O(2)	5507(1)	608(1)	10482(2)	53(1)
P(2)	5166(1)	238(1)	8064(1)	52(1)
Ni(1)	5000	0	10000	46(1)

Table A 1.5. Positional parameters and U(eq) for $[P(CH_2N\text{-}3,5\text{-}(CF_3)_2C_6H_3)_3YTpK]$ (**12c**)

	x	y	z	U(eq)
P(1)	4649(1)	10119(1)	6355(1)	26(1)
Y(1)	6647(1)	9331(1)	7268(1)	24(1)
N(1)	6740(2)	8881(2)	6132(2)	28(1)
N(2)	4909(2)	8849(2)	7902(2)	29(1)
N(3)	6173(2)	11076(2)	6751(2)	29(1)
N(4)	8281(2)	7684(2)	8338(2)	29(1)
N(5)	7540(2)	7696(2)	7925(2)	29(1)
N(6)	7751(2)	9389(2)	8723(2)	30(1)
N(7)	6815(2)	9696(2)	8458(2)	30(1)
N(8)	9188(2)	9344(2)	7450(2)	27(1)
N(9)	8594(2)	9608(2)	6887(2)	27(1)
C(1)	5788(2)	9364(2)	5823(2)	27(1)
C(2)	4165(3)	9304(3)	7388(2)	29(1)
C(3)	5246(3)	11226(2)	6409(2)	28(1)
C(4)	7432(2)	8243(2)	5716(2)	27(1)
C(5)	7297(2)	8053(2)	5034(2)	27(1)
C(6)	7986(3)	7315(2)	4692(2)	29(1)
C(7)	8855(3)	6753(3)	4972(2)	34(1)
C(8)	9025(3)	6969(3)	5626(2)	34(1)
C(9)	8355(3)	7690(3)	5984(2)	32(1)
C(10)	7763(3)	7140(3)	3988(2)	34(1)
C(11)	9940(3)	6352(3)	5955(3)	48(1)
C(12)	4422(3)	8231(3)	8643(2)	30(1)

C(13)	3321(3)	8030(3)	8905(2)	33(1)
C(14)	2899(3)	7365(3)	9652(2)	39(1)
C(15)	3527(3)	6879(3)	10176(2)	40(1)
C(16)	4623(3)	7095(3)	9930(2)	35(1)
C(17)	5054(3)	7751(3)	9200(2)	33(1)
C(18)	1738(3)	7152(4)	9881(2)	59(1)
C(19)	5329(3)	6555(3)	10477(2)	49(1)
C(20)	6520(3)	11994(2)	6719(2)	29(1)
C(21)	6081(3)	12990(3)	6356(2)	33(1)
C(22)	6477(3)	13896(3)	6345(2)	36(1)
C(23)	7304(3)	13861(3)	6685(2)	38(1)
C(24)	7742(3)	12872(3)	7056(2)	34(1)
C(25)	7370(3)	11970(3)	7072(2)	32(1)
C(26)	5982(4)	14902(3)	5924(3)	50(1)
C(27)	8635(3)	12817(3)	7431(2)	42(1)
C(28)	9266(4)	6405(3)	9290(3)	63(1)
C(29)	8515(3)	6692(3)	8750(2)	40(1)
C(30)	7940(3)	6054(3)	8595(2)	45(1)
C(31)	7335(3)	6701(3)	8085(2)	33(1)
C(32)	6545(3)	6414(3)	7751(2)	44(1)
C(33)	8611(4)	9729(4)	9679(3)	62(1)
C(34)	7699(3)	9853(3)	9288(2)	40(1)
C(35)	6717(3)	10451(3)	9403(2)	45(1)
C(36)	6188(3)	10336(3)	8878(2)	36(1)
C(37)	5100(3)	10834(3)	8748(2)	47(1)
C(38)	10932(3)	9742(3)	7601(2)	47(1)

C(39)	10126(3)	9819(3)	7138(2)	33(1)
C(40)	10156(3)	10381(3)	6363(2)	37(1)
C(41)	9198(3)	10234(3)	6232(2)	31(1)
C(42)	8792(3)	10695(3)	5496(2)	40(1)
B(1)	8697(3)	8700(3)	8316(2)	29(1)
F(1)	8282(2)	6253(2)	3828(1)	51(1)
F(2)	6697(2)	7066(2)	4087(1)	46(1)
F(3)	8049(2)	7908(2)	3321(1)	56(1)
F(4)	9864(3)	5343(2)	6179(3)	117(2)
F(5)	10909(2)	6444(3)	5440(2)	109(1)
F(6)	10048(3)	6556(3)	6582(2)	113(2)
F(7)	1326(2)	6741(4)	10617(2)	124(2)
F(8)	1106(2)	7847(3)	9535(2)	105(1)
F(9)	1645(3)	6307(3)	9634(3)	132(2)
F(10)	5647(3)	5568(2)	10470(2)	90(1)
F(11)	4830(2)	6518(3)	11239(1)	79(1)
F(12)	6245(2)	7015(2)	10306(2)	67(1)
F(13)	4881(2)	14971(2)	6138(2)	72(1)
F(14)	6246(3)	15046(2)	5129(2)	82(1)
F(15)	6266(2)	15735(2)	6029(2)	66(1)
F(16)	9586(2)	13000(3)	6895(2)	96(1)
F(17)	8815(3)	11916(2)	7929(2)	92(1)
F(18)	8484(3)	13535(3)	7807(2)	89(1)
O(1)	12225(3)	4136(3)	7604(2)	91(1)
C(43)	13003(5)	3447(6)	7986(4)	121(3)
C(44)	12500(5)	2481(6)	8394(5)	101(2)

C(45)	11303(5)	2741(6)	8471(4)	92(2)
C(46)	11150(5)	3857(6)	8126(4)	98(2)
C(47)	11811(5)	7297(5)	7224(4)	79(2)
C(48)	12043(5)	7863(4)	6467(4)	81(2)
C(49)	13081(6)	7858(5)	6008(5)	113(3)
C(50)	13889(7)	7291(6)	6283(8)	139(4)
C(51)	13729(9)	6724(7)	7051(8)	137(5)
C(52)	12642(9)	6717(6)	7548(5)	113(3)
K(1)	12581(1)	5490(1)	6253(1)	62(1)

Table A 1.6. Positional parameters and U(eq) for $[P(CH_2NHC_6H_4\text{-}2\text{-}CO_2Me)_3]$ **(13)**

	x	y	z	U(eq)
C(28A)	-710(5)	5023(6)	10443(5)	88(1)
C(29A)	-1026(5)	4237(5)	9344(5)	88(1)
C(30A)	-173(6)	4153(5)	8669(3)	88(1)
C(31A)	997(5)	4855(6)	9094(4)	88(1)
C(32A)	1314(5)	5641(5)	10193(5)	88(1)
C(33A)	460(6)	5725(5)	10868(4)	88(1)
C(1)	3632(3)	3328(3)	268(2)	64(1)
C(2)	4738(3)	1305(2)	1090(2)	52(1)
C(3)	6159(3)	3557(3)	1674(2)	57(1)
C(4)	3613(3)	1913(3)	-1645(2)	51(1)
C(5)	4168(3)	1597(3)	-2583(2)	50(1)
C(6)	3666(3)	553(3)	-3471(2)	56(1)
C(7)	2641(3)	-174(3)	-3478(2)	60(1)
C(8)	2080(3)	146(3)	-2584(2)	58(1)
C(9)	2546(3)	1160(3)	-1689(2)	57(1)
C(10)	5241(3)	2367(3)	-2634(3)	61(1)
C(11)	6583(3)	2729(4)	-3765(3)	88(1)
C(12)	2990(3)	281(2)	1605(2)	44(1)
C(13)	1853(3)	-520(2)	1245(2)	44(1)
C(14)	1230(3)	-663(3)	2056(2)	57(1)
C(15)	1697(3)	-67(3)	3200(3)	68(1)
C(16)	2811(3)	699(3)	3547(2)	63(1)
C(17)	3449(3)	863(3)	2776(2)	54(1)

C(18)	1315(3)	-1178(2)	34(2)	48(1)
C(19)	-468(3)	-2350(3)	-1368(2)	68(1)
C(20)	7227(3)	4286(2)	3757(2)	50(1)
C(21)	8214(3)	4230(2)	4732(2)	47(1)
C(22)	8274(3)	5035(3)	5791(2)	57(1)
C(23)	7388(3)	5864(3)	5923(3)	71(1)
C(24)	6417(3)	5914(3)	4988(3)	75(1)
C(25)	6331(3)	5156(3)	3924(3)	66(1)
C(26)	9169(3)	3322(3)	4635(2)	50(1)
C(27)	10871(4)	2412(4)	5656(3)	98(1)
N(1)	4088(3)	2926(3)	-749(2)	65(1)
N(2)	3601(2)	488(2)	833(2)	53(1)
N(3)	7119(3)	3523(3)	2700(2)	62(1)
O(1)	5791(2)	3264(2)	-1880(2)	87(1)
O(2)	5538(2)	2018(2)	-3638(2)	72(1)
O(3)	1890(2)	-1314(2)	-700(2)	68(1)
O(4)	107(2)	-1647(2)	-200(2)	61(1)
O(5)	9302(2)	2662(2)	3758(2)	68(1)
O(6)	9904(2)	3271(2)	5665(2)	74(1)
P(1)	4519(1)	2956(1)	1602(1)	52(1)

Table A 1.7. Positional parameters and U(eq) for $[P(CH_2NC_6H_4\text{-}2\text{-}CO_2Me)_3]Y$ (**14**)

	x	y	z	U(eq)
C(1)	1259(14)	178(16)	5366(9)	48(5)
C(2)	2318(10)	84(14)	6278(7)	64(3)
C(3)	2463(10)	-146(14)	6901(6)	64(3)
C(4)	3371(11)	-166(13)	7063(6)	64(3)
C(5)	4135(9)	44(12)	6604(7)	64(3)
C(6)	3990(10)	274(12)	5982(7)	64(3)
C(7)	3081(12)	294(13)	5819(5)	64(3)
C(8)	1813(16)	-273(16)	7322(9)	47(5)
C(9)	1400(20)	-440(30)	8460(11)	96(8)
N(1)	1388(12)	181(13)	6023(7)	45(4)
O(1)	835(12)	-488(12)	7285(7)	58(4)
O(2)	2151(12)	-373(16)	7950(8)	85(5)
P(1)	0	0	5039(5)	45(3)
Y(1)	0	0	6643(2)	27(1)

Table A 1.8. Positional parameters and U(eq) for [TPP]CoP($CH_2NC_6H_4$-2-$CO_2Me)_3$Gd **(21)**

	x	y	z	U(eq)
C(84)	1005(4)	7982(3)	6783(3)	62(1)
C(85)	1640(4)	7851(4)	6405(3)	70(1)
C(77)	6307(3)	102(3)	1845(2)	54(1)
C(78)	6888(4)	-59(3)	1430(3)	66(1)
C(86)	1994(4)	7075(4)	6310(3)	76(2)
C(89)	725(4)	7238(4)	7091(3)	75(2)
C(88)	1093(4)	6434(4)	6985(3)	72(2)
C(82)	5902(4)	-603(4)	2054(3)	66(1)
C(87)	1718(4)	6379(4)	6601(3)	72(1)
C(80)	6620(4)	-1561(4)	1417(4)	82(2)
C(79)	7043(5)	-873(4)	1213(3)	77(2)
C(81)	6056(4)	-1430(4)	1845(4)	86(2)
C(76)	6114(5)	1005(4)	2048(4)	91(2)
C(83)	612(6)	8845(4)	6877(5)	111(2)
Gd(1)	5555(1)	7547(1)	4128(1)	28(1)
Co(1)	2035(1)	7444(1)	1407(1)	17(1)
P(1)	3490(1)	7470(1)	2603(1)	21(1)
N(5)	1244(2)	6772(2)	1864(1)	19(1)
O(9)	2035(2)	12995(1)	-68(1)	32(1)
N(4)	2345(2)	6368(2)	966(1)	20(1)
N(7)	2699(2)	8118(2)	851(1)	20(1)
O(1)	7209(2)	7292(2)	4278(2)	45(1)
C(36)	832(2)	7084(2)	2372(2)	21(1)

N(6)	1474(2)	8517(2)	1642(1)	19(1)
O(5)	6340(2)	8671(2)	4958(1)	41(1)
C(38)	946(2)	8610(2)	2112(2)	21(1)
O(7)	117(2)	1872(1)	1393(1)	35(1)
C(42)	2118(2)	9579(2)	979(2)	22(1)
O(10)	5489(2)	6423(2)	-1658(1)	43(1)
C(4)	6179(2)	6461(2)	2767(2)	28(1)
C(31)	2028(2)	5544(2)	1024(2)	23(1)
C(40)	1014(2)	9941(2)	1682(2)	26(1)
O(3)	6075(2)	6742(2)	5241(1)	40(1)
C(32)	1422(2)	5311(2)	1415(2)	22(1)
C(37)	700(2)	7946(2)	2506(2)	22(1)
O(6)	6983(2)	9874(2)	5597(2)	53(1)
C(55)	209(2)	8216(2)	3044(2)	25(1)
C(72)	4922(3)	6517(2)	-1222(2)	31(1)
C(66)	2844(2)	11887(2)	773(2)	30(1)
N(3)	4745(2)	8816(2)	3558(2)	27(1)
C(51)	380(2)	2709(2)	1342(2)	25(1)
C(2)	3275(2)	7036(2)	3439(2)	28(1)
C(45)	3690(3)	8507(2)	186(2)	31(1)
C(49)	82(2)	4187(2)	985(2)	32(1)
N(1)	5512(2)	6855(2)	3008(2)	27(1)
O(2)	8650(2)	6766(2)	4325(2)	52(1)
C(29)	2965(3)	5394(2)	319(2)	30(1)
C(65)	1994(2)	12171(2)	173(2)	23(1)
C(47)	3371(2)	6946(2)	293(2)	23(1)

C(3)	3902(2)	8598(2)	2837(2)	28(1)
C(39)	655(2)	9492(2)	2132(2)	26(1)
C(64)	1176(2)	11628(2)	-147(2)	26(1)
N(2)	4139(2)	6842(2)	4146(2)	28(1)
C(9)	7240(2)	6478(2)	3205(2)	34(1)
C(33)	1103(2)	5897(2)	1837(2)	21(1)
C(62)	2074(2)	10494(2)	722(2)	24(1)
O(4)	6364(2)	5725(2)	6121(2)	51(1)
O(8)	-1120(2)	9375(2)	4417(2)	58(1)
C(43)	2702(2)	9004(2)	770(2)	23(1)
C(63)	1230(2)	10797(2)	133(2)	27(1)
C(34)	604(2)	5653(2)	2342(2)	26(1)
C(52)	1395(2)	2895(2)	1717(2)	30(1)
C(12)	3923(3)	6364(2)	4665(2)	28(1)
C(25)	5649(3)	10023(2)	4401(2)	34(1)
C(35)	458(2)	6386(2)	2680(2)	27(1)
C(69)	3914(2)	6758(2)	-231(2)	24(1)
C(74)	4948(2)	6692(2)	56(2)	31(1)
C(30)	2413(3)	4943(2)	622(2)	30(1)
C(70)	3389(3)	6693(2)	-1022(2)	35(1)
C(56)	-817(3)	8231(2)	2798(2)	37(1)
C(28)	2910(2)	6287(2)	522(2)	22(1)
C(50)	-275(2)	3352(2)	965(2)	34(1)
C(48)	1083(2)	4391(2)	1376(2)	23(1)
C(41)	1545(2)	9339(2)	1392(2)	21(1)
C(18)	5734(3)	6186(2)	5537(2)	35(1)

C(26)	6317(3)	9467(3)	4986(2)	37(1)
C(67)	2886(2)	11060(2)	1044(2)	29(1)
C(20)	4888(2)	9682(2)	3703(2)	30(1)
C(1)	4470(2)	6821(2)	2453(2)	26(1)
C(53)	1736(2)	3725(2)	1725(2)	28(1)
C(46)	3279(2)	7813(2)	464(2)	23(1)
C(71)	3890(3)	6575(3)	-1521(2)	39(1)
C(58)	-729(3)	8958(2)	3948(2)	39(1)
C(8)	7902(3)	6095(3)	2900(2)	45(1)
C(73)	5448(3)	6566(2)	-435(2)	32(1)
C(44)	3332(3)	9242(2)	369(2)	31(1)
C(57)	-1297(3)	8603(3)	3240(2)	40(1)
C(17)	4690(3)	5988(2)	5331(2)	33(1)
C(13)	2916(3)	6176(2)	4580(2)	38(1)
C(5)	5880(3)	5987(2)	2053(2)	37(1)
C(14)	2702(3)	5634(3)	5065(2)	49(1)
C(16)	4415(4)	5408(2)	5795(2)	44(1)
C(10)	7667(2)	6879(2)	3958(2)	36(1)
C(22)	4459(3)	11188(3)	3320(3)	48(1)
C(54)	-887(3)	1628(2)	949(3)	57(1)
C(15)	3457(4)	5230(3)	5673(2)	52(1)
C(60)	767(3)	8545(3)	3771(2)	42(1)
C(68)	1180(3)	13313(2)	-682(2)	50(1)
C(23)	5193(3)	11502(3)	3991(3)	51(1)
C(6)	6547(3)	5621(3)	1784(2)	44(1)
C(61)	-2153(3)	9585(3)	4083(3)	61(1)

C(24)	5768(3)	10929(3)	4513(2)	46(1)
C(7)	7572(3)	5688(3)	2204(3)	51(1)
C(21)	4305(3)	10318(2)	3184(2)	39(1)
C(59)	299(3)	8915(3)	4220(2)	51(1)
C(75)	4970(4)	6372(4)	-2467(2)	70(2)
C(11)	9111(3)	7150(3)	5082(3)	63(1)
C(27)	7702(4)	9335(4)	6162(3)	69(2)
C(19)	7417(3)	5908(3)	6321(3)	65(1)

Table A 1.9. Positional parameters and U(eq) for $[P(CH_2NC_6H_5]_3VNMe_2$ (**28**)

	x	y	z	U(eq)
V(1)	1735(1)	2462(1)	4961(1)	22(1)
P(1)	675(1)	2479(1)	2899(1)	29(1)
N(1)	366(1)	1813(1)	4971(1)	27(1)
N(3)	1481(1)	3709(1)	4540(1)	27(1)
N(2)	2698(1)	1971(1)	3970(1)	25(1)
C(10)	3778(2)	1622(1)	4004(2)	25(1)
C(2)	2109(2)	2017(2)	2939(2)	28(1)
C(9)	-164(2)	1668(2)	6795(2)	29(1)
N(4)	2320(2)	2329(1)	6297(1)	28(1)
C(4)	-295(2)	1409(1)	5728(2)	25(1)
C(8)	-796(2)	1268(2)	7552(2)	33(1)
C(3)	763(2)	3644(2)	3583(2)	29(1)
C(16)	1940(2)	4582(2)	4782(2)	30(1)
C(1)	-22(2)	1729(2)	3870(2)	30(1)
C(12)	5518(2)	1416(2)	4968(2)	33(1)
C(11)	4481(2)	1810(2)	4883(2)	29(1)
C(7)	-1597(2)	613(2)	7279(2)	35(1)
C(15)	4180(2)	1069(2)	3192(2)	31(1)
C(14)	5227(2)	686(2)	3291(2)	38(1)
C(21)	3002(2)	4629(2)	5239(2)	42(1)
C(17)	1384(2)	5420(2)	4564(2)	39(1)
C(6)	-1760(2)	374(2)	6228(2)	36(1)
C(13)	5899(2)	852(2)	4174(2)	37(1)

C(5)	-1116(2)	756(2)	5459(2)	30(1)
C(18)	1886(3)	6273(2)	4795(2)	57(1)
C(23)	2668(2)	1413(2)	6690(2)	42(1)
C(22)	2397(2)	3045(2)	7108(2)	44(1)
C(20)	3486(3)	5488(2)	5474(2)	60(1)
C(19)	2937(3)	6306(2)	5242(2)	65(1)

VITA AUCTORIS

Ritu Raturi

Education

2003-2009	Ph.D. Chemistry Department of Chemistry and Biochemistry University of Windsor, Windsor, ON
2000-2002	M.Tech. Food Technology Hartcourt Butler Technological Institute Kanpur, UP, India
1998-2000	M.Sc. Organic Chemistry Department of Chemistrys Kanpur, UP, India
1995-1998	B.Sc. General Science Kanpur University Kanpur, UP, India

Publications

Raturi R., Lefebvre J., Leznoff D. B., McGarvey B. R., Johnson S. J. "A Phosphine-Mediated Through-Space Exchange Coupling Pathway for Unpaired Electrons in a Heterobimetallic Lanthanide-Transition Metal Complex," *Chem. Eur. J.* **2008**, 14, 721-730.

Hatnean J. A., **Raturi R.**, Lefebvre J., Leznoff D. B., Lawes G., Johnson S. A. "Assembly of Triangular Trimetallic Complexes by Triamidophosphine Ligands: Spin-Frustrated Mn^{2+} Plaquettes and Diamagnetic Mg^{2+} Analogues with a Combined Through-Space Through-Bond Pathway for ^{31}P-^{31}P Spin-Spin Coupling," *J. Am. Chem. Soc*, **2006**, 14992.

Raturi R., JohnsonS. A., "Effects of Temperature on Pseudocontact Shifts of Paramagnetic Lanthanide Complexes," (*Manuscript in Preparation*).